7th International Symposium on **Focused Ultrasound** 2020

A Virtual Event, November 9-13, 2020

Abstract Book

Part 1 – Oral Abstracts

Focused Ultrasound Foundation

Sponsor Acknowledgements

Diamond Sponsor

INSIGHTEC

Gold Sponsors

E& Pure Power

PI PIEZO TECHNOLOGY

Silver Sponsors

BRACCO LIFE FROM INSIDE

DAXSONICS ultrasound

UFFC IEEE Ultrasonics, Ferroelectrics, and Frequency Control Society

光 新光人壽 慈善基金會 Shin Kong Life Foundation

SNO 25th Anniversary Society for NeuroOncology

SONIC CONCEPTS

Verasonics® The leader in Research Ultrasound™

Welcome Messages

From the Honorary President

Dear friends:

Though the Symposium experience will be very different than what we imagined a year ago, I am pleased to gather – albeit virtually – with all of you this week. I am proud to be a part of the vast, international focused ultrasound community.

I became interested in focused ultrasound in 2008, when I was desperately seeking a way to extend and preserve quality of life for some of the most challenging, advanced stage patients. My research since then has been dedicated to using it to address gastrointestinal cancers – including those in the pancreas and liver – and soft tissue desmoid tumors.

In these last 12 years, the focused ultrasound community – as well as the body of knowledge around this innovative therapy – has grown immeasurably. I am proud to have contributed to this by growing numbers of patients treated in the clinical setting, and, thanks to my persistence, the possibility of seeing light at the end of the tunnel. This light has come in the form of histotripsy as a wonderful tool to perform fast, more precise, tissue selection and treatments to enhance the immune system.

Despite all that we have learned, there is still much that we don't yet understand about focused ultrasound's vast potential, including how it can be used to modulate the immune system. We are also working to push the technology beyond its known limits to help more and more patients for whom there are no good treatment options.

The Foundation's biennial Symposium plays a critical role in bringing the research community together and reinforcing the importance of our work. Many in the community work in organizations where focused ultrasound is still not widely known, and that can become isolating. This meeting creates a sense of community for us and reminds us we're collectively transforming medicine, advancing science, and improving lives.

This week won't be the same as those in years past for a number of reasons. But, it is my hope and my belief that we will be able to overcome the limitations of a virtual meeting and use this time to grow knowledge, connect, and collaborate. As a passionate man from the Mediterranean sea, I will miss personal interaction with all of you, but better times will come and we will meet then.

Sincerely,

Joan Vidal-Jové, MD, PhD

Director, Comprehensive Tumor Center Barcelona
Institut Khuab for Interventional Oncology

From the Foundation Chairman

Dear Friends,

Welcome to the 7th International Symposium on Focused Ultrasound and our first meeting to be held in an entirely virtual format.

Let me start by saying we will sorely miss the opportunity to visit with you in person. While the scientific portion of the program is extremely robust, unfortunately the social portion is nearly nonexistent this year.

The Symposium has two intersecting purposes: the first is to share information and knowledge, and the second is to create new – and strengthen existing – relationships.

Regarding the first goal, we are optimistic that the virtual format will not only enhance our ability to share information and knowledge, but also enable us to reach a significantly larger audience. We have seen record registrations this year. Undoubtedly, the learning curve of hosting a virtual meeting will be steep, and we apologize in advance for any resulting inconvenience and appreciate your understanding. We are pioneering new territory together this year.

In contrast, the challenge of fostering personal relationships is one for which we do not yet have a solution. To rapidly advance the field, it is critical that we prioritize communication, cooperation, and collaboration of ideas. These values are the keystones to innovation and help to minimize duplication of effort across the field. We feel strongly that, to be most effective, this requires face-to-face interactions. We plan to build on the lessons learned at this year's meeting to craft a hybrid model for future symposia, and we eagerly solicit your ideas to mitigate this gap.

We are enthusiastic about this year's scientific program which will include:

- Keynote and special lectures by:
  - the Symposium's Honorary President, Joan Vidal-Jové, MD, PhD
  - Nobel Laureate, James P. Allison, PhD
  - Milken Institute Chairman, Michael Milken
  - Virginia Governor, Ralph Northam
  - Chairman of the Board of Directors at Medtronic and Intel, Omar Ishrak, PhD
  - Chief of Neurology at Massachusetts General Hospital, Merit Cudkowicz, MD
  - FORTUNE Editor-in-Chief, Clifton Leaf
  - Executive Vice President and Chief Science Officer of the Prostate Cancer Foundation, Howard R. Soule, PhD
- Presentations by award recipients: Lawrence A. Crum, PhD (Visionary Award); Nir Lipsman, MD, PhD (Ferenc Jolesz Memorial Award); and Matthew Bucknor, MD, and Pejman Ghanouni, MD, PhD (Andrew J. Lockhart Memorial Prize).
- Plenary sessions and panel discussions with ample time for Q&A
- Expert-led roundtable discussions on specific topics
- Virtual poster session and industry showcase

This year, we are also devoting portions of our program to the International Society for Therapeutic Ultrasound (ISTU) and the National Institute of Mental Health (NIMH).

The Symposium is taking place in an unprecedented time of unrest and uncertainty as a result of the confluence of multiple threats to our pillars of society and our way of life. Many of the

Continued, next page

ensuing disruptions will be permanent, but on a positive note, many of the changes that would have been inevitable are simply being accelerated.

Fortunately, we in the focused ultrasound community are accustomed to working in a world of disruption. Our community is well positioned to not only survive the challenges currently confronting us but to thrive in this environment.

The important work of our valued community has not only been undiminished but enhanced. We observed a transient slowdown in the development and growth of the field in the early spring, but focused ultrasound is back on track to grow into a multibillion-dollar industry, providing solutions that improve the lives of millions of people around the world.

We appreciate your participation in the Symposium and are very grateful for the generous support of our donors and sponsors which have made it possible. We look forward to a wonderful week together.

Be well,

Neal F. Kassell, MD
Chairman, Focused Ultrasound Foundation

Notes

Table of Contents

Symposium Organizer

FOCUSED ULTRASOUND FOUNDATION

About the Focused Ultrasound Foundation

The Focused Ultrasound Foundation is a medical technology research, education, and advocacy organization dedicated to improving the lives of millions of people with serious medical disorders by accelerating the development and adoption of focused ultrasound.

Positioned at the nexus of a large, diverse group of stakeholders comprising the focused ultrasound community, the Foundation functions as an independent, unbiased third party, aligning organizations into a cohesive ecosystem with a single goal: to make this technology available to patients in the shortest time possible. It strives to catalyze progress while instilling a patient-centric sense of urgency.

The Foundation works to clear the path to global adoption by organizing and funding research, fostering collaboration at our various workshops and symposia, building awareness, and cultivating the next generation through internships and fellowships.

The Foundation is on the leading edge of the venture philanthropy and social entrepreneurship movements and is a model of how private philanthropy can work in concert with academia, industry, and government to bridge the gap between research and commercialization.

To learn more about focused ultrasound and the Focused Ultrasound Foundation, visit the Foundation's website: www.fusfoundation.org

Scientific Program Committee

Matthew Bucknor, MD
University of California, San Francisco
San Francisco, CA, USA

Wen-Shiang Chen, MD, PhD
National Taiwan University Hospital
Taipei, Taiwan

Christian Diederich, PhD
University of California, San Francisco
San Francisco, CA, USA

Mark Emberton, MD
University College London Hospitals
London, UK

Katherine Ferrara, PhD
Stanford University
Stanford, CA, USA

Chandan Guha, MBBS, PhD
Montefiore Medical Center
New York, NY, USA

Joo Ha Hwang, MD, PhD
Stanford University
Stanford, CA, USA

Tatiana Khokhlova, PhD
University of Washington
Seattle, WA, USA

Elisa Konofagou, PhD
Columbia University
New York, NY, USA

Jae Young Lee, MD, PhD
Seoul National University Hospital
Seoul, Korea

Nir Lipsman, MD, PhD
Sunnybrook Health Sciences Centre
Toronto, Ontario, Canada

Chrit Moonen, PhD
University Medical Center Utrecht
Utrecht, Netherlands

José Obeso, MD, PhD
AC Comprehensive Neuroscience Centre (HM CINAC)
Madrid, Spain

Allison Payne, PhD
University of Utah
Salt Lake City, UT, USA

Richard Price, PhD
University of Virginia
Charlottesville, VA, USA

Karun Sharma, MD
Children's National Health System
Washington, DC, USA

Lei Sun, PhD
Hong Kong Polytechnic University
Hong Kong

Clare Tempany, MD
Brigham and Women's Hospital
Boston, MA, USA

Gail ter Haar, PhD
Institute of Cancer Research
Sutton, UK

Zhen Xu, PhD
University of Michigan
Ann Arbor, MI, USA

Keynotes and Special Lectures

Monday, 9 November 2020

8:00 AM | Honorary President's Address

Joan Vidal-Jové, MD, PhD

Joan Vidal-Jové is Director of the Comprehensive Tumor Center Barcelona at the Institut Khuab for Interventional Oncology. As Honorary President of the symposium, he delivered an address entitled, "FUS in Oncology: Strategies of intrusion, anonymity and resistance. The paradigm of pancreas cancer."

8:30 AM | Keynote Address

Ralph Northam, MD

Ralph Northam is the 73rd Governor of Virginia and pediatric neurologist practicing at Children's Hospital of the King's Daughters in Norfolk, Virginia. Governor Northam gave an address about focused ultrasound in Virginia and beyond.

10:19 AM | Special Lecture

Merit Cudkowicz, MD

Merit Cudkowicz is Chief of Neurology at Massachusetts General Hospital (MGH). She gave a lecture entitled, "Therapeutic advances in neurodegenerative disorders: ALS as an example."

1:34 PM | Special Lecture

Renana Eitan, MD

Renana Eitan works in the Functional Neuroimaging Laboratory of Brigham & Women's Hospital and Harvard Medical School. She gave a lecture on "Focused Ultrasound for Psychiatric Disorders."

Tuesday, 10 November 2020

9:29 | Keynote Address

James P. Allison, PhD

James Allison is Chair of Immunology at MD Anderson Cancer Center. He delivered a keynote address entitled, "Immune Checkpoint Blockade in Cancer Therapy: New insights into therapeutic mechanisms of anti-CTLA4 and anti-PD-1."

Chetan Bettegowda

Graeme Woodworth

1:03 PM | Special Lecture

Chetan Bettegowda, MD, PhD and Graeme Woodworth, MD

Chetan Bettegowda is Professor of Neurosurgery at Johns Hopkins Medicine. Graeme Woodworth is Professor of Neurosurgery and Director of the Brain Tumor Treatment & Research Center at the University of Maryland School of Medicine. They gave a special lecture entitled, "Focused Ultrasound and Liquid Biopsy in Brain Tumors: A critical role for the blood brain barrier?"

Keynotes and Special Lectures | continued

Wednesday, 11 November 2020

8:00 AM | Keynote Address

Michael Milken

Michael Milken is Chairman of the Milken Institute. He delivered a keynote address about advances in health care in the 20th and 21st centuries.

9:40 AM | Special Lecture

Howard R. Soule, PhD

Howard Soule is Executive Vice President and Chief Science Officer of the Prostate Cancer Foundation (PCF). He gave a special lecture about PCF's efforts to advance research and improve treatment.

Thursday, 12 November 2020

8:00 AM | Keynote Address

Clifton Leaf

Clifton Leaf is a prominent healthcare journalist and Editor-in-Chief of FORTUNE. He delivered a keynote address entitled, "Want to Go to the Moon? Build a Road."

Friday, 13 November 2020

8:00 AM | Keynote Address

Omar Ishrak

Omar Ishrak is Executive Chairman and Chairman of the Board at Medtronic, and Chairman of the Board at Intel. He gave a keynote address entitled, "The Role of MedTech in Driving Patient Outcomes."

Program at a Glance

Monday 9 November

AM

8:00 — Welcome Message from FUSF Chairman
Honorary President's Address
8:00–8:30

Keynote Address: Ralph Northam
8:30–8:38

9:00 — Movement Disorders Oral Presentation Q&A
8:43–9:04

Parkinson's Disease Panel Discussion
9:04–10:04

10:00

Special Lecture on Neurodegenerative Diseases
10:19–10:43

11:00 — Neurodegenerative Diseases Oral Presentation Q&A
10:43–11:03

Neurodegenerative Diseases Panel Discussion
11:03–11:54

PM

12:00 — Epilepsy Oral Presentation Q&A
11:59–12:19

Epilepsy Panel Discussion
12:19–1:19

1:00

Special Lecture on Psychiatric Disorders
1:34–1:55

2:00 — Psychiatric Disorders Oral Presentation Q&A
1:55–2:15

Psychiatric Disorders Panel Discussion
2:15–3:09

3:00

Neuromodulation Oral Presentation Q&A
3:14–4:35

4:00

Focused Ultrasound for Neuromodulation:
Considerations for Human Translation Panel
4:35–5:17

5:00

Oral presentations, posters, and exhibits are available on-demand all day.

Program at a Glance | continued

Tuesday 10 November

AM 8:00

Brain Tumors Oral Presentation Q&A
8:00–8:22

Brain Tumors Panel Discussion
8:22–9:14

9:00

Keynote Address: James Allison
9:29–10:14

10:00

Cancer Immunotherapy — Brain — Oral Presentation Q&A
10:14–10:36

Cancer Immunotherapy — Breast — Oral Presentation Q&A
10:41–11:03

11:00

Cancer Immunotherapy — Other — Oral Presentation Q&A
11:08–11:28

Cancer Immunotherapy Panel Discussion
11:28–12:19

PM 12:00

Fireside Chat on Cancer Therapy: Beyond Ionizing Radiation
12:19–12:51

1:00

Special Lecture on Liquid Biopsy
1:03–1:24

Special ISTU Session
Updates & Introduction
Lizzi Award Winner Presentations
Remembering Charles Cain: A Pioneer and Leader in Focused Ultrasound
1:29–2:48

2:00

3:00

Roundtable Discussions
3:01–4:01

4:00

Oral presentations, posters, and exhibits are available on-demand all day.

Cancer immunotherapy sessions are sponsored by

CANCER RESEARCH INSTITUTE

Program at a Glance | continued

Wednesday 11 November

AM 8:00
- Keynote Address: Michael Milken
  8:00–8:40

9:00
- Breast Cancer Panel Discussion
  8:40–9:25

10:00
- Special Lecture on Prostate Cancer: Howard Soule
  9:40–10:00
- Prostate Oral Presentation Q&A
  10:00–10:20

11:00
- Prostate Panel Discussion
  10:20–11:22

PM 12:00
- Awards Ceremony
  Visionary Award
  Ferenc Jolesz Memorial Award
  Andrew J. Lockhart Memorial Award
  11:27–12:15
- Pancreatic Cancer Oral Presentation Q&A
  12:30–12:50

1:00
- Pancreatic Cancer Panel Discussion
  12:50–1:39

2:00
- Liver Oral Presentation Q&A
  1:44–2:06
- Miscellaneous Tumors Oral Presentation Q&A
  2:11–2:33

3:00
- Roundtable Discussions
  2:43–3:43

4:00

Oral presentations, posters, and exhibits are available on-demand all day.

Program at a Glance | continued

Thursday 12 November

AM	8:00	Keynote Address: Clifton Leaf 8:00–8:24
		Blood-Brain Barrier Opening — Technical — Oral Presentation Q&A 8:24–8:46
	9:00	Special Lecture on Prostate Cancer: Howard Soule 8:51–9:13
		Drug Delivery Oral Presentation Q&A 9:18–9:38
	10:00	Drug Delivery Panel Discussion 9:38–10:31
	11:00	Fireside Chat with Nathalie LaCave on Gene Therapy 10:46–11:10
		Miscellaneous Indications Oral Presentation Q&A 11:15–11:37
		Musculoskeletal Applications Oral Presentation Q&A 11:42–12:02
PM	12:00	Musculoskeletal Applications Panel Discussion 12:02–12:48
	1:00	Chronic Pain Oral Presentation Q&A 1:03–1:25
	2:00	Women's Health Panel Discussion 1:30–2:17
	3:00	Roundtable Discussions 2:22–3:22
	4:00	

Oral presentations, posters, and exhibits are available on-demand all day.

Program at a Glance | continued

Friday 13 November

AM 8:00

Keynote Address: Omar Ishrak
8:00–8:21

Investor Ecosystem 101; Navigating the Investor Ecosystem
8:21–9:23

Brain Technical — Imaging — Oral Presentation Q&A
8:21–8:41

Brain Technical — Imaging — Panel Discussion
8:41–9:13

9:00

Business Models 101; Business Model Trends in the Med Tech Industry; Dancing with a Giant: Tips for Productive Relationships between Startups and Corporates; Exits: Considering IPOs vs Acquisitions vs Mergers
9:28–11:20

Brain Technical — Miscellaneous — Oral Presentation Q&A
9:28–9:48

Brain Technical — Beyond Ablation Research — Panel Discussion
9:48–10:34

10:00

Technical Research Oral Presentation Q&A
10:49–11:09

11:00

Technology Gaps & Breakthroughs Panel Discussion; Closing Remarks
11:09–12:29

PM 12:00

FDA Town Hall
11:50–12:45

1:00

The Power of Advocacy Organizations; Regulatory; Reimbursement; How Medical Specialty Societies Influence Reimbursement
12:50–2:14

2:00

Real World Examples of FUS Site Success — Panel Discussion
2:19–3:08

3:00

Training Certification and Credentialing — Panel Discussion; Closing Remarks
3:13–4:14

4:00

Oral presentations, posters, and exhibits are available on-demand all day.

Commercialization sessions are sponsored by

AdvaMed
Advanced Medical Technology Association

Session Moderators

Sandra Black
Sunnybrook Health Sciences Centre
Toronto, Ontario, Canada

Matthew Bucknor
University of California, San Francisco
San Francisco, CA, USA

Mark Carol
Focused Ultrasound Foundation
Charlottesville, VA, USA

Elisa Konofagou
Columbia University
New York, NY USA

Rees Cosgrove
Brigham and Women's Hospital
Boston, MA, USA

Katherine Ferrara
Stanford University
Stanford, CA, USA

Paul Fishman
University of Maryland School of Medicine
Baltimore, MD, USA

Nathan Fountain
University of Virginia
Charlottesville, VA, USA

Dheeraj Gandhi
University of Maryland School of Medicine
Baltimore, MD, USA

Wladyslaw Gedroyc
Imperial College Healthcare NHS Trust
London, UK

Pejman Ghanouni
Stanford University
Stanford, CA, USA

Michael Gofeld
Silver Medical Group Centre for Pain Care
North York, Ontario, Canada

Holger Grüll
University of Cologne
Cologne, Germany

Gina Hesley
Mayo Clinic
Rochester, MN, USA

Christy Holland
University of Cincinnati
Cincinnati, Ohio, USA

Joo-Ha Hwang
Stanford University
Stanford, CA, USA

Sasha Klibanov
University of Virginia
Charlottesville, VA, USA

Cyril Lafon
INSERM
Lyon, France

Suzanne LeBlang
Focused Ultrasound Foundation
Charlottesville, VA, USA

Michael Lim
Stanford University
Stanford, CA, USA

Nir Lipsman
Sunnybrook Research Institute
Toronto, Ontario, Canada

Holly Lisanby
National Institute of Mental Health
Bethesda, MD, USA

Subha Maruvada
U.S. FDA Center for Devices & Radiological Health
Silver Spring, MD, USA

Nathan McDannold
Brigham and Women's Hospital; Harvard Medical School
Boston, MA, USA

Jaime Murphy
Imperial College London
London, UK

José Obeso
CINAC; Hospital Universitario HM Puerta del Sur, Móstoles; Universitario CEU-San Pablo
Madrid, Spain

Meaghan O'Reilly
Sunnybrook Health Sciences Center
Toronto, Ontario, Canada

Samuel Peretsman
Urology Specialists of the Carolinas
Charlotte, NC, USA

Richard Price
University of Virginia
Charlottesville, VA, USA

Viola Rieke
University of Utah
Salt Lake City, UT, USA

Narendra Sanghvi
Focused Ultrasound Foundation; SonaCare Medical, LLC
Charlotte, NC, USA

Karun Sharma
Children's National Health System
Washington, DC, USA

Jason Sheehan
University of Virginia
Charlottesville, VA, USA

Craig Slingluff
University of Virginia
Charlottesville, VA, USA

John Snell
Focused Ultrasound Foundation
Charlottesville, VA, USA

Howard Soule
Prostate Cancer Foundation
Santa Monica, CA, USA

Jill O'Donnell Tormey
Cancer Research Institute
New York, NY, USA

Joan Vidal-Jové
Comprehensive Tumor Center Barcelona, Institut Khuab for Interventional Oncology
Barcelona, Spain

Graeme Woodworth
University of Maryland School of Medicine
Baltimore, MD, USA

Seung-Schick Yoo
Harvard Medical School
Boston, MA, USA

Notes

Oral Abstracts

The following abstracts were withdrawn by the authors:

BBB-6	IMM-11	MOV-1	TEC-5
BRT-11	IMM-14	NDG-1	

BBB-1

Topic: Blood-Brain Barrier Opening

Presentation Type: Oral

Bilateral blood-brain barrier opening in mice using acoustic holograms

Sergio Jiménez-Gambín[1], Antonios Pouliopoulos[2], Noé Jiménez[1], Jose M. Benlloch[1], Elisa Konofagou[2], Francisco Camarena[1]

[1]Universitat Politècnica de València, Valencia, Spain
[2]Columbia University, New York, NY, USA

Background: Microbubble-enhanced low-intensity focused ultrasound is the only non-invasive technique to disrupt the blood-brain barrier (BBB) temporally and locally, which allows targeted drug delivery into the central nervous system. However, it is not possible to simultaneously target two or more brain structures, using either a single-element or multi-element transducer. In this work, we present a novel technique using acoustic holograms to perform BBB opening in two mirrored regions in mice brain. The system consists of a single-element transducer and a 3D-printed holographic lens designed to simultaneously create two symmetric foci in anesthetized mice in vivo. This approach has three main advantages: (1) simple and low-cost; (2) aberrations due to skull and water container are corrected; and (3) a single sonication enables multiple BBB opening locations, becoming a time- and cost-effective therapeutic system for neurological diseases.

Materials and Methods: The process of hologram generation is divided in five steps. First, we extract the geometry and acoustic properties of a mouse skull from x-ray micro-CT images and we identify the target structure based on MRI scans. Second, simulated back-propagation and phase-conjugation are used to calculate the acoustic wavefront at the holographic surface. Third, a phase-only lens is generated from both the phase and magnitude of the recorded wavefront. Fourth, the lens is manufactured using Formlabs ClearResin (sound speed: 2580 m/s; density: 1171 kg/m3) by stereolithographic 3D-printing. Finally, the target acoustic image is generated by exciting the lens with the single-element transducer. For the in-vivo experiment, 1µl/g Definity microbubbles were injected intravenously and 1.68-MHz FUS (400 kPa peak-negative pressure, PRF: 5 Hz, pulse length: 1 ms) was applied for 2 minutes. Then, 0.2 ml of gadolinium tracer was injected intraperitoneally, and post-treatment BBB opening was assessed using T1-weighted MRI. Figure 1 shows the experimental and simulated configuration consisting of the single-element FUS transducer (diameter: 64mm, focal depth: 62.6mm; H-204, Sonic Concepts, WA, USA), the acoustic lens to compensate the skull aberrations and split the focus in two, the high-frequency 10-MHz PCD was used for targeting purposes, the water cone for acoustic coupling between the lens and the head of the animal, and the shaved head of the mouse where the bifocal target was reconstructed.

Results: T1-MRI shows gadolinium extravasation at two symmetric focal spots. The two experimental BBB openings are separated 3.0 ± 0.7 mm (n=5 mice) compared to 5.3 mm in full-wave simulations. The discrepancy was likely due to the differences between the skull scanned with micro-CT for manufacturing the lens and the skulls of the treated mice. Furthermore, air pockets trapped within crevices of the lens may have contributed to the field distortion. Using the micro-CT scan of the treated subjects would lead to a better ultrasound location prediction. Nevertheless, we show here the capability of bifocal ultrasound generation in different animals using a separate unique micro-CT scan.

Conclusions: A bilateral BBB opening is possible employing one single sonication with a holographic lens in mice, thus improving the treatment efficiency for several neurodegenerative diseases targeting symmetric brain structures, e.g. hippocampus, putamen and caudate. This work demonstrates the feasibility of hologram-assisted BBB opening for targeted drug delivery in the central nervous system in symmetric regions in separate hemispheres.

Acknowledgements: This research has been supported by the Spanish Ministry of Science, Innovation and Universities (MICINN) through grant "Juan de la Cierva - Incorporación" (IJC2018-037897-I) and PID2019-111436RB-C22, by the Agència Valenciana de la Innovació through gran [omitted].

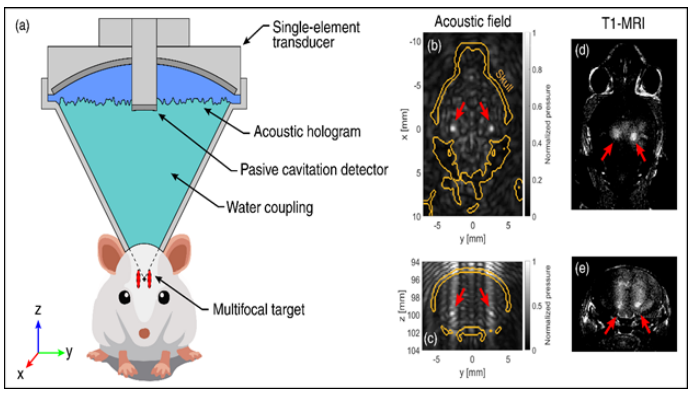

Figure 1. (a) Experimental configuration. (b,c) Simulated ultrasound negative-peak pressure distribution. (d,e) Axial and coronal T1-MRI, showing localized BBB opening by gadolinium extravasation.

BBB-2

Topic: Blood-Brain Barrier Opening

Presentation Type: Oral

Transplantation of exogenous mitochondria after ischemic stroke via FUS-mediated BBB opening

Catherine Gorick, Pedro Norat, Jennifer Sokolowski, Sauson Soldozy, Alexander Klibanov, Petr Tvrdik, M. Yashar Kalani, Richard Price

University of Virginia, Charlottesville, VA, USA

Background: Stroke is a leading cause of death and disability in the United States, with ischemic stroke accounting for the majority (87%) of these injuries. Many studies of neuroprotective agents have been unsuccessful, and treatments focus primarily on reperfusion only. Mitochondrial transplantation has been explored in animal models and in the clinic as a therapeutic approach for cardiovascular disease, effectively improving post-ischemic myocardial function. There is evidence that mitochondrial uptake by neurons can improve cell viability and recovery after stroke, and that ventricular delivery of muscle-derived mitochondria can reduce infarct size in the stroked brain. We thus sought to determine if it is possible to use focused ultrasound (FUS) to further disrupt the blood-brain barrier (BBB) in the infarcted brain region to enhance the delivery of mitochondria and potentially improve neuronal function after ischemic injury.

Materials and Methods: Male or female C57BL/6 mice were used in all studies. Mitochondria were extracted and purified from dissected gastrocnemius skeletal muscle, and stained with MitoTracker Red solution. Mice underwent unilateral transient proximal middle cerebral artery occlusion (tpMCAo) with arterial occlusion lasting 1 hour. At the end of the occlusion, the existing arteriotomy in the central cerebral artery was used to insert an intra-arterial catheter, which would be used to deliver mitochondria, microbubbles, or buffer solution. Immediately following reperfusion, mice received intra-arterial mitochondria or FUS treatment followed by intra-arterial mitochondria. For the FUS treatments, a 1 MHz transducer was aligned to target the infarct volume and cationic lipid-shelled microbubbles (MBs) were injected intra-arterially. Following a 2-minute pulsing protocol optimized for BBB disruption, mitochondria were delivered via the same arterial catheter. Infarct size was assessed by tetrazolium chloride (TTC) staining, and BBB disruption was assessed by T1-weighted contrast-enhanced MRI and Evans Blue dye extravasation. Immunofluorescence was used to assess mitochondrial extravasation and distribution in the brain tissue.

Results: Intra-arterial delivery of exogenous mitochondria to stroked brain results in reduced infarct volume as evidenced by TTC staining (Fig. 1). We next sought to determine whether MRgFUS could be used to further enhance therapeutic delivery to an infarct. T2-weighted MRI was used to identify FUS targets within the stroke volume, and T1-weighted images confirmed increased contrast agent extravasation following FUS (Fig. 2). This enhanced BBB disruption was confirmed by Evans Blue dye measurements. We observed a 3-fold increase in dye volume between the stroke brains treated with FUS vs intra-arterial delivery alone (Fig. 3). Finally, we tested whether exogenous mitochondria would display the same pattern of increased delivery. Immunofluorescent staining illustrated widespread mitochondria distribution in the infarct following FUS, a result of increased extravasation from the vasculature into the surrounding brain tissue (Fig. 4).

Conclusions: Here, we demonstrate the capacity of FUS to enhance delivery of exogenous mitochondria into infarcted brain tissue following ischemic stroke. Mitochondrial transplantation, previously shown to aid in recovery following myocardial infarct, similarly reduces infarct volume in our stroke study. FUS can be used to further the disrupt the already-altered BBB in the stroked tissue, allowing for increased accumulation of a therapeutic from the bloodstream. By increasing mitochondrial extravasation into the damaged brain parenchyma, FUS may therefore be able to speed neuronal recovery after ischemic stroke.

Acknowledgements: Supported by National Institutes of Health Grants R01EB020147 and R21EB024323 to R.J.P. C.M.G. was supported by American Heart Association Fellowship 18PRE34030022.

Figure 1. A,B: Infarct size decreases after intra-arterial mitochondrial infusion. C:Evaluation of infarct size.

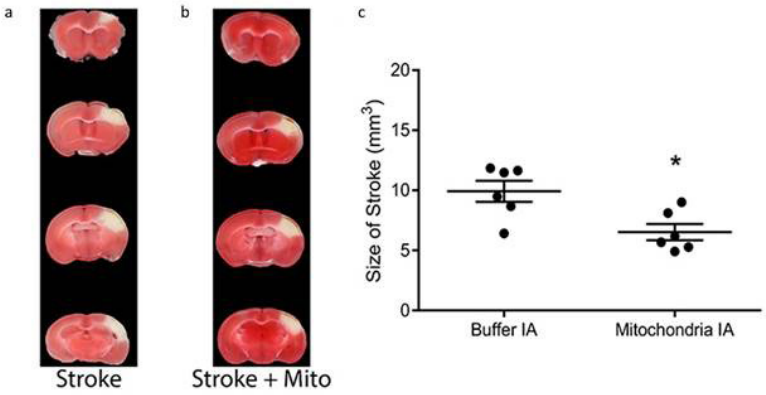

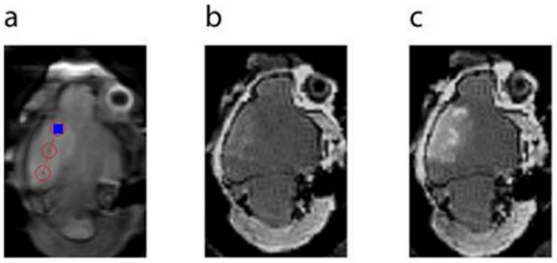

Figure 2. A: T2 MRI post-stroke. B: Red circles = treatment plan. B: Pre-FUS contrast MRI. C: Post-FUS contrast MRI.

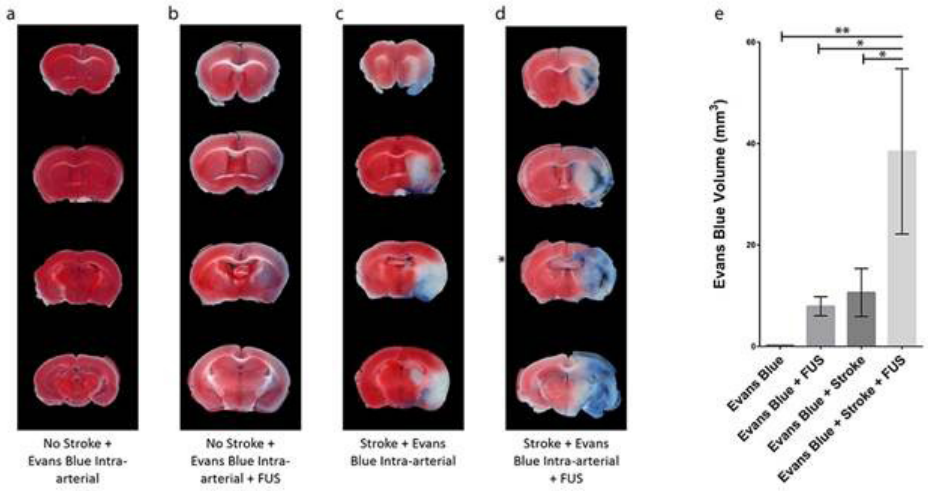

Figure 3. A-D: Evan Blue extravasation images. E: Volume of Evans Blue dye extravasation in the four groups. Bars: mean +/- SD. *, $p<0.05$; **, $p<0.01$, one-way ANOVA, n=3.

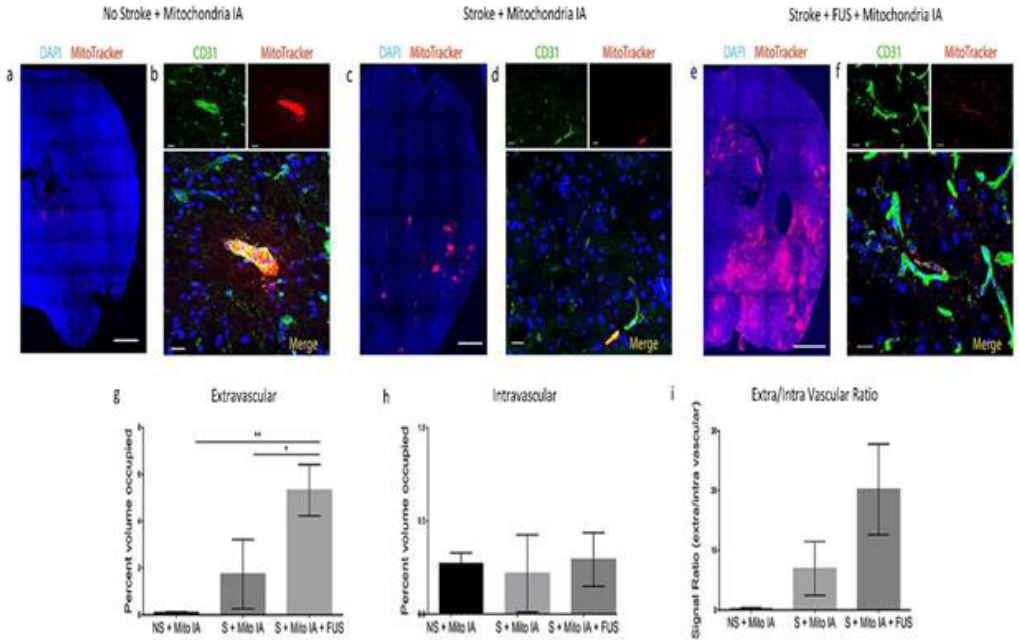

Figure 4. FUS can enhance delivery of intra-arterially infused mitochondria to cross the ischemic blood-brain barrier.

BBB-3

Topic: Blood-Brain Barrier Opening
Presentation Type: Oral

Characterization of nucleic acid nanomedicine delivery in brain tumors with microbubble-enhanced focused ultrasound at subcellular resolution

Yutong Guo[1], Anastasia Velalopoulou[2], Jinhwan Kim[1], Midhun Ben Thomas[3], YongTae Kim[1], Daniel Pomeranz Krummel[4], Soma Sengupta[4], Tobey J. MacDonald[3], Costas Arvanitis[1]

[1]Georgia Institute of Technology, Atlanta, GA, USA
[2]Georgia Institute of Technology, University of Pennsylvania, Philadelphia, PA, USA
[3]Emory University, Atlanta, GA, USA
[4]University of Cincinnati, Cincinnati, OH, USA

Background: The systemic delivery of nucleic acid-based drugs in brain tumors, such as small interfering RNA (siRNA), remains a major problem as unmodified nucleic acids are readily broken down in biological fluids, have poor accumulation in the brain, and cannot penetrate into target cells even if they get into the brain. While nanoparticle encapsulation can prolong circulation time and facilitate cellular uptake, their accumulation in brain tumor remains particularly poor due to their low permeability across the blood-brain/blood tumor barriers (BBB/BTB) and limited interstitial transport. In our recent investigations, we showed that focused ultrasound (FUS), when combined with circulating microbubbles, promotes interstitial convective transport in solid tumors, in addition to increasing the BBB/BTB permeability. Therefore, we hypothesized that FUS enhanced convective transport in brain tumors may lead to improved delivery of nanomedicine whose transport is mediated by convection.

Materials and Methods: To test our hypothesis, we employed 40nm size cationic lipid-polymer hybrid nanoparticle (LPH) (≈+11 mVolt zeta potential) loaded with siRNA in tandem with fluorescent microscopy and physiologically based pharmacokinetic mathematical modeling. Both the LPH and the siRNA were labeled with fluorescent molecules allowing assessing their distribution in vivo. BBB/BTB opening was performed using a custom-built 0.5 MHz FUS system and concurrent i.v. administration of microbubbles in GL261 glioma mice tumor model followed by an administration of LPH-siRNA particles. The physiologically based pharmacokinetic (PBPK) mathematical model simulates the diffusive and convective transport of nanoparticles along with their cellular uptake in brain tumor microenvironment.

Results: Fluorescence microscopy indicates a 13-fold increase in the LPH accumulation in the tumor at 8 hours after FUS treatment, as compared to non FUS-treated tumor ($P=0.044$). Importantly, immunofluorescence staining of vessels shows a ten-fold increase in nanoparticle penetration and a 5-fold increase in siRNA uptake after FUS treatment compared to control. Crucially, up to 50% of the LPH-siRNA are taken up by cancer cells among all cell types, demonstrating good specificity against the GL261 glioma cell line. Integration of the experimental data with the PBPK model for parameter identification, revealed increased vessel effective diffusion coefficient and hydraulic conductivity (convective transport) in interstitial space after FUS. Interestingly, sensitivity analysis indicates that the optimum particle size for LPH-siRNA delivery to brain cancer cell shifts from 20nm (non-FUS) to 40-50nm after FUS, and the transvascular transport increases with a higher cationic charge of the particles.

Conclusions: Microbubble enhanced FUS combined with nanomedicine provides unique opportunities for targeted drug delivery in the brain and brain tumor microenvironment. By explaining and underscoring the importance of particle size and surface charge in FUS-enhanced drug delivery in the brain, our findings provide important scientific principles for the more rational design of focused-ultrasound-based treatment.

Acknowledgements: This study was supported by the CURE foundation and NIH Grant R00EB016971 (NIBIB).

BBB-4

Topic: Blood-Brain Barrier Opening

Presentation Type: Oral

Acoustic cavitation dependent immune response to FUS-induced blood-brain barrier opening

Robin Ji, Maria Eleni Karakatsani, Mark Burgess, Morgan Smith, Maria Murillo, Elisa Konofagou

Columbia University, New York, NY, USA

Background: Focused ultrasound (FUS) induced blood-brain barrier (BBB) opening without intravenous administration of drugs have been shown to be able to provide a therapeutic effect on both wild-type and transgenic neurodegenerative mouse models. Though the exact mechanism has yet to be elucidated, the current hypothesis is the immune response to FUS-mediated BBB opening can lead to such therapeutic effects. Extensive research has been conducted in understanding the parameter space and relationship between microbubble cavitation and BBB opening size using contrast-enhanced MRI, however limited research has been done in fully understanding the immune response to BBB opening, and whether it can be controlled. Therefore, this study aims to investigate the relationship between acoustic cavitation during focused ultrasound (FUS) induced blood-brain barrier (BBB) opening and the resulting immune response in mice.

Materials and Methods: A single-element 1.5MHz FUS transducer with a confocally aligned single-element 7.5MHz passive cavitation detector (PCD) was used for BBB opening in mice. A pulse sequence with a peak-negative pressure of 490kPa (MI = 0.4), pulse length of 10ms, and a pulse frequency of 2Hz was used throughout all sonication. The cavitation dose was quantified by the power spectrum of the cavitation signals over a bandwidth between 4.5 MHz and 13.5 MHz. Real-time cavitation dose monitoring was used to calculate the cumulative cavitation dose (CCD), at which the sonication would be terminated. A bolus injection of Definity microbubbles (10x clinical dose) was administered at the start of each sonication and readministered based on the cavitation levels, until the targeted CCD was reached. The immune response to FUS-induced BBB opening was quantified using the RT2 Profiler PCR Array Mouse Inflammatory Cytokines & Receptors kit. For this study, three different CCD thresholds (low, medium, high) and three different sacrifice time-points post-FUS (6hrs, 24hrs, 72hrs) were employed in this study.

Results: Contrast-enhanced, T1-weighted MRI images confirmed successful BBB openings in all three CCD thresholds 30 minutes after sonication, with significant BBB opening volume differences between all CCC thresholds. Additionally, qPCR analysis captured different immune response to the different CCD thresholds (Figure 1). The low CCD threshold resulted in a slower immune response that peaked at 24hrs, while the medium and high CCD thresholds resulted in a more immediate immune response, i.e. at 6h peaking at around 24h. Finally, the immune response for all CCD thresholds returned close to baseline values by 72h post-FUS.

Conclusions: In this study, the relationship between acoustic cavitation and the immune response after FUS-mediated BBB opening was explored. With fixed sonication parameters, different BBB opening sizes and immune responses were achieved using a cavitation-based controller system. Furthermore, the inflammation response due to BBB opening was observed to transient, as within 72h, the majority of the genes observed return to baseline. In conclusion, these results suggest a relationship between cavitation dose and the immune response to FUS-induced BBB opening, which ultimately may be used to modulate the immune response for more effective therapies.

Acknowledgements: National Institutes of Health (R01AG038961 and R01EB009041) and the Focused Ultrasound Foundation.

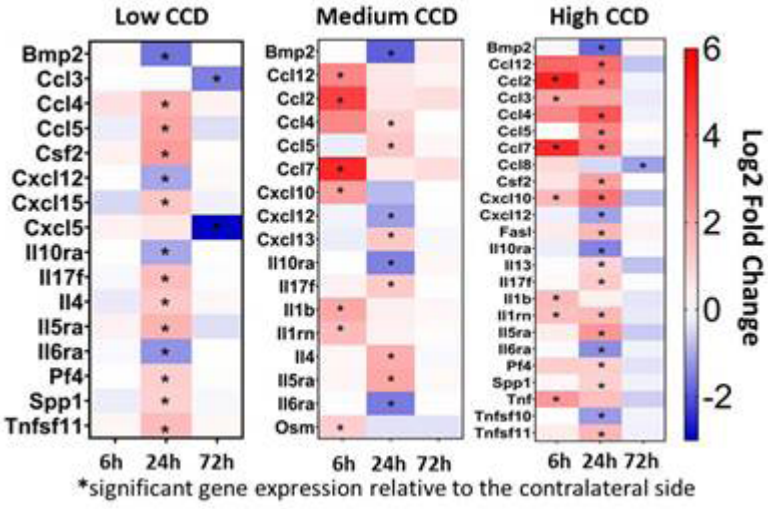

Figure 1. Heat maps of genes with significant expression changes for all three CCD targets and all three time points.

BBB-5

Topic: Blood-Brain Barrier Opening

Presentation Type: Oral

Contrast-free detection of focused ultrasound-induced blood-brain barrier opening using diffusion tensor imaging

Maria Eleni Karakatsani, Antonios Pouliopoulos, Michael Liu, Sachin Jambawalikar, Elisa Konofagou

Columbia University, New York, NY, USA

Background: Contrast-enhanced Magnetic Resonance Imaging has been extensively used for the detection and confirmation of the blood-brain barrier (BBB) opening induced by focused-ultrasound (FUS) coupled with the administration of microbubbles. The translation of the technique to the clinic may be challenged by potential for toxicity of the currently available contrast agents (gadolinium (Gd)) as well as the lack of diffusion information. In this study we investigate the feasibility of diffusion-tensor imaging (DTI) in the detection of the BBB opening and the directionality of the flow.

Materials and Methods: For this study, a non-human primate (NHP) was repeatedly treated with FUS and preformed circulating microbubbles to transiently disrupt the BBB (n = 4). The scanning routine involved a diffusion sequence followed by the injection of Gd and the acquisition of a contrast-enhanced T1-weighted image, enabling comparison with the emerging protocol. This routine was implemented once before the onset of the experiments (DTIPRE, Gd-T1wPRE and was repeated after every sonication (DTIPOST, Gd-T1wPOST). The DTIPOST was registered to the DTIPRE by a deformable deformation matrix and corrected for eddy current distortions before the calculation of the tensor with the associated eigenvalues and eigenvectors. The fractional anisotropy map (FA) was constructed based on the eigenvalues and the difference ΔFA=FAPOST-FAPRE is reported herein.

Results: DTI detected an increase in the fractional anisotropy from 0.21 ± 0.02 to 0.38 ± 0.03 (82.6 ± 5.2 % change) within the targeted region 1 h after BBB opening. Enhanced DTI contrast overlapped by 77.22 ± 9.2% with hyper-intense areas of gadolinium-enhanced T1-weighted scans, indicating diffusion enhancement only within the BBB opening volume. Diffusion enhancement was highly anisotropic and unidirectional within the treated brain region, as indicated by the direction of the principal diffusion eigenvectors. Polar and azimuthal angle ranges decreased by 35.6% and 82.4%, respectively, following BBB opening.

Conclusions: DTI may be used as a contrast-free MR imaging modality in place of contrast-enhanced T1 mapping for detecting BBB opening during focused-ultrasound treatment or evaluating BBB integrity in brain-related pathologies.

Acknowledgements: NIH (EB009041 and G038961)

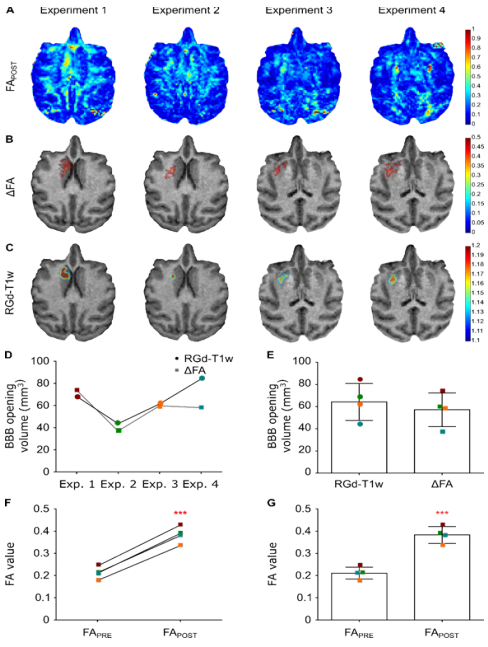

Figure 1: BBB opening detection with FA map, ΔFA and Gadolinium-Enhanced T1-weighted imaging for the four successfully completed experiments targeting a similar structure (Caudate nucleus region) in the NHP.

BBB-7

Topic: Blood-Brain Barrier Opening

Presentation Type: Oral

ScRNA-seq reveals FUS pressure dependent enrichment of transfected cell populations and their differential transcriptional responses after BBB opening

Alexander Mathew, Catherine Gorick, Richard Price

University of Virginia, Charlottesville, VA, USA

Background: Gene delivery to brain parenchyma may be achieved by Focused Ultrasound (FUS) mediated disruption of the blood brain barrier (BBB) via activation of IV infused plasmid-coupled microbubbles (MB). Recently, we demonstrated that the specificity of transfection of endothelial cells of the BBB is inversely proportional to peak-negative pressure (PNP), a phenomenon we term "sonoselective" transfection. While sonoselective transfection occurs at PNPs too low to disrupt the BBB, we next asked how BBB-disruptive PNPs skew distributions of transfected cell populations and their transcriptomes. To address this question, we performed single cell RNA-sequencing (scRNA-seq) on transfected cells from brains treated with low and high PNP FUS BBB disruption followed by bioinformatics analyses.

Materials and Methods: Male C57BL/6 mice were anesthetized and acoustically coupled to an MR-compatible small animal FUS system. Mice received an injection of cationic MBs conjugated to mRuby plasmid (2e5 MBs/g body weight), followed by injection of additional free plasmid to reach a total plasmid dose of 40 ug. Sonications were performed at 0 MPa (control), 0.2 MPa, or 0.4 MPa using a 1.1 MHz single element focused transducer operating in 10 ms bursts, 0.5 Hz pulse repetition frequency for 2 minutes. 48 h after treatment, front right quadrants of each brain were excised, pooled by treatment condition, and dissociated. Live, mRuby+ cells were isolated from 0.2 MPa, and 0.4 MPa cell suspensions by FACS (Figure 1). Control (unsorted), 0.2 MPa (mRuby+), and 0.4 MPa (mRuby+) single cell libraries were generated using the 10X Chromium Controller and V3 chemistry. An average of 1482 cells per condition were sequenced at an average depth of 92,409 reads per cell. The CellRanger pipeline was implemented for raw read processing, filtering and alignment. All further analyses were performed in R using Seurat with default parameters. Cell clusters were computed by graph-based clustering and subsequently identified by comparing the top 20 globally distinguishing markers with those having high cell-type specificity scores in the PanglaoDB webserver. Differential gene expression between each FUS treated cell population and control was computed using the MAST framework.

Results: t-SNE followed by graph based clustering of all sequenced cells led to identification of 6 distinct brain-resident cell populations (Figure 2A). FUS PNP elicited unique distributions of mRuby-transfected cell types, with 0.4 MPa having a distribution most similar to the control condition (Figure 2B). Thus, we hypothesize that cells of the neurovascular unit (NVU) apposed to the circulation (i.e. endothelial cells, pericytes, and astrocytes) are relatively enriched at lower FUS PNP while those farther from the BBB (neurons, oligodendrocytes, and microglia) are enriched at higher FUS PNP (Figure 2C). We observed robust, PNP-dependent differential gene expression for multiple cell types when compared to matching cell types from untreated, untransfected control brain tissue (Figure 3). Interestingly, several genes associated with the stress response were upregulated proportional to PNP but independent of cell type including Ctsd, Ly86, Cd68, and Tyrobp (Figure 4).

Conclusions: Cells of the NVU (neurons, astrocytes, microglia, endothelial cells, pericytes, and oligodendrocytes) are differentially transfected and transcriptomically impacted by low vs high PNP in the context of FUS mediated BBB disruption. We propose a model in which a cell's transfection likelihood increases with PNP and decreases with distance from the circulation. Identification of PNP-dependent, cell-type independent transcriptional regulation points to activation of a common cellular stress signaling response following FUS treatment and/or transfection. Our results generalize sonoselective transfection to non-endothelial cell types, enabling optimal targeting of genes to the NVU.

Acknowledgements: Supported by National Institutes of Health Grants R01EB020147 and R21EB024323 to R.J.P. A.S.M. was supported by an NIH F30 Fellowship. C.M.G. was supported by American Heart Association Fellowship 18PRE34030022.

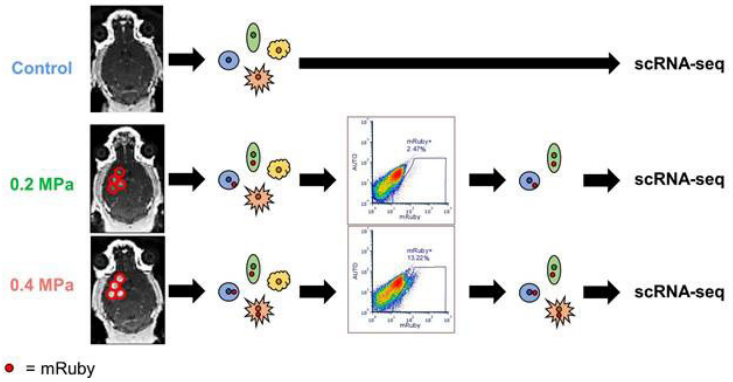

Figure 1. Using cells from the control condition to define the mRuby gating strategy, mRuby+ cells were sorted from FUS-treated brains by FACS. Single cell RNA-sequencing was then performed.

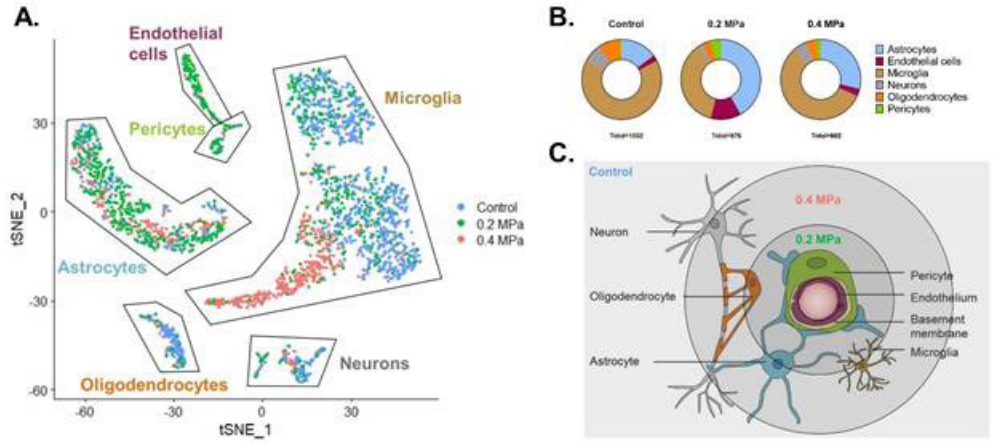

Figure 2. A) t-SNE plot showing all sequenced cells. B) Proportions of each of the 6 identified cell types for each condition. C) Proposed model in which transfection frequency is proportional to FUS PNP.

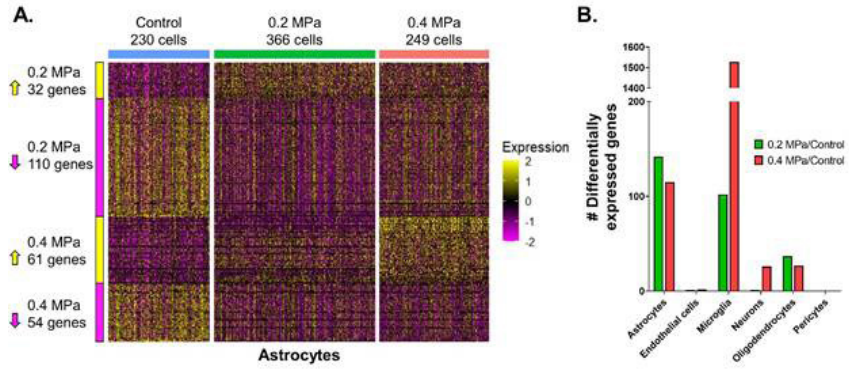

Figure 3. A) Gene expression heatmap for astrocytes from each condition. B) Magnitude of significant (p adjusted < 0.05) differential gene expression (upregulated or downregulated) for each cell type.

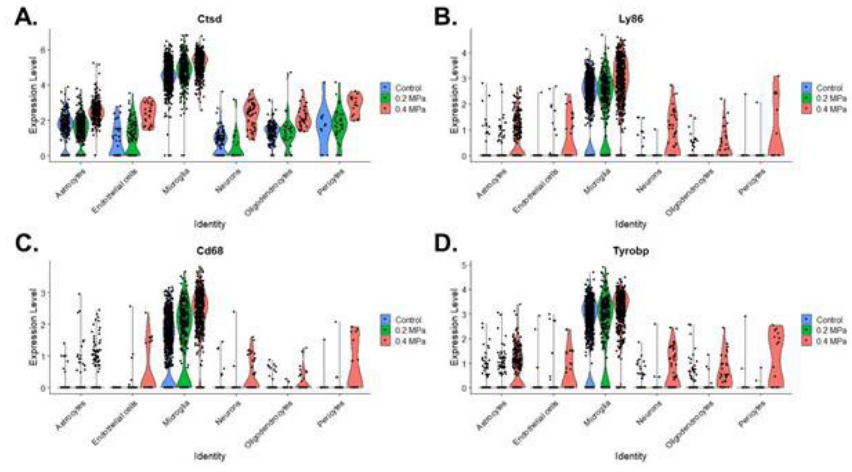

Figure 4. Violin plots of normalized expression levels for selected transcripts. Each dot represents a single cell, grouped by cell type and treatment condition.

BBB-8

Topic: Blood-Brain Barrier Opening

Presentation Type: Oral

Transcriptomic response of brain tissue to focused ultrasound-mediated blood-brain barrier disruption depends strongly on anesthesia

Alexander Mathew, Catherine Gorick, E. Andrew Thim, William Garrison, Grady Wilson Miller, Natasha Sheybani, Richard Price

University of Virginia, Charlottesville, VA, USA

Background: Focused ultrasound (FUS) mediated blood brain barrier disruption (BBBD) with microbubbles (MB) is a promising strategy for the targeted delivery of systemically-administered therapeutics to the central nervous system (CNS). Pre-clinical investigations of FUS+MB BBBD have been performed on different anesthetic backgrounds; however, the potential influence of the choice of anesthetic on the molecular response to BBBD is unknown. We hypothesize that anesthetics may differentially alter the underlying reactivity of the brain parenchyma, yielding anesthesia-dependent synergies and conflicts with respect to sterile inflammation, drug metabolism, or neuronal damage. Herein, we test this hypothesis by detailing the cumulative transcriptome and pathway level impacts of anesthesia, MB, and FUS+MB on the brain parenchyma.

Materials and Methods: C57BL/6 mice were anesthetized with either isoflurane in medical air (Iso) or ketamine/dexmedetomidine (KD). After i.v. MB injection, FUS (1.1 MHz, 0.4 MPa, 10 ms pulse, 2 s pulse interval, 2 min) was targeted to the right or left striatum and applied to open the BBB. Bulk RNA sequencing was performed on mRNA extracted from the FUS+MB treated regions 6h post-treatment. Brains extracted from naïve mice, mice treated with each anesthetic alone, and mice treated with each anesthetic and MB were also sequenced. RNA seq data were used to assess differential gene expression and gene set enrichment. We also performed histological analysis of brains treated with combinations of Iso, KD, and FUS+MB. Brains treated with 0.8 MPa FUS+MB were positive controls for damage. We scored multiple transverse sections from each condition for RBC extravasation and vacuolation.

Results: Post-BBBD MRI contrast was greater with Iso vs. KD, yet no differences in cavitation were detected (Figure 1A). In normal brain, Iso alone elicited minimal differential gene expression (DGE), while KD alone led to massive DGE (Figure 1B). Regardless of the anesthetic, FUS+MB BBBD enriched genes involved in endothelial cell activity (Figure 1C). Iso-FUS+MB induced these pathways more significantly and enhanced genes associated with leukocyte adhesion. Both conditions led to activation of inflammation pathways, with responses substantially enhanced in Iso-FUS+MB. Iso-FUS+MB repressed metabolic programs, while several were enriched by KD-FUS+MB. With respect to BBB tight junction transcripts, FUS+MB upregulated Cldn5 and Emp1 independent of anesthetic (Figure 2). KD led to more DGE in transporter- and transcytosis-associated transcripts than Iso (Figure 2). With the exception of the 0.8 MPa positive control group, no conditions elicited damage (Figure 3).

Conclusions: Our study addressed how choice of general anesthetic shapes acute transcriptomic responses to FUS with respect to sterile inflammation, endothelial activity, metabolism, platelet activity, repair, molecular signaling, and BBB-associated genes. We conclude that the underlying transcriptomic response to FUS-mediated BBBD may be strongly influenced by the choice of anesthetic. Such responses may synergize and/or conflict with responses generated by the therapeutic approach itself. Thus, our results provide a framework for rational anesthesia selection for preclinical BBBD studies and will likely find utility when comparing clinical outcomes to pre-clinical results for FUS mediated BBBD drug and gene delivery approaches.

Acknowledgements: Supported by National Institutes of Health Grants R01EB020147, R01CA197111, R01NS111102, and R21EB024323 to R.J.P. and R01EB023055 to A.L.K. A.S.M. was supported by National Institutes of Health Training Grant T32LM012416. C.M.G. was supported by American.

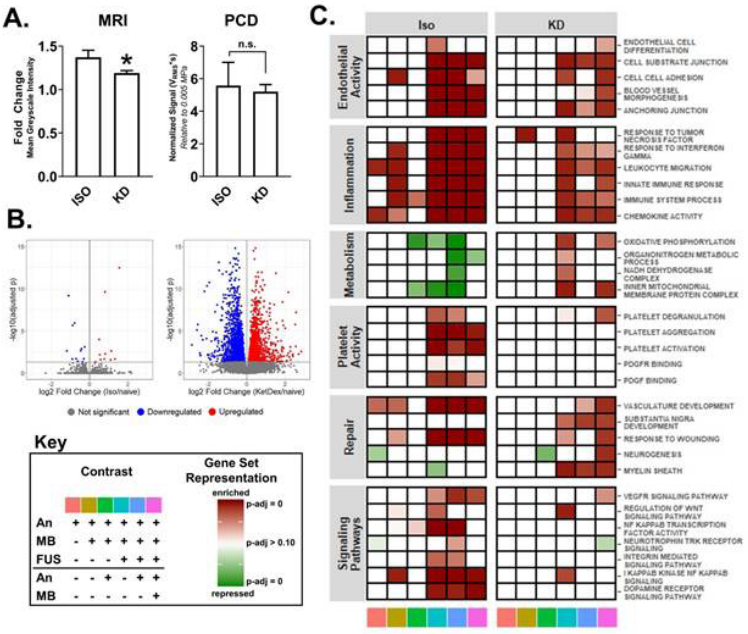

Figure 1. (A) Contrast enhancement and acoustic emissions. (B) Differential gene expression. (C) Gene set pathway enrichment analysis.

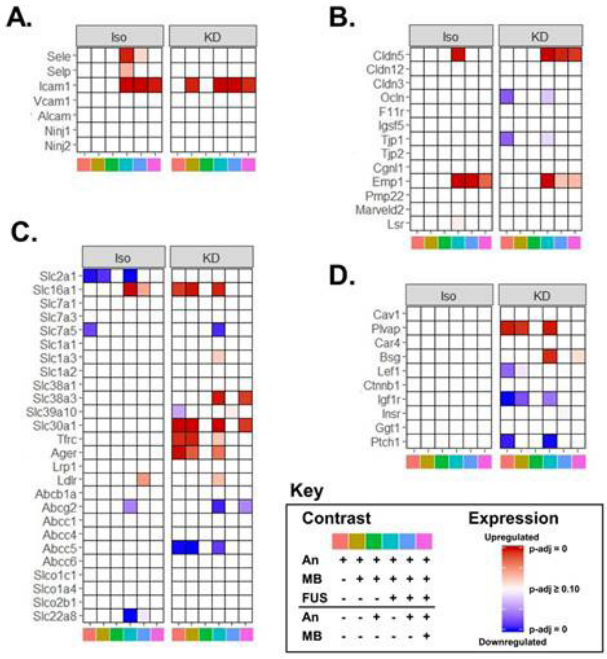

Figure 2. Heatmaps of significance of upregulation (red) or downregulation (blue) for selected genes (rows) across multiple contrasts (columns).

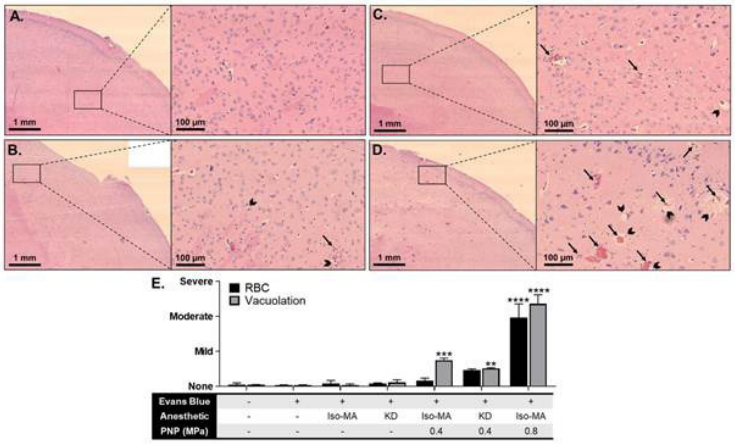

Figure 3. H&E images of (A) untreated, (B) IsoMA-FUS at 0.4 MPa, (C) KD-FUS at 0.4 MPa, or (D) IsoMA-FUS at 0.8 MPa. (E) Scoring of RBC extravasation and vacuolation.

BBB-9

Topic: Blood-Brain Barrier Opening

Presentation Type: Oral

MR-guided focused ultrasound trastuzumab delivery for intracranial metastases in patients with Her2-positive breast cancer

Ying Meng[1], Raymond Reilly[2], Maureen Trudeau[1], Rossanna Pezo[1], Arjun Sahgal[1], James Perry[1], Amit Singnurkar[1], Suganth Suppiah[1], Clement Hamani[1], Maheleth Llinas[1], Yuexi Huang[1], Kullervo Hynynen[1], Nir Lipsman[1]

[1]Sunnybrook Research Institute, Toronto, ON, Canada
[2]University of Toronto, Toronto, ON, Canada

Background: Microbubble-mediated temporary opening of the BBB using low-intensity MR-guided focused ultrasound (MRgFUS) is a non-invasive approach for targeted drug delivery. This approach has shown promise in improving the tissue concentration of large molecular therapies, such as trastuzumab and trastuzumab-based therapies in animal Her2+ brain metastases models. The goal of this study is to establish the safety and feasibility of MRgFUS to enhance the delivery of trastuzumab to brain metastases and tumor margins in patients with Her2-positive breast cancer.

Materials and Methods: This is a phase I single-arm, open-labelled study in patients with metastatic Her2-positive breast cancer and intracranial metastatic disease between 18 and 80 years of age (NCT03714243). Participants will undergo up to six MRgFUS BBB opening procedures with the 220 kHz ExAblate Neuro 4000 type 2.0 (InSightec®, Israel) device. The procedures will overlap with the standard dosing regimen of trastuzumab or trastuzumab-based therapies.

Results: Primary outcomes for this trial will examine safety and feasibility. Safety will be measured by clinical and MRI assessments, and reported as treatment related adverse events according to the Common Terminology Criteria for Adverse Events recommendations. Feasibility and extent of BBB opening of intracranial metastatic lesion(s) will be assessed by contrast enhancement on T1-weighted MRI. Further, the second outcome will consist of efficacy measures such as the change in tumor volume on structural MRI.

Conclusions: Results from this trial will determine the utility of MRgFUS to enhance the delivery of large molecular therapies in patients with brain tumors.

Acknowledgements: This study is supported by the Focused Ultrasound Foundation

BBB-10

Topic: Blood-Brain Barrier Opening

Presentation Type: Oral

Rapid short-pulse sequences deliver drugs across the blood-brain barrier with a low level of microglial activation and a low amount of blood-borne proteins released into the brain

Sophie Morse, Tiffany G. Chan, Nicholas J. Long, James J. Choi

Imperial College London, London, United Kingdom

Background: Focused ultrasound and microbubbles can alter the blood-brain barrier (BBB) permeability in a non-invasive, local and reversible manner, allowing drugs into the brain (Hynynen et al 2001). Recently, we showed that by rapidly emitting short ultrasound pulses – known as Rapid Short-Pulse (RaSP) sequences – the distribution and safety of drug delivery can be improved (Morse et al 2019). With RaSP, the BBB permeability was altered for less than 10 minutes, which contrasts with the several hours of opening produced with traditional, long-pulse (>1ms) sequences. A prolonged duration in BBB opening exposes the brain to bloodborne proteins, such as albumin and immunoglobulin, which leak through the disrupted BBB and produce an inflammatory response involving glial cell activation (Kovacs et al 2016). Here, we characterised the brain microenvironment following RaSP exposure by assessing the amount of albumin and immunoglobulin extravasating into the brain and whether glial cells were activated.

Materials and Methods: A RaSP sequence is composed of short, microsecond pulses emitted at rapid, kilohertz rates grouped into bursts. Using a 1-MHz focused transducer, we applied ultrasound to the left hippocampus of mice using either a RaSP sequence (5 cycles at 1.25 kHz grouped into 10 ms bursts at 0.5 Hz) or ms-long sequence (10,000 cycles at 0.5 Hz) at a de-rated peak-negative pressure of 350 kPa (n = 5). The right hippocampus was used as a control. A model drug, fluorescently-tagged Texas Red 3kDa dextran, was systemically administered before the injection of SonoVue® microbubbles. Brains were extracted either 0, 10 or 20 min after the ultrasound treatment to assess the extent of albumin and immunoglobulin extravasation, or 0, 2, 24 or 48 h after ultrasound exposure to investigate the involvement of microglia and astrocytes. Brains were cut into 30-µm-thick slices with a cryostat and imaged with a fluorescence microscope. To identify the amount of albumin and immunoglobulin in the brain, immunofluorescence staining was performed and the increase in intensity in the targeted region was quantified with respect to the control region. To identify the location and morphology of microglia and astrocytes, immunofluorescence staining was carried out (Iba1 for microglia and GFAP for astrocytes).

Results: In RaSP-treated brains, less albumin and immunoglobulin were detected in all brains compared to long-pulse-treated brains. Immediately after the ultrasound treatment, 3.7-fold less albumin was detected in RaSP-treated brains and undetectable levels were observed 10 and 20 min after the sonication. No immunoglobulin was detected at all time points with RaSP, whereas long pulses resulted in albumin and immunoglobulin being detected in the brain at all time points tested.

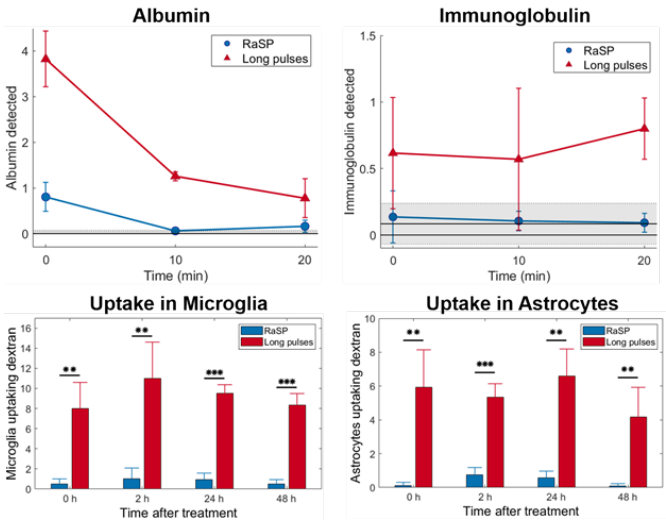

Figure 1. Safety features of RaSP and ms-long pulse sequences. Less albumin and no immunoglobulin extravasate and little or no immune response from glial cells by emitting a RaSP sequence.

Immunofluorescence staining showed little or no uptake of our model drug in microglia and astrocytes in RaSP-treated brains. However, with long pulses, a higher uptake was observed in microglia, which also had a more rounded shape, a sign of activation. Uptake within astrocytes was also higher in long-pulse-treated brains. Future work will involve quantifying the number of activated microglia within the ultrasound targeted region of the brain by using DAB staining.

Conclusions: Emitting ultrasound in a RaSP sequence reduced the number of bloodborne proteins extravasating into the brain and led to less uptake of the model drug by microglia and astrocytes. These results indicate that RaSP sequences can deliver molecules to the brain with a negligible level of disruption to the BBB and the brain tissue microenvironment, improving the performance and safety of ultrasound methods beyond what has been possible.

Acknowledgements: EPSRC Centre for Doctoral Training in Medical Imaging (EP/L015226/1)

BBB-11

Topic: Blood-Brain Barrier Opening

Presentation Type: Oral

Recurrent micro-seizure like activity following focused ultrasound and microbubble induced Blood-Brain Barrier opening

Mehmet S. Ozdas[1,2,3], Aagam[1], S. Shah[1,2,3], Paul M. Johnson[1,2,3] , Javad Nazarian[2], Wolfger von der Behrens[1,2,3], Mehmet Fatih Yanik[1,2,3]

[1] Institute of Neuroinformatics, ETH Zurich, Switzerland
[2] Neuroscience Center Zurich, Switzerland
[3]DIPG Research Center, University Children's Hospital Zurich, Switzerland

Background: Focused ultrasound (FUS) and microbubble (MB) induced Blood-Brain Barrier (BBB) opening is a promising method for targeted delivery of drug molecules which do not cross the BBB otherwise. It has been shown that BBB can be transiently and repeatedly opened in rodents, non-human primates, and in humans in a 'safe' manner. However, other recent studies have shown that FUS+MB induced BBB opening may cause sterile inflammation at similar levels to those observed in traumatic brain injury and ischemia although counter claims suggest inflammations depend on microbubble concentrations. It has been also shown that FUS+MB induced BBB opening can suppress sensory evoked potentials and even induce behavioral changes. Here, we report recurrent micro-seizure like activity following BBB opening using in vivo cellular electrophysiology.

Materials and Methods: Female Long Evans rats (200-300 g, n=4) were anesthetized under isoflurane (1.5-2%). A Neuronexus probe (A2x16-10mm) was inserted in the vibrissae motor cortex (vM1) for electrophysiological recordings. A custom 2.5 MHz FUS transducer (Sonic Concepts) was positioned on the skull such that it targets vibrissae sensory cortex (vS1) with the aid of an ultrasound collimator and sterile gel (Fig. 1). vS1 and vM1 are functionally connected however anatomically distant regions from each other. This electrode configuration was used to avoid confounding effects due to possible mechanical FUS effect on the electrodes and the BBB disruption upon electrode insertion itself. Custom-made MBs or MBs conjugated with liposomes were injected through the tail-vein (0.2mL/min,5e9/mL over 3-7 mins). FUS (0.5-0.7 MPa, stable cavitation regime verified by PCD in separate cohort) was applied 30s following MBs injection. The micro-seizure like activity were observed during sonication and the timing of the first seizure depended on the pressure of the FUS. BBB disruption was verified with Evans Blue. For evoked local field potential (eLFP) analysis, the raw data was low pass filtered at 300 Hz. The eLFPs were aligned to the whisker stimulus averaged over 2 mins and then normalized to the average response amplitude of the baseline. Extracellular spike detection and sorting was done with Klustakwik. Electrophysiological data analysis was done in Python. Data shown is mean ± s.e.m.

Results: Micro-seizures are recurrent and uncontrolled hyperactivity with post-ictal periods, causing transient circuit dysfunction such as suppression of behaviorally relevant evoked responses. Micro-seizures can lead to aberrant circuit wiring, neuronal degeneration and cellular loss in the long term. Our results suggest that FUS induced BBB opening can cause micro-seizure like activity. Applying FUS combined with MBs to vS1 resulted in transient and recurrent micro-seizure like activity in vM1 (Fig. 2A-B). Following cessation of seizure-like activity, we observed a complete silencing of extracellular spikes in vM1 for several mins. After that, the spontaneous spiking rate returned to baseline (Fig. 2A). However, following the first seizure-like activity, which is expected to occur during BBB opening in vS1, a persistent inhibition of eLFPs was observed (Fig. 2C). The micro seizure-like activity oscillated at 73 Hz on average (Fig. 2D) and spread from deep to upper cortical layers of vM1 (Fig. 2E).

Discussion: We provide insight into the consequences of BBB opening by in-vivo cellular-resolution electrophysiology. Our approach allowed observation of recurring micro-seizure like activity post BBB opening as well as propagation of seizure-like activity within cortical lamina. Such seizure-like activity could be occurring as excitotoxic molecules such as excitatory neurotransmitters cross from blood to interstitial cellular space upon BBB opening. Although we do not yet know the cellular and molecular mechanisms triggering this seizure-like activity and silencing of the spontaneous multi-unit activity during post-ictal periods, our findings indicate 'repeated' opening of BBB by FUS may pose safety concerns.

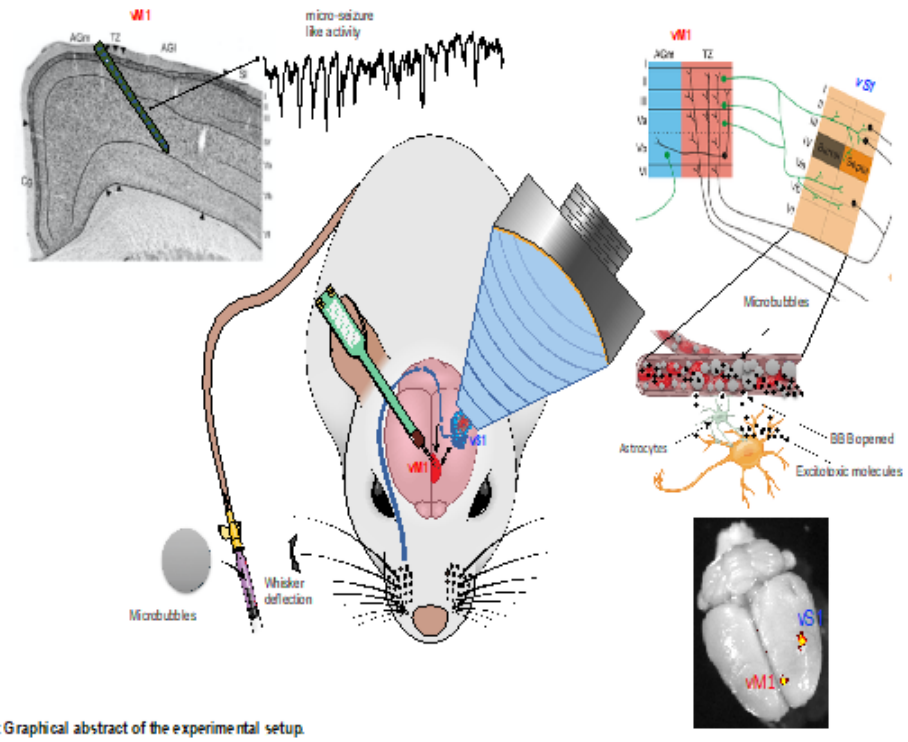

Figure 1: Graphical abstract of the experimental setup.

Whiskers were mechanically deflected at 0.3 Hz. vM1 coronal section (top-left) and vS1-vM1 projections illustration (top-right) are modified with permission of Chakrabarti and Schwarz (http://www.scholarpedia.org/article/Whisking_control_by_motor_cortex). IVIS spectrum imaging of whole brain demonstrates Evans Blue for BBB opening in vS1 due to FUS and in vM1 due to electro insertion (bottom-right).

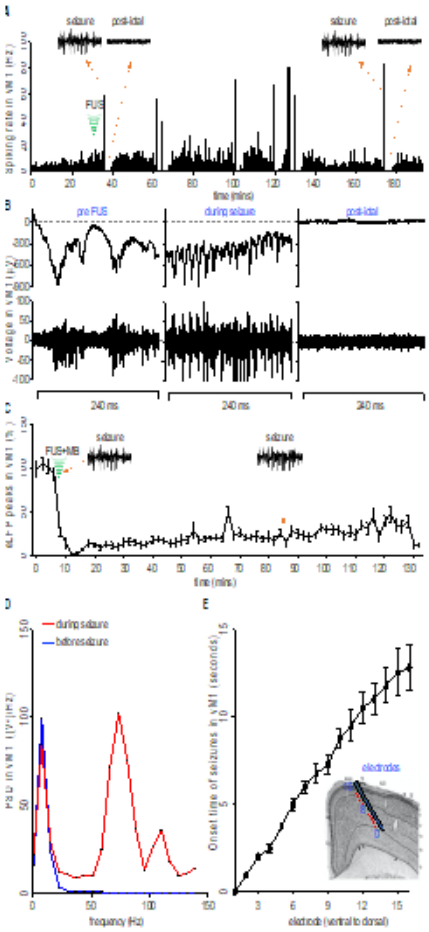

Figure 2: FUS induced cortical micro-seizure like activity.

(A) Example of multi-unit spiking rate in vM1, from one electrode in one animal with 1 second bin size. Each peak represents a high number of spontaneous extra-cellular spikes during seizure-like activity.

(B) Example of raw (top) and high-pass filtered (bottom) recordings before FUS treatment, during seizures (after FUS treatment), and during post-ictal periods. Representative "Pre FUS" is shown 10 mins before microbubble injection and FUS sonication (left). Representative "during seizure" is showing high-frequency activity following FUS sonication of circulating microbubbles in vS1. The "post-ictal" period shows silencing of neuronal activity during the first 1 min following seizure-like activity.

(C) Example of evoked LFP amplitudes in vM1 by somatosensory whisker stimulation before and after FUS+MB induced BBB opening in vS1. Following the first seizure-like activity the evoked LFPs in vM1 are persistently suppressed although seizure-like activity can repeat multiple times after only one time FUS+MBs application. The onset of seizure-like activity depends on bubble concentration and FUS intensity. Lower bubble concentration and/or FUS intensity can delay the onset of seizure-like activity or prevent BBB opening. Suppression of evoked LFPs in vM1 begins with BBB opening and can last more than 2 hrs depending on FUS intensity and microbubble concentration. The insets show examples of seizure-like activity during eLFP recordings.

(D) Power spectral density (PSD) of raw data in vM1 before and during seizures, n=4. The peak mean power is detected at 73.2 Hz, Power=102 ± 36.4 in (V^2/Hz). All data are mean ± s.e.m.

(E) Propagation of seizure-like activity through cortical layers of vM1, n=4 animals. Seizure-like activity first occur in the deep layers of vM1 then propagate to upper layers. All data are mean ± s.e.m.

BBB-12

Topic: Blood-Brain Barrier Opening
Presentation Type: Oral

A neuronavigation-guided clinical ultrasound system for blood-brain barrier opening at the bedside with real-time cavitation monitoring – pre-clinical evaluation in non-human primates with behavioral amelioration and immunogenicity

Antonios Pouliopoulos, Nancy Kwon, Greg Jensen, Anna Meaney, Yusuke Niimi, Mark Burgess, Robin Ji, Shih-Ying Wu, Maria Eleni Karakatsani, Alicia McLuckie, Fabian Munoz, Hermes Kamimura, Andrew Teich, Vincent Ferrera, Elisa Konofagou

Columbia University, New York, NY, USA

Background: Blood-brain barrier (BBB) opening using focused ultrasound (FUS) is currently being tested in multiple clinical trials. Most trials are conducted with either an implanted transducer following craniotomy or a multi-element array for MRgFUS. We recently developed a clinical system to treat Alzheimer's disease (AD) patients based on a neuronavigation-guided FUS transducer that can achieve non-invasive BBB opening while eliminating the need of on-line MRI. Previous studies in rodents treated with FUS have shown an acute inflammatory response in the murine brain, which is resolved within 7 days after treatment. Here, we investigated the immune response in non-human primates (NHPs) treated with our clinical FUS system. Behavioral testing through a visuomotor task was also performed to assess cognitive function following BBB opening. Our aim was to investigate the effects of clinically-relevant FUS exposure in an animal model which closely resembles the human brain.

Materials and Methods: A 0.25-MHz, single-element FUS (Sonic Concepts, Bothell, WA) transducer was developed for neuronavigation-guided clinical BBB opening. The transducer's design was based on k-wave simulations, which provided the optimal combination of aperture size and radius of curvature. Human skull-induced beam aberrations and skull heating were estimated during therapeutic sonication (MI: 0.4-0.8), using a hydrophone and a thermocouple, respectively. Four NHPs were treated in the prefrontal cortex (PFC) and motor cortex using the single-element FUS transducer (fc: 0.25 MHz, Ppk-neg: 200 - 400kPa, MI: 0.4 - 0.8, PL: 10 ms, PRF: 2 Hz, duration: 2 min) and the FDA-approved dose of Definity microbubbles (10 μl/kg). Two NHPs were treated bilaterally (MI: 0.4 and 0.8 - left and right hemispheres), and were sacrificed at the acute (48-h post-FUS) and chronic (18-days post-FUS) timepoints. Real-time cavitation monitoring was performed using a 1.5MHz passive cavitation detector. The NHP brains were stained for Iba1 and CD68 to evaluate microglia spatial distribution. Two NHPs performed a transitive inference test daily for up to 4 weeks before FUS treatment and were then treated unilaterally (MI: 0.4 and 0.8 - left hemisphere). A new set of images were presented on each day, to ensure that performance was only due to inference capacity. Behavioral testing using touch panels in the NHP home cage was conducted daily for 3 weeks post-FUS to evaluate changes in touch accuracy and reaction times.

Results: Numerical simulations showed that our system can target the human midbrain (fig. 1a). Transcranial transmission caused a lateral and axial shift of 0.5 ± 0.4 mm and 2.1 ± 1.1 mm, while the focal size decreased by 3.3 ± 1.4% and 3.9 ± 1.8% along the lateral and axial dimension, respectively (fig. 1b-d). The maximum temperature increase was 0.16 ± 0.03°C at MI of 0.8 (fig. 1e). Clinically-relevant FUS treatments led to BBB opening volumes (fig. 2a) of 680 ± 236 mm3 at MI of 0.4, and 1413 ± 299 mm3 at MI of 0.8 (n = 3). The density of Iba1+/CD68+ cells within regions exposed to FUS was higher than in non-treated areas at the acute timepoint and MI of 0.8 (fig. 2b). By day 18 post-FUS, cell numbers returned to baseline. The increased cell number at MI of 0.8 was due to microglia migration towards blood vessels (fig. 2c). Accuracy increased for both NHPs (figs. 2d-e), but significantly only at MI of 0.8. The reaction time increased at MI of 0.4, but significantly decreased at MI of 0.8.

Conclusions: We developed a clinical setup for BBB opening based on a single-element transducer with neuronavigation guidance and real-time cavitation monitoring. Transcranial ultrasound propagation caused a moderate focal shift and distortion, while the skull heating was negligible. Our pre-clinical findings in NHPs demonstrated that FUS-induced immune response can be triggered at high MI but is reversible, while BBB opening may be associated with improvement in NHP cognitive performance, both in terms of touch accuracy and reaction time. The clinical setup described here has been granted an investigational device

exemption (IDE G180140) by the FDA, to achieve non-invasive and targeted BBB opening at the bedside in 6 AD patients.

Acknowledgements: NIH 5R01EB009041 and 5R01AG038961. Focused Ultrasound Foundation.

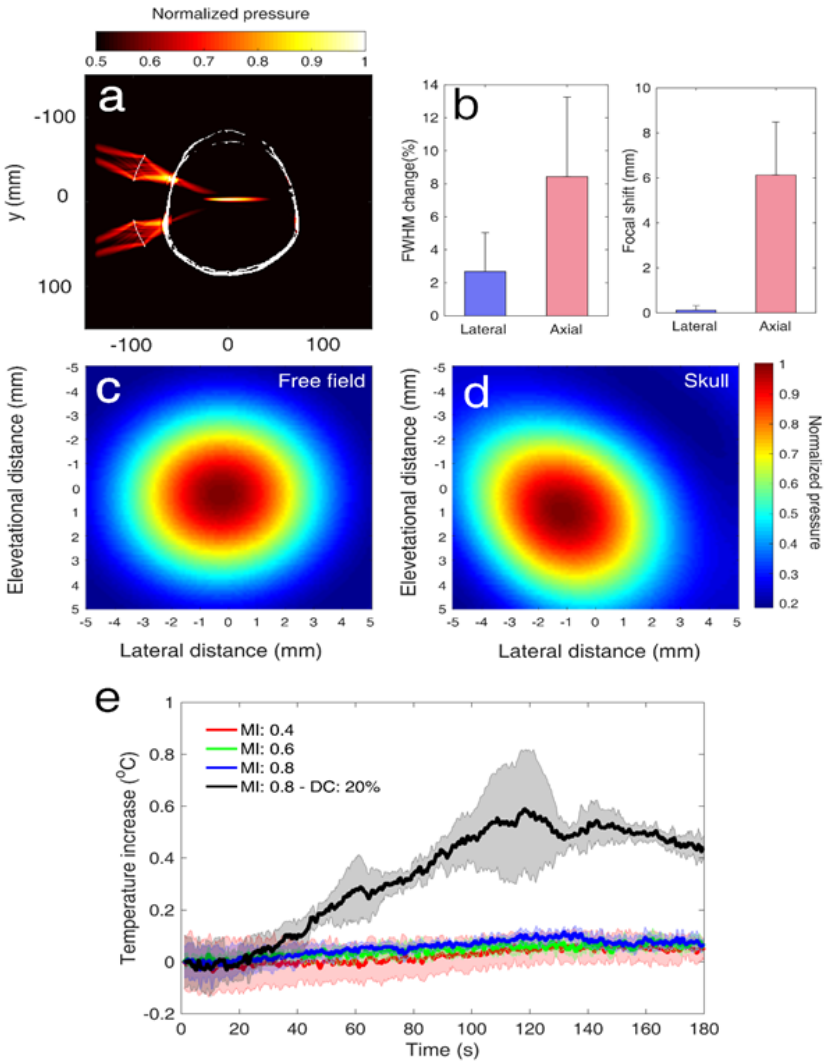

Figure 1. a) Numerical simulations. b) Focal volume change and shift. c)-d) Beam transverse profile in free field and through a human skull. e) Skull heating at clinically relevant MI (0.4 - 0.8).

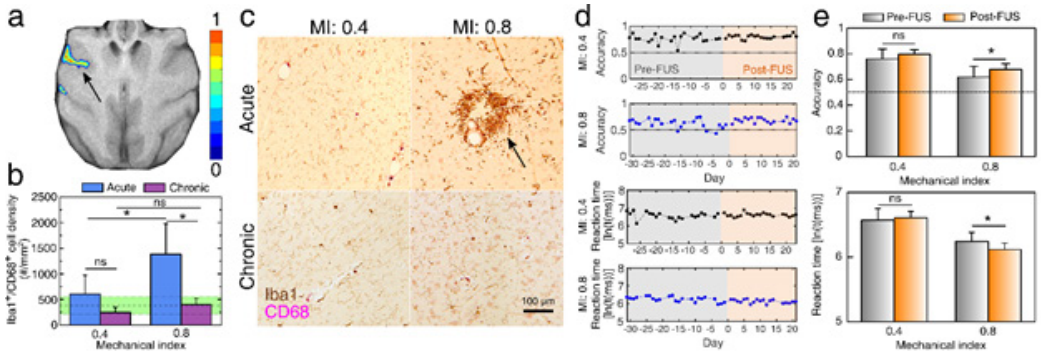

Figure 2. a) BBB opening in a NHP (MI: 0.8). b) Inflammatory cell density after FUS. c) Iba1/CD68 stain, showing migration of microglia. d-e) Accuracy and reaction time before and after FUS.

BBB-13

Topic: Blood-Brain Barrier Opening

Presentation Type: Oral

Quantitative analysis of in-vivo microbubble distribution in the human brain: Impact on imaging and treatment

Francesco Prada[1], Antonio Gennari[1], Linvillle Ian[2], Michael Muterbaugh[2], Zhihang Chen[2], Natasha Sheybani[2], Francesco DiMeco[1], Frederic Padilla[3], John Hossack[2]

[1]Fondazione IRCCS Istituto Neurologico "C. Besta", Milan, Italy
[2]University of Virginia, Charlottesville, VA, USA
[3]Focused Ultrasound Foundation, Charlottesville, VA, USA

Background: Microbubbles (MB) serve as a powerful component in the contexts of both ultrasound imaging and therapy. They are widely used as contrast agents to enable contrast-enhanced ultrasound (CEUS) imaging and as acoustic "amplifiers"of mechanical bioeffects incited by therapeutic-level ultrasound. The distribution of MBs in the brain is not yet fully understood, thereby limiting the guidance available for CEUS surgery or MB-based FUS treatments. In this paper, we describe a robust platform for intraoperative quantification of MB distribution in different regions of the human brain. We demonstrate that it is feasible to quantitatively discriminate between tumoral and normal brain tissues and introduce new information relating to real-time brain vascularization.

Materials and Methods: Among patients with primary brain neoplasms who underwent intraoperative CEUS imaging during standard surgical tumor resection at Fondazione IRCCS C. Besta in Milan, Italy, between June 2013 and July 2018, 21 had image sets of adequate length. Following curation of acquisitions for image quality and presence of motion artifacts, 19/21 ultrasound image sets were retrospectively analyzed using a newly developed custom image processing software for quantitative analysis of echo power. Regions of interest (ROIs) were drawn on key structures by a blinded neurosurgeon, following which peak enhancement and time intensity curves (TICs) were quantified.

Results: CEUS images revealed clear qualitative differences in MB distribution: in all cases arteries showed the highest enhancement among all structures, followed by tumor and white matter regions, respectively. The custom software built for quantitative analysis effectively captured these differences. Quantified peak intensities (i.e. maximum intensity value for each ROI) corroborated qualitative observations on CEUS, with regions containing artery, tumor or white matter structures having an average MB intensity of 0.584, 0.436 and 0.175 units, respectively. Interestingly, peak intensity values were found to be lower for brain than for tumor and artery and lower for tumor than for artery. Moreover, the normalized area under TICs revealed the time of flight for MB to be significantly lower in brain tissue as compared with tumor tissue. Significant heterogeneities in TICs were also observed within different regions of the same brain lesion.

Conclusions: In this study, we provide one of the earliest and the most comprehensive strategies for accurate quantitative analysis of human brain CEUS intraoperative images. Taken together, our results demonstrate that such quantification from CEUS imaging enables discernment between different types of brain tumors as well as comparison among different regions of (e.g. white vs. grey matter) and structures within the brain. Similar considerations will be important for the planning and implementation of MB-based imaging or treatments in the future.

Acknowledgements: Focused Ultrasound Foundation

BBB-14

Topic: Blood-Brain Barrier Opening

Presentation Type: Oral

A viral vector engineered for improved focused ultrasound BBB opening gene delivery

Jerzy Szablowski[1], Hongyi Li[2], John Heath[2], Mikhail Shapiro[2]

[1]Rice University, Houston, TX, USA
[2]California Institute of Technology, Pasadena, CA, USA

Background: Gene delivery is a promising therapeutic approach. Recently, multiple gene therapies were approved for clinical use, including for blindness, hemophilia, and muscular atrophy, with many more in clinical trials. A large fraction of these trials use adeno-associated virus (AAV), but few target the brain due to the difficulty of gene delivery across the blood-brain barrier (BBB). Focused ultrasound (FUS) can be used to open the BBB (FUS-BBBO) to enable the delivery of AAVs into the brain from the blood. Recent studies optimized the ultrasound parameters, and choice of serotypes for more efficient delivery. However, the delivery of large molecules, e.g. AAVs, remains challenging. AAV delivery requires FUS pressures close to the safety margins of the FUS-BBBO; intravenous injection of AAVs exposes peripheral organs to the virus, leading to off-target peripheral tissue transduction. Here, we engineer a new AAV with improved brain transduction efficiency and tissue specificity after FUS-BBBO.

Materials and Methods: To obtain a new AAV strain optimized for FUS-BBBO we modified a viral vector engineering method called Cre-recombination-based AAV targeted evolution (CREATE). In CREATE, a library of AAVs with mutated capsid proteins (Fig. 1a) is injected intravenously into mice. When a particular AAV clone transduces a cell expressing Cre, its viral genome is modified and becomes detectable by a Cre-dependent PCR (Fig. 1b). We modified CREATE to engineer a FUS-BBBO-optimized AAV, which we called AAV.FUS. We first generated a library of viral vectors with a capsid modified by insertion of randomized 7 amino-acid sequence between residues 588 and 589 of the AAV9 capsid (Fig. 1a). We chose AAV9 due to our preliminary studies and published work showing its efficient gene delivery in mice. We then used FUS-BBBO to deliver the AAV library (Fig. 1c) to one hemisphere of hSyn1-Cre mice that express Cre in neurons. We used our previously published ultrasound parameters but using a lower pressure (0.33 MPa). After 2 weeks, the DNA from targeted and control hemispheres (Fig. 1c) was extracted and sequenced using next-generation sequencing (NGS). The clones with sequences detected uniquely in the targeted hemisphere were then subjected to the second round of screening to quantify the performance of each clone in greater detail. Following this round, we identified 5 clones most enriched in the FUS-targeted hemisphere and evaluated their transduction efficiency and tissue tropism compared to AAV9.

Results: FUS-BBBO was used to deliver an AAV library to one hemisphere (Fig. 2, a-b). Subsequent DNA extraction and NGS resulted in the recovery of ~15,500 unique AAV clones. The top 2,098 clones were used for second round of screening, which allowed us to rank-order each clone by the transduction efficiency in the targeted hemisphere. The efficiency of transduction was evaluated using NGS, where a higher number of reads was ascribed to more effective transduction. Based on the NGS data we obtained 5 new AAV.FUS candidates (Fig. 2c). Histological analysis revealed higher numbers of transduced cells in the brain for all candidates (Fig. 3a, b; range: 20-130% improvement over AAV9). At the same time, each serotype transduced the liver less effectively (Fig. 3c, d; range: 13 – 643% reduction compared to AAV9). Liver is strongly transduced by many AAVs, e.g. AAV9. The top AAV.FUS candidate (AAV.FUS.3) showed 12.1-fold improvement in overall brain-tissue specificity after FUS-BBBO (Fig. 4).

Conclusions: FUS-BBBO gene delivery can be improved by engineering new AAV viral vector strain - AAV.FUS. To engineer AAV.FUS we introduced mutations into AAV9 capsid proteins which improved its transduction efficiency and tissue specificity. We have delivered AAV.FUS using safe ultrasound pressures (0.33 MPa at 1.5 MHz) and observed significantly improved transduction in the brain and significantly reduced transduction of a peripheral tissue (liver). This study opens possibilities for further improvement of gene delivery with FUS-BBBO where AAVs are optimized for e.g. FUS-BBBO in different species, or for different ultrasound pressures. It is also the first example of a viral vector engineered for targeting molecular features of FUS-opened BBB.

Acknowledgements: JOS and HL contributed to this work equally. Corresponding

authors: MGS and JOS. Authors would like to thank the following funding agencies: NIH (1UG3MH120102-01) grant to MGS and BBRF NARSAD Young investigator #27737 award to JOS.

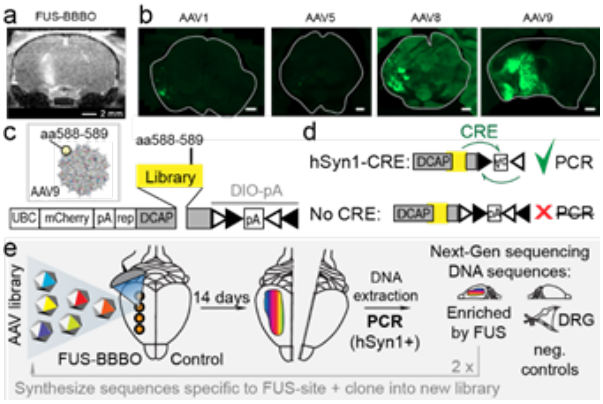

Figure 1. Design of the screening methodology for generation of improved AAV for FUS-BBBO delivery.

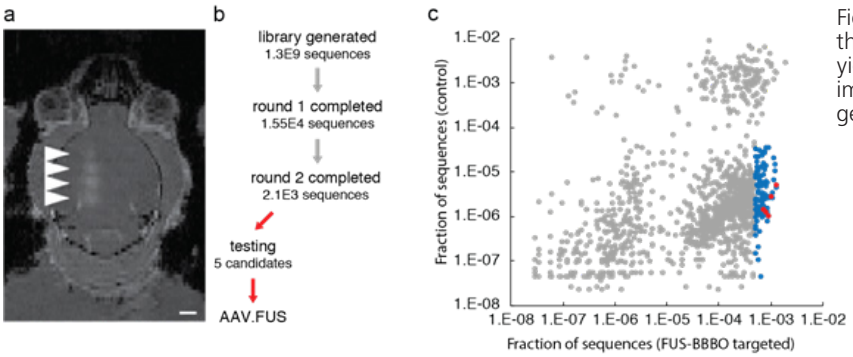

Figure 2. High throughput screening yields vectors with improved FUS-BBBO gene delivery.

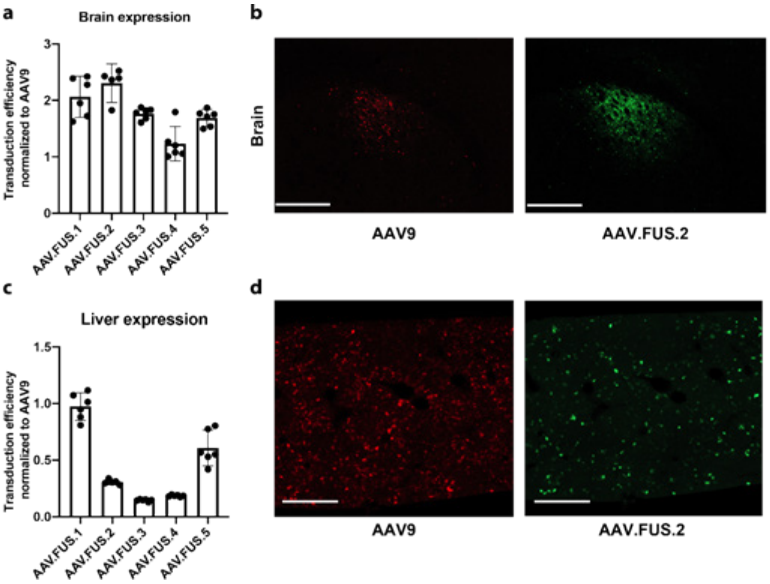

Figure 3. AAV.FUS improves gene delivery with FUS-BBBO by improving brain transduction efficiency and reducing off-target peripheral tissue expression, such as liver that is commonly targeted by AAVs.

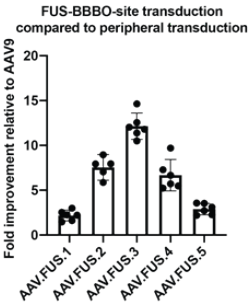

Figure 4. AAV.FUS candidates improve the tissue selectivity of FUS-BBBO gene delivery to the brain by up to 12.1-fold.

BRT-1

Topic: Brain Technical
Presentation Type: Oral

Computationally efficient transcranial ultrasonic focusing: Taking advantage of the high correlation length of the human skull

Thomas Bancel, Guillaume Maimbourg, Julien Guilbert, Alexandre Houdouin, Guillaume Raybaud, Mickael Tanter, Jean-François Aubry

Physics for Medicine Paris, Paris, France

Background: The phase correction necessary for transcranial ultrasound therapy requires numerical simulation to non-invasively assess the phase shifts induced by the skull. In order to be suitable for clinical use, simulations should take less than a few seconds to be acceptable from the practitioner standpoint.

Propagating a full-wave through the patient's skull from the target up to the elements of the transducer enable to take into account the 3D internal structure of the skull, based on a previously acquired CT. However, computation times can take up to a few hours.

We propose here to perform numerical simulations at half the treatment frequency to reduce the computation time, by taking advantage of the wide coherence length of the skull. We assess the efficiency of this approach by experimentally measuring the pressure field restored through 5 human skulls.

Materials and Methods: Refocusing was experimentally achieved at 900kHz through 5 human skulls with a 512-element array. Cross-correlation maps of the phase shifts induced by the skull were first computed to determine the average correlation length of the skull at 900kHz.

Phase shifts for aberration correction were computed by numerically propagating both a 450kHz and a 950kHz tone burst from the target through the skulls. We used the k-wave toolbox to perform such simulations, and previously acquired CTs to model the acoustic properties of the skulls. However, to reduce computation time, the numerical propagation was limited to a volume located between a spherical surface centered on the target as close as possible from the inner surface of the skull, up to an envelope surrounding the skull and positioned 5 pixels away from its outer surface. Propagation was then analytically propagated in water from this envelope up to the transducer elements using the Rayleigh 2nd integral formulae. Simulations were performed on 32 GB RAM, 2x intel Xeon® CPU E5-2630 v3 at 2.40 GHz equipped with a GPU unit GeForce GTX-Titan-X (NVIDIA).

Transfer matrices for each skull were also acquired experimentally to assess the performance of our simulation. A time reversal experiment with an implanted hydrophone was used as gold standard and pressure fields restored by simulated corrections were compared to pressure fields restored with the measured gold standard correction.

Results: The average correlation length of the 5 skulls was found to be 12.63mm and 8.77mm in the anterior-posterior and left-right axis respectively.

We demonstrate that a 450kHz simulation restores 94.6% of the pressure as compared to a simulation performed at 900kHz. Compared to gold standard correction, this corresponds to 85.0% of pressure restoration whereas 900kHz simulation restores 90.2%.

The spatial resolution of the simulation grid could be decreased to 0.94 mm corresponding to $\lambda/3.5$(where λ is the ultrasound wavelength at 450kHz in water) and respecting the stability criteria of the k-wave pseudo-spectral finite-difference resolution scheme. This decreased grid resolution (as compared to the one at 900kHz) resulted in a simulation grid eight times smaller and a computation time divided by ten, dropping from 31s at 900kHz to 3s at 450kHz.

Conclusions: With this approach, we could speed up the computation of the phase delay induced by the skull. We were able restore a pressure amplitude of 85.0% of the gold standard hydrophone-based correction with a 3s simulation time. The resolution (0.94mm) of the simulation grid at 450kHz remains smaller than the smallest correlation length of the skulls (4.71mm) and close to the resolution of the CT (0.5 mm). This technique could be used in future algorithms modelling shear wave inside the skull bone. It could contribute to reduce the computation time by an order of magnitude.

Acknowledgements: This work was supported by the Bettencourt Schueller Foundation and the "Agence Nationale de la Recherche" under the program "Future Investments" with

the reference ANR-10-EQPX-15. The work performed in this publication was performed with the support of the Inserm Technology Research Accelerator (Inserm ART) in Biomedical Ultrasound, Paris, France.

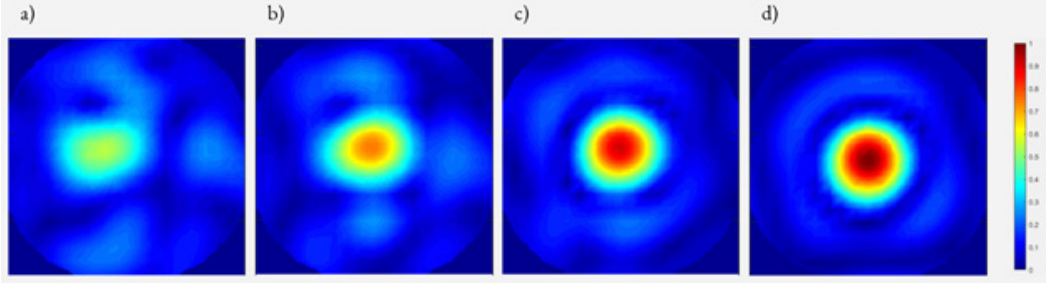

Figure 1. Pressure field measured in the focal plane a) without correction b) with correction from simulation run at 450kHz c) with correction from simulation run at 900kHz d) with gold standard correction.

Simulation frequency (kHz)	900	450
Spatial grid resolution (mm)	0.47	0.94
Grid size (pixel)	384 x 320 x 128	192 x 160 x 64
Average pressure restored compared to gold standard (%)	90.2 (+/- 3)	85.3 (+/- 4)
Average volume at -3dB (mm3)	3.2 (+/- 0.6)	3.5 (+/- 0.7)
Computation time (s)	31	3

Figure 2. Computation time and performance of 450 kHz and 900 kHz simulations.

BRT-2

Topic: Brain Technical
Presentation Type: Oral

Comparing ray-tracing algorithm and finite differences modelling on a clinical device for HIFU brain therapy using the transfer matrix formalism

Thomas Bancel[1], Alexandre Houdouin[1], Philippe Annic[1], Itay Rachmilevitch[2], Yeruham Shapira[2], Mickael Tanter[1], Jean-François Aubry[1]

[1]Physics for Medecine Paris, Paris,France
[2]Insightec, Tirat Carmel, Israel

Background: On the only HIFU clinical device used for brain surgery, adaptive delay corrections needed to compensate skull aberrations are computed using a manufacturer proprietary ray-tracing algorithm. Corrections are then applied on each transducer element during the clinical procedure.

In this work, we quantitatively assessed the clinical ray-tracing performance and compare it to an in-house 3D finite difference algorithm on N=5 human skulls. The use of the transfer matrix formalism was beneficial to compare both techniques in an identical setup, and to identify insights on how to improve performance.

Materials and Methods: All experiments were run on an Exablate Neuro 4000 clinical system manufactured by Insightec Ltd. The transducer is made of 1024 elements distributed on a 30-cm diameter hemisphere operating at 650kHz.

After being degased for 12 hours, skulls were positioned inside the probe using a home-made 3D-printed positioning apparatus. Transfer matrices were acquired for each skull (N=5) and each target (T=2 targets per skull) using a needle hydrophone scanning a 6mm x 6mm x 9.6mm ellipsoidal volume around the target. Gold standard corrections were also acquired for each skull and target by positioning the hydrophone at focus and measuring phase delays for each element sonicating one after another.

Ray-tracing corrections were provided by the manufacturer based on previously acquired CTs of the skulls and on the position of the skulls with respect to the probe for each target. Restored pressures were measured by scanning the same volume around the target with an hydrophone; and also computed using the transfer matrix. The two pressure fields could then be compared.

Our in-house 3D finite-differences algorithm modelled the skull density and sound speed based on a linear interpolation of the Hounsfield Unit from the CT. Bone speed of sound and density were used as inputs in the k-Wave toolbox on Matlab, in order to propagate a 650kHz toneburst from the target to the transducer.

The phase shift computed for each transducer element was then inverted and used as a correction.

Results: Pressure fields and resulting intensities computed with the transfer matrix and measured with an hydrophone were compared on four different corrections' sets: ray-tracing correction, in-house 3D finite-differences correction, gold standard correction and no correction. We showed that the average difference between measured and calculated pressures is 0.67 +/- 4.4 % on a total of more than 13.000 volumic points.

Our in-house algorithm restored 85.6 +/- 4.6 % and 84.1 +/- 4.8 % of the gold standard correction for the first and second targets respectively; whereas the manufacturer ray-tracing algorithm restored 83.9 +/- 4.9 % and 83.1 +/- 6.2 %.

Using the transfer matrices and isolating elements based on their incident angles, we showed that, for both algorithms, performance degrades as incident angles increase. For the 3D-finite differences algorithm, performance drops from 89.5 +/- 3.3 % for incident angles below 5° to 65.2 +/- 20.7 % for incident angles higher than 25°.

Conclusions: In this study, we quantitatively assessed the performance of the clinical correction based on their proprietary ray-tracing algorithm. We could compare it to our own 3D finite difference correction and show that we obtain slightly higher performance. We also demonstrated that the transfer matrix is a robust methodology for computing pressure fields resulting from any correction.

Finally, performance degradation for higher incident angles suggests that shear-wave propagation inside the skull might play a significant role in the induced phase shift at angles reaching 25°. This leaves room for improvement modelling transverse propagation inside the skull.

Acknowledgements: This work was achieved in collaboration and with the financial support of Insightec ltd, to which we are grateful. We are also thankful to the Centre de Neuro-Imagerie (CENIR) of ICM (Institut du Cerveau et de la Moëlle Épinière) Paris, where the experiments were conducted. This work was supported by the Bettencourt Schueller Foundation and the "Agence Nationale de la Recherche" under the program "Future Investments" with the reference ANR-10-EQPX-15. The work performed in this publication was performed with the support of the Inserm Technology Research Accelerator (Inserm ART) in Biomedical Ultrasound, Paris, France.

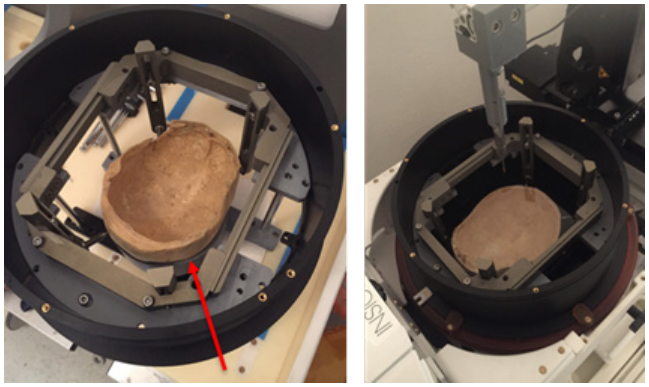

Figure 1. Left picture: 3D-printed positioning system (red arrow). Right picture: skull positioned inside the transducer for transfer matrix acquisition and pressure fields measurement.

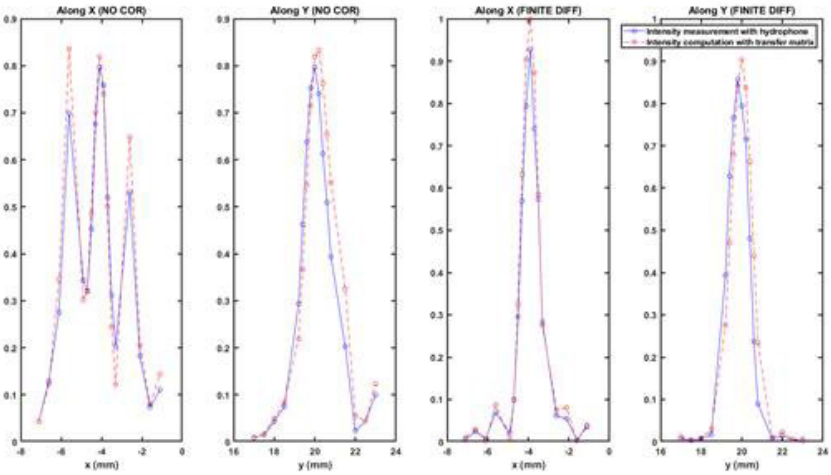

Figure 2. Intensity comparison for skull #2 between measurement with an hydrophone (plain blue line) and computation using transfer matrix (red dashed line) for 2 different corrections.

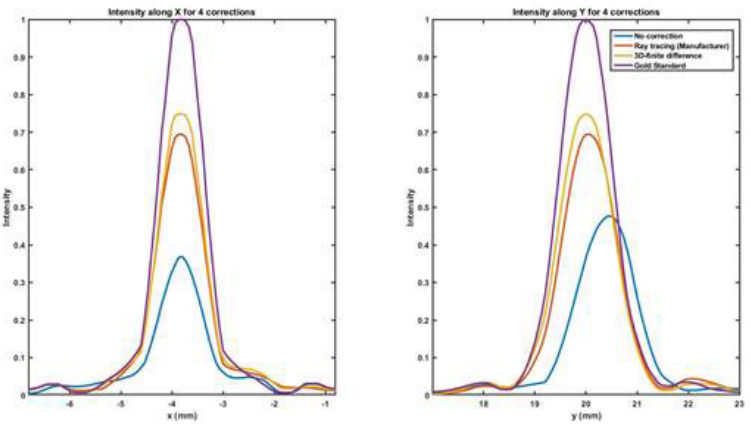

Figure 3. Comparison of the restored intensity for different corrections: no correction (blue), ray tracing algorithm (orange), 3D finite-difference algorithm (yellow) and gold standard (purple).

BRT-3

Topic: Brain Technical
Presentation Type: Oral

Aberration correction for the transskull focusing of high-intensity ultrasound at various depths in brain

Daria Chupova, Vera Khokhlova, Oleg Sapozhnikov, Leonid Gavrilov, Pavel Rosnitskiy

Lomonosov Moscow State University, Moscow, Russian Federation

Background: Multi-element focused phased arrays have been successfully used in clinics for thermal lesioning in deep brain structures. Despite undoubted advantages of the existing hemispherical transducers, several limitations in their surgical application have been revealed. For example, overheating of non-targeted tissues and skull bones may occur due to thermal spread. Furthermore, hemispherical array geometry restricts mechanical displacement of the transducer, thus the treatment envelope of the existing systems is limited to the central part of the head. This study is aimed at evaluating the potential of a new design of less focused fully populated array (Fig. 1) for mechanical tissue ablation using boiling histotripsy (BH) method. The proposed approach could potentially enlarge the treatment region and expand the range of bioeffects. The possibility of tight transskull focusing at different depths with aberration correction was examined using linear and nonlinear field modeling.

Materials and Methods: Three models of 1 MHz 256-, 512-, and 1024-element arrays (Fig. 1a) with 200 mm aperture and 60° focusing angle were developed. A novel algorithm based on the capacity-constrained tessellation was used to develop a fully populated random pattern of equal area elements (Fig. 1b). A realistic 3D acoustical model of the head was built using MRI open database and included in simulations (Fig. 1c). A combination of different approaches was used in the acoustic field modeling and aberration correction. For linear simulations, the Rayleigh integral was used for propagation in water outside the head and pseudo-spectral time domain simulation (k-Wave software) based on the Kelvin–Voigt rheological model for propagation through the skin, skull, and brain (Fig. 2a). Aberration correction was based on the phase-conjugation method. A spherically divergent wave propagating from the focal point to the "Boundary 1" was simulated. Then the phase delays were defined at the array elements by calculating backpropagation using the Rayleigh integral (Fig. 2b). Nonlinear simulations were similar to the linear ones, but the Westervelt equation was used inside the homogeneous brain tissue and outside the head to account for strong nonlinear effects and a linear Kelvin–Voigt model was applied inside the skull and adjacent tissues (Fig. 2c). It was assumed that only the 1-MHz fundamental harmonic passes through the skull because bones induce strong frequency-growing ultrasound transmission losses.

Results: Linear simulations with aberration correction were performed at 5 focal depths, 25–65 mm from the inner skull surface (Fig. 2a). Pressure distributions for the deepest (a), central (b) and outer (c) positions of the focus are presented in Fig. 3 for the 256-element array showing that aberration correction provides the tight focal lobe for all cases. For deeper focusing (Fig. 3a,b), the acoustic intensity near skull bones is relatively low (7–15%) compared to the focal intensity. For shallow focusing (Fig. 3c), the increased intensity near skull (40%) could be compensated in pulsed BH exposures by using low pulse repetition rates. To demonstrate the feasibility of nonlinear focusing through the skull, the central position of the focus (red circle in Fig. 2a) was simulated for the intensity at the array elements of 30 W/cm2 and 40 W/cm2 (typical technical limitations). The resulting focal waveforms contain developed shocks of >60 MPa (Fig. 4) and thus can be used to realize a BH method.

Conclusions: This study demonstrates that the proposed new type of fully populated multi-element phased arrays can provide tight focusing through an intact skull at least over a 40 mm range of depths. Future work is planned to develop BH pulsing schemes for transskull sonication, evaluate electronic steering capabilities of the arrays with aberration correction, and determine safe levels of nonlinear pressure fields near skull bones.

Acknowledgements: This study was funded by RSF 19-12-00148, RFBR 19-02-00035, the Ph.D. student stipend from "Basis" Foundation, the stipend of the President of Russia SP-2644.2018.4, and FUSF summer 2020 Internship Program.

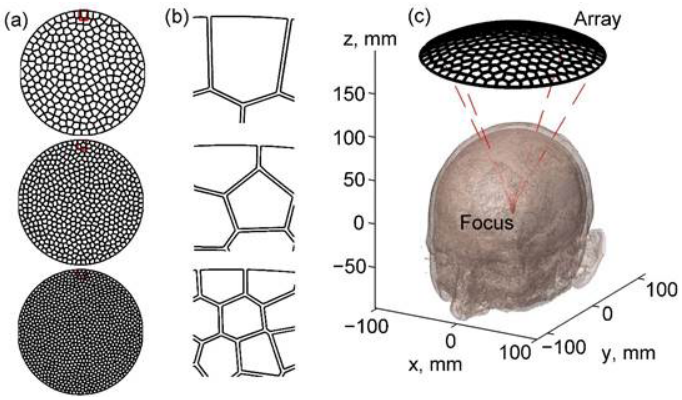

Figure 1. Front view sketches of 256-, 512-, and 1024-element 1 MHz fully populated arrays (a) and array elements (b). A 3D sketch of the simulation geometry (c).

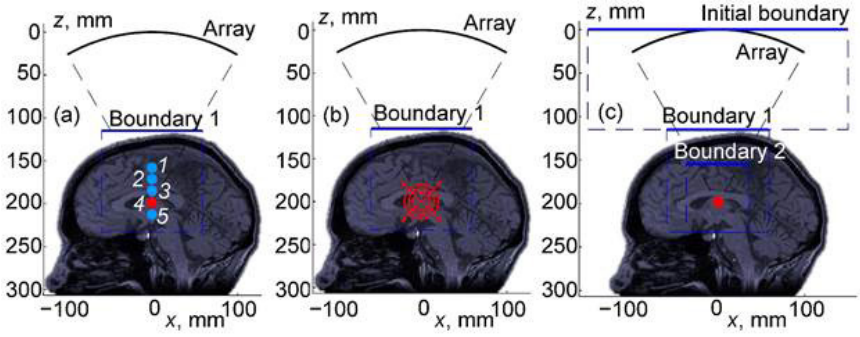

Figure 2. Setting boundary conditions for (a) simulating a linear beam, (b) aberration correction, and (c) simulating a nonlinear beam. Points 1–5 in the figure (a) represent simulated positions of the focus.

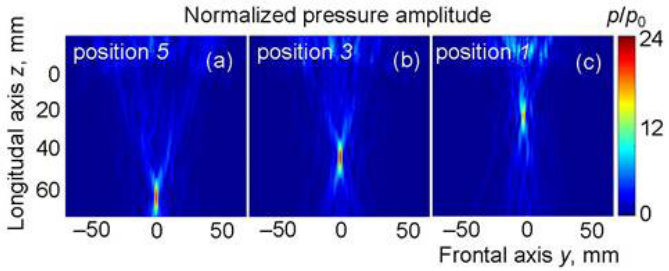

Figure 3. Linearly simulated distributions of the normalized pressure amplitude inside the head for different positions of the focus after aberration correction. Positions 1, 3, and 5 are marked in Fig. 2a.

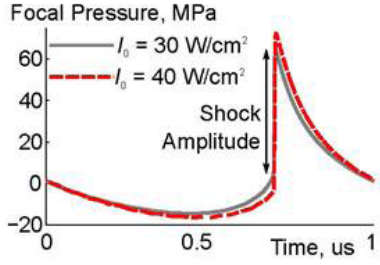

Fiigure 4. Results of nonlinear simulations in the brain with aberration correction for position 3 of the focus. One cycle of the focal waveforms simulated for given initial intensities.

BRT-4

Topic: Brain Technical
Presentation Type: Oral

Three-dimensional transcranial cavitation localization by four sensors

Zhongtao Hu, Lu Xu, Yaoheng Yang, Yan Gong, Dezhuang Ye, Christopher Pacia, Hong Chen

Washington University in St. Louis, St. Louis, MO, USA

Background: Cavitation is the dominant physical mechanism for focused ultrasound (FUS)-activated cavitation-mediated therapies in the brain. Accurately knowing the 3D location of cavitation in real time can beneficially improve the treatment targeting accuracy and avoid off-target tissue damage. However, the skull induces strong phase and amplitude aberration to the cavitation signals and presents significant challenge to the transcranial cavitation localization. Existing techniques for 3D cavitation localization use hemispherical multi-element arrays combined with passive beamforming and adaptive skull-specific correction algorithm. However, these techniques require expensive equipment. Their time-consuming computation limits applications in real-time cavitation localization, which is urgently needed to ensure the safety and efficacy of the FUS treatment. The object of this study was to investigate the feasibility of using a four-sensor network to transcranially locate cavitation source in 3D.

Materials and Methods: A device for 3D cavitation localization was designed and fabricated (Fig. 1(A)). It consists of four sensors (Olympus V323-SM) distributed on a hemisphere with a diameter of 18 cm. The performance of the device was evaluated using an ex vivo human skull setup (Fig. 1(B)). In this setup, microbubbles (~1×106 microbubbles/mL) were injected into a tube phantom (3 mm inner diameter and 5 mm outer diameter) positioned inside the skull cavity (Fig. 1(C)). The microbubbles were activated by a FUS transducer (1 Hz pulse repetition frequency, 75 cycles in pulse length, and 1.5 MHz driving frequency) at an estimated in situ peak negative pressure of 6.5 MPa. The FUS transducer and the tube was moved by a 3D stage to different locations. The FUS transducer was coaxially aligned with an ultrasound imaging probe. B-mode images were acquired before and after FUS sonication to determine the location of the cavitation event based on image contrast changes. The acoustic emissions from the FUS-activated microbubbles were passively detected and saved for post-processing. The signals were filtered to only keep the subharmonic frequency (750 kHz with 300-kHz bandwidth), which were used to represent the cavitation signals. Then, the time delay between signals received by the four sensors were measured by detecting the maximum inter-correlation of them. The position of the cavitation source was calculated using a method similar to that usually used in the global positioning system (GPS).

Results: Fig. 2(A) shows the schematic diagram of the experimental setup. Fig. 2(B) shows the positional error along x-, y-, z-axis both with and without skull, error bars denote standard deviation of measured locations. The positional error of transcranial cavitation localization along x, y, z axis were 1.7±1.2 mm, 1.6±1.7 mm, and 4.1±1.5 mm, respectively. For comparison, the positional error of cavitation localization without skull were 1.2±1.8 mm, 0.9±1.6 mm, and 3.1±2.3 mm, respectively. Figs. 2(C) and (D) present the tracking accuracy of transcranial cavitation localization in the xy plane and xz plane, and the magenta circle markers represent the mean value over four replicates and the bars represent the upper and lower deviation along horizontal and vertical directions. Higher accuracy was achieved along x and y axes than along z axis. Larger deviation was observed at locations away from the center than close to the center.

Conclusions: This study evaluated the feasibility of using a four-sensor network for transcranial cavitation localization in 3D. This proposed method achieved a mean accuracy of 1.7 mm, 1.6 mm and 4.1 mm along the x, y, z axes. This method could determine the cavitation location in 3D with a low computation cost, making it possible for real-time cavitation localization in 3D. Future work is needed to further improve the localization accuracy and evaluate its application in vivo.

Acknowledgements: This work was supported by the US Office of Naval Research #N0014-19-1-2335.

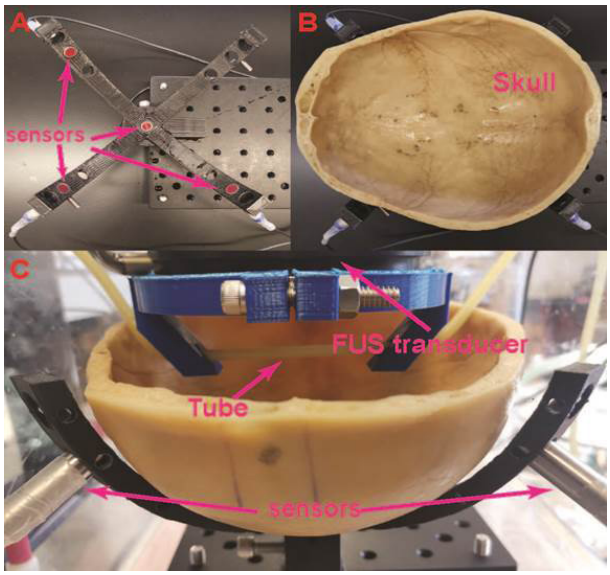

Figure 1. (A) The proposed device. (B) The device with skull. (C) Transcranial Localization experimental setup.

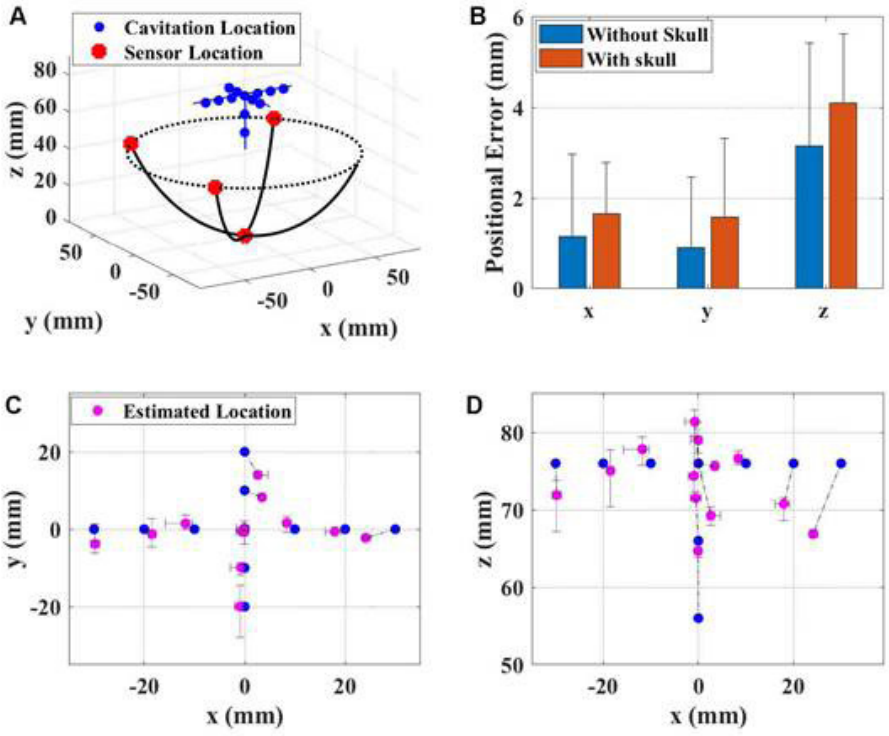

Figure 2. (A) Schematic diagram of the experimental setup. (B) Positional error both with and without skull. (C) and (D) show the transcranial cavitation source positions and estimated locations.

BRT-5

Topic: Brain Technical
Presentation Type: Oral

Rapid autofocusing of MR-guided focused ultrasound acoustic pressure fields using MR-ARFI with spatially coded emissions

Sumeeth Jonathan, M Anthony Phipps, Charles Caskey, William Grissom

Vanderbilt University, Nashville, TN, USA

Background: Magnetic resonance-guided focused ultrasound (MRgFUS) has many potential neurological applications. However, skull-induced aberrations of the acoustic pressure field limit its specificity and safety. The pressure field can be refocused in situ using MR-acoustic radiation force imaging (MR-ARFI), which maps the displacement (proportional to acoustic intensity) caused by the acoustic beam's radiation force. Current MR-ARFI-based refocusing methods require 4 spatially coded emissions per element to recover the complex-valued aberrations. However, reported scan times (2 hours/512 elements) are too long for practical in vivo use. We developed a rapid autofocusing method which can recover the aberrations with many fewer MR-ARFI images by fitting a set of pre-calibrated pressure field maps to the acquired images in a "multi-voxel" magnitude least-squares approach.

Materials and Methods: An MRI-compatible, 128-element FUS transducer (Image Guided Therapy; Bordeaux, FR) was used to sonicate a human brain tissue-mimicking phantom in a water tank. Sonications were performed at 650 kHz for 10 ms (PNP = 4.8 MPa). Displacement images were acquired using a spin echo 2D MR-ARFI sequence implemented on a 7 Tesla scanner (Phipps & Jonathan, 2019).

Transducer elements were randomly grouped into 4 logical elements. A known phase aberration pattern was programmatically added to each logical element of the transducer during transmission (Fig 1). The "single-voxel" refocusing method (Larrat et al, 2010) was implemented to recover the programmed aberrations using 4 spatially coded emissions per logical element (16 MR-ARFI acquisitions or 32.0 min scan time). Though the MR phase was imaged over a 2D plane, this method only uses the mean acoustic intensity across a few image voxels near the acoustic focus (hence "single-voxel" method).

Our autofocusing method can recover the complex-valued aberrations from many fewer MR-ARFI images by fitting a set of pre-calibrated pressure field maps to the acquired images (Fig 2). This is a "multi-voxel" approach that can recover the complex-valued aberrations from the entire MR-ARFI image using magnitude least-squares optimization. The aberrated images used in the fit were those already acquired for the single-voxel method. We evaluated the performance of our method using 1, 2, and 8 aberrated MR-ARFI images in the least-squares fit.

Results: Figure 3 compares phase aberration estimates obtained by the canonical single-voxel MR-ARFI-based refocusing method and our proposed multi-voxel method. Our multi-voxel method recovered the programmed aberrations with lower RMSE than the single-voxel method when 2 or 8 MR-ARFI acquisitions were used in the least-squares fit, which represents a 87.5% and 50% reduction in the number of required acquisitions, respectively.

Figure 4 shows representative MR-ARFI images acquired using our MRgFUS transducer. When the estimated aberrations were applied to refocus the programmatically aberrated pressure field, our multi-voxel method recovered the acoustic focus with higher peak displacement than the single-voxel method when 2 or 8 MR-ARFI acquisitions were used in the least-squares fit.

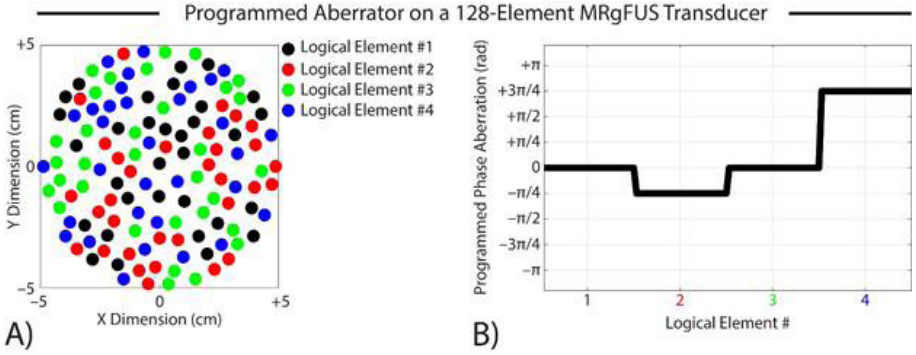

Figure 1. (A) Transducer elements were randomly grouped into 4 logical elements. (B) A known phase aberration pattern ([0, −π/4, 0, 3π/4] rad) was programmatically added.

Conclusions: A multi-voxel MR-ARFI-based autofocusing method was proposed for rapid aberration correction of MR-guided focused ultrasound acoustic pressure fields. We compared our proposed method to the canonical single-voxel MR-ARFI-based refocusing method and demonstrated that as few as two MR-ARFI acquisitions can be used to refocus a programmatically aberrated pressure field. Future work will evaluate the multi-voxel method using more complex aberration patterns and on

our group's in vivo platform for transcranial FUS neuromodulation in non-human primates (Phipps & Jonathan, 2019).

Acknowledgements: This work was supported by NIH grants R01 MH 111877, R24 MH 109105, U18 EB 029351, and F31 EB 026928.

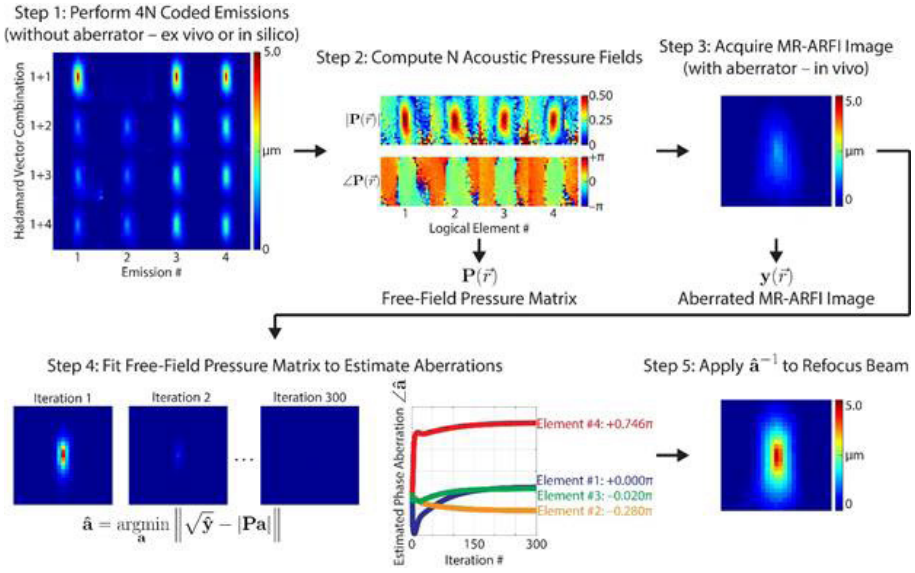

Figure 2. Our method can recover complex-valued aberrations with many fewer MR-ARFI images by fitting a set of pre-calibrated pressure field maps to the acquired images in a magnitude least-squares approach.

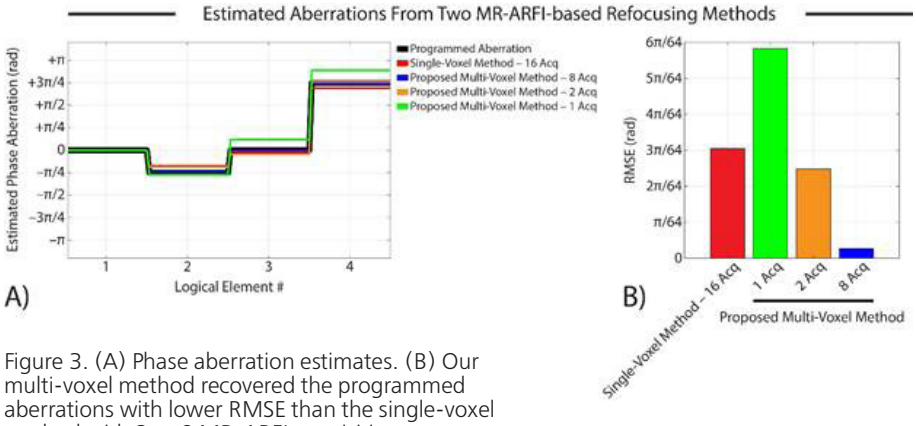

Figure 3. (A) Phase aberration estimates. (B) Our multi-voxel method recovered the programmed aberrations with lower RMSE than the single-voxel method with 2 or 8 MR-ARFI acquisitions.

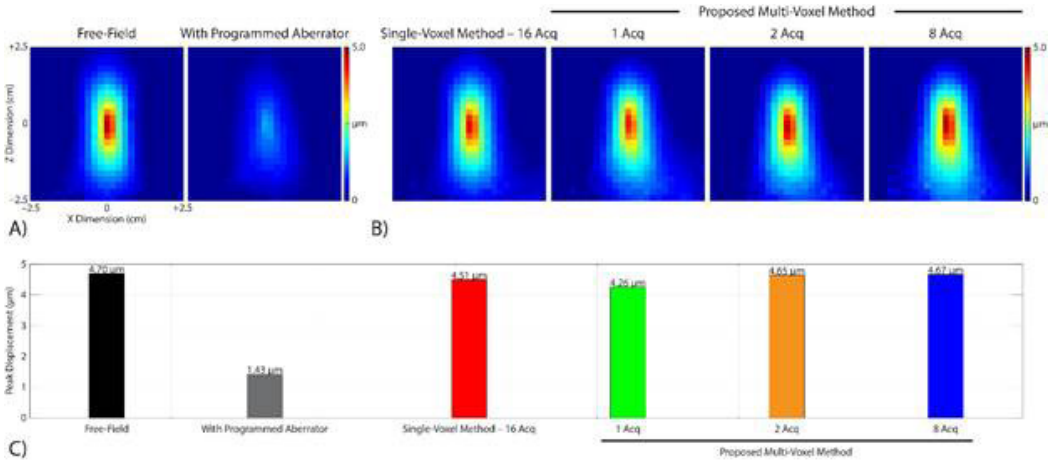

Figure 4. (A) Representative MR-ARFI images. (B) and (C) Our multi-voxel method recovered the acoustic focus with higher peak displacement than the single-voxel method with 2 or 8 MR-ARFI acquisitions.

BRT-6

Topic: Brain Technical
Presentation Type: Oral

Comparison of transcranial focused ultrasound treatment planning using MR and CT images

Steve Leung[1], David Moore[2], Yekaterina Gilbo[3], John Snell[2], Taylor Webb[1], Craig H. Meyer[3], Wilson Miller[3], Kim Butts Pauly[1]

[1]Stanford University, Stanford, CA, USA
[2]Focused Ultrasound Foundation, Charlottesville, VA, USA
[3]University of Virginia, Charlottesville, VA, USA

Background: Currently, treatment planning of transcranial focused ultrasound is performed with CT images of patient skulls. However, the use of CT images has two main downsides: 1) it requires exposing patients to ionizing radiation and 2) it adds to treatment time overhead. Using MR in place of CT can bypass these downsides and may also expand the eligible pool of patients. This study aims to compare the performance of MR and CT images when used for treatment planning.

Materials and Methods: Three degassed ex vivo human skulls were used for experimentation. Ultrashort echo time MR scans were performed on a Siemens 3T Prisma system at two echo times (50 μs and 2510 μs). Images were post-processed to generate MR-simulated-CT images that achieved CT-like bone contrast. CT scans were performed on a GE Discovery CT750 HD system at 120 kVp using the BONEPLUS reconstruction kernel.

The degassed skulls were attached to skull frames, which were secured to the InSightec Exablate 4000 head transducer. The MR and CT images were input into the InSightec Exablate software to calculate phase corrections for two targets: the geometric focus and 5 mm steering. The resulting focal spots were measured with an Onda HNA-0400 hydrophone mounted on a 3-axis positioner system.

Results: For targets at the geometric focus and with 5 mm steering, the MR-simulated-CT correction resulted in focal spot intensities that were comparable to the CT correction.

Conclusions: MR-simulated-CT images are a promising alternative to CT images for treatment planning of transcranial focused ultrasound.

Acknowledgements: Supported by InSightec and the Focused Ultrasound Foundation.

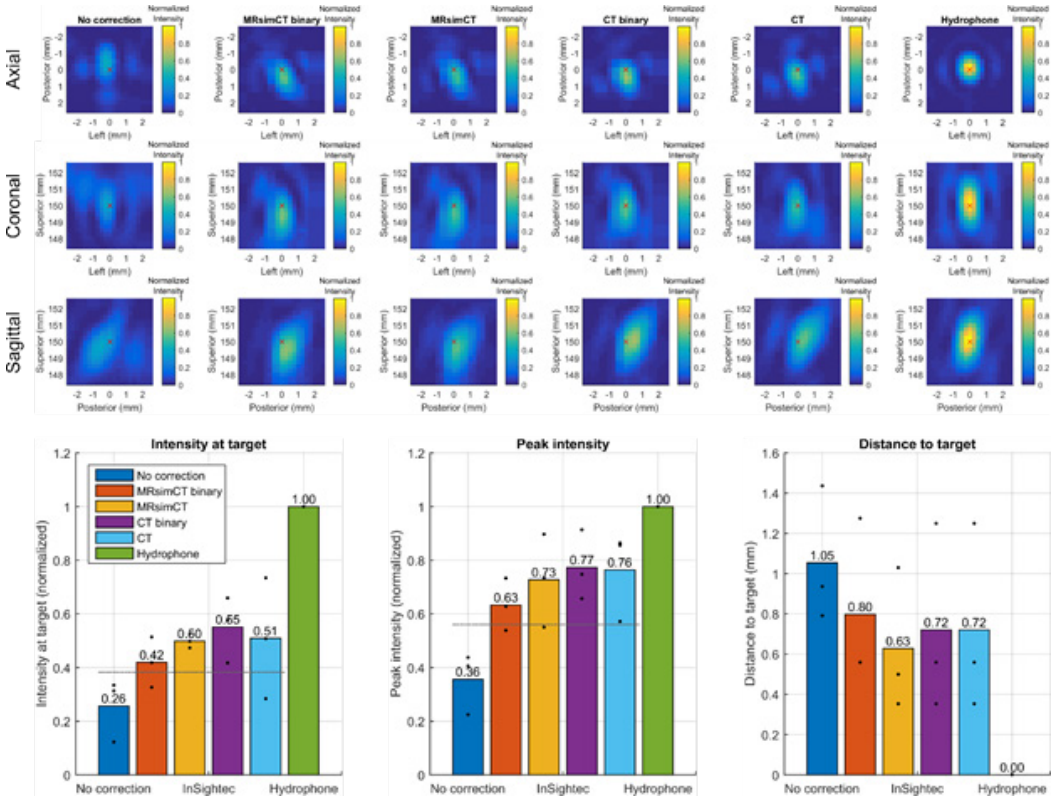

Figure 1. Focal spots at the geometric focus achieved using InSightec phase correction and different image inputs. a) 3D hydrophone raster scans of the focal spots for Skull B. b) Averaged focal spot metrics for all three skulls. The dashed line marks the mean of the no correction and CT correction values.

BRT-7

Topic: Brain Technical
Presentation Type: Oral

Transcranial MR-guided histotripsy treatment: An in-vivo pig study

Ning Lu, Dinank Gupta, Badih Daou, Jonathan Sukovich, Adam Fox, Dave Choi, Aditya Pandey, Timothy Hall, Douglas Noll, Zhen Xu

[1]University of Michigan, Ann Arbor, MI, USA

Background: Histotripsy has been previously used to treat a wide range of locations in vitro through an excised human skull, offering a non-invasive treatment option for brain applications including the treatment of brain tumors. The goal of this study is to demonstrate the feasibility and safety of in vivo transcranial MR-guided histotripsy in the pig brain through an excised human skullcap.

Materials and Methods: A 700-kHz, 128-element MR-compatible phased-array transducer built in-house was used to apply histotripsy to the pig brain through an excised human skullcap. As the pig skull is too flat and thick for ultrasound propagation, a 60 mm diameter circular region of the pig skullcap was surgically removed to provide an acoustic opening. The skin was sutured over the pig brain after craniotomy. The craniotomy was performed 2 days prior to the histotripsy treatment to remove any air bubbles between the brain and the skin. On the day of the treatment, the ultrasound array was placed in a water bucket inside a 3T GE MRI scanner. The pig head was placed above an excised human skull held by a skull holder inside the array. The MR images were acquired using surface coil pads attached to left and right side of the pig head. Pre-treatment MRI scans were used to align the geometric focus of the array within the target brain tissue based on fiducial markers on the array. A target zone of 27-216 mm3 was treated by electronically steering the focus with 1-3 mm between adjacent focal locations. Each focal location was treated with 50 pulses with a pulse repetition frequency of 10 Hz and an estimated peak-negative pressure of 51 MPa at the geometric focus. T2 and T2* images were acquired immediately after and 2 hours post-treatment to evaluate the treated zone and any off-target brain damage, including hemorrhage and edema. The pig brains were harvested for pathological examination.

Results: Histotripsy ablation was successfully generated in the thalamus of three pig brains adjacent to the third ventricle, as confirmed by MRI. T2-weighted MR images showed hyperintense histotripsy ablation zones compared to the surrounding untreated tissue. These hyperintense regions were well confined within the targeted volume and did not demonstrate significant brain edema. T2* images, as a measure of iron and hemosiderin in the brain, demonstrated no excessive bleeding in peri-target zones. Histology revealed complete cellular disruption within the ablation zones and a great correlation to the identified treatment zones on MRI.

Conclusions: This study provides initial results demonstrating the feasibility and safety of transcranial MR-guided histotripsy in the in vivo pig brain through an excised human skull. MRI and histology results showed a well-confined histotripsy ablation zone without significant hemorrhage or edema outside the target region. This study is still ongoing with more porcine experiments and further investigation on MR guidance and real-time monitoring.

Acknowledgements: This study is supported by Focused Ultrasound Foundation.

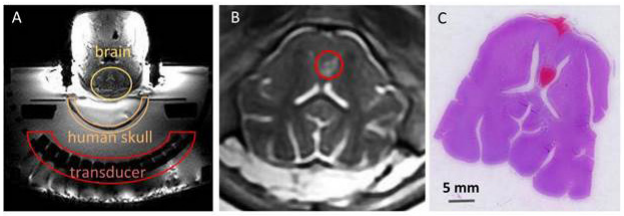

Figure 1. A: Experimental setup for transcranial histotripsy treatment in the MR scanner. B: High-resolution T2 image acquired 2 hours post-treatment. The ablation zone is labeled in red circle. C: The histology slice of pig brain corresponding to B. The bleeding shown on the slice is well confined within the target volume.

BRT-8

Topic: Brain Technical
Presentation Type: Oral

Using phase data from MR temperature imaging to visualize anatomy during MRI-guided focused ultrasound neurosurgery

Nathan McDannold, P. Jason White, G. Rees Cosgrove

Brigham and Women's Hospital, Harvard Medical School, Boston, MA, USA

Background: Neurosurgery targets in the thalamus can be challenging to identify during transcranial MRI-guided focused ultrasound (MRgFUS) thermal ablation due to poor image quality. They also neighbor structures that can result in side effects if damaged. Here we demonstrate that the phase data obtained during MRgFUS for MR temperature imaging (MRTI) contains anatomic information that could be useful in guiding this procedure. Structures such as the red nucleus (RN), substantia nigra (SN), and the subthalamic nucleus (STN), contain higher concentrations of iron. This iron in the tissue consists largely of ferritin and hemosiderin and is paramagnetic. The magnetic field thus becomes slightly increased in these structures, which leads to a more phase accumulation between excitation and readout of the MRI data. The phospholipids in heavily myelinated white matter are diamagnetic, leading to decreased phase accumulation. These structures can be used to refine atlas-based targeting.

Materials and Methods: The same data obtained for MRTI was used to create the filtered phase maps. First, we averaged all the complex images acquired during and after each sonication. After masking the images with segmentations of the brain, the phase was then unwrapped. We removed the low spatial frequency components of the phase maps resulting from static magnetic field inhomogeneities, which we found using an averaging filter in the spatial domain with a kernel size of nine voxels. This low pass filtered phase map was subtracted off, leaving only the high spatial frequency components that contained anatomic information (Figure 1). This approach was evaluated in 68 thalamotomies for essential tremor (ET) and four pallidotomies for Parkinson's Disease. The coordinates of the voxels within the segmentations of the RN, STN, and IC along with those within the accumulated thermal dose contours were rotated to a common reference frame so that the PC was located at the origin and the ACPC line was oriented along the anteroposterior direction. For visualization, this information was used to generate maps of the probability for each voxel to be within a segmentation of the RN, STN, or IC, or within the accumulated thermal dose contour.

Results: We found that we could readily visualize the red nucleus and subthalamic nucleus, and those nuclei were consistently aligned with the sonication target coordinates. We also could consistently visualize the internal capsule, which needs to be protected from thermal damage to prevent side effects (Figure 2-3). The average locations of these structures agree well with stereotactic atlas (Figure 4). Preliminary results from four pallidotomies in Parkinson's disease patients suggest that this approach might also be useful in visualizing the optic tract in addition to the internal capsule.

Conclusions: The image data used to create MRTI during MRgFUS thermal ablation contains anatomic information that is relevant for refining lesion placement in atlas-based targeting of the VIM and preventing unwanted damage to the IC. This anatomic information is automatically registered to the thermal mapping, does not suffer from uncertainty due image distortion, and requires no extra time to acquire. This approach could be useful in improving efficacy, safety and treatment time during this noninvasive neurosurgical procedure.

Acknowledgements: NIH grant R01EB025205.

Figure 1. (left) Processing phase data obtained during sonication in two ways: (a) Phase-difference relative to a pre-sonication image for MRTI; (b) Average of all images and high pass filter for anatomy.

Figure 2. (right) Annotated filtered phase maps. CN: caudate nucleus; EC: external capsule; GP: globus pallidus; IC: internal capsule; RN: red nucleus; SN: substantia nigra; STN: subthalamic nucleus.

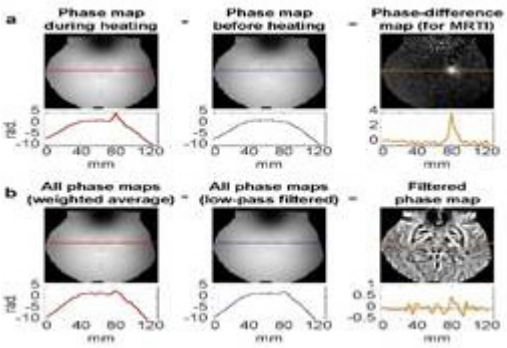

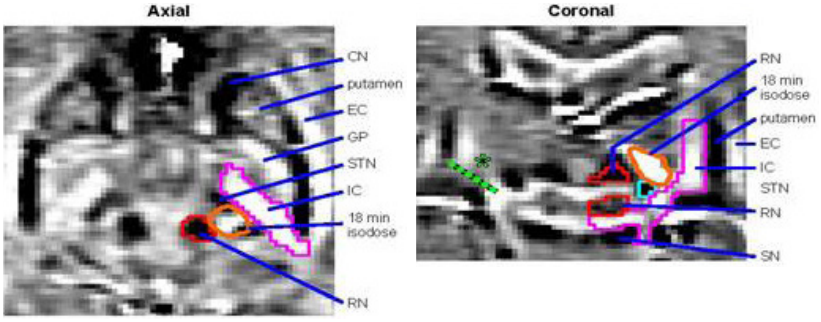

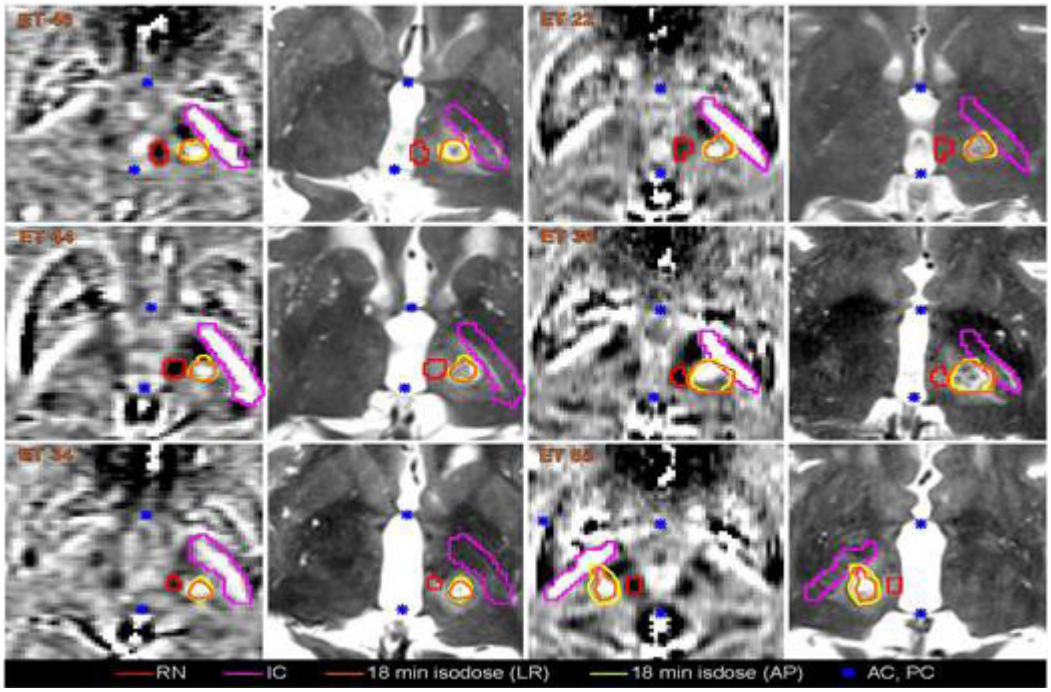

Figure 3. Axial phase maps (left) and T2-weighted images acquired 24 h later (right) for six ET treatments. The segmentations and accumulated thermal dose contours were generated from the same image data.

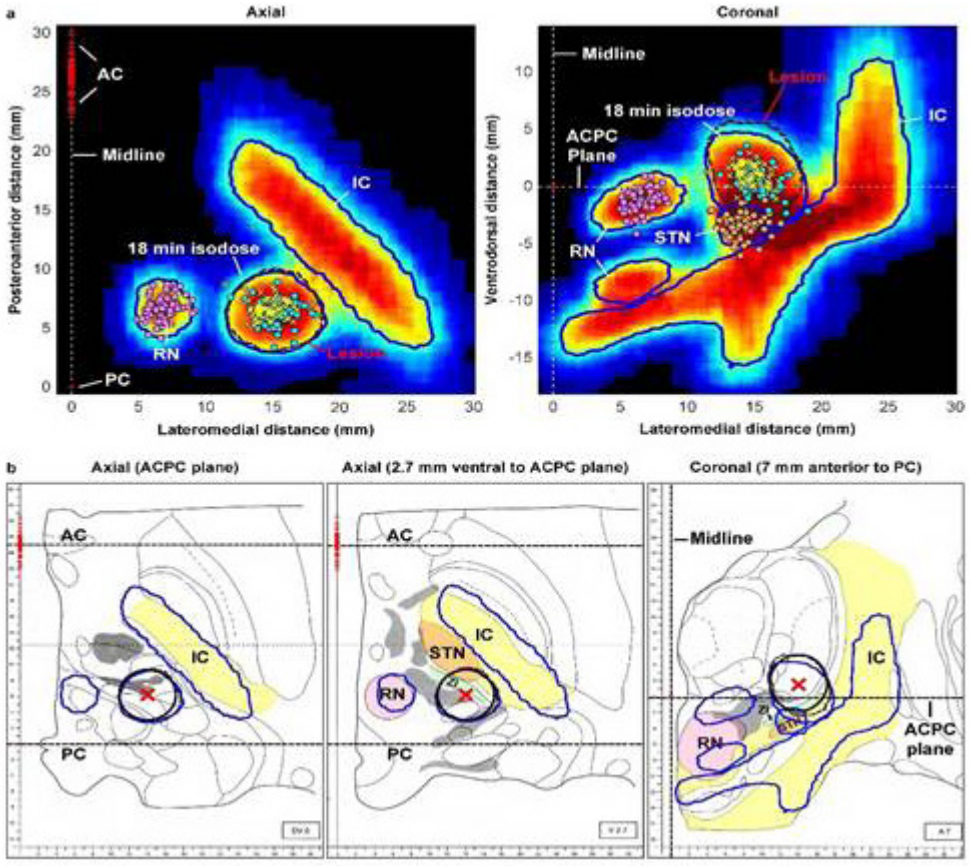

Figure 4. (a) Probability for each voxel from 68 treatments to be within the RN, STN, or IC segmentations, or within the accumulated 18 CEM43 dose contour. (b) 50% contours superimposed on Morel thalamus atlas.

BRT-9

Topic: Brain Technical
Presentation Type: Oral

MRI-based thermal dosimetry during focused ultrasound thalamotomy

Nathan McDannold, P. Jason White, G. Rees Cosgrove

Brigham and Women's Hospital, Harvard Medical School, Boston, MA, USA

Background: Transcranial MRI-guided focused ultrasound (MRgFUS) is a noninvasive thermal ablation method approved for the treatment of essential tremor and tremor-dominant Parkinson's disease. This method uses MR temperature imaging (MRTI) to monitor the treatment. Accurately tracking the accumulated thermal dose is important for both safety and efficacy. Currently, MRTI is obtained in a single plane that varies between sonications, preventing direct tracking of the accumulated dose. In this work, we tested a method to estimate this dose during 70 MRgFUS treatments.

Materials and Methods: This method used the MRTI obtained during treatment and exponential fits of the focal heating to create simulated thermal images for sonications when the imaging plane was changed. The accumulated thermal dose was estimated in coronal and axial imaging planes. Tissue swelling was evaluated by measuring the mean shift in the ventricle wall between pre-treatment MRI and imaging obtained 24 h after MRgFUS. The Sørensen-Dice similarity coefficient (DSC) was used to compare the accumulated dose to lesion segmentations in T2-weighted MRI obtained one day after MRgFUS. The distance between thermal dose contours at 17 cumulative min at 43°C (CEM43) and the lesion segmentations was measured, and the probability for thermal damage was estimated using probit analysis.

Results: The threshold that maximized the DSC was found for each treatment. Figure 1 superimposes the regions where the dose exceeded these patient-specific thresholds onto the lesion segmentations for coronal MRTI. The mean DSC between the lesion segmentations and dose regions at the 17 CEM43 threshold used by the device software was 0.83, but it varied among different treatments (range: 0.41-0.95). Mismatch was greater in cases with more tissue swelling. Overall, the mean distance between the lesion segmentations and the 17 CEM43 dose contours was 0.34 ± 0.56 mm (Figure 2a). Good agreement was observed over a range of dose thresholds (Figure 2b). The probability for thermal damage was estimated to be 50% at 14.9 CEM43 (Figure 3). Due to large thermal gradients, which exceeded 90 CEM43/mm, the area where the probability for thermal damage was uncertain was narrow.

Conclusions: This approach accurately predicted the lesion shapes on average. Tissue swelling appeared to explain when mismatch occurred, although other errors probably contributed. Overall, these results show that the 17 CEM43 threshold is a good predictor for

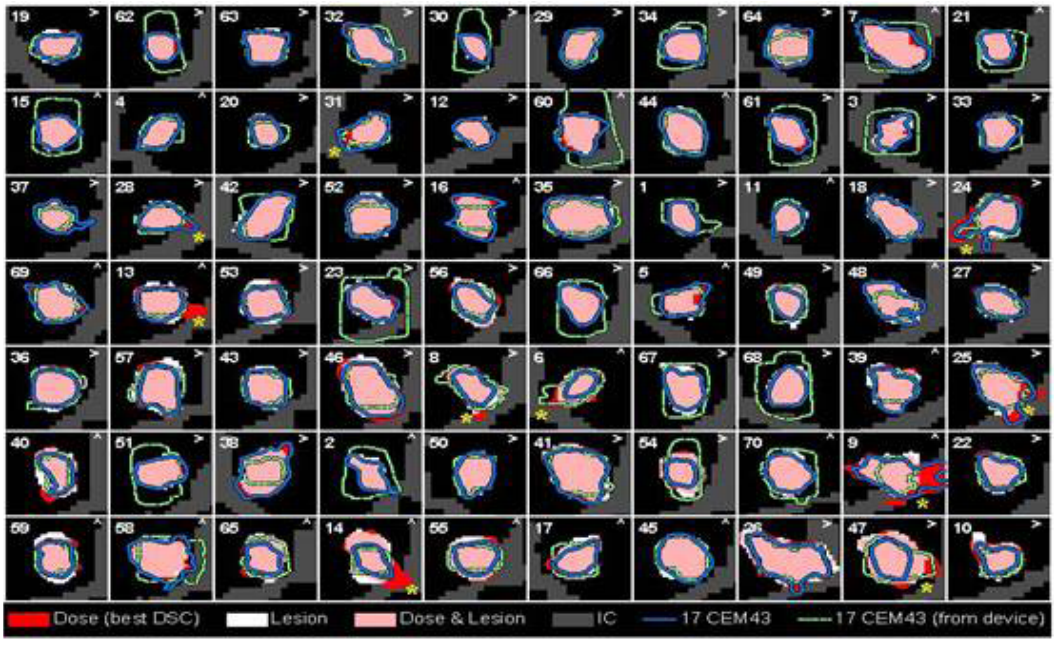

Figure 1. Comparing lesion shapes and accumulated isodose contours. Patients are sorted by ventricle shift resulting from swelling. With more shift, the 17 min contours underpredicted the lesions.

thermal lesions, although there will always be a narrow margin where the fate of the tissue is uncertain.

Acknowledgements: NIH grant R01EB028686

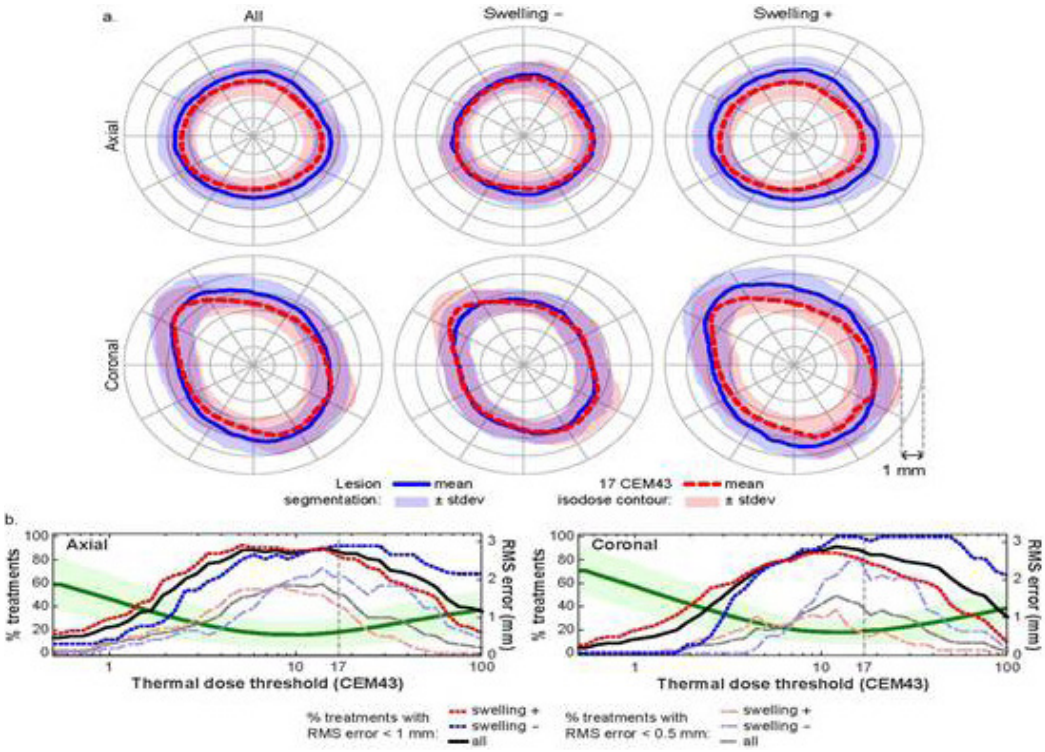

Figure 2. (a) Distances between the 17 CEM43 contours and lesion segmentations. For treatments with more swelling, the dose underpredicted the lesion edge. (b) Agreement vs. dose threshold.

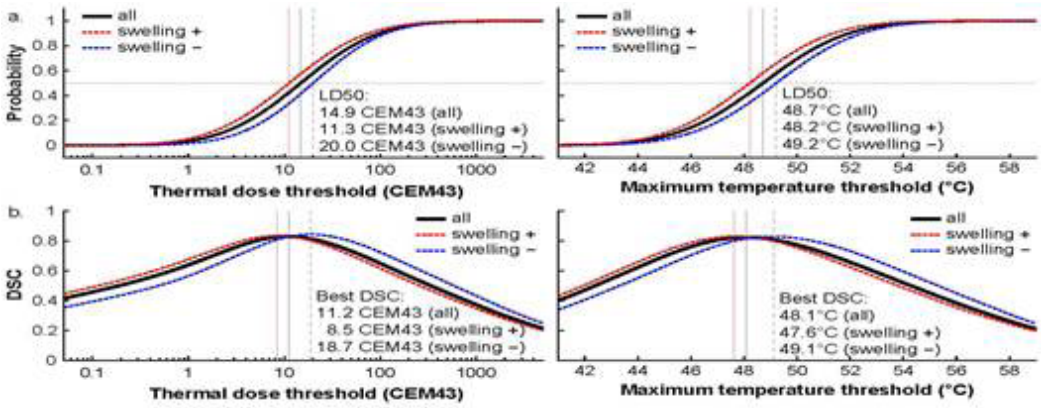

Figure 3. (a) Probability for each MRTI voxel being within a lesion segmentation as a function of the thermal dose and maximum temperature. (b) DSC between isodose/isotherm contours and lesion segmentations.

BRT-10

Topic: Brain Technical
Presentation Type: Oral

Transmit-receive capable histotripsy transducer systems for real-time treatment localization and mapping and evaluating induced tissue damage

Jonathan Sukovich, Timothy Hall, Ning Lu, Zhen Xu

University of Michigan, Ann Arbor, MI, USA

Background: Histotripsy has been demonstrated to be safe and effective for the ablation of various tissues in a wide range of locations in the body including through the ribs and skull. A primary challenge associated with delivering histotripsy treatment in practice is localizing and mapping the generated cavitation events and monitoring induced tissue damage within the treatment target during therapy in real-time. The goal of this study is to demonstrate the capabilities of a new, transmit-receive capable histotripsy transducer systems with the potential to enable both.

Materials and Methods: A modularly extensible array of transmit-receive capable histotripsy transducer elements, and a system for independently controlling them, was designed and implemented. The histotripsy transducer elements' outputs were driven using custom amplifier systems. Receive functionality was achieved using 12-bit, 50MHz ADCs wired in parallel across the transducer elements. Control over the transducer outputs, and acquisition of signals received through them, were achieved using system-on-a-chip (SoC) devices. The settings for the outputs of the transducers (firing phase and amplitude) and their acquisition parameters (sampling frequency & duration, gain, etc) could be set uniquely on each array element. Communications with the SoCs to control the array and transfer data was achieved via ethernet. A 700-kHz, 360-element histotripsy transducer designed and built in-house for transcranial histotripsy, and controlled by the described system, was used to demonstrate the system's capabilities. Bovine brain samples were treated through excised human skullcaps and acoustic cavitation emission (ACE) signals generated during treatment were acquired using the array elements as receivers. Cavitation was localized by back-projecting the ACE signals into the field to generate maps of their amplitudes. Induced tissue damage was evaluated by monitoring the evolution of bubble lifespans by tracking the timings of the ACE signals associated with each bubble's growth and collapse during treatment.

Results: All transmit and receive parameters could be set independently on each array element. On transmit, the firing phase and amplitudes of the elements could be set arbitrarily with 10ns resolution. On receive, the sampling frequencies of the elements could be adjusted individually from 3.125MHz to 50MHz; maximum record lengths ranged from 655us to 10.4ms depending on sampling frequency. ACE signals from both the growth and collapse of cavitation bubbles could be acquired transcranially using the array elements. The localized positions of the generated bubbles from the acquired signals were in good agreement with morphological observations of induced damage based on the geometry of the treatment volumes. Assessments of the bubble lifespans from the acquired signals were observed to correlate with induced damage, where they were observed to grow during treatment with increasing degree of tissue fractionation until fractionation was complete, at which point the lifespans became stable.

Conclusions: We have demonstrated the capabilities of the new transmit-receive capable histotripsy system. We have shown that the ACE signals received by it can be used to localize cavitation events as well as to evaluate induced damage. Maps of the localized cavitation events were shown to be in good agreement with morphological assessments of induced damage, and the induced damage was observed to correlate with the measured lifespans of the generated bubbles. Although this study only demonstrated these capabilities using a transcranial array, the technologies enabling the transmit-receive capabilities shown, and the methods for localizing and monitoring damage, can readily be integrated or applied in other systems for treatment of other locations.

Acknowledgements: FUSF Grant 24332. NIH R01-CA211217, NIH R01-NS108042, ONR Grant N00014-17-1-2058 (under Dr. Tim Bentley)

BRT-12

Topic: Brain Technical
Presentation Type: Oral

"Propeller Beanie" passive antennas to alleviate dark bands in transcranial MR-guided focused ultrasound

Xinqiang Yan[1], Steven P. Allen[2], William Grissom[3]

[1]Vanderbilt University Medical Center, Nashville, TN, USA
[2]University of Virginia, Charlottesville, VA, USA
[3]Vanderbilt University, Nashville, TN, USA

Background: Transcranial MR-guided focused ultrasound (tcMRgFUS) neurosurgery is a non-invasive treatment for essential tremor and many emerging applications [McDannold 2005 & 2010]. In the FDA-approved Insightec tcMRgFUS system, however, RF reflections inside the transducer create a curved dark band in brain images, which limits the set of scans that can be performed during treatment (Fig. 1). To address this, researchers have proposed doping the water, and placing RF coils inside the water bath [Leung JTU 2015 &Watkins ISMRM 2014]. This work proposes a simpler solution that almost completely alleviates the problem, which is to place a passive reflecting antenna or resonator above the patient's head, with a "propeller-beanie" crossed-wire shape (Fig. 2a). The proposed antennas alleviate the wave cancellation by reflecting the incoming RF waves back down into the head before they arrive at the transducer's upper surface and reflect [Yan Concept MR 2018].

Materials and Methods: Methods:

Electromagnetic (EM) Simulation — Fig. 2b shows a simulation model in the EM Solver Ansys HFSS. The body coil was modeled as a low-pass birdcage with a diameter/length of 60cm/100cm. The transducer bowl was modeled as a conductive surface on a 35 cm-diameter hemisphere. It was filled with tap water (conductivity=0.01 S/m, relative permittivity=81.) The head model was positioned at the center of the coil and immersed in the tap water. A pair of 26-gauge crossed tin-coated copper wires was placed ~1cm above the head. The wires' lengths were 12cm, which equals the half-wavelength of the 3T Larmor frequency in the water. The simulations used the EM and RF circuit co-simulation method.

Experiment — An imaging experiment was conducted to validate the signal improvements. A 3D-printed holder was made to attach to the top of a swim cap and hold a pair of 12 cm 26-gauge wires 1 cm above the head. The cap was placed on a head-shaped plastic mold containing 4% agar gel doped with approximately 2 mM CuSO4 as well as onions for contrast, which was then placed in the Insightec ExAblate Neuro 4000 system (Insightec Ltd, Tirat Carmel, IL) installed at a GE Discovery MR750T 3T scanner (GE Healthcare, Waukesha, WI). Sagittal gradient-recalled echo (GRE) images (TE 6 ms, TR 50 ms, 2 NEX, 40 cm FOV, 40 degrees flip (nominal), slice thickness 3 mm, 256 x 256 matrix, 62.5 kHz bandwidth) were acquired with and without the wires.

Results: Fig. 3 shows simulation and experimental results. Without water bath filled, B1+ field in the brain contains characteristic center brightening. With water, a dark band appears where B1+ is attenuated approximately 4x, and B1+ is attenuated at least 30% everywhere in the brain. The B1- field is similarly impacted, which compounds the signal loss in practice. The experimental images in the second row of Fig. 3 show the phantom wearing the "propeller beanie" antenna, and two GRE images measured without and with the crossed wires present. The wires alleviated the dark band in the brain and shifted it up in the water bath.

Fig. 4 shows10-gram local SAR distributions without and with passive wires. Even with the unoptimized antenna, the worst 10-gram Specific Absorption Rate (SAR) only increases by 31%. This is because the passive wires increase the 10-local SAR nearby (i.e., at the top of the head) while the highest SAR without the wires appears in the middle of the head.

Conclusions: In this work, we explained how the dark band is generated in the Insightec tcMRgFUS system and proposed simple crossed-wire "propeller beanie" passive antennas to alleviate it. In practice, the wires can be a high gauge to prevent interference with the FUS beam (which may be a problem for metal screen reflectors [Hadley ISTU 2019]), and they can be strung across the inside of the transducer or held in place by a holder that runs along the transducer seams, so that the patient need not wear a cap.

Figure 1.

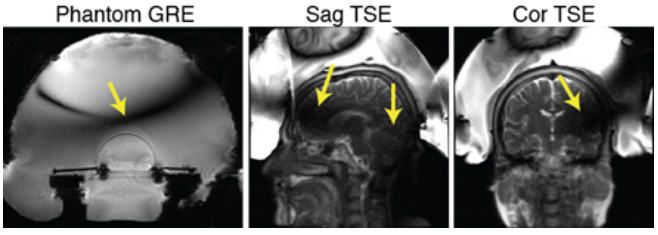

Acknowledgements: This work was supported by NIH R01 EB 016695.

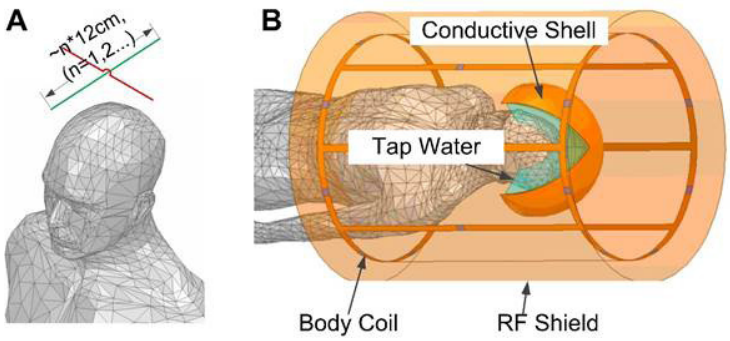

Figure 2.

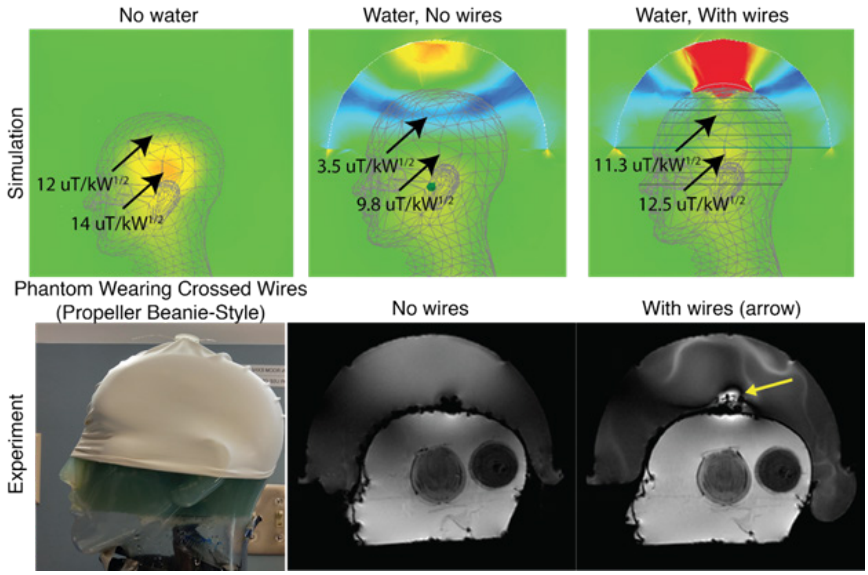

Figure 3.

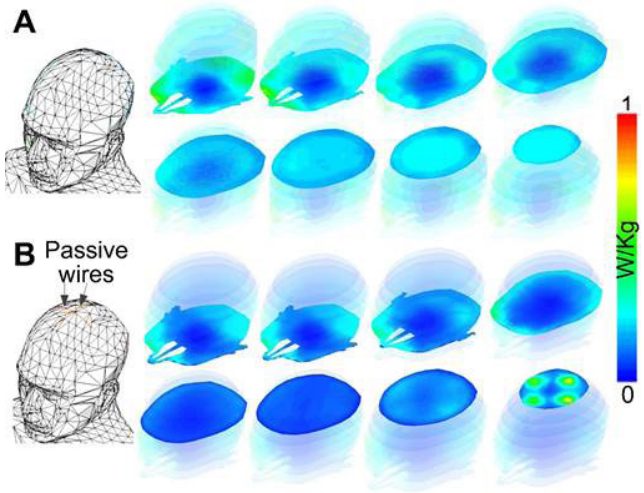

Figure 4.

BRT-13

Topic: Brain Technical
Presentation Type: Oral

First in history remote start of MRgFUS treatment procedures due to COVID-19 epidemic

Rezida Galimova[1], Olga Kachemaeva[1], Igor Buzaev[2], Dmitrii Krekotin[1], Shamil Safin[3], Sergei Illarioshkin[4]

[1]Intelligent Neurosurgery Clinic, Ufa, Russian Federation
[2]Republic Cardiac Center, Ufa, Russian Federation
[3]Republic Clinic Hospital, Ufa, Russian Federation
[4]Scientific Center of Neurology, Moscow, Russian Federation

Background: Intelligent Neurosurgery Clinic in Ufa is the first medical center adopting MR guided focused ultrasound therapy to treat movement disorders in Russia. Due to the new coronavirus epidemic, the company (Insightec) specialists were not able to be on the site to start the first treatment procedures.

The decision to treat the first patient remotely with the help of modern digital technology came spontaneously during the studying process with the medical center's specialists in April 2020.

Materials and Methods: Studying materials were sent to the Center to conduct one week of online training. Secured VNC access was organized to the equipment, Remote Desktop Sharing, and Port Address Translation allowed the use of the working station by all participants, four videoconference cameras were installed in MRI rooms, Microsoft Teams program was used for the online communication (Image 1).

The first MRgFUS procedure was performed by the Intelligent Neurosurgery Clinic doctors under the online guidance of the company specialists to the 68-year-old male patient with a drug-resistant tremor-dominant form of Parkinson disease (Hoehn Yahr stage 2, symptoms duration 4 years, UPDRS-III 46 before the therapy, the skull density ratio (SDR) 0.45) in 5th of May, 2020. The procedure was performed in a 1.5T MR imaging system (GE Optima 450, GE Healthcare, USA) using the ExAblate 4000 (InSightec, Israel).

Unilateral ablation of the ventral intermediate nucleus was chosen as the target for tremor-dominant PD. Series of low-powered sonications at 43C were administered to confirm the accurate thermal focusing in all three planes using magnetic resonance thermography. The number of total sonications – 12, the number of the therapeutic sonications – 6, the therapeutic temperature – 57C, the mean duration for each sonication - 13 to 16 sec., the maximum of the delivered energy – 22 000J, time from the first sonication to treatment completion 174 min., the size of the thalamotomy lesion was 5.2 mm to 5 mm

Results: The patient developed significant improvement of performance on UPDRS-III after MRgFUS (41) and reduction of tremor by 38.5% and demonstrated significant improvement of rest tremor in the treated hand after the procedure.

Figure 1. The MRgFUS working station with remote connection of participants.

Conclusions: MRgFUS is one of the treatment options for medication-resistant PD with satisfying efficacy and safety.

Despite the COVID infection limitations innovative digital technologies connect enthusiastic people and allow patients' to have high-quality medical care that they deserve. Our experience shows that even very difficult neurosurgical procedures can be performed with a good result after proper preparation and education under online supervision. Supportive teamwork from both sides is achievable. Intelligent Neurosurgery Clinic was able to perform eight treatments after the first procedure under the online supervision in June, July 2020.

BTU-1

Topic: Brain Tumors
Presentation Type: Oral

Focused ultrasound mediated blood-brain barrier opening following radiation is safe in a murine pontine glioma model

Zachary Englander[1], Hong-Jian Wei[1], Antonios Pouliopoulos[1], Xu Zhang[1], Tony Wang[1], Jeffrey Bruce[1], Peter Canoll[1], Neil Feldstein[1], Zhiguo Zhang[1], Oren Becher[2], Stergios Zacharoulis[1], Elisa Konofagou[1], Cheng-Chia Wu[1]

[1]Columbia University, New York, NY, USA
[2]Lurie Children's Hospital, Chicago, IL, USA

Background: Diffuse intrinsic pontine glioma (DIPG) is a devastating pediatric brain cancer with limited treatment options and poor survival. Drug delivery is a major therapeutic obstacle in this disease, as the blood brain barrier (BBB) limits the distribution of intravenous therapies to the brainstem. Focused ultrasound is a revolutionary technology that, when combined with the administration of microbubbles (FUS+MB), can effectively open the BBB permitting the entry of drugs across the cerebrovasculature. Given that the utility of FUS in brainstem tumors remains unknown, the purpose of our study was to determine the safety and feasibility of this technique in a preclinical murine pontine glioma model following radiotherapy, the current mainstay of treatment for this disease.

Materials and Methods: A syngeneic orthotopic model was established by stereotactic injection of PDGF-B+p53-/-H3.3 K27M+ murine glioma cells (100,000/1ul) into the pons of B6 albino mice. During post-injection week three, mice underwent 9 Gy of radiation to the brainstem in three fractions using the small animal radiation research platform. Animals were randomized to control (n=3) or FUS groups (n=3). A single-element, spherical-segment 1.5 MHz ultrasound transducer driven by a function generator through a power amplifier was used with concurrent intravenous microbubble injection for tumor sonication. BBB opening was confirmed with gadolinium-enhanced MRI. Sequential weight lifting scores measured motor function before and after treatment. Mice were serially monitored for survival with daily weights.

Results: FUS+MB successfully caused BBB opening while preserving normal motor function (pre-FUS mean = 9 points, post-FUS mean = 11 points, $P>0.05$). Furthermore, there was no difference in survival between the groups (control mean = 32 days, FUS mean = 33.6 days, $P>0.05$).

Conclusions: FUS+MB is a safe and feasible technique for BBB opening in a preclinical pontine glioma model following radiation therapy.

Acknowledgements: Herbert Irving Cancer Center CAPRI Grant (NIH R38CA231577-01)

BTU-2

Topic: Brain Tumors
Presentation Type: Oral

Microbubble-facilitated focused ultrasound induces cerebral oxygenation to enhance brain tumor suppressive response In radiation therapy

Chia-Jung Lin[1], Chiung-Yin Huang[2], Kuo-Chen Wei[2], Hao-Li Liu[3]

[1]NaviFUS Co. LTD, Taipei, Taiwan (Republic of China)
[2]Chang Gung Memorial Hospital, Tauyuan, Taiwan (Republic of China)
[3]Chang Gung University, Tauyuan, Taiwan (Republic of China)

Background: One standard treatment of malignant brain tumor is surgical resection followed by radiotherapy (RT). However, the hypoxia condition may cause systemic delivered oxygen in solid tumors insufficient for ionizing radiation to produce cytotoxic effect, which leads to tumor recurrence and poor survival.

Ultrasound has been reported to induce systemic oxyhemoglobin change in animal brain tissue. A study reported focused ultrasound (FUS) combined with oxygen-contained microbubbles prior to RT significantly increased the oxygen content in breast cancers and prolonged animal survival. Therefore, microbubble facilitated FUS may change the tumoral oxygen dynamic and be benefit for RT.

We hypothesize that FUS combined with clinical microbubble (MB-FUS) can locally enhance the cerebral oxygenation. This may sensitize brain tumor's response to RT and enhance therapeutic efficacy. Animal cerebral oxygenation, brain tumor progression and animal survival will be accessed to evaluate the efficacy.

Materials and Methods: To observe the animal cerebral oxygen dynamic of ICR mice (n=4), two circular regions of skull were removed to reveal brain tissue. Animal was intravenously injected with 4μl microbubbles (SonoVue®) and FUS was immediately delivered at one circular region (400kHz, 0.27MPa, duty=1%, PRF=1Hz, duration=60s). The cerebral oxygenation of revealed regions was real-time observed via a tissue oxygenation imager before and after FUS exposure for 90 seconds. To evaluate the effect of MB-FUS on sensitizing brain tumors to radiation, mouse glioma cell GL261 was implanted in the right cerebral hemisphere of C57BL/6 mice. Animal were assigned into three groups: control (n=5), RT (received radiation, n=7) and MB-FUS+RT (received MB-FUS and the subsequent radiation, n=7). On the 5th and 7th day, animal was intravenously injected with 4μl microbubbles. FUS was immediately delivered at implanting site (500kHz, duty=1%, PRF=1Hz, duration=120s) with two output stages. In first stage, the acoustic level ramps up from 0.107 to 0.191MPa. In the second stage, the acoustic level ramps down to 0.107MPa and continuously proceeds to complete the exposure. The mouse brains were than exposed to a single radiation (2Gy). Tumor progression was monitored via MRI and animals were sacrificed at the humane endpoints. Statistical analysis was calculated by a one-way ANOVA, a two-way ANOVA test and a Mantel-Cox log-rank test, respectively. Statistical significance was assumed at $p < 0.05$.

Results: The cerebral perfusion and oxygen dynamic were observed before and after MB-FUS treatment. The relative mean oxyhemoglobin concentration of FUS-treated regions ($\Delta AU=26.60\pm14.28$ at 90s, $p < 0.05$) was significantly elevated after FUS compared to the control regions ($\Delta AU=-5.95\pm14.12$ at 90s) (Fig. 1b). The relative mean perfusion level of FUS-treated regions ($\Delta PU= -40.15\pm76.82$ at 90s) was slightly higher than the control regions ($\Delta PU= -54.80\pm65.71$ at 90s) after FUS (Fig. 1a).

The repetitive treatments of MB-FUS and RT was performed on glioma-bearing animal on day 5 and 7 after tumor implanting. MB-FUS and the combined RT provided most profound brain tumor suppression effect (MB-FUS+RT, 43.43 ± 22.92 on day 26, $p < 0.0001$) compare to control (184.85 ± 10.75) and RT (86.13 ± 14.59) (Fig. 2). This combined treatment also improved the animal survival significantly (MB-FUS+RT, median survival 31 days, $p < 0.01$) compared to control (25 days) and RT (28 days) (Fig. 3).

Conclusions: In this study, we showed that FUS combined with clinical microbubble (i.e. clinical ultrasound contrast agent which is non-oxygen bearing) can locally enhance the cerebral oxygenation. The change of oxygen dynamic in brain tissue may be the important factor of MB-FUS to sensitize brain tumors to the subsequent radiation, which leads to profound tumor growth suppression and animal survival improvement. In summary, FUS combined with clinical microbubble is feasible to serve as a RT sensitizer in brain tumor therapy.

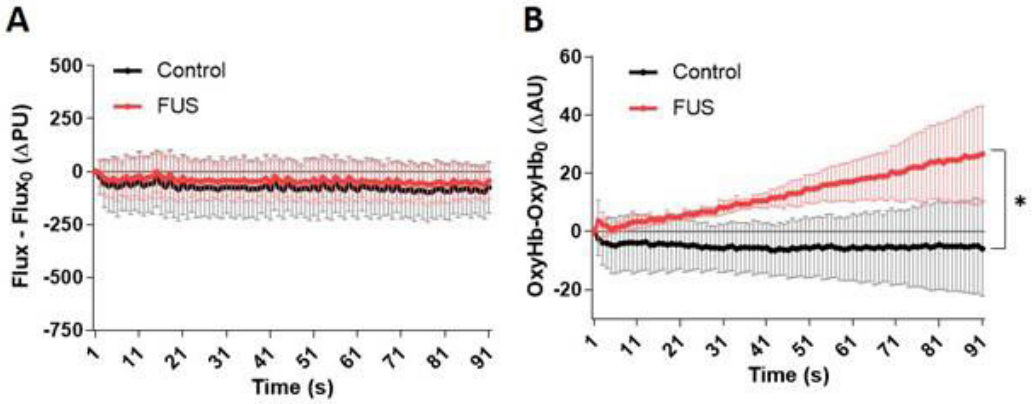

Figure 1. (A) The relative perfusion level (ΔPU) and (B) the relative oxyhemoglobin concentration (ΔAU) dynamic of control and FUS-treated regions before and after MB-FUS treatment. * represents $p < 0.05$.

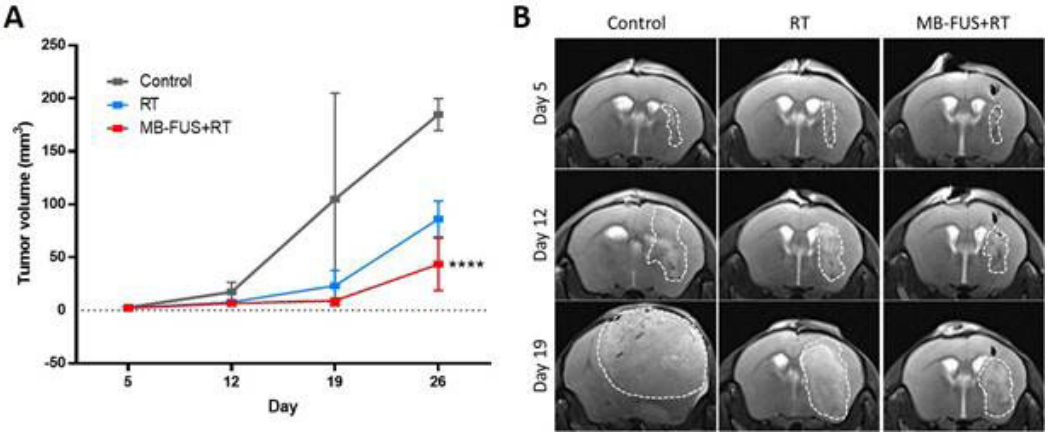

Figure 2. (A) Tumor progression and (B) the representative T2-weighted MR imaging of the brain tumor progression among three animal groups. **** means $p < 0.0001$.

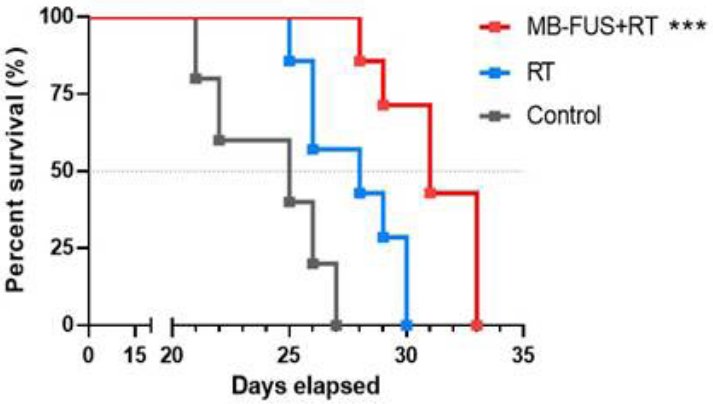

Figure 3. Kaplan–Meier plot demonstrating animal survival among three animal groups. *** means $p < 0.01$.

BTU-3

Topic: Brain Tumors
Presentation Type: Oral

Optimization of focused ultrasound-enabled liquid biopsy (FUS-LBx) in a murine glioblastoma model

Christopher Pacia, Lifei Zhu, Arash Nazeri, Yimei Yue, Jinyun Yuan, Hong Chen

Washington University in St. Louis, St. Louis, MO, USA

Background: Though blood-based liquid biopsy enables noninvasive acquisition of a tumor's molecular profile for diagnosis, the blood-brain barrier (BBB) hinders the efficient release of brain tumor biomarkers into the bloodstream. In our previous studies, we demonstrated the feasibility for focused ultrasound-enabled liquid biopsy (FUS-LBx) to increase BBB permeability and enhance the release of glioma-specific biomarkers into the bloodstream in mice. The objective of this study was to optimize the safety and efficacy of FUS-LBx by evaluating the impact of three key parameters on biomarker release efficiency and safety: FUS pressure, microbubble dose, and blood-collection time.

Materials and Methods: Enhanced green fluorescence protein (eGFP)-transfected murine glioma cells were implanted in mouse brains. Mice were randomly assigned to different groups to evaluate the impact of three key parameters on the efficacy and safety of FUS-LBx: post-FUS blood collection times (10, 30, and 60 min), FUS pressures (0.5, 1.0, and 1.5 MPa), and microbubble doses (8e8, 40e8, and 80e8 microbubbles/mL). A magnetic resonance (MR)-guided FUS system was used to perform FUS sonication after intravenous injection of microbubbles. Contrast-enhanced T1-weighted MR imaging (MRI) was used to evaluate the BBB permeability change post-FUS compared with pre-FUS. Blood was collected after FUS and plasma eGFP mRNA levels were analyzed with quantitative polymerase chain reaction. Mouse brains were collected for H&E analysis of potential FUS-induced hemorrhage.

Results: Contrast-enhanced T1-weighted MRI confirmed successful FUS-induced BBB opening (Fig. A). The robustness of our technique was demonstrated through consistent volumes of contrast enhancement when FUS pressure and microbubble dose were constant. There was a significant increase (p=0.0015) in eGFP mRNA levels in the plasma when the blood samples were collected 10 minutes post-FUS compared with the control group (Fig. B). With longer delays, the average mRNA levels decreased. There were significant increases (p=0.0298, p=0.0013) at 1.0 and 1.5 MPa, respectively (Fig. C). And there were significant increases (p=0.0027, p=0.0023) at 40×108 and 80×108 microbubbles/mL, respectively (Fig. D). There was a non-significant increase in the extent of FUS-induced hemorrhage with increasing FUS pressures and microbubble doses.

Conclusions: This study revealed that FUS pressure, microbubble dose, and blood collection time were important in determining the efficacy of tumor-specific biomarker release and the extent of associated hemorrhage. This study suggested that optimization of FUS-LBx operation parameters could improve the potential for FUS-LBx to be a safe and sensitive technique to diagnose brain tumors.

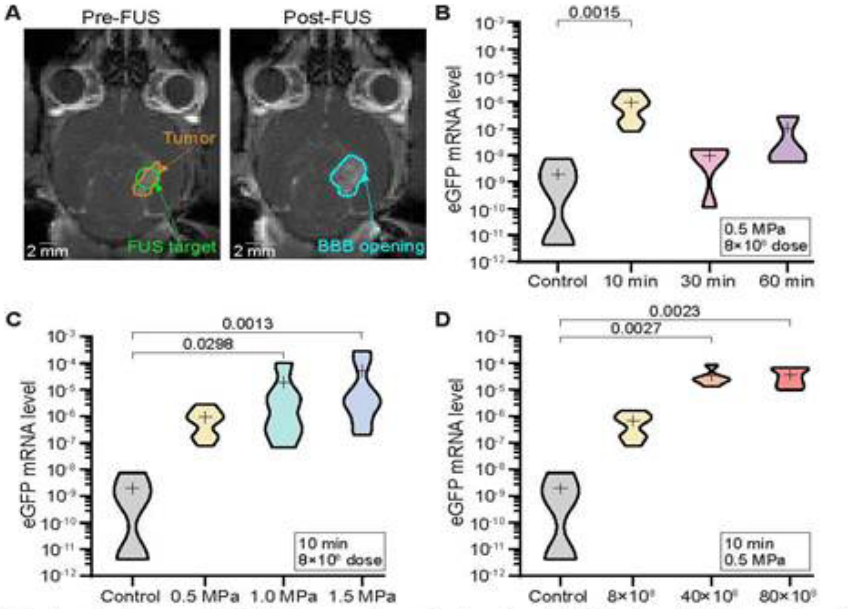

(A) Contrast-enhanced T1W MRI scan shows the localized FUS-induced BBB opening at the target tumor. (B) A significant increase in plasma eGFP levels was only observed when the blood was collected 10 minutes post-FUS. The FUS pressure and microbubble dose were kept constant at 0.5 MPa and 8×108, respectively. (C) There is a positive trend for increasing levels of plasma eGFP mRNA for higher FUS pressures, where the levels are significantly higher at 1.0 and 1.5 MPa. The blood collection time and microbubble dose were kept constant at 10 min and 8×108, respectively. (D) The eGFP mRNA levels in the plasma increased with greater microbubble doses and was significantly higher at 40×108 and 80×108 doses compared with non-treated mice. The blood collection time and FUS pressure were kept constant at 10 min and 0.5 MPa, respectively. The mean of each group is indicated by +.

Acknowledgements: This work was in part supported by the National Institutes of Health (NIH) grants R01MH116981 and R01EB27223. This publication was also partially supported by the NIH/National Center for Advancing Translational Sciences (NCATS) grant UL1TR002345.

BTU-4

Topic: Brain Tumors
Presentation Type: Oral

One-year outcome of multiple blood-brain barrier disruptions with temozolomide for the treatment of glioblastoma

So Hee Park, Jin Woo Chang

Yonsei University College of Medicine, Seoul, South Korea

Background: To overcome the blood-brain barrier (BBB) which interferes with the effect of chemotherapeutic agents, we performed multiple disruption of BBB (BBBD) with magnetic resonance-guided focused ultrasound (MRgFUS) on patients with glioblastoma (GBM) during standard adjuvant temozolomide (TMZ) chemotherapy (Clinical trial registration no.: NCT03712293 (clinicaltrials.gov)). We report a one-year follow-up result of BBBD with TMZ for GBM.

Materials and Methods: From September 2018 to January 2019, six patients were enrolled (4 men and 2 women, median age: 53 years, range: 50-67 years). Of the six patients, five underwent a total of 6 cycles of BBBD during standard TMZ adjuvant therapy. One patient underwent 3 cycles of BBBD but continued with TMZ chemotherapy. The one-year follow-up results of these 6 patients were reviewed.

Results: The mean follow-up duration was 15.17±1.72 months. Two patients showed recurrence of tumor at 11 months and 16 months, respectively. One underwent surgery, and the other patient was restarted with TMZ chemotherapy due to the tumor location with highly possibility of surgical complications. The survival rate up to 1 year was 100% and the other four patients are on observation without recurrence. None of the six patients had immediate or delayed BBBD-related complications.

Conclusions: Multiple BBBDs can be regarded as a safe procedure without long-term complication and it seems to have some survival benefits. However, since TMZ partially crosses the BBB, further extended study with large numbers would be needed to evaluate the benefits of BBBD resulting in an increase of TMZ concentration. This study opened a new therapeutic strategy for GBM by combining BBBD with a larger molecular agent.

Acknowledgements: This study was supported by a grant of the Korea Health Technology R&D Project, Ministry of Health & Welfare.

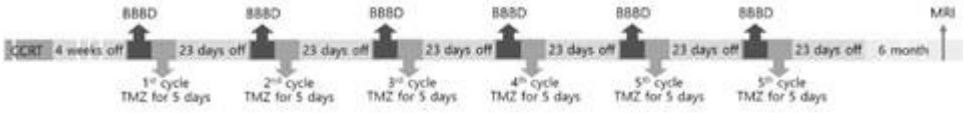

Figure 1.

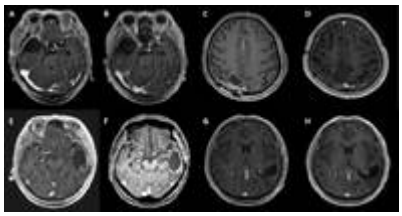

Figure 2.

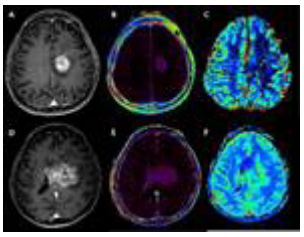

Figure 3.

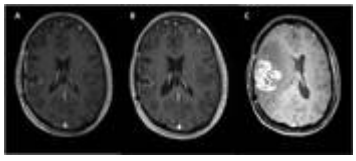

Figure 4.

BTU-5

Topic: Brain Tumors
Presentation Type: Oral

Perfluorobutane phase shift nanoemulsions-facilitated ablation: a transcranial ablation platform with improved lesion localization and tumor ablation efficiency

Chenguang Peng[1], Yongzhi Zhang[2], Chanikarn Power[2], Nathan McDannold[2], Tyrone Porter[3]

[1]Brigham and Women's Hospital, Brookline, MA, USA
[2]Brigham and Women's Hospital, Harvard Medical School, Boston, MA, USA
[3]Boston University, Boston, MA, USA

Background: Microbubble-facilitated ablation is an emerging technology to noninvasively ablate brain tissues. Studies have shown that microbubbles (MBs) excited with ultrasound can impair blood flow, resulting in localized lesion formation. Spatial control of the forced MB oscillation is critical to limit the lesion to the targeted area of the brain. In this study, perfluorobutane (PFB) phase-shift nanoemulsions (PSNE) and ultrasound contrast agents (UCA) were tested for MB-facilitated ablation in the brain. PSNE are nanodroplets that can be vaporized with ultrasound at the transducer focus whereas UCA have a gas core and oscillate throughout the ultrasound beam path. Therefore, it was hypothesized that PSNE would confer greater spatial control of MB-facilitated ablation than UCA. To test the hypothesis, the location and size of lesions of each agent in healthy rats were compared. Additionally, the effectiveness of MB-facilitated ablation of murine brain tumors using each agent was compared.

Materials and Methods: PFB PSNE were synthesized by compressing (~45 psi) PFB MB under dry ice bath (approximate -10 – 15 oC). Sonications were performed using two high intensity focused ultrasound (HIFU) transducers operating at 837 kHz and positioned such that the focal regions overlapped. Sonications were targeted in the left stratum without contrast agents, and then repeated in the left stratum within 1 min after intravenous injection of PFB PSNE (1.5 x 1010 droplets/kg) or Definity UCA (20 µl/kg; ~2.5x106 MBs). In each sonication, we started with ramping pressure pulses (water equivalent pressure ranging from 1.7 to 4 MPa for PFB PSNE and 0.15 to 1.3 MPa for UCA) to determine the IC threshold. For ablation studies, the peak negative pressure of tone bursts (burst length: 10 ms, pulse repetition cycle: 1 Hz) was 5% or 30% above the IC threshold determined for each agent. A combination of MRI and histology was used to compare quantitatively the size and location of lesions resulting from UCA- or PSNE-facilitated ablation in healthy rat brains. T2* images were acquired after sonications using a 7T MRI (Biospin 7T, Bruker) to identify the microhemorrhages that may have resulted from UCA- or PFB PSNE-nucleated cavitation in the blood vessels. In a second study, F98 gliomas established in the caudate putamen of Fischer rat brains were treated with UCA- or PSNE-facilitated ablation. The animals were sacrificed 5 days after treatment for histological analysis of the tumors.

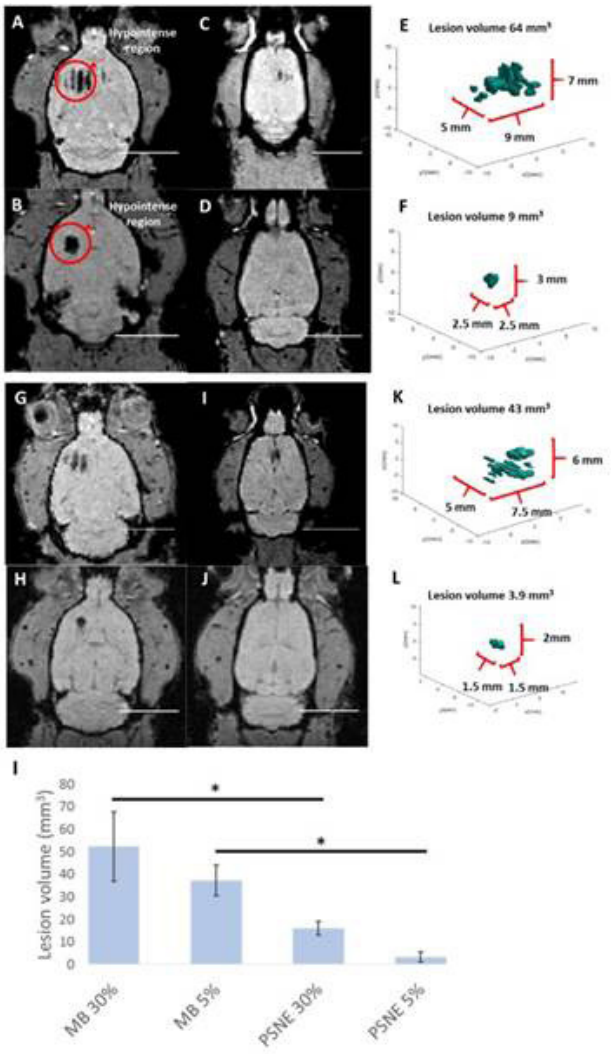

Figure 1. Representative MRI T2* images of subjects received with PSNE or MB ablation at acoustic pressure 30% or 5% higher than the inertial cavitation threshold.

Results: As shown in Figure 1, PFB PSNE-facilitated ablation generated smaller lesions than UCA-facilitated ablation at both 5% and 30% above the IC threshold (Figure 1A, B, G&H). The mean lesion size in the UCA group at 5% and 30% above the IC threshold was 37.3±6.8 mm3 and 52.4±15.4 mm3 while PFB PSNE generated a significantly smaller lesion (3.3±2.4 mm3 and 16.0±3.1 mm3, respectively). Unlike the PSNE group, there was pre-focal damage in the UCA group (Figure 1C, D, I&J).

Figure 2 presents MRI examples of brain tumors before and after different treatments. In the UCA group, a hypointense ring formed at the periphery of the tumor, suggesting that microhemorrhages were concentrated in blood vessels at the tumor rim. Conversely, PSNE-facilitated ablation created a hypointense region that covered the whole tumor area. H&E staining confirmed this finding (Figure

3). A larger fraction of treated brain tumor was killed in the PFB PSNE group (89.4 ± 6.3%) than in the UCA group (11.1 ± 7.7%).

Conclusions: In this study, PFB PSNE- and UCA-facilitated ablation were used to create lesions in healthy tissue and showed distinctive damage patterns. PFB PSNE-facilitated ablation generated smaller lesions than UCA-facilitated ablation while preventing pre-focal damage. In addition, PFB PSNE-facilitated ablation was able to destroy tumors more effectively than UCA-facilitated ablation. The IC from MB created damage predominantly at the periphery of the tumors. On the contrary, PFB PSNE-FA induced mechanical destruction of a large fraction of the tumor volume. These results demonstrate that PFB PSNE can facilitate safe and effective brain tumor ablation via improved spatial control of cavitation-mediated tumor destruction and lesion formation.

Acknowledgements: NIH grant P01CA17464501 and R21EB027506, BU-BWH partnership

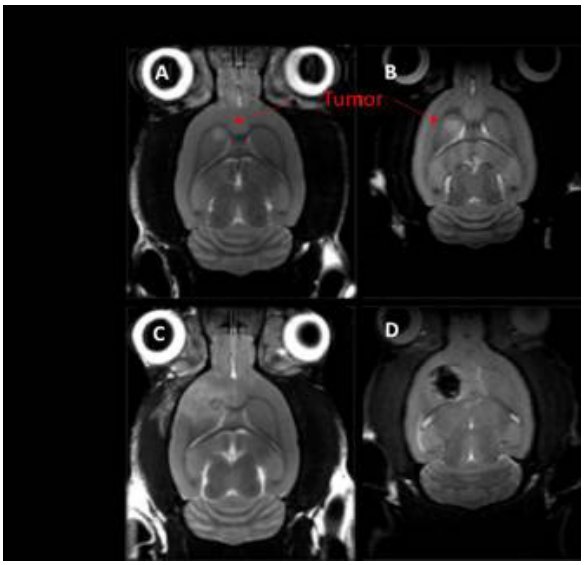

Figure 2. T2-weighted images of MB-facilitated ablation and PFB PSNE-facilitated ablation.

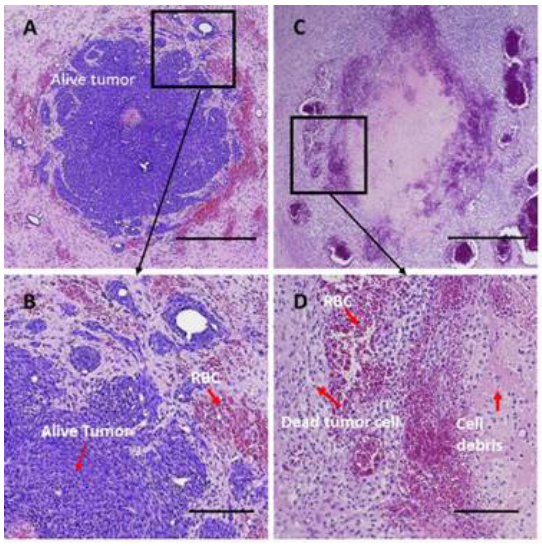

Figure 3. Histology of tumors after MB- or PFB PSNE-facilitated ablation.

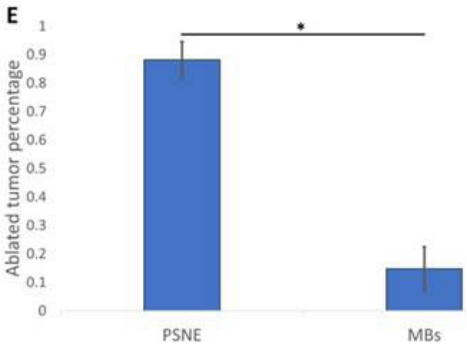

BTU-6

Topic: Brain Tumors
Presentation Type: Oral

Focused ultrasound enhances checkpoint blockade immunotherapy for glioblastoma via targeted immunomodulation

Tao Sun[1], Meenal Datta[2], Sampurna Chatterjee[2], Yongzhi Zhang[1], Chanikarn Power[1], Yan Gao[3], Pragya Kumar[2], Gino Ferraro[2], Gordon Freeman[3], David Reardon[3], Rakesh Jain[2], Nathan McDannold[1]

[1]Brigham and Women's Hospital, Harvard Medical School, Boston, MA, USA
[2]Massachusetts General Hospital, Harvard Medical School, Boston, MA, USA
[3]Dana-Farber Cancer Institute, Harvard Medical School, Boston, MA, USA

Background: Conventional checkpoint blockade immunotherapy (CBI) for treating glioblastoma (GBM) is challenged by its immunosuppressive microenvironment, with insufficient T lymphocyte infiltration and excessive M2-like myeloid cells. To improve the efficacy of CBI, novel approaches that can reverse this 'cold' immune microenvironment are desperately needed. Such interventions are particularly expected to enhance the delivery of immunotherapeutics across the blood brain/tumor barriers, lymphocyte infiltration, and reprogramming of macrophages/microglia. Here we report the use of microbubble-mediated focused ultrasound (FUS) to alter the tumor microenvironment in a targeted manner during CBI. FUS is hypothesized to open the blood-tumor barrier for enhanced antibody delivery and immune cell trafficking, and to facilitate controllable inflammation for the recruitment and activation of immune effectors.

Materials and Methods: Tested in a GBM murine model GL261-Luc2, FUS immunomodulation effects were compared with or without anti-PD1 treatment. To characterize the immune response, brains (tumors), spleens, and superficial cervical lymph nodes were harvested and homogenized for flow cytometry. In the survival study, FUS was applied on Day 14 and Day 20 after the tumor inoculation. Therapeutic antibodies and isotype controls were administered via intraperitoneal injection beginning on Day 11 (500 μg) after tumor implantation with repeat injections every 3 days (250 μg/dose) for a total of four injections. Bioluminescent imaging and MRI were used for monitoring tumor growth and FUS treatment planning. Long-term survivors who survived over 90 days were re-challenged by injecting the same tumor cells intracranially into the contralateral hemisphere.

The sonication was performed using a house-made single-element transducer (f-number = 0.875) operating at 690 kHz. To monitor the bubble activities, a passive cavitation detector (f0 = 1.5 MHz, 25% bandwidth) recorded the acoustic emissions produced during each burst. For each animal, we sonicated at four locations (a 2 by 2 grid with 1-mm spacing) to cover the whole tumor. A pulse train containing 10-ms pulses at 4-Hz pulse repetition frequency was applied at each target at the acoustic pressure of 320 kPa. Optison bubbles were injected through the tail vain at a dose of 100 μL/kg.

Results: In a GBM murine model treated with PD-1 inhibitors, our results demonstrate that FUS enhances T cell infiltration and macrophage reprogramming locally. Flow cytometry results (Fig. 1) show that the combination treatment significantly enhanced CD3+ T cell infiltration (Fig. 1A) and TIM3 expression on cytotoxic T cells (Fig. 1B). In addition, FUS was found to be able to polarize tumor-associated macrophages (Fig. 1C) towards the M1 phenotype (defined as CD86+ CD206- subpopulation in the cells of interest). Similar M1 polarization effects were also observed in macrophages in the cervical lymph nodes and spleen. Finally, the FUS-aPD1 approach ($n = 8$) provided significantly increased survival benefits (Fig. 2) compared to aPD1 monotherapy ($n = 7$, $P < 0.05$) and IgG control group ($n = 6$, $P < 0.001$). Due to the outbreak of COVID-19, the survival study of IgG + FUS group could not be finished at the time of abstract submission.

Conclusions: Our results provide important preclinical proof-of-principle for pairing FUS with CBI in treating GBM. Given the potential for microbubble-mediated FUS to enhance anti-tumor immunity and reduce tumor burden in combination with CBI, ongoing works are evaluating 1) the dynamics of immune cell infiltration into the GBM microenvironment with FUS, and 2) optimized protocols of FUS and CBI for superior treatment efficacy.

Acknowledgements: Focused Ultrasound Foundation (NJM and DAR), NIH R35CA197743 (RKJ).

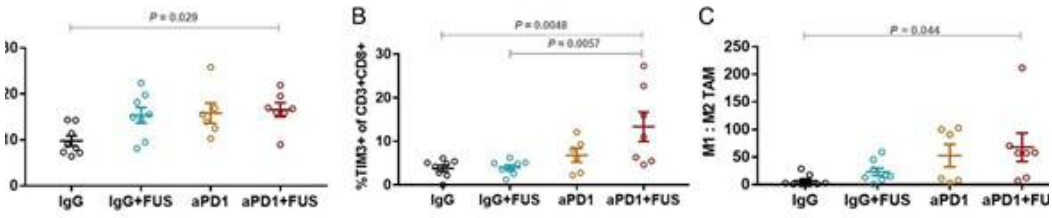

Figure 1. Flow cytometry results in brain show that FUS enhances T cell infiltration and macrophage reprogramming locally. Statistical significance was determined by one-way ANOVA with Tukey post hoc tests.

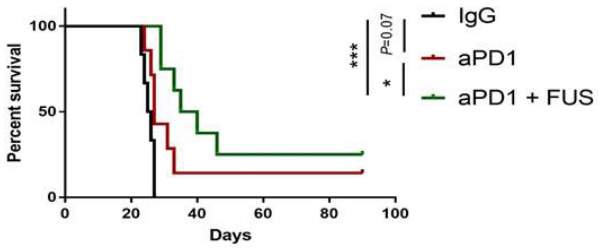

Figure 2. Long-term survival curves comparing IgG control (n = 6), aPD1 only (n = 7), and FUS-PD1 combination therapy (n = 8) groups.

BTU-7

Topic: Brain Tumors
Presentation Type: Oral

Initial experience with focused ultrasound surgery for central brain lesions in children and young adults

Shelly Wang[1], Kambiz Alavian[2], Nolan Altman[1], Michael Duchowny[1], Ian Miller[1], John Ragheb[1], Travis Tierney[2]

[1]Nicklaus Children's Hospital, Miami, FL, USA
[2]Imperial College London, Hammersmith Hospital, London, United Kingdom

Background: We are evaluating the safety and feasibility of transcranial magnetic resonance image-guided focused ultrasound thermoablation for the treatment of benign centrally-located brain tumors in 10 children and young adults (IDE no. G160189). This report describes our first five cases.

Materials and Methods: IRB approval and informed consent were obtained to treat 3 females and one male with hypothalamic hamartomas and one male with a subependymal giant cell astrocytoma associated with tuberous sclerosis complex (TSC). All patients were treated under general anesthesia using the Exablate 4000 system (INSIGHTEC Ltd., Tirat Carmel, Israel). The study is open to subjects 8 to 22 years of age who require surgical intervention for a benign centrally-located brain tumor. Please see ClinicalTrials.gov identifier NCT03028246 for full exclusion and inclusion criteria.

Results: Thermoablation of target tissue was achieved in 3 patients (21, F; 22, F; 19, M) with epilepsy related hamartomas with immediate cessation of gelastic seizures in 2 of these 3 patients (Figure 1). Another patient (15, F) with hyperphagia and obesity (but not epilepsy) related to her hamartoma experienced an effortless 13kg weight loss over six months after her surgery (Figure 2). Near-field calcium and acoustic cavitation events precluded complete thermal ablation of the subependymal giant cell astrocytoma in the patient (19, M) with TSC. No postoperative endocrine, cognitive or motor complications occurred in any case.

Conclusions: Focused ultrasound surgery can be used safely to treat epilepsy and hyperphagia associated with hypothalamic hamartomas. It is less certain that calcium-bearing tumors like subependymal giant cell astrocytomas can be treated with focused ultrasound. More work is necessary to further refine optimal patient selection criteria, determine the long term therapeutic durability of this approach, and definitively demonstrate the safety of focused ultrasound in younger children with other begin central tumors.

Acknowledgements: The Focused Ultrasound Foundation of Virginia (grant no. FUS 530 to TST) funded this trial (ClinicalTrials.gov identifier NCT03028246). The device manufacturer, InSightec Ltd., is our FDA regulatory sponsor but we have not requested any commercial financial support for this study. We thank Mor Dayan, B.Sc. and Jacob Chen, B.Sc. (InSightec Ltd.) for technical support of these cases. Patricia Dean, ARNP, MSN coordinates the comprehensive epilepsy center at Nicklaus Children's Hospital and skillfully cared for our patents.

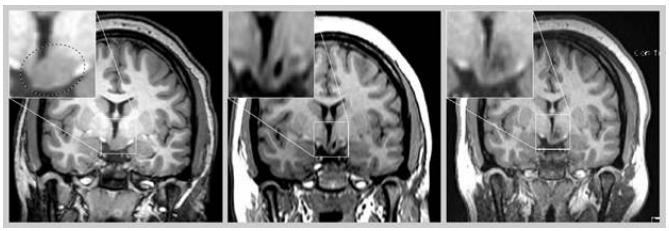

Figure 1.

Figure 2.

BTU-8

Topic: Brain Tumors
Presentation Type: Oral

Blood-brain barrier opening by focused ultrasound enhances etoposide delivery for glioblastoma treatment

Hong-Jian Wei, Pavan Upadhyayula, Antonios Pouliopoulos, Zachary Englander, Xu Zhang, Chia-Ing Jan, Jia Guo, Angeliki Mela, Zhiguo Zhang, Tony Wang, Jeffrey Bruce, Peter Canoll, Neil Feldstein, Stergios Zacharoulis, Elisa Konofagou, Cheng-Chia Wu

Columbia University, New York, NY, USA

Background: Glioblastoma (GBM) is a devastating disease and even with the current treatment of surgery followed by chemoradiation, the outcomes remain poor with a median survival of 15 months and 5-year survival of 6.8%. The heterogeneous integrity of the blood-brain barrier (BBB) in GBM tumors largely limits the bioavailability of systemic treatments to the brain. There is a growing interest in enhancing drug delivery by overcoming the BBB limits with the use of focused ultrasound (FUS). Herein we hypothesize that FUS-mediated BBB opening can enhance the delivery of etoposide for a therapeutic benefit in GBM.

Materials and Methods: A murine glioma cell line (Pdgf+, Pten-/-, P53-/-) was intracranially injected into B6(Cg)-Tyrc-2J/J mice to establish the syngeneic GBM model for this study. Animals were treated with FUS and microbubbles (MBs) to open the BBB and to enhance the delivery of systemic etoposide. We used passive cavitation detection (PCD) transducer to acquire acoustic emissions from MBs and magnetic resonance imaging (MRI) to evaluate BBB opening and tumor progression. Liquid chromatography-mass spectrometry was used to measure the concentrations of etoposide concentrations in the GBM tumors.

Results: The murine glioma cell line was sensitive to etoposide in vitro and generated xenografts with diffusely infiltrative features of GBM. MRI and PCD demonstrated the successful BBB opening by FUS and persistent stable cavitation activity during sonication with minimal inertial cavitation. The treatment combining FUS and etoposide decreased tumor growth by 45% and prolonged median overall survival by 31.58%. FUS-mediated BBB opening increased not only the brain tumor-to-serum ratio of etoposide by 3.5-fold but also the etoposide concentration in brain tumor tissue by 8-fold as compared to without BBB opening.

Conclusions: Our study currently demonstrates that BBB opening with FUS enhances intratumoral delivery of etoposide in the brain resulting in local control and overall survival benefits of GBM tumors in mice.

Acknowledgements: We thank Maggie and Jacob Dyson, and the Zuckerman Mind Brain Behavior Institute MRI Platform, a shared resource. This research was funded by the Gary and Yael Fegel Family Foundation, Star and Storm Foundation, Matheson Foundation (UR010590), Herbert Irv

BTU-9

Topic: Brain Tumors
Presentation Type: Oral

Neuronavigation-guided focused ultrasound (navifus) for transcranial blood-brain barrier opening in recurrent glioblastoma patients

Kuochen Wei, Koting Chen

Chang Gung Memorial Hospital, Kweishan, Taiwan (Republic of China)

Background: Blood-brain barrier (BBB) limits over 95% of drugs' penetration into brain, which has been a major obstacle in treating patients with glioblastoma. Transient BBB opening in glioblastoma (GBM) is feasible by combining focused ultrasound (FUS) with systemic infusion of microbubbles (MB).

Materials and Methods: OBJECTIVES neuronavigaiton-guided focused ultrasound, a novel device that integrates neuronavigation and FUS-MB system, is able to intraoperatively direct the ultrasound energy precisely and repeatedly at targeted CNS areas. This clinical trial evaluates the safety and feasibility of NaviFUS in recurrent glioblastoma patients.

METHODS The study is a first-in-human, prospective, open-label, single-center, single-arm, dose escalation phase 1 clinical trial. A total of 6 patients will be enrolled. Patients will be enrolled into three groups, each group receiving an escalating dose of FUS energy (acoustic power is 4, 8, and 12W) with concomitant systemic microbubbles (0.1ml/kg) applied 1 week before surgical resection.

Results: Dynamic contrast-enhanced MRI will be obtained immediately and 24 hours after FUS procedures, while heavily T2-weighted sequence will be obtained to evaluate for any micro-hemorrhages. We anticipate that there will be minimal side effects associated with neuronavigaiton-guided focused ultrasound-mediated transient BBB opening.

Conclusions: Obtained results will support a planned phase 2 trial to evaluate whether neuronavigaiton-guided focused ultrasound can effectively enhance the delivery of chemotherapeutic agents and improve tumor control.

Acknowledgements: NaviFUS inc

CHP-1

Topic: Chronic Pain
Presentation Type: Oral

Young Investigator

Bilateral magnetic resonance-guided focused ultrasound thalamotomy of the central lateral nucleus for medically-refractory neuropathic pain

Abdul-Kareem Ahmed, Jiachen Zhuo, Joel Greenspan, Howard Eisenberg, Charles Sansur, Elias Melhem, Rao Gullapalli, Dheeraj Gandhi

University of Maryland School of Medicine, Baltimore, MD, USA

Background: Neuropathic pain (NP) is a chronic pain syndrome resulting from lesions involving the central or peripheral somatosensory nervous system. It is a highly prevalent disorder that is often resistant to pharmacotherapy. Therefore, there is a need for more effective therapies that demonstrate greater specificity, reduced potential for abuse, and potential improvement of other facets of pain such as its debilitating effect on behavior and cognition. This early phase I trial is aimed to determine the safety and efficacy of

MR-guided focused ultrasound (MRgFUS) central lateral thalamotomy (CLT) for NP.

Materials and Methods: Seven patients have been enrolled at University of Maryland with medically-refractory NP, all with at least 6 months of symptoms and with an eligible skull density ratio (SDR≥0.40) (NCT03111277). Primary outcomes of this study are the safety and feasibility of MRgFUS CLT, and secondary outcome is effectiveness, assessed by widely used and validated tools. These tools include the pain Numeric Rating Scale (NRS), the Pain Disability Index (PDI), and the Brief Pain Inventory (BPI). The central lateral nucleus was first targeted with stereotactic coordinates. The location was adjusted based on magnetic resonance data and patient feedback before thermal ablation was made permanent. Patients were continuously monitored for side effects.

Results: This interim analysis presents the results after the completion of the first five patients. Four men and one woman were treated (mean age 53.6±11.0 years). No serious adverse events were noted and all mild adverse events, including headache or headframe discomfort, resolved within two weeks. Four patients underwent bilateral CLT with MRgFUS, one unilateral secondary to tolerating the procedure (Figure 1). The average SDR was 0.49±0.03 (range 0.45-0.53). At 3 months, mean reduction in BPI was 59.9 percent (p=0.003) (Figure 2), and mean reduction in PDI was 42.0 percent (p=0.044) (Figure 3). Reduction in pain metrics was maintained at one year in four patients with follow-up data. All patients had some reduction in their daily use of analgesic medications.

Conclusions: MRgFUS thalamotomy of the central lateral nucleus may offer a promising technique for patients with neuropathic pain. CLT in this series caused no serious adverse events. The treatment results in meaningful reduction in pain scores as reported. Compared to prior series, patients had a more uniform response. Pain medication use decreased, suggesting a role for CLT in providing analgesic-sparing relief. Long-term data are needed to assess durability of response and to identify subgroups of patients most likely to benefit from this procedure.

Figure 1. Axial T1-weighted MRI demonstrating central lateral thalamotomy at 1 day, 30 days, and 12 months post-procedure.

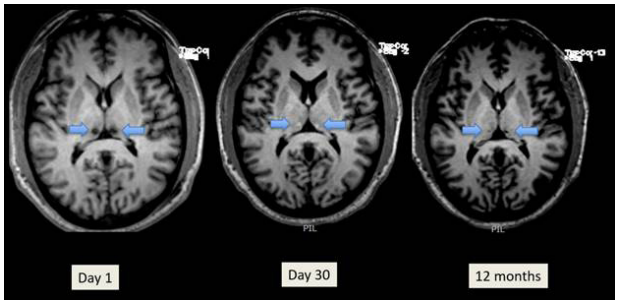

Figure 2. Brief Pain Inventory (BPI) scores at 3 and 12 months after MR-guided focused ultrasound central lateral thalamotomy (CLT)

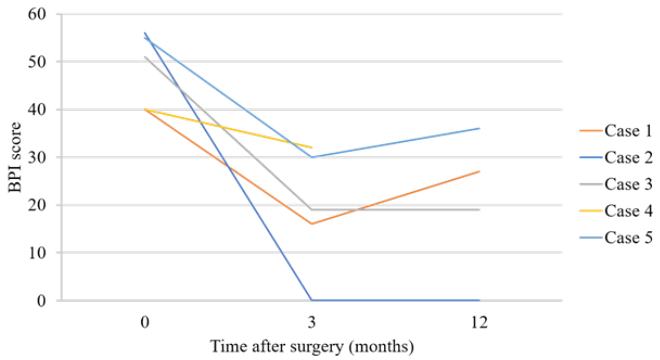

Figure 3. Pain Disability Index (PDI) scores at 3 and 12 months after MR-guided focused ultrasound central lateral thalamotomy (CLT)

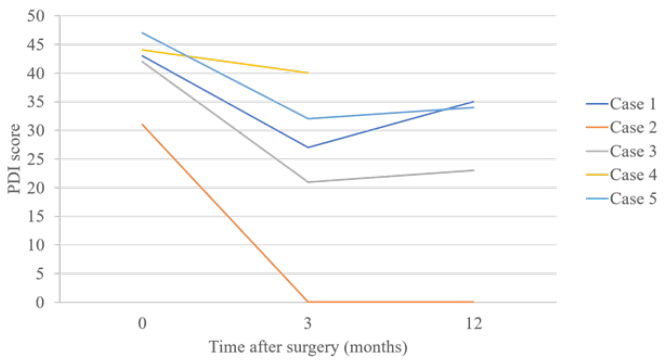

CHP-2

Topic: Chronic Pain
Presentation Type: Oral

MRI-guided transcranial focused ultrasound to modulate pain thresholds in healthy adults: A double-blind, concurrent tFUS/MRI study

Bashar Badran[1], Kevin Caulfield[1], Sasha Stomberg-Firestein[1], Philipp Summers[1], Logan Dowdle[2], Matt Savoca[1], Xingbao Li[1], Christopher Austelle[1], Baron Short[1], Jeffrey Borckardt[1], Norman M Spivak[3], Alexander Bystritsky[3], Mark George[1]

[1]Medical University of South Carolina, Charleston, SC, USA
[2]University of Minnesota, Minneapolis, MN, USA
[3]University of California, Los Angeles, Los Angeles, CA, USA

Background: Transcranial focused ultrasound (tFUS) via low intensity focused ultrasound pulsation (LIFUP) is a noninvasive brain stimulation method that may modulate deep brain structures. We investigated whether sonication of the right anterior thalamus would modulate thermal pain thresholds in healthy individuals.

Materials and Methods: We enrolled 19 healthy individuals in this three-visit, double-blind, randomized, sham-controlled, crossover trial. Participants had a first structural MRI scan for LIFUP targeting. They then attended two identical experimental LIFUP/MRI visits (counterbalanced by condition) at least one week apart. Within the MRI scanner, participants received two, 10-minute sessions of either active or sham LIFUP spread 10 minutes apart to the right anterior thalamus [frequency: 650kHz, pulse repetition frequency: 10 Hz, pulse width: 5ms, duty cycle: 5%, sonication duration: 30s, inter-sonication interval: 30s, number of sonications: 10/session, ISPTA3 = 719 mW/cm2]. The primary outcome measure was quantitative sensory thresholding (QST), measuring sensory, pain, and tolerance thresholds to a thermal stimulus applied to the left forearm before and after right anterior thalamic LIFUP.

Results: The right anterior thalamus was sonicated in 17 of the 19 subjects. Thermal sensitivity was significantly attenuated after active LIFUP (0.51 degree change, SE=0.30) relative to sham stimulation (1.08 degree change, SE=0.28) ($p = 0.046$). LIFUP also changed sensory and tolerance thresholds however this was not statistically significant.

Conclusions: Two 10-minute sessions of anterior thalamic LIFUP has antinociceptive effects in healthy individuals. Future studies should optimize the parameter space, dose and duration of this effect which may lead to multi-session LIFUP interventions for pain disorders.

Acknowledgements: The Tiny Blue Dot Foundation provided financial support for this study.

CHP-3

Topic: Chronic Pain
Presentation Type: Oral

Modulation of pain in humans via ultrasound peripheral nerve stimulation

Stephen Lee, Hermes Kamimura, Elisa Konofagou

Columbia University, New York, NY, USA

Background: The peripheral nervous system translates all motor and sensory signals, including noxious pain, from the periphery to the brain. Our previous findings demonstrated that focused ultrasound (FUS) applied to the sciatic nerve in mice can evoke [1] and suppress [2] motor responses. Though many neuroscientific questions can be explored in animal models, the understanding of pain remains elusive; thus, studies in humans are necessary. We have shown in preliminary results that FUS can suppress electrically-induced somatosensory evoked potentials [3]. Currently, we are evaluating the capability of FUS for the suppression of pain from the C6 dermatome. Thus, we asked whether direct nerve FUS neuromodulation can alter pain sensation levels in healthy human subjects.

Materials and Methods: Eleven (n=11) healthy human volunteers were enrolled in this study. All methods were performed with the approval of the Columbia University Institutional Review Board. We developed a dual-mode ultrasound system composed of a confocal 7.8 MHz imaging probe and a 1.1 MHz, 4-annular array FUS transducer to both target with displacement imaging and stimulate the median nerve at the distal region of the forearm. Both transducers were driven with a single 256 Verasonics Vantage system. The imaging reconstruction was CUDA-accelerated using an NVIDIA Tesla k40c GPU to enable real-time displaying of both B-mode and displacement imaging. Noxious thermal stimuli at the skin of the subject's palm were used to elicit pain via TRP channels in free nerve endings of c-fiber neurons using a custom-built thermal stimulation device. The heat pulse signal consisted of a 5-s baseline at skin temperature (30-32°C) followed by a 2-s rise to the subjects' perceived threshold for pain (37-40°C), which was acquired at baseline. Subsequently, there was a 2-3 minute-interval (randomized) in between pulses to allow for the cessation of peptidergic release, i.e., upregulation of peptides (calcitonin gene-related peptide, substance P, neuropeptide Y) in the skin, responsible for either reducing the threshold or enhancing the magnitude of response to a stimulus. Subjects received 15 thermal stimulations with randomized FUS/sham pulses and rated their pain sensation using the Wong-baker pain scale.

Figure 1. B-mode imaging of the median nerve and displacement imaging technique.

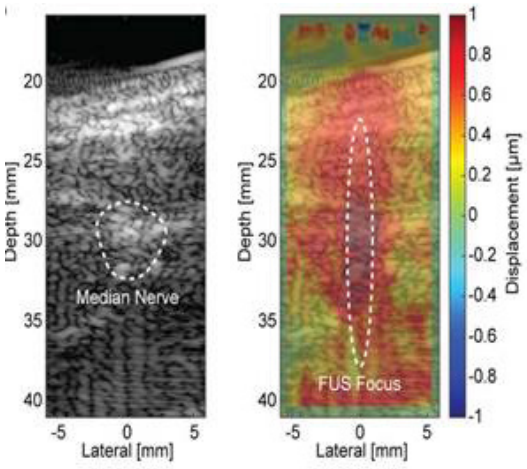

Results: A correlation with the interframe displacement induced during FUS was found with reported pain sensation between FUS and sham pulses. FUS decreased subjective pain ratings significantly in two subjects ($p < 0.05$) and trending in another two subjects but not significantly ($p = 0.0713$ and $p = 0.1108$) using a paired t-test. Subjects were grouped into 3 groups based on displacement measured during FUS (Fig. 1). A 2-way ANOVA indicated that the decrease in pain ratings between the two groups was significantly different (Fig. 2). Multiple comparisons show that the group receiving nerve displacements between 28 and 62 microns had significantly different changes in sensations than the other groups.

Figure 2. Double-blinded results of within-subject changes in pain ratings over 15 thermal stimulations with randomized FUS and sham pulses.

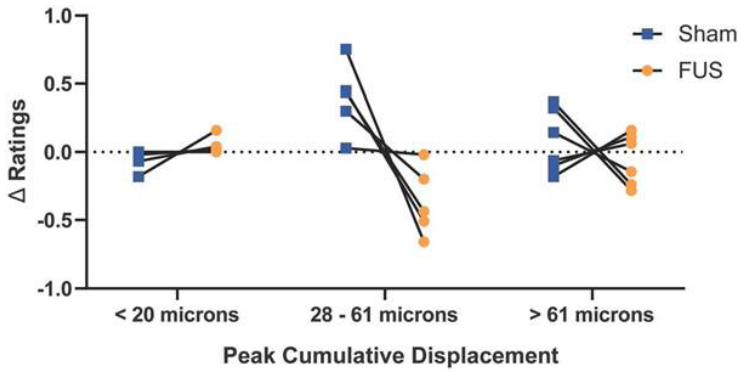

Conclusions: FUS applied to the median nerve consistently reduced pain sensation elicited by noxious heat pulses delivered on the dorsum of the hand of healthy subjects. Our results indicate that sufficient nerve displacement >28 microns) must be achieved to cause changes in nociceptive pain within subjects. Our method revealed that displacement, rather than transducer driving pressure, is a more accurate measure of therapeutic dosage to the nerve. Using FUS at the peak of thermal stimulation may acutely decrease reported pain sensations. This study thus provides the basis for further development of a FUS-based therapeutic technique for peripheral pain control.

DRD-1

Topic: Drug Delivery
Presentation Type: Oral

Acoustically detonated biomolecules for targeted and genetically encoded cavitation

Avinoam Bar-Zion, Atousa Nourmahnad, David R. Mittelstein, Shirin Shivaei, Ojas Pradhan, Dina Malounda, Mohamad Abedi, Audrey Lee-Gosselin, David Maresca, Mikhail G. Shapiro

California Institute of Technology, Pasadena, CA, USA

Background: Despite the many achievements of nanomedicine, passive delivery of anti-cancer drugs is frequently limited to the proximity of functional blood vessels, resulting in heterogeneous therapeutic effects. Cell therapy is an emerging approach for active drug delivery based on engineered cells that can home to tumor cells, colonize their cores, and produce drugs in-situ. However, this technology has limited mechanisms for non-invasive control and physical action. In this work, we propose to use ultrasound cavitation to selectively activate these cells and equip them with a new mechanical toolbox. Our approach is based on gas vesicles (GVs), a family of gas-filled protein nanostructures. Our lab recently introduced GVs as the first acoustic reporter genes, heterologously expressing them in both bacteria and mammalian cells. Here we demonstrate the use of GVs as genetically encoded cavitation nuclei in vitro and in vivo and investigate the resulting bioeffects on surrounding cells and tissues.

Materials and Methods: Although single GVs have nano-scale sizes, they are frequently found in multi-GV aggregates when expressed in bacterial and mammalian cells (Fig. 1). Similarly, when attached to mammalian cells, they usually form multi-GV patches. We hypothesized that low-frequency ultrasound could collapse the shells of GVs, and use the released gas to nucleate cavitation activity. Passive acoustic measurements and high-frame-rate microscopy were used to quantify cavitation activity and validate our model for GV cavitation. The ability of GVs to facilitate controlled release of co-expressed therapeutics from tumor-homing Salmonella typhimurium bacteria was tested using a bioluminescent protein as a payload model. Next, we compared the number of colony-forming units with and without ultrasound exposure to test for selective lysis of GV expressing bacteria. Similarly, controlled lysis of mammalian HEK cells was evaluated using flow cytometry. The ability of GV cavitation to propel payload molecules was tested using tissue-mimicking phantoms. Finally, we studied GV cavitation in vivo using BALB/c mice models. In vivo cavitation of GVs administered into MC26 tumors was measured using passive cavitation detection. The effect of GV cavitation on surrounding tissue was evaluated by systemic tail-vein injection of GVs and subsequent insonation of the medial liver lobe. We selected this tissue as our target due to its homogeneity and the natural accumulation of circulating GVs inside it.

Results: Passive cavitation measurements from purified GVs (f0 = 0.67MHz) and GV expressing cells (f0 = 0.33MHz) were significantly higher than all the controls. High-frame-rate microscopy at 5Mfps captured the collapse of GV and subsequent formation of large micro-scale bubbles over time scales of several cycles. The insonation of GV-expressing bacteria leads to their lysis, with a 42% decrease in the number of colony-forming units. As a result, we measured a 16-fold increase in the released concentration of the co-expressed payload (Fig. 2). Likewise, insonation triggered the lysis of GV-expressing mammalian cells. Moreover, GV cavitation propelled and dispersed payload molecules into tissue-mimicking agarose phantoms. Finally, we showed that GVs taken up by in vivo tissues can seed cavitation activity, producing local hemorrhage and necrosis (Fig. 3). GVs administered to subcutaneous tumors nucleate robust cavitation, quantified using passive cavitation measurements.

Conclusions: In this work, we demonstrated the use of GVs as genetically encoded cavitation nuclei. Cavitation activity nucleated by GVs can lyse tumor-homing engineered cells and release co-expressed molecular payloads. In vivo, GV seeded cavitation produced direct damage to the surrounding tissue. The selective production of GVs and their contrast in many imaging modalities, such as ultrasound and MRI imaging, could be used for treatment guidance and monitoring. In situ expression of GVs in tumor-colonizing bacteria would allow these cells to nucleate deep-tissue drug delivery and disruption of tumors, opening a range of new theranostic possibilities. Similarly, the recent expression of GVs in mammalian cells could enable new immunotherapy approaches.

Acknowledgements: This project was supported by the David and Lucile Packard Fellowship for Science and Engineering (MGS) and the Heritage Medical Research Institute (MGS). In addition, this project has received funding from the European Union's Horizon 2020 research and innovation programme under the Marie Skłodowska-Curie grant agreement No. 792866 (AB-Z).

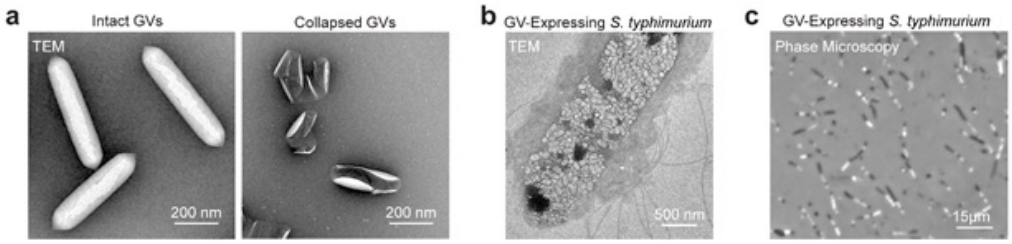

Figure 1. a, Purified Anabaena flos-aquae GVs. b, TEM image of GV expressing S. typhimurium cells. c, Phase-contrast microscopy of GVs (in white) inside S. typhimurium cells.

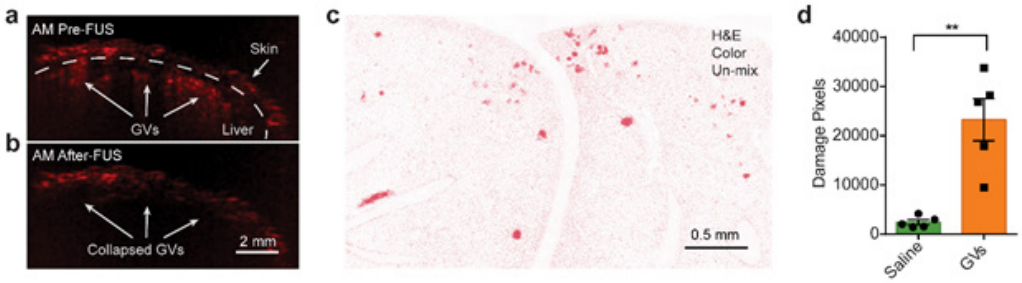

Figure 2. a, Illustration of intra-cellular GV cavitation. b, Structure of the plasmid containing the gas vesicle gene cluster, and the payload gene. c, Controlled payload release using ultrasound.

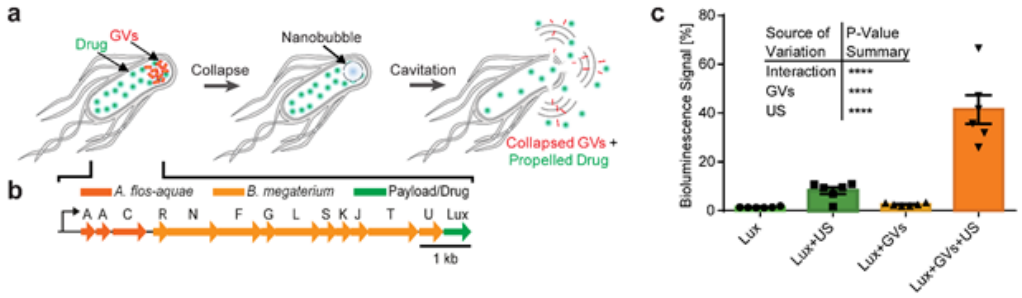

Figure 3. a, Ultrasound scan showing GV accumulation inside the liver. b. The signal is erased after insonation. c, GV cavitation produces local tissue damage. d, Number of pixels with damaged tissue.

DRD-2

Topic: Drug Delivery
Presentation Type: Oral

Validation of SonoTran®: A cavitation-enhanced drug delivery system

Calum Crake[1], Paul Boulos[1], Maura Power[1], Edward Ellis[1], Florian Monnier[1], Alessandro Polcaro[1], Massimo Masiero[1], Michael Gray[2], Robert Carlisle[2], Constantin Coussios[2], Christian Coviello[1], Cliff Rowe[1]

[1]OxSonics Therapeutics, Oxford, United Kingdom
[2]University of Oxford, Oxford, United Kingdom

Background: Cavitation-enhanced delivery has been shown to improve the dose, distribution, and efficacy of oncology agents across all drug classes including small-molecules, oncolytic viruses, monoclonal antibodies and antibody-drug conjugates (ADCs). This could lead to both improved anti-tumor response and reduced systemic toxicity through a lowered therapeutic dose. The SonoTran System, a mobile therapeutic ultrasound platform featuring a novel handheld probe has been developed to be used in combination with infusion of a gas-stabilizing cavitation agent, SonoTran Particles, to enhance drug delivery of any systemically-administered oncology agent. One of the key features of the system is real-time cavitation monitoring using passive acoustic mapping (PAM), which has been shown in pre-clinical experiments to provide an effective marker for drug delivery. This work describes translation and validation of laboratory and in-vivo experimental methods into a calibrated and safe clinical system.

Materials and Methods: The SonoTran System performs three functions: B-mode imaging for guidance, long-duration therapeutic ultrasound pulsing for instigation of cavitation from SonoTran Particles to promote active transport of therapeutics, and PAM for real-time monitoring of treatment. Imaging and therapy output were assessed following established international standards, while the combined probe system, performance with SonoTran Particles and PAM were assessed using novel methods. The SonoTran System probes were first individually matched and calibrated in an acoustic test tank. Receive performance for PAM was calibrated using point source and hydrophone measurements, and was subsequently tested in-vitro for monitoring of cavitation from flowing SonoTran Particles in a multi-layer abdominal phantom. The complete system was then tested in-vivo for enhanced drug delivery of an approved antibody (Erbitux®/Cetuximab) administered intravenously in a murine model via the tail vein (bi-lateral subcutaneous H292 tumors in CD1 nude mice). Delivery was assessed using ELISA to quantify Erbitux, while efficacy was assessed using tumor growth curves. Finally, the complete system was tested in both terminal and recovery (animal monitored for >2 weeks post-treatment) experiments at full scale in a porcine model (n=8, 50-60kg, large white hybrid pigs) to validate in-vivo cavitation performance and safety at clinical length scales in a realistic acoustic environment representative of a human abdomen.

Results: Acoustic measurements showed the SonoTran System performed both imaging and therapy in accordance with the applicable international standards. Receive calibration of probes was determined acoustically and the specificity, repeatability and precision were measured. Calibrations were successfully used in-vitro to monitor cavitation of flowing SonoTran Particles in an abdominal phantom. In-vivo, cavitation-enhanced treatment of murine tumors using the SonoTran System increased antibody delivery, resulting in reduced tumor growth and improved cure rate with cavitation compared to antibody alone. Additionally, large animal experiments demonstrated cavitation was instigated and reliably mapped for 30 minutes or more using the handheld probes at clinical length scales in both porcine liver and pancreas. Blood biochemistry, macroscopic assessment (including recovery of experimental animal), and post-treatment histology of targeted porcine tissue demonstrated safety of the SonoTran System.

Conclusions: The SonoTran System's imaging, therapy and treatment monitoring functionality were assessed in-vitro and in-vivo to assess performance and safety. In-vitro results confirmed that the system could perform all three functions and the methods used were validated. Subsequent in-vivo murine results confirmed that the SonoTran System and SonoTran Particles can enhance delivery and efficacy of a clinical antibody. Further results in porcine liver and pancreas showed that prolonged cavitation treatment is possible across a large tissue volume and that cavitation can be monitored in real-time using PAM. Finally, blood analyses and post-treatment tissue histology showed that the delivered level of cavitation and ultrasound exposure is safe.

DRD-3

Topic: Drug Delivery
Presentation Type: Oral

Liposomal drug delivery of doxorubicin and cisplatin using MR-HIFU in a large animal model

Juan Castillo[1], Lukas Sebeke[2], Edwin Heijman[1], Pia Rademann[1], Alexandra Claudia Maul[1], Holger Grüll[2]

[1]University Hospital of Cologne, Berlin, Germany
[2]University of Cologne, Cologne, Germany

Background: Chemotherapeutic APIs like doxorubicin and cisplatin and are characterized by low tumor specificity and a rapid clearance from the blood stream. Their encapsulation in liposomal nanoparticles reduce extravasation and uptake in healthy tissue and provide increased blood circulation time, while tumor uptake is mediated by the enhanced-permeability-and-retention effect (EPR). This effect is less pronounced in human tumors and furthermore liposomal encapsulation reduces drug bioavailability. A promising concept to solve these problems is the use of temperature-sensitive-liposomes (TSLs) with local hyperthermia (42-45°C). The latter can be achieved with high-intensity-focused-ultrasound under magnetic-resonance guidance (HIFU-MR). In this work we present the localized release of doxorubicin and cisplatin using MR-HIFU mediated hyperthermia (42°C) in a swine model. A large animal model was chosen since it better approaches a human setting than preclinical work with small animals.

Materials and Methods: German landrace pigs received an infusion of doxorubicin or cisplatin containing TSLs. Potential anaphylactic reactions to the liposomes were prevented by administration of methylprednisolone acetate 24h prior to the start of the liposome infusion as well as methylprednisolone, diphenhydramine, and ranitidine 1h prior to the start of the liposome infusion. The pigs were intubated and ventilated under pressure-control. A catheter with three lumens for the continuous administration of propofol and Ringer's solution and for the administration of the TSLs was placed in the right external jugular vein. The animals were placed inside the MRI scanner in left lateral recumbency with the biceps femori above the acoustic window of the HIFU table (Figure 1). Blood samples of approx. 4 ml were drawn at 0, 2, 8, 15, 20, 28, 32, 38, 45, 50, 60, 80, 100, 140 and 180 minutes after start of the infusion (see Figure 2). Two local hyperthermia treatments with target temperatures of 42 °C were initiated at 10 minutes and 60 minutes after beginning of the TSL infusion, targeting two spherical volumes with a diameter of 18 mm in the biceps femori, and were continued for up to 30 minutes. 180 minutes after the start of the TSL infusion, animals were euthanized using sodium pentobarbital and all relevant organ and tissue samples where extracted. The cisplatin, doxorubicin and lipid concentrations in the blood, organ and tissue samples were determined using ICP-MS, fluorescence-HPLC and ESI-MS.

Results: We were able to find a 15-fold increase in the concentration of doxorubicin in the treated volumes of the first hyperthermia treatment and a 7-fold increase in the treated volumes of the second hyperthermia treatment compared to the values for the untreated muscle (see Figure 3). For cisplatin, a 2.5-fold increase in concentration was found for both hyperthermia treatments.

The pharmacokinetic curves show a steady increase in blood concentrations of both the active drugs and the lipid, to about 60 %ID at around 30 min, since also during the infusion there is considerable extravasation and excretion. For doxorubicin-TSLs, an experimental half-life $t1/2,exp$ of 16.4 min could be determined for the API. cisplatin-TSLs shows a higher $t1/2,exp$ of 40.1 min for the API.

Conclusions: We have shown that HIFU-Hyperthermia is a suitable method for local drug release of DOX using thermosensitive liposomes in non-moving targets in large animals. Concentration increases of 15-fold for doxorubicin or 2.5-fold for cisplatin were achieved. No serious adverse effects could be observed during the whole experiments. The used premedication and the infusion time of 30 min prevented anaphylactic shocks. This makes this method suitable to treat tumors located in non-moving regions like different types of sarcomas. The present study is of high importance for translational purposes, as we managed to show an increase in concentration of the API after hyperthermia treatments with HIFU in an experimental set up comparable to a human case.

Acknowledgements: Supported by the European Union FP7 Health program Health

("IPaCT", grant agreement no. 603028) and German Federal Ministry of Education and Research ("TSL-LIFU", FKZ: 13XP5014C).

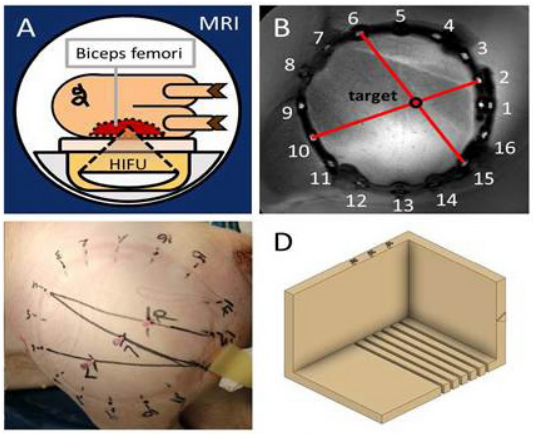

Figure 1. Experimental setup. (A) Positioning of the pig in lateral recumbency. (B) Example for the localization of the treated areas. (C) Localization of the targeted areas. (D) Cutting guide used.

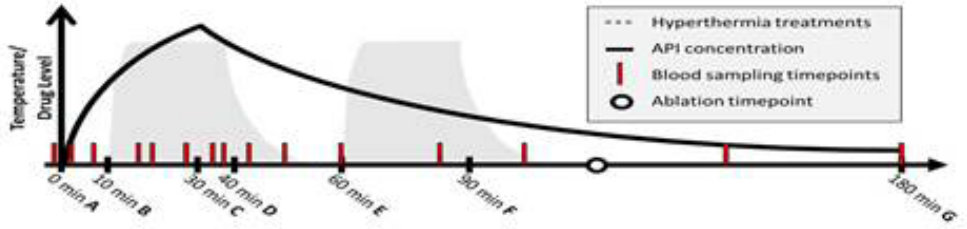

Figure 2. Experimental Timeline. Blood was sampled at 0, 2, 8, 15, 20, 28, 32, 38, 45, 50, 60, 80, 100, 140 and 180 minutes after start of infusion.

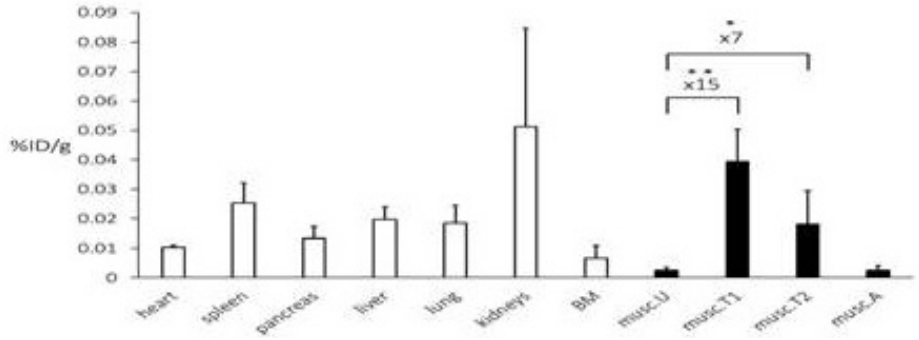

Figure 3. Biodistribution of doxorubicin 3 h after start of infusion of TSLs in pigs. Dose: 50 mg/m2.

DRD-4

Topic: Drug Delivery
Presentation Type: Oral

Ultrasonic thermal stress promotes acute changes in the transvascular transport dynamics in brain tumors and promotes targeted delivery of chemotherapy encapsulated in heat sensitive nanoparticles

Chulyong Kim[1], Yutong Guo[1], Anastasia Velalopoulou[2], Jahannes Leisen[1], Anjan Montamarry[3], Dieter Haemmerich[4], Costas Arvanitis[1]

[1]Georgia Institute of Technology, Atlanta, GA, USA
[2]Georgia Institute of Technology, Philadelphia, PA, USA
[3]Massachusetts General Hospital, Boston, MA, USA
[4]University of South Carolina, Charleston, SC, USA

Background: While therapeutic strategies based on nanoparticles delivery hold great promise for targeted drug delivery to glioblastomas (GBMs) and reduced systemic toxicity, their effective translation to the clinics remains limited due to high heterogeneity and low drug accumulation throughout the tumor. In this study, we examined the abilities of trans-skull MR-guided focused ultrasound (MRgFUS)-mediated hyperthermia to promote the targeted delivery of chemotherapy encapsulated in heat sensitive nanoparticles in glioma tumor models in rodents. In parallel to these investigations we explored the role thermal stress on the transvascular transport dynamics using dynamic contrast enhanced MR imaging (DCE-MRI).

Materials and Methods: For this study we employed i) a custom built MR-guided FUS-system for closed-loop trans-skull hyperthermia ($\Delta T<1°C$), ii) heat-sensitive liposomal Doxorubicin (HSL-Dox), iii) dynamic contrast enhanced MR imaging (DCE MRI) and iv) GL261 (mice) glioma tumor model. Prior to the experiments, we optimized the FUS system for attaining maximum tissue to skull heat deposition using mathematical modeling that we prospectively validated in mice. Subsequently, we applied FUS transcranial hyperthermia (~41.5°C) for 10 min with concurrent administration of HSL-Dox. Hour post treatment we sacrificed the animals and assessed Dox delivery using fluorescence microscopy. To better understand the FUS-hyperthermia mediated changes in tumor perfusion and vessel permeability during the sonications and identify potential synergies for drug delivery, we also measured, in a separate cohort, the ktrans using dynamic contrast enhanced MRI. In these experiments we also assessed the impact of FUS-hyperthermia on the uptake of free dox infusion during and post FUS-hyperthermia. Finally, we integrated the experimental measurements with physiologically based pharmacokinetic modeling (PBPK) using parameter optimization procedures and inferred transport dynamics in the brain tumor microenvironment under US thermal stress.

Results: Analysis of the extracted tumors with fluorescence microscopy showed significantly higher Dox penetration (distance from CD31 positive cells) and cellular uptake (~3.5-fold increase, $p<0.001$) for HSL-Dox +FUS in comparisons to the non-FUS groups. The ktrans values from DCE-MRI, which provide a measure of capillary permeability and tissue perfusion, indicate that moderate thermal stress by US (≈41.5°C for up to 10 mins) can promote acute changes in the transport dynamics in the brain tumor microenvironment (Ktrans value for control vs. FUS was 0.095 and 0.15 min-1, respectively $p=0.028$). Interestingly, FUS hyperthermia combined with free Dox also resulted in ~1.6-fold increase in Dox delivery as compared to the non-FUS group. Finally, sensitivity analysis from the refined PBPK modeling indicates that increasing the vessel permeability may lead to even higher chemotherapy delivery, suggesting that pretreatment with microbubble-enhanced FUS can be a reasonable therapeutic strategy.

Conclusions: Collectively our data demonstrate that localized transcranial MRgFUS-hyperthermia can increase Dox accumulation in brain tumors by HSL-Dox and support the hypothesis of synergistic effects between FUS-triggered drug release and hyperthermia-mediated changes in key transport parameters. Our findings can help to refine our understanding on the role of US thermal stress in modulating mass transport in brain tumors and reveal new therapeutic strategies against brain tumors.

DRD-5

Topic: Drug Delivery
Presentation Type: Oral

Lower interstitial fluid pressure and enhanced delivery and penetration of nanoparticles in solid tumors using nondestructive pulsed focused ultrasound

Ali Mohammadabadi[1], Ruby N. Huynh[2], Aniket S. Wadajkar[1], Rena G. Lapidus[1], Anthony J. Kim[1], Christopher B. Raub[2], Victor Frenkel[1]

[1]University of Maryland School of Medicine, Baltimore, MD, USA
[2]The Catholic University of America, Washington, DC, USA

Background: Nanocarriers have many benefits in cancer therapy, improving payloads of chemotherapeutics while minimizing off-target delivery and the associated side effects. Factors in the tumor microenvironment (TME) including high interstitial fluid pressure (IFP) and fibrillar collagen in the extracellular matrix can reduce extravasation and penetration of these large agents, limiting their potential therapeutic advantage. We previously demonstrated that pretreatment of solid tumors with pulsed focused ultrasound (pFUS) improves the delivery and subsequent therapy of various therapeutic formulations (small molecules, liposomes, antibodies, & DNA) in solid tumor models. These results were associated with expanded extracellular spaces, an increase in hydraulic conductivity, and a decrease in tissue stiffness. In this study, we investigate the effects of pFUS on IFP and the fibrillar collagen network, and their relation to delivery and penetration of systemically administered nanoparticle probes.

Materials and Methods: A head and neck xenograft flank tumor model was used for all investigations. Cells were inoculated subcutaneously in the right flank of female athymic nude mice, and tumors measured daily. A single element 500 kHz FUS transducer was used for all pFUS treatments and coupled to the tumors using a plastic cone that was filled with degassed water and sealed with an acoustically transparent silicone membrane (Fig. 1A). pFUS exposures were carried out at 80 W; 10 ms bursts and a 10% duty cycle for 2 minutes per treatment location (spacing 1.5 mm). IFP in the tumors was measured from the surface to the tumor center using the wick-in-needle method (step size: 0.5 mm) (Fig. 1B). For the in vivo imaging study, control and pFUS treated animals were imaged using IVIS® Spectrum in vivo imaging system at 24 hr following systemic administration of 40 nm fluorescently labeled NPs (n = 5 per group). For characterizing NP penetration, whole tumors were resected after euthanizing animals at 24 hr following systemic administration of 200 nm fluorescent NPs (n= 7 per group). Tumors were sectioned (200 μm slices) and imaged with a fluorescence imager. The distribution of NPs was evaluated in 3 concentric regions of interest. The effects of pFUS on the general macroscopic structure and the fibrillar collagen microstructure were characterized by staining tumor sections with hematoxylin and eosin (H&E) and Masson's Trichrome (MTC), using standard light and polarized light microscopy, respectively.

Results: IFP (5.87 ± 0.48 mm Hg) was 28% lower in the center of pFUS treated tumors compared to the untreated controls (8.15 ± 0.87 mm Hg) ($p = 0.04$; $n = 10$) (Fig. 2B). The slope and coefficient of variability of the measured values from the tumor periphery to the center were also lower in the pFUS treated tumors (25% vs 42%) (Fig. 2A). In the in vivo imaging study mean epifluorescence signals were 49% greater in the pFUS treated tumors (2.49 ×1010 RLU ± 0.72) compared to the controls (1.67 ×1010 RLU ± 0.45) ($p = 0.03$; $n = 5$) (Fig. 3A, B). Significantly greater numbers of NPs (57%) were also found to penetrate into the center of the tumors pretreated with pFUS compared to controls ($P = 0.03$; $n = 7$) (Fig. 3C, D). Polarized light microscopy of the fibrillar collagen network showed nondestructive alterations to birefringent microstructure in response to pFUS. However, whole-scale damage to the tumors was not detected in features of stained histological sections.

Conclusions: pFUS pretreatment of tumors was shown to nondestructively reduce IFP, where effects were associated with greater penetration and overall delivery of NP probes. We propose that pFUS effects generated in the fibrillar collagen network increased hydraulic conductivity of the fluid in the TME, improving fluid flow from the tumor center to the periphery, which was subsequently taken up by peritumor lymphatics to lower IFP (Fig. 4A). Lowering the IFP gradient, as well as the gradient of NP distribution, demonstrates a less heterogenous TME, being the goal of TME modulating therapies (Fig. 4B). These results support those of our earlier therapeutic studies and may facilitate the clinical translation of this procedure for treating cancer patients.

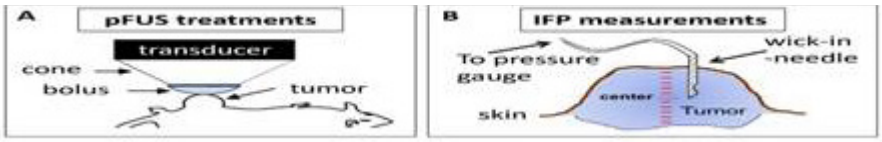

Figure 1. Schematic of pFUS treatments and IFP measurements. (A) A water-filled cone sealed with a flexible membrane (bolus) coupled the pFUS transducer to the tumor. (B) IFP measurements.

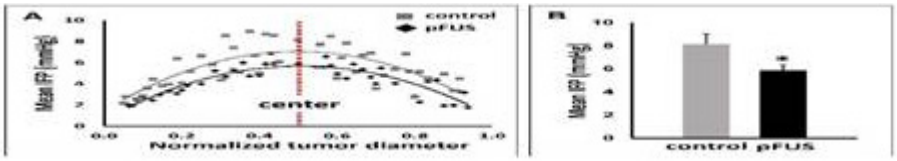

Figure 2. IFP measurements in solid tumors. (A) Compared mean IFP between controls and pFUS treated tumors. (B) pFUS treatment reduced the mean IFP by 28% at the center of tumors compared to controls.

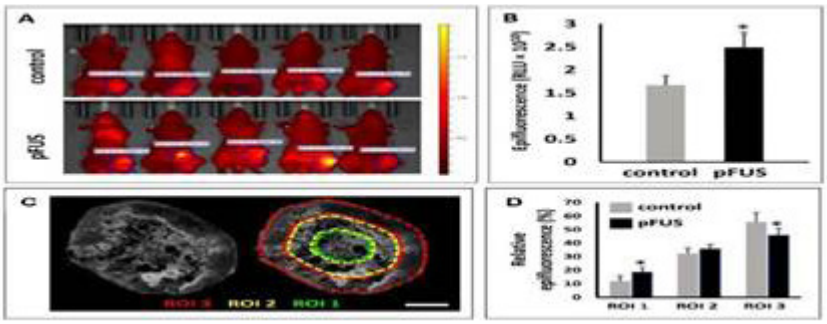

Figure 3. pFUS and NP delivery. (A) In vivo NP (40 nm) epifluorescence. (B) Mean NP (40 nm) epifluorescence. (C) The distribution of NPs (200 nm) in ROIs. (D) Relative NP (200 nm) epifluorescence.

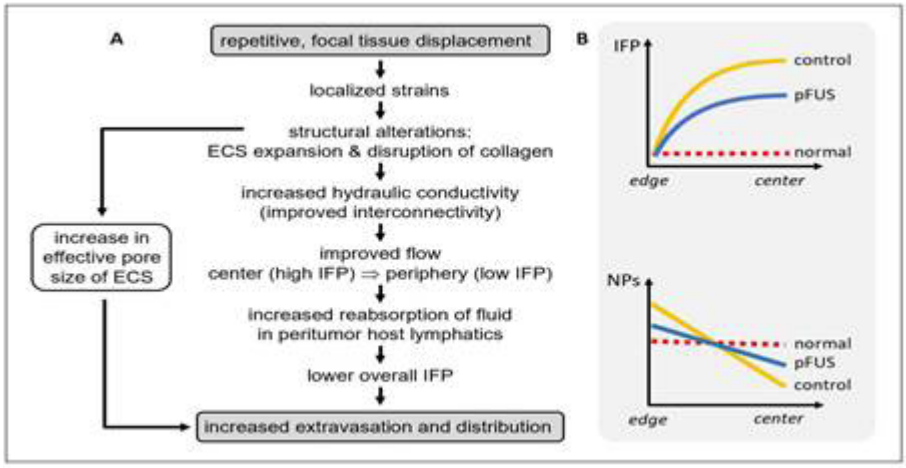

Figure 4. (A) A proposed model for the mechanism of pFUS treatment on the TME. (B) A graphical representation of reduced IFP and NP gradients after pFUS treatment, rendering the TME more uniform.

DRD-6

Topic: Drug Delivery
Presentation Type: Oral

Improved monitoring of ultrasound-enhanced drug delivery by passive acoustic mapping with spatial selectivity

Cameron Smith[1], Christophoros Mannaris[1], Luca Bau[1], Megan Jackson[2], Robert Carlisle[1], Constantin Coussios[1]

[1]University of Oxford, Oxford, United Kingdom
[2]OxSonics Ltd, Oxford, United Kingdom

Background: Ultrasound mediated cavitation can produce a wide range of desirable bioeffects. However, due to the stochastic nature of cavitation and the irregularities in tumour perfusion real time treatment monitoring is essential to allow for reliable, safe therapies. Passive acoustic mapping (PAM) has shown to be capable of localizing and determining the extent of cavitation activity. In this work, a PAM derived cavitation dose metric is related to extravasation of a drug into solid tumours, exploring whether PAM derived cavitation dose can be used to monitor the levels of drug delivery achieved and how cavitation occurring outside the tumour affects this relation.

Materials and Methods: CD-1 nude mice were subcutaneously inoculated with HT-29 tumour cells. Once the tumours reached 90-150 mm^3, the mice were intravenously injected with cetuximab and a submicron sized cavitation agent (SonoTran® Particles, SPs) at two different concentrations, and treated with focused ultrasound (0.5 MHz, 50,000 cycle pulses, 0.5 Hz PRF) for 10 minutes (figure 1). Cavitation throughout the treatment was monitored using frequency domain robust Capon beamforming PAM from data recorded using two 90-degree coplanar L11-4v linear arrays, which were also used between pulses to acquire B-Mode images to guide the treatment with PAM overlay (figure 2a). Intratumoural cetuximab concentrations were then assessed via ELISA and compared to PAM derived cavitation dose estimates (figure 2b). Using data from the B-Mode images collected PAM energy was spatially selected in two ways, one to exclude cavitation occurring within the skin of the mice (figure 3a), and the second method was to exclude all cavitation occurring outside of the tumour (figure 3b).

Results: The use of cavitation nucleation agents and ultrasound was found to increase the concentration of drug delivered to the tumour in all cases, compared to the non-ultrasound-treated passive delivery controls. The cavitation dose following exclusion of cavitation activity within the skin was found to improve the correlation between the cavitation dose and the concentration of Cetuximab delivered (figure 4). The coefficient of determination R^2 increased from 0.57 with no exclusion to give an R^2 of 0.62 post skin exclusion. In the case of exclusion of all cavitation activity occurring in either skin or muscle outside the tumour the correlation coefficient increased further to an R^2 value of 0.74. The relationship between cavitation dose and drug delivered to the tumour appears to be linear within the parameter range explored, and the strong correlation indicates that the amount of cavitation generated within the tumour is critical in determining the levels of drug delivery achieved.

Conclusions: This study demonstrates that PAM derived cavitation dose can monitor the levels of ultrasound enhanced drug delivery to solid tumours. PAM's ability to spatially localize cavitation can be utilized to exclude cavitation occurring from locations outside of the tumour, thereby improving the correlation between cavitation dose and drug delivered, with both cavitation occurring in the skin in front of the tumour and in the vascular bed behind the tumour artificially increasing the cavitation dose estimates if not properly accounted for. These results show the advantages that PAM offers over single element methods and demonstrates that PAM can be used to reliably monitor cavitation enhanced drug delivery therapies.

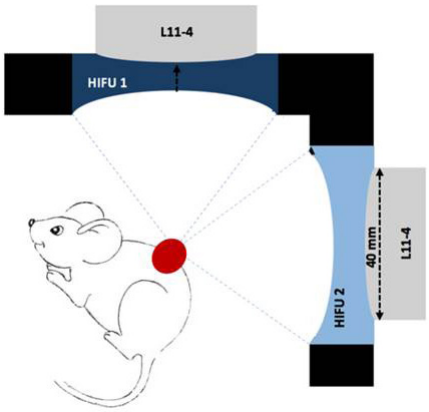

Figure 1. CD-1 nude mice with tumours ranging from 90-150 mm^3 were intravenously injected with Cetuximab antibody and SonoTran Particles (SPs). Tumours were then exposed ultrasound.

Acknowledgements: The authors gratefully acknowledge support from the UK's Engineering and Physical Sciences Research Council under the Oxford Centre for Drug Delivery Devices (OxCD3) programme grant (EP/L024012/ 1), and thank OxSonics Therapeutics Ltd.

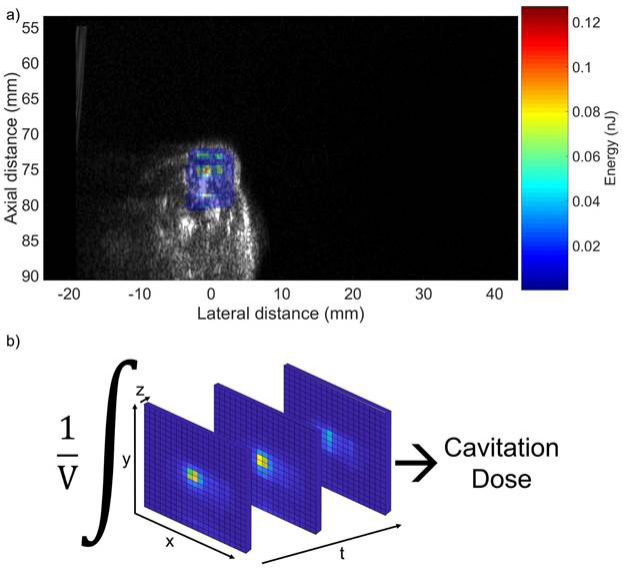

Figure 2. a) Example PAM map overlaid on its corresponding B-mode image. b) The cavitation dose for each treatment was calculated as the integral of the PAM power maps normalised by the tumour volume.

Figure 3. Example B-mode with overlay of a binary mask used to exclude cavitation occurring within the skin (a), or outside the tumour (b). Red corresponds to included, blue to excluded.

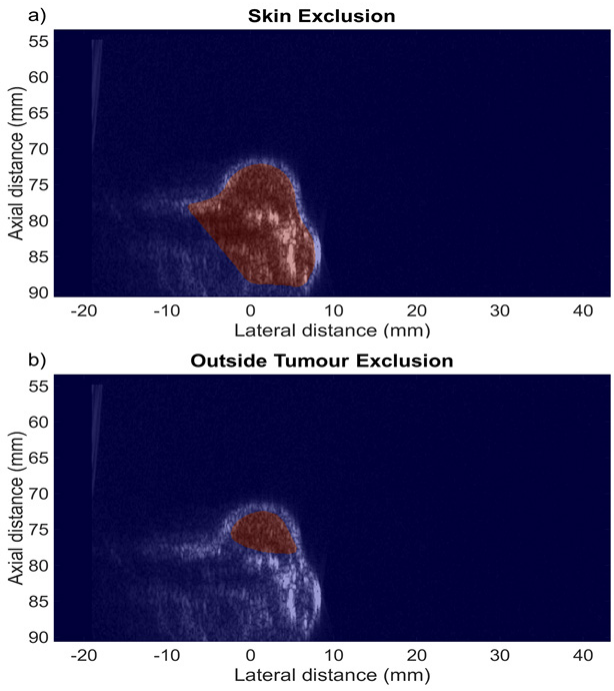

Figure 4. Cavitation dose for each tumour against the concentration of Cetuximab (Cetux) delivered to that tumour. The R^2 for each method are 0.57, 0.62, and 0.74 respectively.

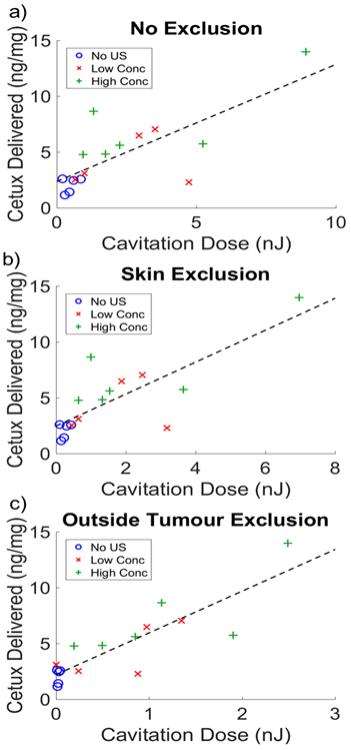

DRD-7

Topic: Drug Delivery
Presentation Type: Oral

Magnetic resonance guided high intensity focused ultrasound generated non-invasive hyperthermia releases thermosensitive doxorubicin in a rhabdomyosarcoma murine model

Claire Wunker[1], Karolina Piorkowska[2], Benjamin Keunen[3], Warren Foltz[4], Maximilian Regenold[4], Maryam Siddiqui[5], Michael Dunne[4], Samuel Pichardo[5], Christine Allen[4], Adam Waspe[2], Rebecca Gladdy[4], J. Ted Gerstle[6]

[1]Luenfeld-Tanenbaum Research Institute, Toronto, ON, Canada
[2]The Hospital for Sick Children, Toronto, ON, Canada
[3]SickKids, Palmerston, ON, Canada
[4]University of Toronto, Toronto, ON, Canada
[5]University of Calgary, Calgary, Canada
[6]Memorial Sloan Kettering Cancer Center, New York, NY, USA

Background: Rhabdomyosarcoma (RMS) is a tumor of skeletal muscle that most commonly affects children and young adults. Current treatment involves surgery, vincristine-based chemotherapy, and radiation with five-year survival of ~30% in the most aggressive type. In cases of relapsed or metastatic RMS, alternate chemotherapies include doxorubicin, which causes cardiotoxicity. Thus, new treatments are needed with increased efficacy and reduced toxicity in these vulnerable patients. An alternate form of doxorubicin is encapsulated in a thermosensitive liposome (TLD) and has been used to treat other malignancies. Magnetic resonance guided high intensity focused ultrasound (MRgHIFU) combines real-time MR imaging and open source software libraries (Proteus) that modulate and monitor ultrasound (US) function based on the thermometry from the imaging (Fig. 1). The software controls the operation of the US which generates localized hyperthermia (HT) in a region of interest (ROI) centered in the tumor.

Materials and Methods: We localized HT in an RMS mouse model through Proteus, which generates closed-loop controlled HT, using a Bruker 7T MRI and IGT small animal HIFU system. Core temperature is monitored to ensure no systemic heating. An initial scan determines the location of the tumor and targets the ROI. Proteus produces thermal maps to monitor the procedure. The US has a focal point with assumed uniform distribution in all directions to create an ellipsoid for temperature control. Short sequences of heating confirm adequate HT and allow for adjustments prior to drug delivery. Once appropriate heating profiles are obtained, a preheating cycle for 1.5 minutes is started to bring the tumor to the target temperature and then the drug is injected. HT temperature (41°C ± 2°C) is maintained in the tumor for the duration of the treatment. The mouse is sacrificed immediately after treatment and tissues are collected. These tissues are analyzed using high-performance liquid chromatography (HPLC) for drug accumulation.

10-(n=19) and 20-(n=23) minutes of HT were used to determine optimal HT duration for drug delivery. After completing 10- and 20-minutes of HT, the duration between injection of the drug and time of death was calculated and averaged. This average time for each duration group was used as the time to allow the drug to circulate in the control animals. There were 4 treatment groups at both treatment durations: HT + TLD, HT + standard doxorubicin (Dox), TLD, Dox (Fig. 2).

Results: Using an RMS mouse model with MRgHIFU, we generated and optimized a reproducible and consistent treatment with the ROI temperature maintained at 41±1.6°C (Fig. 3). Maintaining the animal's core normothermia was confounded during prolonged HT treatment and was rectified with a 3D printed holder combined with forced air heating or cooling.

Significantly higher concentrations of TLD were measured in tumors of mice treated with 20-minute HT compared to 20-minute control mice (Fig. 4, $p = 0.0163$). We found no statistical difference in the tumor accumulation of drug between TLD and Dox for 10- or 20-minute HT durations ($p > 0.05$). Non heated TLD remained in the plasma and was significantly higher than standard doxorubicin in the plasma at all time points ($p = 0.002$). Hence, we decided to treat our next study survival animals for 20 minutes of HT. There was no correlation between tumor size and either plasma or tumor drug amounts ($r(59) = 0.11$ $p = 0.42$, $r(60) = -0.14$ $p = 0.30$).

Conclusions: With the collaboration of a multidisciplinary translational team (computer

engineering, imaging, biology, pharmacology), we have successfully developed non-invasive MRgHIFU to examine the utility of TLD as a less toxic therapy for advanced RMS. We found significantly higher amounts of TLD in the tumor with 20 minutes of heating. Next steps include survival studies comparing treatment responses as well as analysis of drug accumulation in systemic tissues to determine systemic toxicity. Our preclinical models have begun to provide us data that tumors are responsive to this modality however additional validation is required. Ongoing studies will specifically address if HT can induce an immune response in our RMS mouse model.

Acknowledgements: C17 Research Grant

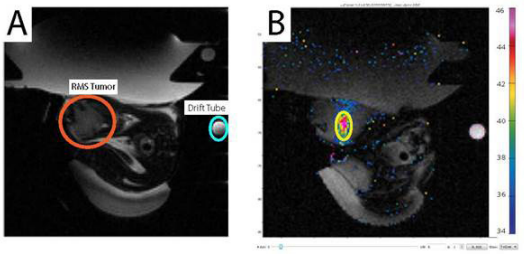

Figure 1. A- MRI axial image displaying the tumor in the hindlimb of the mouse (circled in orange), B- During hyperthermia treatment with thermometry overlayed and region of interest circled in yellow.

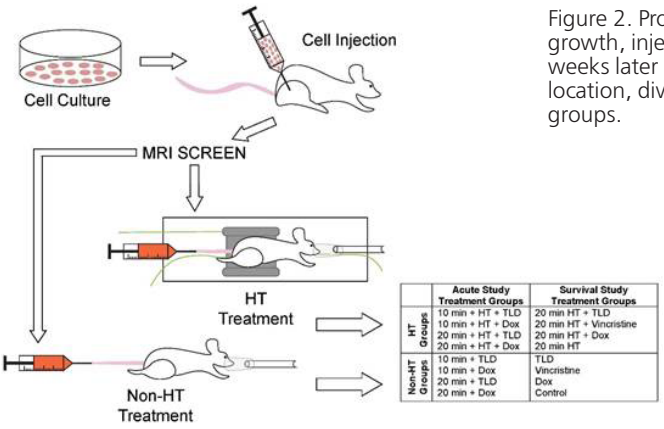

Figure 2. Protocol for treatments: tumor cell growth, injection into the right hindlimb, 2-3 weeks later 7T MRI screening for tumor size and location, division into HT and non-HT treatment groups.

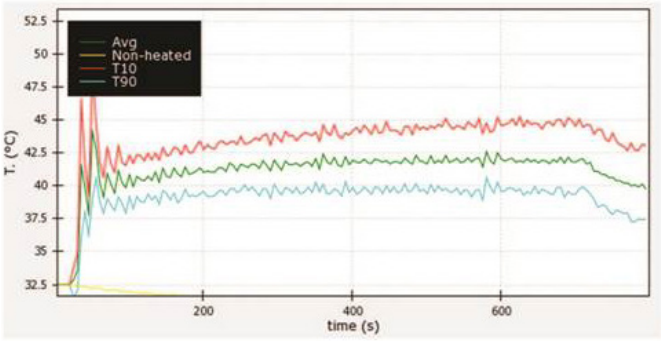

Figure 3. Temperature calculated within the ROI during HT treatment. Preheating cycle initial spike followed by stable temperatures. Average (green), 10th percentile (red), 90th percentile (cyan).

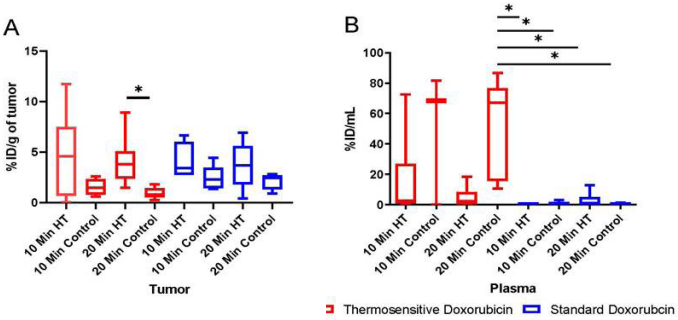

Figure 4. HPLC results with significance ($p<0.05$) of the amount of doxorubicin in the tumor (A) with 20 minutes of HT in combination with TLD treatment and all levels of Dox and TLD in the plasma (B).

DRD-8

Topic: Drug Delivery
Presentation Type: Oral

Focused ultrasound-mediated brainstem delivery of intranasal administered agents

Dezhuang Ye, Jingyi Luan, Hannah Pang, Yaoheng Yang, Hong Chen

Washington University in St. Louis, St. Louis, MO, USA

Background: FUS-mediated intranasal (FUSIN) delivery is a recently proposed brain drug delivery technique that capitalizes on the unique advantages of the IN route for direct nose-to-brain drug administration as well as FUS in combination with microbubbles for generating localized mechanical forces on the vasculature that enhances the penetration of IN-administered drugs. The objective of this study was to characterize FUSIN drug delivery regarding its dependency on different experimental factors, including the time interval between intranasal (IN) administration and focused ultrasound (FUS) sonication (Tlag1), the FUS parameters, and the elapsed time to sacrifice the mice post-FUS (Tlag2).

Materials and Methods: Wild-type mice were treated by FUSIN to deliver the near-infrared fluorescent dye-labeled bovine serum albumin (800CW-BSA) to the brainstem. The mice were divided into multiple groups (Tabel 1) to determine the dependence of FUSIN delivery efficiency on the time interval between IN administration and FUS sonication (Tlag1 = 0.5 h, 1.5 h, and 4.0 h), the FUS pressure (0.43 MPa, 0.56 MPa, and 0.70 MPa), and the elapsed time of sacrificing the mice post-FUS (Tlag2 = 0.5 h, 1.0 h, and 4.0 h). 800CW-BSA was intranasally administered to the mice and followed by intravenous injection of microbubbles and then FUS sonication. Mice were sacrificed at different time points post-FUS. The mouse brains were excised and sliced into 2-mm coronal sections for fluorescence imaging in order to quantify the delivery efficiency of 800CW-BSA to the brainstem. All the major organs, including heart, lung, spleen, kidney, liver, stomach and intestines, nose, and trigeminal nerve were also harvested to assess the biodistribution of 800CW-BSA using fluorescence imaging.

Results: The FUSIN delivery efficiency reached the highest at Tlag1 = 0.5 h, which was on average 24.5×, 5.4×, and 21.6× higher than those of the IN only, Tlag1 = 1.5 h, and Tlag1 = 4.0 h, respectively (Fig. A). FUSIN achieved the highest delivery to the brainstem at the lowest tested pressure, 0.43 MPa with a delivery efficiency that was 1.8× and 3.7× higher than those at 0.56 MPa and 0.70 MPa, respectively (Fig. B). The 800CW-BSA concentration in the brainstem after FUSIN decreased by 5.5 fold from 0.5 h to 4.0 h post-FUS. The accumulation of 800CW-BSA was low in major organs such as heart, lung, spleen, kidney, and liver, but high in stomach and intestines.

Conclusions: FUSIN is a promising technique for brain drug delivery that integrates FUS and microbubbles to enhance the accumulation of intranasally administered agents at the FUS-targeted brain location. The current study found that FUSIN delivery to the brainstem depends on several critical experimental parameters, including the time interval between IN and FUS, the FUS pressure, and the elapsed time between FUS treatment and mouse sacrifice. This study revealed the unique characteristics of FUSIN as a noninvasive, efficient, and localized brain drug delivery technique with minimal systemic exposure. Findings from this study provide guidance for selecting optimal treatment parameters and insight into the mechanisms of FUSIN.

Acknowledgements: National Institutes of Health (NIH) grants R01EB027223 and R01MH116981

Figure.1. FUSIN delivery of 800CW-BSA to brainstem (A) at different time intervals between IN and FUS (Tlag1), (B) at different FUS pressure levels.

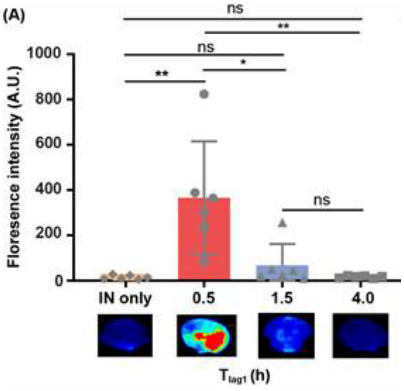

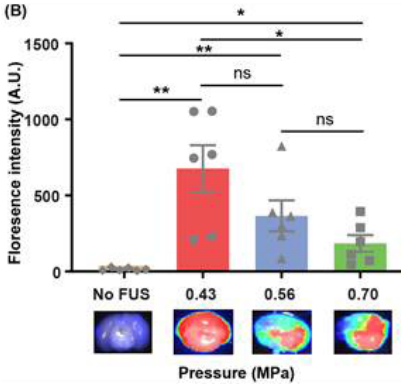

Figure 2. Summary of all study groups

Group #	Animal #	T_{lag1}	Pressure	T_{lag2}
1	6		Control (IN only)	
2	6	0.5 h	0.56 MPa	0.5 h
3	6	1.5 h	0.56 MPa	0.5 h
4	6	4.0 h	0.56 MPa	0.5 h
5	6	0.5 h	0.56 MPa	1.0 h
6	6	0.5 h	0.56 MPa	4.0 h
7	6	0.5 h	0.43 MPa	0.5 h
8	6	0.5 h	0.70 MPa	0.5 h

T_{lag1}: Time delay between IN and FUS; T_{lag2}: Time of sacrifice after FUS

DRD-9

Topic: Drug Delivery
Presentation Type: Oral

Extracellular vesicles combined with microbubble-assisted ultrasound for drug delivery in cancer

Yuana Yuana

Technical University of Eindhoven, Eindhoven, Netherlands

Background: Microbubble-assisted ultrasound (USMB) has been used for decades for diagnostic imaging. Its application for localized drug delivery is emerging. Hitherto, the micron size of MB may limit the drug uptake by USMB application only to cells adjacent to vessels. We have demonstrated that USMB triggers the release of cell-derived lipid bilayer-enclosed nanoparticles known as extracellular vesicles (EVs) with a diameter <200 nm, smaller than MB, and thus may potentially bypass the multiplicity of biological barriers. In the current study, we investigated if (i) USMB could generate EVs containing drug cargo, and (ii) the recipient tumour cells could take up these EVs.

Materials and Methods: Using pulsed US (10% duty cycle, 1 kHz pulse repetition frequency, and 100 μs pulse duration), different pressures (0.6, 0.7, and 0.8 MPa) were applied to load the model drug, Cell Tracker Green fluorescent probe (10 nM CTG) or bovine serum albumin conjugated with fluorescein isothiocyanate (50 μg/mL BSA FITC), into primary human endothelial cells (HUVECs) in vitro. To investigate if model drugs were present in the cells and EVs, cells and cell supernatants were harvested within 2 h after treatments and measured using flow cytometry, electron microscopy, and fluorescent microscopy. EVs were isolated from cell supernatants and co-cultured with head-and-neck carcinoma (FaDu) or breast carcinoma (MDA-MB-231) cells. EV uptake was monitored at 0, 2, and 4 h. The Cre-LoxP system using EVs carrying active Cre recombinase and reporter-expressing T47D human mammary cells was used to confirm the uptake of EV containing cargo by the recipient tumour cells.

Results: HUVECs could be loaded with CTG by incubating CTG for 30 min. However, USMB did not enhance the loading of CTG in HUVEC. In case of BSA-FITC, at 0.6 MPa, BSA FITC signal intensities were the highest compared to untreated and treated HUVECs at 0.7 and 0.8 MPa. This molecule was localized in the cell lysosomal compartment indicating its degradation in this compartment. Cell supernatants collected from CTG/BSA FITC-loaded HUVECs within 2 h incubation contained EVs with CTG/BSA FITC cargo, with increasing concentrations with higher pressures. Co-culturing these EVs resulted in uptake by the recipient tumour cells within 4 h. EVs containing BSA FITC taken up by cells were not present in the cell lysosomal compartment, and its FITC fluorescent signal was observed in the cell cytoplasm or in the vicinity of cell nucleus. A red-to-green colour switch was observed in reporter cells confirming the uptake of USMB-generated EV carrying active Cre recombinase and transfer of its cargo.

Conclusions: In conclusion, the type of the model drug is one of parameters which may clearly influences the loading using USMB. It is also clear that this loading would not be optimal if the model drug would be trapped in the lysosomal compartment. USMB simultaneously triggered the release of EVs carrying model drugs. These EVs were taken up by the recipient tumour cells, highlighting the potential of EVs combined with USMB for drug delivery.

Acknowledgements: This work was funded by Focused Ultrasound Foundation (High Risk Track grant).

Figure 1. Loading CTG or BSA FITC to HUVEC cells using USMB.

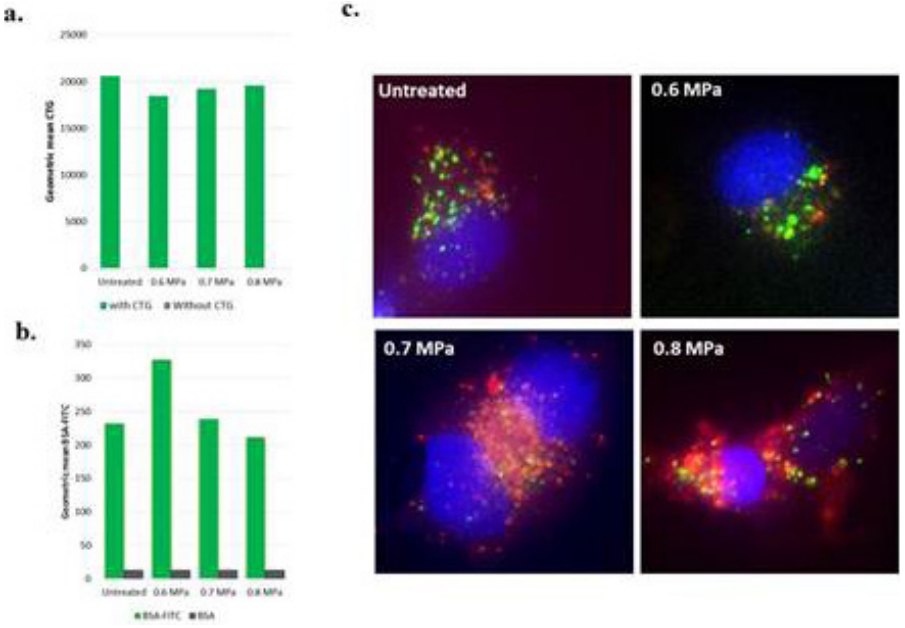

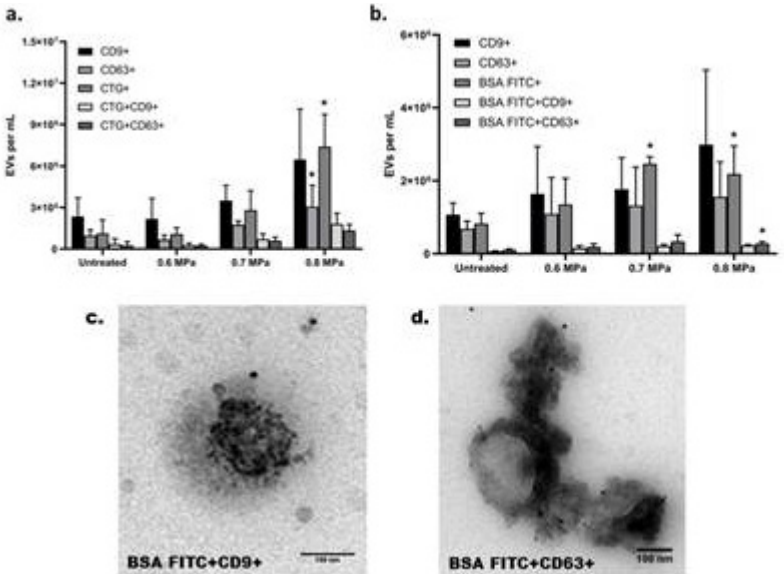

Figure 2. CTG or BSA FITC-containing EVs generated by USMB.

Figure 3. Uptake of EVs containing BSA FITC by FaDU cells.

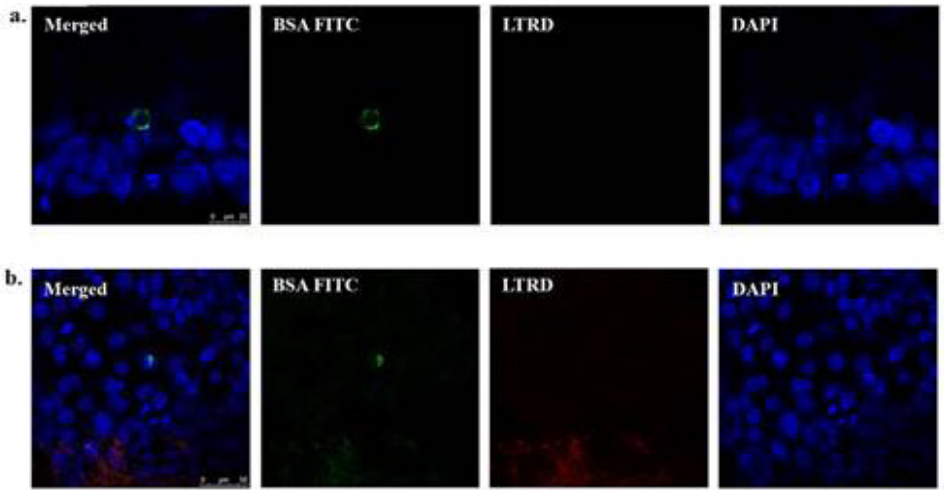

Figure 4. Uptake of EVs carrying Cre-recombinase by T47D recipient cells

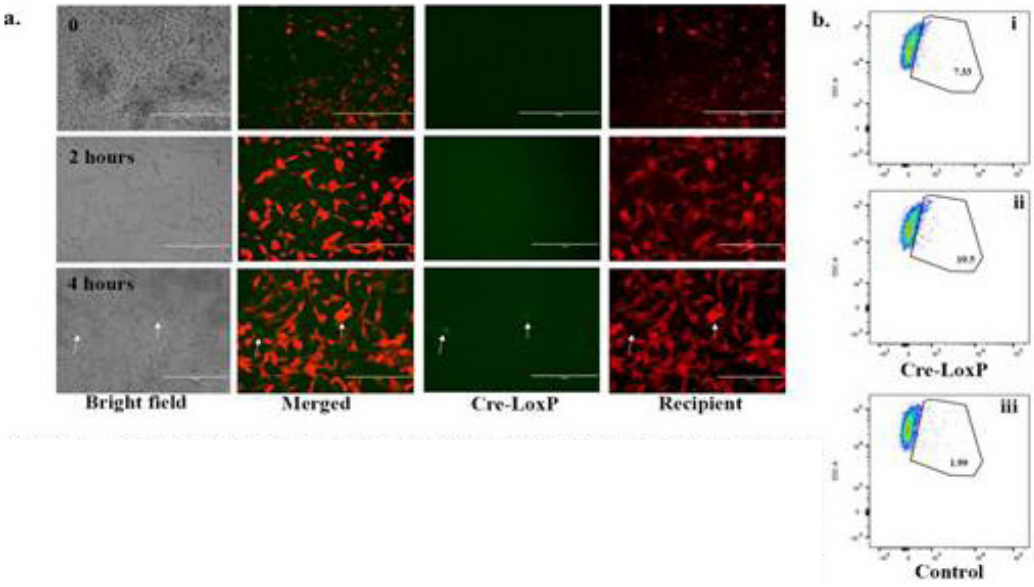

EPI-1

Topic: Epilepsy
Presentation Type: Oral

Investigating the feasibility of MRgFUS for minimally invasive heating of mesial temporal lobe structures

Sijia Guo[1], John Snell[2], Jiachen Zhuo[1], Dheeraj Gandhi[1], Paul Fishman[1], Rao Gullapalli[1]

[1]University of Maryland School of Medicine, Baltimore, MD, USA
[2]Focused Ultrasound Foundation, Charlottesville, VA, USA

Background: The main obstacle to applying current transcranial MR-guided focused ultrasound (tcMRgFUS) technology to temporal lope epilepsy (TLE) is the location of the mesial temporal lope (MTL) with respect to the base of the skull. The MTL is considered outside the "treatment envelope" of current clinically approved devices due to the potential skull heating which also results in low energy deposition at the focal target. Strategies using focused ultrasound safely for thermal ablation of the MTL have not been adequately explored. Our hypothesis is that the effective combination of the longer sonication time, element blocking algorithms, and multiple-target sonication strategies will allow for a safe and robust ablation of MTL. Our hypothesis will be verified by acoustic simulation work and experiments on a cadaver skull filled with tissue-mimicking phantom.

Materials and Methods: The acoustic simulation model will employ numerical simulations using a three-dimensional full-wave model based on the Westervelt equation. Spatial maps of the acoustic properties of the skull will be extracted from CT data based on the relationship between density and longitudinal sound speed/attenuation for skull bone, and we will use the CT-based analytical method for phase aberration. For the experimental validation, we will use the InSightec 670kHz system to target at the MTL region of a cadaver skull filled with tissue-mimicking phantom (Figure 1). Target temperature will be recorded based on MR thermometry and skull temperature will be measured using 4 thermocouples at the potential heating spots predicted by the simulation. Element blocking algorithm and multiple-target sonication were only employed in acoustic simulation, which will be verified in the future experiments. In the element blocking algorithm, the transducer elements whose beams pass through the most heated skull region will be turned off. Sonications at 1-5 targets within the MTL with 5-7 mm gap between each target, and 0-4 min cooling between each sonication will be simulated to achieve the heated volume that reached 50°C.

Results: An example of the acoustic simulation (Figure 2(a)) and the MR thermometry images when targeting the MTL (Figure 2(b)) are shown. The measured target and skull heating are agreed with the simulation results (Figure 2(c)). The highest target temperature rise we achieved is 14°C with a 900W sonication for 30 seconds, while the skull temperature rise is 10.2°C. It was found that by blocking the transducer elements whose beams caused the skull base heating can help to decrease skull heating by 4 °C without disturbing the focal shape (Figure 3). Figure 4 summarized the simulated accumulated volume that reached 50°C for 1-5 targets, 5-7 mm gap between each target, and 0-4 min cooling between each sonication. With 5 targets (distance between target: 5 mm, cooling duration: 2 min) being treated for 30 s each continuously, the accumulated volume that reached 50°C can reach 1.5~2 cc.

Figure 1. The skull and gel phantom preparation.

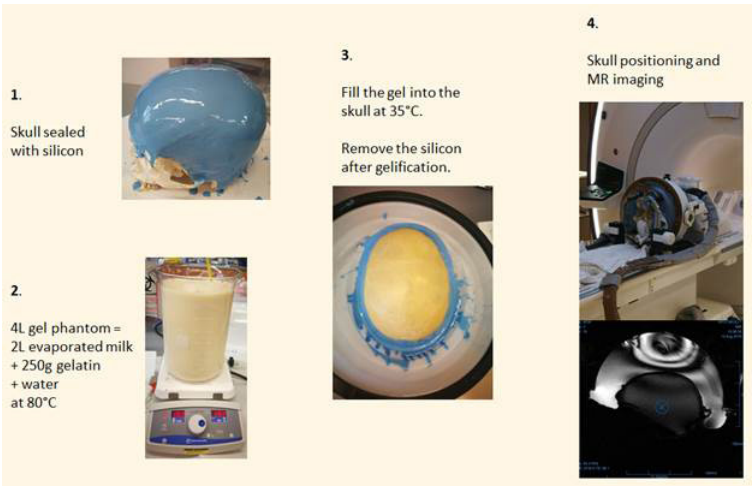

Conclusions: On a cadaver skull, we were able to achieve 14°C temperature rise with a 30-second sonication while the skull temperature rise is 10.2°C, which agreed with our simulation results. Blocking less than 100 elements can help to decrease skull heating by 4 °C without disturbing the focal shape while keeping the temperature rise the same at the MTL target. The accumulated volume that reached 50°C can reach 1.5~2 cc by sonicating 5 targets within MTL with a distance of 5 mm and a cooling duration of 2 min.

Acknowledgements: We would like to thank the funding from FUS Foundation.

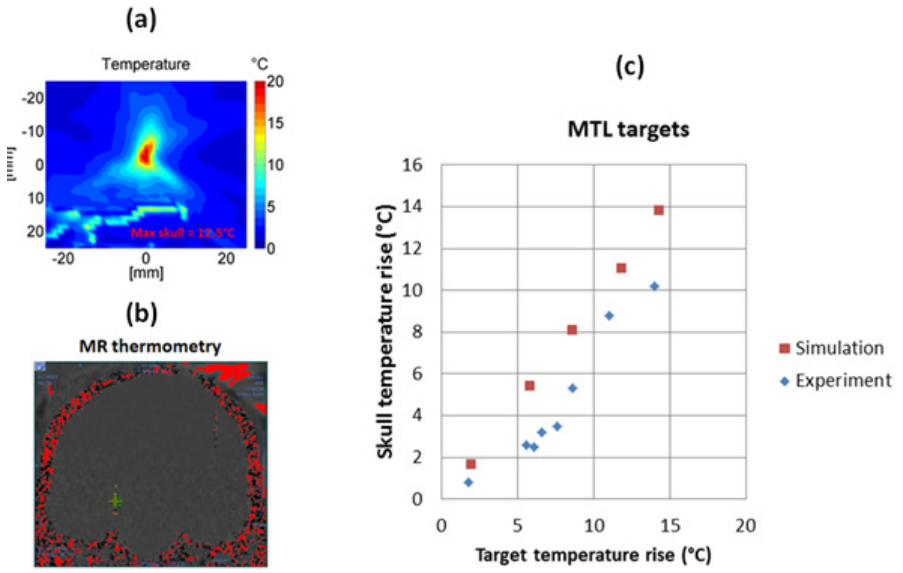

Figure 2. An example of the acoustic simulation (a) and the MR thermometry images (b) when targeting the MTL. (c) shows the comparison between experimental and simulation results.

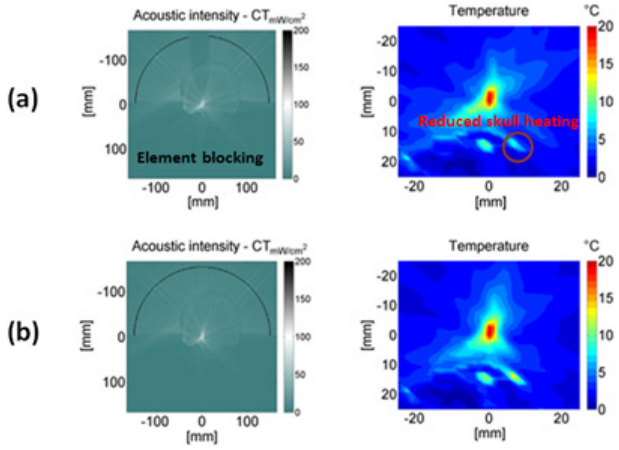

Figure 3. (a) shows that element blocking can help to decrease skull heating by 4 °C compared with a sonication without element blocking (b).

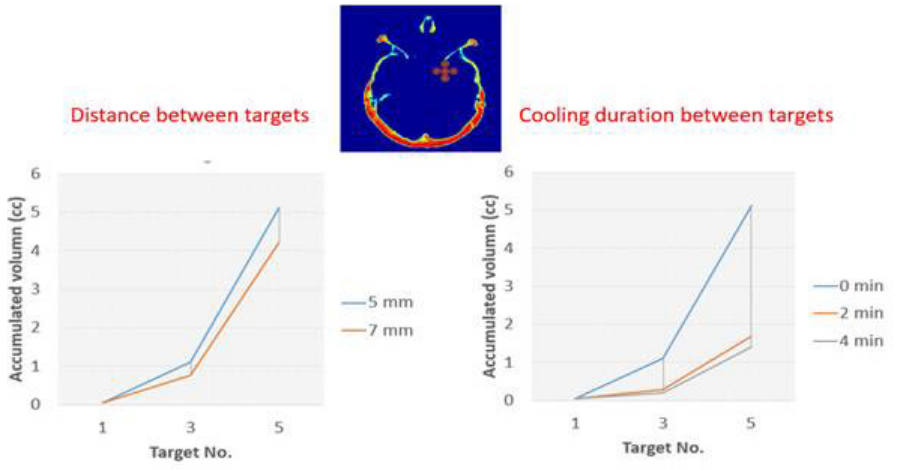

Figure 4. Simulated heating volumes that reached 50 °C for 1-5 targets within MTL, 5-7 mm gap between each target, and 0-4 min cooling between each sonication.

EPI-2

Topic: Epilepsy
Presentation Type: Oral

Focused ultrasound ablation of the anterior thalamus for epilepsy

Vibhor Krishna, Francesco Sammartino, William Bell, Jacquelyne Cios, Jesse Mindel

Ohio State University Wexner Medical Center, Columbus, OH, USA

Background: Focused ultrasound ablation (FUSA) is an emerging treatment for neurological and psychiatric diseases. Here, we describe the results of feasibility studies and the first human application of anterior thalamic nucleus (ATN) ablation using FUSA in a patient with epilepsy who had treatment-refractory, focal onset seizures with secondary generalization.

Materials and Methods: Feasibility analysis was performed with simulations and phantom study. An investigational device exemption was obtained from the FDA to test the safety of unilateral ATN FUSA.

A 57-year-old man with a long-standing history of medically intractable, focal-onset seizures with secondary generalization from a presumed R temporal cavernous malformation was enrolled. He was maximized on Keppra and Phenytoin and failed Lamotrigine and Oxcarbazepine. Besides clinical assessments, high-resolution structural and diffusion MRI were obtained at baseline, 1 day post and 3 months post FUSA. We performed microstructural analysis with restricted diffusion imaging (RDI) and used differential tractography (DDI) to define microstructural changes at the ablation site and network-level effects of ATN FUSA respectively.

Results: Following the establishment of feasibility, the patient successfully underwent FUSA of the left ATN (coordinates X: 6.5mm lateral / Y: 0mm / Z: 8mm above mid-commissural point) using the Exablate 4000 device. Eight therapeutic sonications (peak temperature >55 0C) were performed. The ATN lesion contained two distinct clusters of RDI change at 24-hours post-FUSA, and both were detectable at 3-months imaging (Figure 1).

The patient tolerated the procedure well without neurological deficits or serious adverse events. A detailed neuropsychological assessment at 3 months revealed a decline in verbal fluency, immediate verbal memory, and psychomotor speed. The patient remains seizure free at 12 months follow-up. The DDI analysis showed significant microstructural changes in the ipsilateral fornix, corpus callosum, and cingulum (Figure 2).

Conclusions: This report represents the first ATN ablation using focused ultrasound in a patient with medically intractable epilepsy. Further safety of this procedure will be carefully assessed during this Phase-1 trial.

Acknowledgements: Focused Ultrasound Foundation

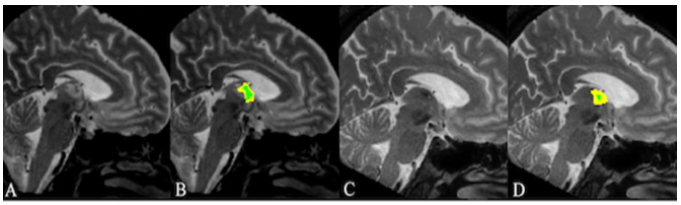

Figure 1. Sagittal image showing the ATN lesion (1day post FUSA)on T2-weighted imaging (A), and the clusters with significant RDI change between baseline and 24 hours imaging (B; clusters based on percentage RDI increase from baseline – green: 61.7% increase and yellow: 30.6%). The insets C&D are show the 3 months imaging results for T2-weighted and RDI analysis respectively (percentage RDI increase from baseline – green: 17%, yellow: 7%).

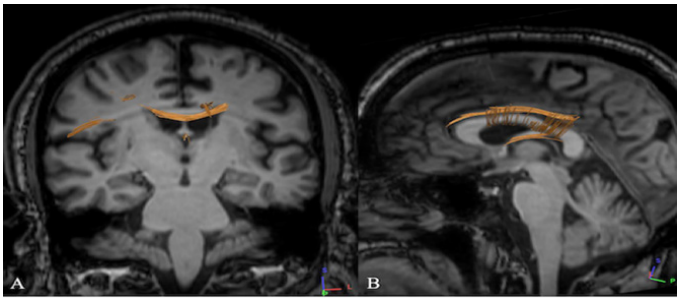

Figure 2. Differential tractography reveals significant changes in white matter microstructure in the left fornix, corpus callosum, left cingulum, right centrum semiovale and perisylvian white matter. Results comparing baseline and 3 months post-FUSA diffusion MIRI on coronal (A) and sagittal (B) projections.

EPI-3

Topic: Epilepsy
Presentation Type: Oral

Safety and feasibility of neuromodulation for drug-resistant epilepsy by low intensity focused ultrasound, an intracranial EEG study

Hsiang-Yu Yu[1], Chien-Chen Chou[1], Cheng-Chia Lee[1], Fu-Jung Hsiao[2], Syu-Jyun Peng[1]

[1]Taipei Veterans General Hospital, Taipei, Taiwan (Republic of China)
[2]National Yang Ming University, Taipei, Taiwan (Republic of China)

Background: Low intensity focused ultrasound (LIFUS) had neuromodulation effect in epilepsy in animal experiment. The safety and effect are not well established in human. Patients who have finished their intracranial EEG (iEEG) studies with conclusive results of epileptogenic foci could provide an opportunity to investigate the safety and effect of neuromodulation of LIFUS by targeting at the planned resection region. The iEEG recording could also provide real time information during the treatment.

Materials and Methods: Adult patients who received stereo-electroencephalography (SEEG) surgery for determining the epileptogenic zone (EZ) were screened for participating this study. Eligible patients were enrolled before removal of the SEEG electrodes. After skull attenuation simulating and treatment planning, the NaviFUS system (Fig. 1A) delivered the neuromodulating FUS (ultrasound parameter: ISPTA 2.8 W/cm2, duty: 30%, modulating duration: 10 minutes) to targeted brain area under the guidance of neuronavigation system (Fig. 1B). Simultaneous iEEG recordings were performed during the sonication and continuous recording for at least 72 hours after sonication. Brain MRI was done on the 14th day after sonication. Band power changes (delta, theta, alpha and beta) of the target electrodes during the sonication and a 10-minute duration after sonication were analyzed.

Results: Four patients (4 males, aged 26 to 42 years) met the criteria and completed the clinical trial. The FUS targeted the EZs for each patient (right frontal in x1, left frontal x1, and left temporal x2). One patient experienced hot sensation over the scalp during treatment. Otherwise, there were no reported unanticipated adverse events during the sonication or the 2-weeks period follow up. Significant band power increased during sonication was noted in two cases, and significant decreased after sonication was noted in three cases (Table 1). There was no increased in seizure frequency or epileptogenic biomarkers in the 72-hour iEEG follow-up. Brain MRI after sonication showed no lesioning effect on the targeted brain parenchyma.

Conclusions: LIFUS is a safe and feasible in neuromodulation of a targeted region for DRE. Simultaneous iEEG recording showed power changes during and short period after treatment. More cases and different sonication settings are necessary to determine the significance of the iEEG changes and future application in clinical practice.

Acknowledgements: NaviFus

Figure 1. A. The NaviFUS system

Figure 2. FUS neuromodulation guided by neuronavigation system

Figure 3. Target electrode band power changes compared to baseline in sonication and after sonication

	During sonication				After sonication			
	Delta	Theta	Alpha	Beta	Delta	Theta	Alpha	Beta
Case 1	-	-	-	-	-	↓**	-	-
Case 2	-	↑**	↑**	↑*	↓**	↓**	↓**	↓**
Case 3	-	↑*	-	-	-	-	-	-
Case 4	-	-	-	-	↓**	↓**	↓**	↓**

-: no change, ↑: increased power, ↓: decreased power
*: $p < 0.05$, **: $p < 0.01$

IMM-1

Topic: Immuno-oncology
Presentation Type: Oral

Immunological and therapeutic effects of focused ultrasound in canine cancer patients

Harshini Ashar, Danielle Dugat, Kalyani Ektate, Ashish Ranjan

Oklahoma State University, Stillwater, OK, USA

Background: Spontaneous canine cancers are often well-established when detected in the patients, and in some cases metastasize aggressively. Several canine tumor types (e.g. melanoma, sarcoma, etc.) demonstrate similar incidence rates and tumor immune-environment like human cancer. A growing set of immunological reagents are also available for dogs, thereby making them an excellent resource for understanding the antitumor immune effects of focused ultrasound (FUS) in a clinical setting. The objectives of this study were to understand the therapeutic effectiveness of FUS treatment in dogs with spontaneously occurring local and malignant cancers and assess local and systemic immune effects by characterizing the cytokine and immune cell populations in the blood and tumor samples.

Materials and Methods: Eight canine patients varying in tumor types (e.g. ameloblastoma, melanoma, plasmacytoma, etc.) underwent FUS ablative treatments. For tumor treatments, a dry type platform with 1MHz transducer under ultrasound guidance was employed. Transducers were moved in a rastered fashion in the 3D space under ultrasound guidance with 3 degrees of freedom to adjust both the shape and size of the treated regions and conform sonication to tumors. We performed core-ablations of the tumor (~50-60%), and this took about 3-5 min of treatment time. The primary endpoints were to determine the cytokine profile of blood 6h post-FUS exposure, and local control of tumors 3 wks post-treatment. Additionally, the populations of CD4+ and CD8+ cells in sarcoma and melanoma bearing patients (n=1) were assessed.

Results: In some cases, complete local remission of tumors was noted with FUS (especially for the benign indications). Cytokine assessment of blood performed using a multiplex array system showed significant enhancement of monocyte chemoattractant protein 1 (MCP-1) at 6h post-treatment in all dogs, suggesting an anti-tumoral macrophage activation and recruitment. FUS ablative treatment in melanoma patient caused a significant increase in the T-cell population in the blood (2-4-fold increase in CD3+ and CD3+CD8+ T-cell populations) and tumors (30-fold enhancement in CD3+ CD4+T-cell and ~8-fold increase in CD3+ CD8+T-cell) 2-wks post-treatment. In the sarcoma patient, a 4-fold increased expression of the IFNγ producing CD-4+ T cells was seen in the blood, however, the population of CD-8+Tcells remained unchanged 2wks post-treatment.

Conclusions: Our early data suggests that FUS is capable of achieving promising local remissions of canine cancers. FUS ablations can also enhance the tumor immunogenicity and populations of antigen-presenting cells and T-cells at local and systemic sites. Research is currently underway in our laboratory to understand the role of FUS parameters on the immune system in a larger set of patients varying in tumor types. We anticipate finishing the comprehensive immune evaluations in the patients before the FUS symposium.

Acknowledgements: We thank the National Cancer Institute of the National Institutes of Health under Award numbers 5R37CA239150 (Ranjan), Focused Ultrasound Foundation, PETCO and the Kerr Endowed Chairship at Oklahoma State University for support.

IMM-2

Topic: Immuno-oncology
Presentation Type: Oral

Immune cell modulation of pulsed focused ultrasound in murine melanoma and breast cancer models

Parwathy Chandran, Gadi Cohen, Scott Burks, Joseph Frank

National Institutes of Health, Bethesda, MD, USA

Background: Major therapeutic advances in the field of tumor immunotherapy are hindered by the ability to overcome the immunosuppressive tumor microenvironment (TME), which prevents the immune system from mounting an efficient anti-tumor response. Image guided pulsed focused ultrasound (pFUS) has shown promise as an immunomodulatory strategy for altering TME, predominantly through mechanotransductive forces (arising from acoustic radiation and cavitation forces) rather than elevated temperatures. This study evaluated the temporal changes following non-ablative pFUS on spleen (Sp), inguinal lymph nodes (LN), and tumor immune cell profiles in murine B16 melanoma and 4T1 mammary carcinoma flank tumor models.

Materials and Methods: Murine B16 melanoma and 4T1 mammary carcinoma cells (2×106 cells) were subcutaneously, bilaterally implanted into flanks of C57BL/6J and BALB/c mice (n=10 tumors/group/time point), respectively, and allowed to reach ~5 mm in diameter. Ultrasound-guided pFUS (VIFU 2000, Alpinion) was administered at 1 MHz, at a peak negative pressure (PNP) of 6 MPa. The entire tumor volume was sonicated with a 2-mm spacing between points using a 10-sec pulse length, 10% duty cycle and a pulse repetition frequency of 10 Hz. On days 1, 3, and 5 post-sonication, Sp, LN and tumors were harvested, fixed and processed for flow cytometry (FACS) analysis of immune cell populations [cytotoxic (Tcyt), helper (Th), and regulatory (Treg) T cells, B, natural killer (NK), dendritic cells (DC), F4/80+ macrophages (M1 and M2), myeloid-derived suppressor cells (MDSC)] and checkpoint markers (CTLA-4 and PD-1). Non-sonicated tumors along with Sp and LN harvested on days 1, 3, and 5 served as time-matched controls. Heat map was generated from the flow cytometry analysis calculated from the mean of percentage of all treated samples of each immune cell type normalized to the average of the control group (0 MPa) for each time point.

Results: Flow cytometry analysis revealed varying immune responses between B16 and 4T1 tumor bearing mice, with differences in the temporal migration of immune cells between the B16 and 4T1 Sp-LN-tumor triad over 5 days. pFUS treated B16 tumors compared to control tumors demonstrated a shift from an immunosuppressive, 'cold' TME on day 1, which progressed to a pro-inflammatory, 'hot' tumor on day 3 with elevated cell counts of tumor infiltrating T cells (Th and Tcyt), pro-inflammatory M1 macrophages and NK cells, which decreased by day 5. On day 5, a shift of cell populations toward B16 LN, with increased Treg, Tcyt, NK, F4/80, M1 and M2 activity was observed. Alternatively, post-pFUS, 'cold' 4T1 TME on day 1, evolved to exhibit an entirely diverse 'hot' tumor profile by day 5 with high cell counts for Th, Tcyt, B, NK and DC along with suppression of tumorigenic Treg, MDSC, PD-1+ and CTLA4+ numbers. 4T1 mice also showed high levels of Tcyt in Sp on day 1, and NK cells on day 3 in LN.

Conclusions: These results suggest that pFUS altered the TME by inducing anti-tumor responses by engaging both innate (macrophages, NK cells) and adaptive (Tcyt, Th cells) arms of immunity. This study reveals the differences in immune cell profiles following sonication between two tumor types, and underscores the importance of not generalizing pFUS effects on the TME. The global changes to the immune cell landscape represent a shift from anti-inflammatory, immunosuppressive TME towards a pro-inflammatory and anti-tumor TME. Optimizing pFUS parameters to enhance immune cell infiltration, would presumably lead to slowing tumor growth rates, and when coupled with immune checkpoint inhibitors could serve as a neoadjuvant approach in treating malignancy.

Acknowledgements: This study is supported by Intramural Research Programs at the NIH Clinical Center, and the National Institute of Biomedical Imaging and Bioengineering.

IMM-3

Topic: Immuno-oncology
Presentation Type: Oral

Temporal immune changes of murine breast and melanoma tumor microenvironments following pulsed focused ultrasound

Gadi Cohen, Parwathy Chandran, Rebecca Lorsung, Lauren Tomlinson, Robert Rosenblatt, Scott Burks, Joseph Frank

[1]National Institutes of Health, Bethesda, MD, USA

Background: Various cellular and biological immunotherapies have revolutionized the treatment of human malignancies by augmenting endogenous immune responses within the tumor microenvironment (TME). Despite significant advances in the field, these immune responses against cancer cells are often hinder by immunosuppressive milieu capable of mounting an anti-inflammatory effect. Non-ablative pulse focused ultrasound (pFUS) has long been recognized as a promising approach to overcome these tolerizing effects while eliciting an efficient anti-tumor response. However, cellular and molecular changes within the TME following pFUS exposure have not been thoroughly investigated. In the present study, we interrogated the immune-modulatory changes that occur following non-ablative pFUS exposure within the TME of murine B16 melanoma and 4T1 breast flank tumor models.

Materials and Methods: Murine B16 melanoma and 4T1 mammary carcinoma cells were subcutaneously implanted into both flanks of C57BL/6J and BALB/c mice, respectively (n=10 tumors/group/time point). The natural expression of the cytokines, chemokines, trophic factors (CCTFs), and cell adhesion molecules (CAM) was evaluated within the TME of untreated 4T1 and B16 flank tumors over 11 days. Ultrasound-guided pFUS (VIFU 2000 Alipinion) at 1 MHz and peak negative pressures of 6 MPa was administered to tumors after reaching an average of 5 mm in diameter. The entire tumor volume was sonicated with a 2-mm spacing between points using a 10% duty cycle, 20-msec pulse length, and a pulse repetition frequency of 5 Hz. Temporal immune-related changes in tumors were assessed 1, 8, 24, 48 and 72 hours following sonication using proteomic profiling and histological analyses. Furthermore, we performed a transcriptomic analysis of these tumors and explored the potential gene pathways accountable for the immune response induced by pFUS treatment. Causal networks were constructed from were extracted from tumors samples 0, 1, 6, 12 hours post-sonication using ingenuity pathway analysis software. A gene was considered differentially expressed if an adjusted p-value < 0.05 compare to sham untreated tumors.

Results: Natural history growth characteristics during 11 days showed a progressive increase in size for both tumors, and proteomic analysis revealed a shift toward an immunosuppressive TME. An anti-tumor TME was detected following pFUS treatment with increased expression of various pro-inflammatory CCTF and CAM as well as reduced tumor growth rates. This pro-inflammatory shift lasted for up to 24 hours and returned to the immunosuppressive TME by 72 hours. Interestingly, cross-comparison of the tumor transcriptomes identified inversed gene expression patterns, which was further validated by histological examination. Transcriptomic analyses following sonication identified inverted gene expression patterns in the two tumor types. Functional analysis of B16 tumors revealed increased intracellular signaling pathways associated with immune response regulations, while 4T1 tumors demonstrated reduced expression of proliferation genes.

Conclusions: This study provides a macroscopic overview of the effects of non-ablative pFUS sonication on the TME of two different types of tumors. The induced immune-modulation change suggests that pFUS may alter the expression of pro-inflammatory CCTF, CAM, and likely cause tropism of cytotoxic cell populations into the tumors, thus creating a more profound immunogenic response. These results provide insight into the temporal dynamics in the treatment-associated TME and underscore the potential use of pFUS as neoadjuvant treatment approaches in cancer immunotherapy.

Acknowledgements: The Intramural Research Programs at the NIH Clinical Center and the National Institute of Biomedical Imaging and Bioengineering have supported this study. The authors have no conflicts of interest.

IMM-4

Topic: Immuno-oncology
Presentation Type: Oral

Pilot evaluation of focused ultrasound ablation and focused ultrasound ablation plus pd-1 anti-body blockade in advanced solid tumors

Lynn Dengel, Nolan Wages, Kim Bullock, Rachita Khot, Craig L. Slingluff

University of Virginia, Charlottesville, VA, USA

Background: The treatment of many cancers has been revolutionized by checkpoint blockade therapies. Despite the extraordinary value of immunotherapy advances, the majority of patients (60-80%) do not respond to systemic therapy. There are pre-clinical and clinical data to support focused ultrasound ablation (FUSA) benefit in several malignancies. In addition to direct effect of tumor ablation, there are data demonstrating positive effects of FUSA on the tumor microenvironment, which may lead to enhance immunologic control of malignancy beyond the local treatment region.

Materials and Methods: The present non-randomized clinical trial applies FUSA to accessible lesions in metastatic cancers. FUSA is administered alone or combined with FDA-approved systemic immunotherapy. The primary objectives are to assess the safety and to test whether spot FUSA increases CD8+Tcell infiltration in treated metastasis. Secondary objective is to test whether spot FUSA increases CD8+ Tcell infiltration in untreated metastasis. Finally, when feasible the clinical effect on treated and untreated metastasis will be assessed as an exploratory objective.

The eligible participants must have ≥1dermal, subcutaneous or nodal metastases from an advanced solid tumor that is accessible for FUSA and biopsy. Tumor biopsy is performed pre-, post- and 3 weeks following FUSA. When possible, the peripheral zone of tumor is targeted. FUSA is administered to a single lesion with a goal of treating 33% or 1cc of the lesion volume to induce the immune response.

Safety stopping rules are evaluated by dose limiting toxicities. All eligible participants will be evaluated for the following immune response parameters. Infiltration of CD8+ T cells in treated metastases will be evaluated by immunohistochemistry (IHC). In addition, infiltration of CD8+ T cells in untreated metastases, when available, will be evaluated by IHC along with cellular and structural changes in the tumor microenvironment. Clinical benefit to treatment will be assessed by RECIST 1.1. Target enrollment is 32 participants.

Results: The trial has been approved by institutional IRB and the FDA and opened to enrollment 11/21/2019 (ClinicalTrials.gov Identifier: NCT04116320). To date, two participants have enrolled. Participant 1 with metastatic colon cancer underwent FUSA to a metastatic deposit in left groin. Participant 2 with metastatic thyroid cancer underwent FUSA to a metastatic deposit in the right axillary node.

Conclusions: This is clinical trial in progress for which 2/32 participants have undergone FUSA without immediate complications, supporting ongoing enrollment of participants with accessible metastatic tumor deposits for FUSA of advanced solid malignancy.

Acknowledgements: Focused Ultrasound Foundation and the University of Virginia

IMM-5

Topic: Immuno-oncology
Presentation Type: Oral

PD-1 inhibition to modulate response to FUS in metastatic breast cancer

Patrick Dillon, David Brenin, Timothy Bullock, Bethany Horton, Christiana Brenin

University of Virginia, Charlottesville, VA, USA

Background: FUS is an ablative therapy using high energy ultrasound waves to induce heat shock proteins, cytokine release and cellular mediated mechanisms resulting in T cell activation and recognition of tumor antigens. FUS has been demonstrated to be an effective method for inducing tumor antigen exposure and presentation to dendritic cells, thus acting as an auto-vaccine. Pembrolizumab is a PD-1 targeted antibody used in multiple solid tumors to augment T cell activation. It is hypothesized that the combination of these two modalities will result in T cell infiltration into breast tumors as well as systemic immune responses.

Materials and Methods: In this pilot study, we examine pembrolizumab therapy in combination with FUS (Echopulse device) to assess for immune stimulation and antitumor effects at local ablation sites, distant non-treated sites and in the blood. Biopsy is performed before and after treatment to assess ductal, fibroblast and immune cells in the peripheral zone of ablation as well as at distant metastatic sites. Immunologic assessments of CD8/CD4 T cells, MDSC's, T-regulatory cells and cytokine are performed. Patients were randomized to receive either PBZ 14 days before or 7 days after a single time FUS partial tumor ablation on day 15. Biopsies were done on days 1, 22 and 64 and tumor imaging was every 12 weeks.

Results: Seven patients with varying ER/HER2 status were enrolled and completed treatment. Technically, the FUS ablation of in situ breast or axillary tumors in metastatic breast cancer patients was performed with real time US guidance. Side effects include ablation site pain, fatigue, nausea, dyspnea. No adverse skin reactions nor systemic reactions were observed. Biopsies were obtained from 7 patients before and after FUS + pembrolizumab. Immunohistochemistry for CD8/CD4 and myeloid derived suppressor cells was performed. Massively parallel sequencing of cDNA (RNAseq) for markers of immune response was performed using the NextSeq to a minimum depth of 100 M 2 x 76 bp and alignment using TopHat. Preliminary results of the analysis will be presented.

Conclusions: Focused ultrasound ablation with a clinically cleared, US guided, device was safely combined with a PD-1 checkpoint inhibitor in metastatic breast cancer patients of varying receptor phenotypes. Toxicity was tolerable. Immunologic outcomes are described. Preliminary evidence suggests that FOXP3 and PD-L1 staining cells are altered in the tumor center and periphery by the application of focused ultrasound plus pembrolizumab.

IMM-6

Topic: Immuno-oncology
Presentation Type: Oral

Young Investigator

Immune sensitization and therapeutic impact of boiling histotripsy in refractory murine neuroblastoma

Avinash Eranki[1], Mario Ries[2], Priya Srinivasan[3], Xiaofang Wu[3], Tatiana Khokhlova[4], AeRang Kim[3], Karun Sharma[3], Anthony D. Sandler[3], Peter C.W. Kim[5], Bradford J. Wood[6], Chrit T.W. Moonen[2]

[1]India Institute of Technology, Bengaluru, India
[2]University Medical Center Utrecht, Utrecht, Netherlands
[3]Children's National Medical Center, Washington, DC, USA
[4]University of Washington, Seattle, WA, USA
[5]Warren Alpert Medical School of Brown University, Providence, RI, USA
[6]National Institutes of Health, Bethesda, MD, USA

Background: Neuroblastoma (NB) is the third most common childhood cancer and arises from the developing sympathetic nerve ganglia in the abdomen, chest or neck. Survival rates are only about 20-40% in high-risk patients, even with intense multimodal therapy. Immunotherapy promises exceptional benefits to cancer patients. However, the majority of cancer types, including high-risk NB remain immunologically unresponsive, possibly due to a weak or small scale mutanome and unfavorable regulation of immunity. We previously demonstrated on a clinical MR-HIFU system that boiling histotripsy (BH) is capable of producing controlled, spatially precise mechanical tissue fractionation. The goal of this study was to evaluate the role of BH in sensitizing the immune system to checkpoint inhibitor therapy in a refractory murine NB tumor model.

Materials and Methods: This study was approved by the IACUC at Children's National. NB tumors (Neuro2a) were grown unilaterally or bilaterally in A/J mice via subcutaneous hind limb injection of 1×106 tumor cells. Once the tumors reached 1200-1750 mm3, they were treated with 1) BH alone (N = 10), 2) αCTLA-4 + αPD-L1 (N = 10), 3) BH + αCTLA-4 (N = 10), 4) BH + αPD-L1 (N = 10), or 5) BH + αCTLA-4 + αPD-L1 (unilateral tumors, N = 16), and 6) BH + αCTLA-4 + αPD-L1 (bilateral tumors, N = 18, unilateral BH treatment). Control group (N=10) received no drug nor BH. Checkpoint antibodies were administered intraperitoneally at 100 µg/antibody/time-point at three time points (Figure 1a). Mice were anesthetized and positioned using a custom-built holder and a 3-axis linear stage. Three adjacent foci (1.5×1.5×6 mm @-6dB, Figure 1b) were targeted within each tumor by a 1.5 MHz HIFU transducer (aperture diameter = 75 mm, focal length = 56 mm) under coaxial b-mode ultrasound imaging guidance. Sonication parameters were shock amplitude of 80 MPa, pulse length = 13.33 ms, PRF = 1 Hz, total sonication time/focus = 15 s. Pain medication was administered at least once in all mice immediately post-BH, and mice were monitored for any adverse events. ELISA of cardiac blood serum, and flow cytometry of tumor, draining & contralateral lymph nodes, and spleen were performed. Mice surviving for >300 days were re-challenged with 2x initial tumor burden (2 × 106 cells), to test long-term immune memory effect.

Results: BH alone caused upregulation of splenic and lymph node NK and DC's and circulating IL-2, GM-CSF, IFN-γ, and IL-6, whereas immune regulators like CD4+Foxp3+, IL-10, and VEGF-A are significantly reduced (Figure 2). BH + αCTLA-4 + αPD-L1 induced significant CD8α+CD11c+ cells in the spleen and draining lymph nodes, increase in CD11c+ in draining lymph nodes, circulating IFN-γ and, further decrease in circulating IL-10 and IL-6 compared to untreated group (Figure 3). Combining BH + αCTLA-4 + αPD-L1 significantly enhances anti-tumor response, improving survival from 0 to >60% in mice with unilateral tumors (Figure 4a). This drug-device combination also results in an abscopal effect with unilateral treatment of refractory bilateral tumors (>62% survival, p<0.0001, Figure 4b). Further, this combination treatment significantly induces CD4+CD44+hiCD62L+low (Figure 4c) and CD8α+CD44+hiCD62L+low (Figure 4d) cells in the spleen, demonstrating significant effector memory response to NB tumor cells.

Conclusions: BH + αCTLA-4 + αPD-L1 is capable of treating large established NB tumors in mice, resulting in an abscopal response, long-term survival and immune memory. BH increased anti-tumor cytokine and cellular

Figure 1. a. Pictorial representation of treatment protocol of BH + αCTLA-4 + αPD-L1 in mice with unilateral or bilateral NB tumors. b. Placement of three adjacent BH foci within the NB tumors.

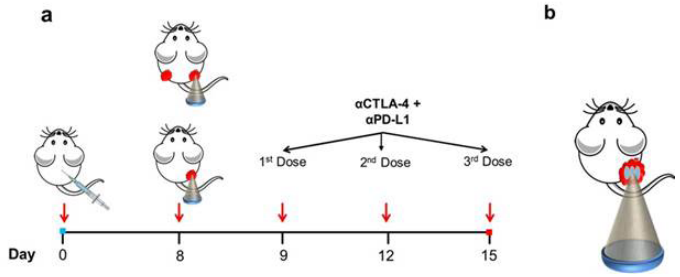

populations while downregulating immune suppressive factors, making the tumor more immunogenic (converting from immune-cold to hot). BH can sensitize the immune response to checkpoint inhibitors, and may be achieved on a clinical HIFU system, making this device-drug combination an appealing candidate for rapid clinical translation. For a more complete account, see Eranki et al. Clinical Cancer Research, 2020.

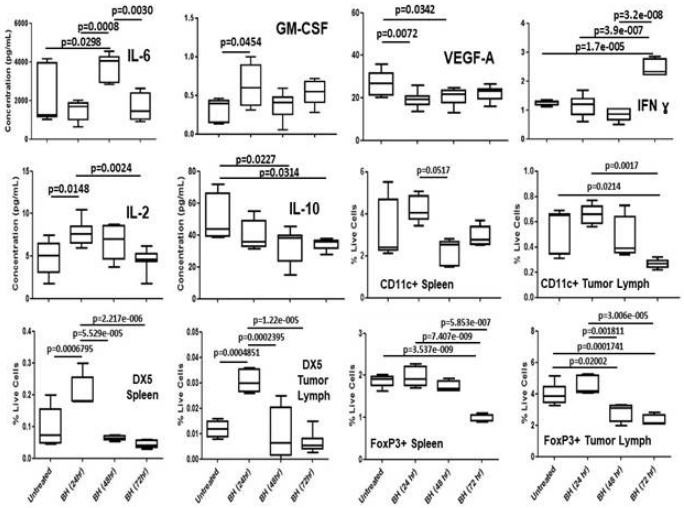

Figure 2. Systemic cellular and cytokine effect of BH in mice with NB tumors. BH resulted in an upregulation of cytokines (IL-6, GM-CSF, IL-2), and downregulated pro-tumoral cytokines (IL-10, VEGF-A). In addition, there was an increase in concentration of NK −cells (DX-5), and dendritic cells (CD11c+), and a decrease in concentration of regulatory T-cells (FoxP3+).

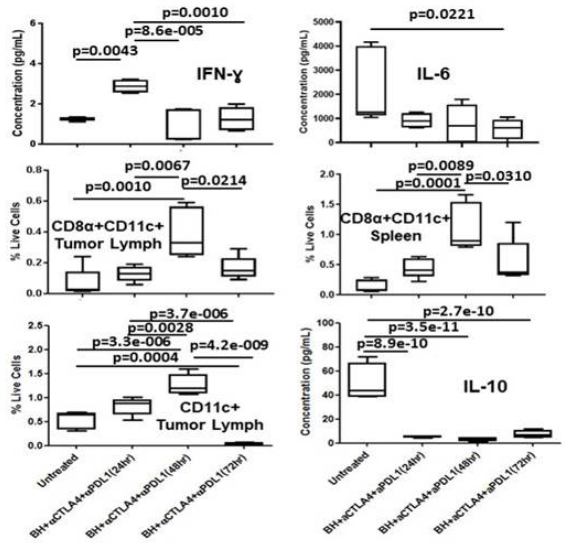

Figure 3. The systemic immune response remained more towards anti-tumoral when treated with BH + αCTLA-4 + αPD-L1.

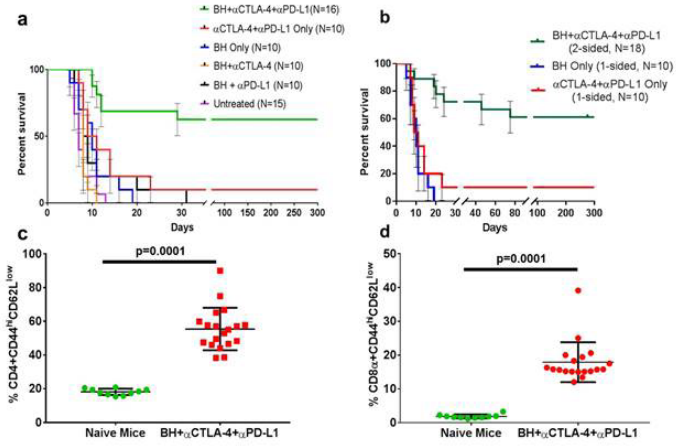

Figure 4. Kaplan-Meier plot post-BH + αCTLA-4 + αPD-L1 therapy of a. Unilateral tumors b. Bilateral tumors c. CD4+ effector memory response d. CD8+ effector memory response

IMM-7

Topic: Immuno-oncology
Presentation Type: Oral

Temporal dynamics of intratumoral immune cell infiltration triggered by boiling histotripsy

Avinash Eranki[1], Mario Ries[2], Priya Srinivasan[3], Tatiana Khokhlova[4], Xiaofang Wu[3], AeRang Kim[3], Karun Sharma[3], Anthony D. Sandler[3], Peter C.W. Kim[5], Chrit T.W. Moonen[2], Bradford J. Wood[6]

[1]India Institute of Technology, Bengaluru, India
[2]University Medical Center Utrecht, Utrecht, Netherlands
[3]Children's National Medical Center, Washington, DC, USA
[4]University of Washington, Seattle, WA, USA
[5]Warren Alpert Medical School of Brown University, Providence, RI, USA
[6]National Institutes of Health, Bethesda, MD, USA

Background: Neuroblastoma (NB) is a common high-risk childhood cancer, with poor outcomes (20-40% survival) even with multimodal therapies, possibly due to lack of mutations, and unfavorable regulation of the immune system. Boiling histotripsy (BH) has been shown to be capable of producing mechanically fractionated lesions in a spatially precise manner on a clinical high intensity focused ultrasound (HIFU) system. The goal of this work is to characterize the role of BH in a temporally evolving intratumoral immune response in a murine NB model and resulting in enhanced survival.

Materials and Methods: This study was approved by the Institutional Animal Care and Use Committee. NB tumors (Neuro2a) were grown unilaterally in A/J mice via subcutaneous hind limb injection of 1 million tumor cells. Once the tumors reached 1200-1750 mm3 (~13-15 mm diameter), they were treated with BH. Data from treated mice were compared against untreated mice (N=5 per time point). Treated mice were anesthetized and positioned on a 3D printed holder, controlled with a 3-axis linear stage. Three adjacent foci (1.5×1.5×6 mm @-6dB, Figure 1b) were targeted by a 1.5 MHz single-element HIFU transducer (aperture diameter = 75 mm, focal length = 56 mm), and treated with BH within each tumor, guided by b-mode ultrasound imaging. Sonication parameters were fc = 1.5 MHz, PRF = 1 Hz, total sonication time/focus = 15 s, and pulse length = 13.33 ms. Pain medication was administered in all mice immediately post-BH, and mice were monitored for adverse events. Tumors were excised at 24, 48, and 72 hours after BH (Figure 1), and fixed in 10% neutral buffered formalin solution for ~ 72 hours. Subsequently, tumors were sectioned using a microtome into 5 μm slices, and stained with H&E, CD68+, CD4+, CD8α+, and PD-L1. Stained tissue sections were imaged under a slide scanning bright field microscope (TissueScope LE, Ontario, Canada).

Results: BH tumor therapy resulted in fractionated tumor debris at 24-hrs post-therapy, with a tight margin separating structurally intact tumor surrounding this treated region (Figure 1). Compared to untreated tumors, the tumors treated with BH 24, 48, and 72-hrs later demonstrated a significant immune cell infiltration post BH-therapy. Specifically, there was a significant intratumoral increase in CD68+ (macrophages) at 48-hrs post-BH, with a sustained increase of CD68+ population observed at 72-hrs post-BH (Figure 2). In addition, we observed a significant increase in intratumoral infiltration of CD4+ at 24-hrs after BH therapy, but returned to baseline at 48 and 72-hrs after BH therapy (Figure 2). CD8α+ population also saw a significant increase at 24-hrs post-BH, but their population quickly reduced to pre-treatment levels at 48 and 72-hrs after BH (Figure 2). Our results show that BH significantly increase the expression of PD-L1 on tumor cells at 72-hrs after BH therapy.

Conclusions: BH therapy resulted in a significant intratumoral immune cell infiltration that is temporally dependent and dynamic. BH therapy of refractory NB tumors results in immunocyte recruitment and upregulation of a major checkpoint inhibitor drug target. This may in part explain the enhanced tumor regression and survival outcomes for immunotherapeutic intervention associated with BH and check point inhibition in this model, and merits further consideration for translation.

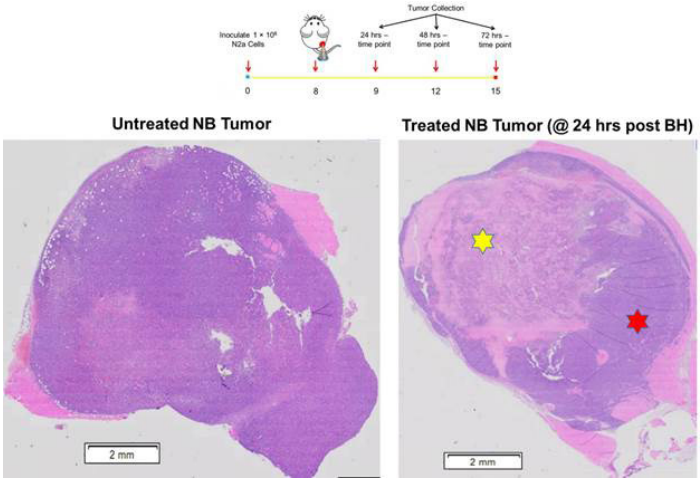

Figure 1. Hematoxylin and Eosin (H&E) stained tumors pre and post-BH (72-hrs).

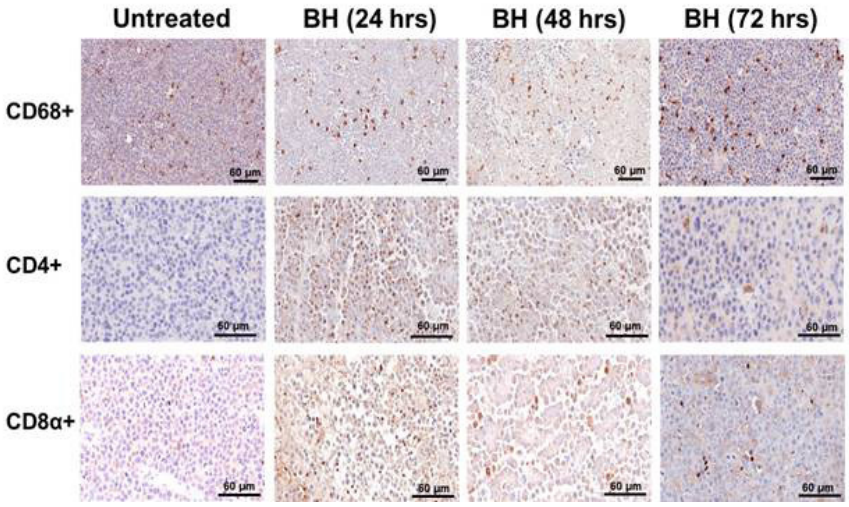

Figure 2. Representative immunohistochemistry images of untreated tumors compared against, tumors excised at 24, 48, and 72-hrs post-BH.

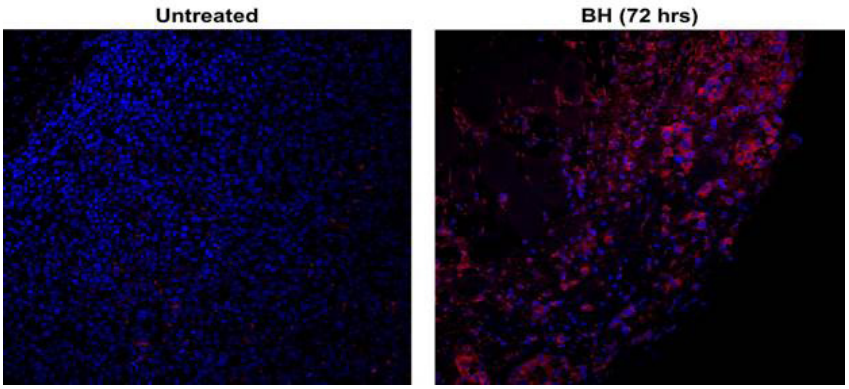

Figure 3. Response of intratumoral PD-L1 to BH therapy. BH therapy to tumors results in a significant upregulation of PD-L1 on tumor cell surface, 72-hrs after BH.

IMM-8

Topic: Immuno-oncology
Presentation Type: Oral

Impact of a combined immune checkpoint inhibitor and mechanical focused ultrasound treatment in a MC38 preclinical model

Fant Cécile[1], Chloé Grasselly[2], Morgane Denis[2], Doriane Mathé[2], Pierre-Antoine Choffour[2], Loic Daunizeau[1], Jean Louis Mestas[1], Cyril Lafon[1], Tianxi Li[3], Christophe Caux[4], Stephane Depil[4], Charles Dumontet[5], Frédéric Padilla[6]

[1]LabTAU INSERM U1032, Lyon, France
[2]Antineo, Lyon, France
[3]University of Virginia, Charlottesville, VA, USA
[4]CRCL INSERM U1052, Lyon, France
[5]Anticancer Antibodies INSERM U1052, Lyon, France
[6]Focused Ultrasound Foundation, Charlottesville, VA, USA

Background: Immune checkpoint inhibitors (ICI) counteract the local immunosuppression in the tumor environment, but are so far effective in only 20-40 % of treated patients due to a lack of a baseline immune response. ICI response can be enhanced in poor or non-responder patients by combination with focal therapies such as Focused ultrasound (FUS). Recent preclinical and clinical data have shown that FUS can enhance host antitumor immune response in numerous ways. Combining FUS and ICI could be a clinically relevant approach but the choice of modality, dosage and treatment schedule are still open questions. Here, we report the effect of a combined ICI and mechanical FUS treatment on tumor growth, survival and intratumoral immune infiltrate in a MC38 preclinical model.

Materials and Methods: Mice were exposed to mechanical FUS using a confocal device generating and monitoring pulsed cavitational ultrasound (frequency 1.1MHz, PRF 250 Hz, DC 1%, peak negative pressure -20.5MPa). Anti-PD1 antibodies were administrated each week intraperitoneally at the dose of 12.5 mg/kg. Different schedules of treatment were investigated: simultaneous treatment of FUS and ICI, delivery of ICI three days before or three days after FUS. A longitudinal follow-up of tumor growth and overall survival was performed during 50 days. Lymphoid and myeloid intratumoral immune cells were assessed by flow cytometry on days one, three and six after the start of the combined treatment, including expression levels of co-inhibitory and co-stimulatory molecules such as PD-1, PD-L1, TIGIT, LAG3, TIM-3 and ICOS. To study the impact of immune response, combined treatment were performed on Rag2 -/- mice, and on CD8 T-cell depleted wild-type mice.

Results: Significant increased survival and tumor growth control were observed when ICI was delivered three days before or three days after FUS, with better results when FUS was delivered first, with an increased survival up to three-fold for the combination compared to control. Simultaneous treatment did not impact survival or tumor growth. When T cells were depleted, combined treatment did not lead to increased survival or control of tumor growth. Flow cytometry revealed that combined treatment may lead to increased antigen priming as increased CD11c+ CMHIIhigh conventional dendritic cells (DC), activated CD8- and Sirpa-CD24- subpopulations were found. As for co-inhibitory and co-stimulatory molecules expression at cell surface, flow cytometry showed increased PD1 and LAG3 expression by CD8+ cells as well as increased expression of various co-inhibitory molecules at CD4+ and tumor cells surface for combined group. Flow cytometry data were also analysed with unsupervised approach.

Conclusions: Combining ICI with mechanical FUS results in a significant improvement in tumor growth control and survival, depending on the treatment schedule. This response is immune dependent, certainly through a CD8-mediated response, as depleted mice are not responsive to the combination. Significant changes in immune infiltrate such as increased DC-mediated response are potential candidates to explain this enhanced response. However, the combined treatment led to increased PD1 expression, as well as of other co-inhibitory molecules, by CD4+, CD8+ and tumor cells possibly explaining the transient effect of the combination. These results carry important implications for future combined FUS/ICI therapies.

Acknowledgements: This work was supported by the LabEx DEVweCAN (ANR-10-LABX-0061) of the University of Lyon, within the program "Investissements d'Avenir" (ANR-11-IDEX-0007) operated by the French National Research Agency (ANR) and the FUS Foundation.

IMM-9

Topic: Immuno-oncology
Presentation Type: Oral

Non-thermal histotripsy focused ultrasound tumor ablation as a means of generating immunostimulatory tumor vaccines

Amy Felsted[2], Ryan Hubbard[2], Ashley Pepple[1], Ryan McGinnis[2], Tejaswi Worlikar[2], Anutosh Ganguly[1], Zhen Xu[2], Clifford Cho[1]

[1]University of Michigan Medical School, Ann Arbor, MI, USA
[2]University of Michigan, Ann Arbor, MI, USA

Background: We recently demonstrated that tumor treatment with histotripsy, a non-thermal method of focused ultrasound ablation, generates a profound local and systemic anti-tumor immune response that is strong enough to induce abscopal inhibition of distant tumors and potentiate the efficacy of checkpoint inhibition immunotherapy.

Materials and Methods: To gain mechanistic insight into these potentially therapeutic effects, we used a murine model of melanoma therapy to compare the immunological impact of histotripsy with thermal focused ultrasound ablation.

Results: Whereas subtotal tumor treatment with histotripsy and thermal focused ultrasound ablation were comparable in their ability to inhibit tumor growth, abscopal inhibition of contralateral, untreated tumors was only observed with histotripsy. Histotripsy stimulated larger populations of infiltrating myeloid and lymphocyte populations in treated and untreated tumors than thermal focused ultrasound. Tumor homogenates created by histotripsy but not thermal focused ultrasound were capable of activating tumor antigen-specific CD8+ T cells in vitro, suggesting that only histotripsy ablation releases immunogenically-intact tumor antigen peptides. Moreover, tumor homogenates generated by histotripsy but not thermal ablation conferred immunoprotection to naïve mice against tumor challenge when used as a vaccine; indeed, the pattern of intratumoral cell infiltration seen after histotripsy homogenate vaccination was similar to that observed in abscopal tumors after histotripsy ablation.

Conclusions: These findings suggest that the ability of histotripsy to induce mechanical cell death without the potentially denaturing effects of heat may be critical for its potently immunostimulatory effect.

Acknowledgements: Department of Veterans Affairs; National Institutes of Health; Focused Ultrasound Foundation; Forbes Institute for Cancer Discovery

IMM-10

Topic: Immuno-oncology
Presentation Type: Oral

Ultrasound stimulated microbubbles enhance the potency and durability of anti-PD-L1 checkpoint blockade therapy in an orthotopic breast tumor model

Sharshi Bulner[1], William Cruz[1], Alex Wright[1], Robert Kerbel[1], David Goertz[2], Kullervo Hynynen[1]

[1]Sunnybrook Research Institute; University of Toronto, Toronto, ON, Canada
[2]University of Toronto, Toronto, ON, Canada

Background: Immune checkpoint inhibitor therapies (CITs) are fundamentally impacting the treatment landscape of many cancer types. Unfortunately, only limited subsets of patients show durable complete responses (CRs). Considerable efforts are therefore being made to combine CITs with other therapies. However, a significant issue with drug based combinatorial approaches is the associated increase in systemic toxicity, which limit the number of combinations of anticancer agents that can be used. Therefore, there is strong interest in combining CITs with localized physical therapies, since it does not add to systemic toxicity and can promote aspects of the innate and/or adaptive immune system, which can complement CITs. Here we investigate if the use of focused ultrasound and microbubbles (FUS/MBs) to disrupt tumor vasculature can enhance the effects of a clinically relevant combination of anti-PD-L1 (aPD-L1) antibody + paclitaxel (PTX) in the treatment of triple negative breast cancer (TNBC).

Materials and Methods: Murine mammary tumors (EMT6) were initiated in the mammary fat pads of Balb/c mice. At day 8 post tumor implantation, experiments were conducted with 4 groups: sham, FUS/MBs, aPD-L1+PTX, FUS/MBs+aPD-L1+PTX (combo). The aPD-L1 antibody (5 mg/kg; Genentech) was given i.p. every 3-4 days for a total of 10 doses. PTX (20 mg/kg) was administered i.p. biweekly for a total of 3 doses. FUS/MBs treatments consisted of two MRI guided FUS treatments with the LP100 system (FUS Instruments) administered 10 mins apart with Definity MBs (60 μL/kg) using 3 MPa 580 kHz 10ms pulses at 5s intervals for 3 minutes following the bolus injection of MBs (Fig. 1). Tumor growth was monitored longitudinally until tumor volumes reached 1700 mm3 or ethical endpoints.

A passive cavitation detector confirmed the presence of broadband emissions, consistent with inertial cavitation. Perfusion shutdown elicited by FUS/MBs treatment was assessed in separate acute experiments (1 and 24-hr points) using Hoescht perfusion dye. Tumors were sectioned and analyzed with custom written MATLAB code to evaluate perfusion. H&E staining was conducted to assess necrosis.

To determine if an immune memory response is generated by FUS/MBs treatment, re-challenge experiments were conducted. To determine if a T-cell response is elicited by FUS/MBs treatment and whether it enhanced the aPD-L1+PTX combination, we repeated the above longitudinal experiments but instead used a Balb/c nude mouse model (devoid of T-cells).

Results: FUS/MBs treatment resulted in a substantial shutdown of blood flow compared to the sham group along with increased levels of necrosis. Survival studies demonstrated that the addition of FUS/MBs treatment profoundly enhances the effects of the aPD-L1+PTX and resulted in a CR for 7/8 tumors (Fig. 2). Re-challenge experiments in the contralateral fat pad of CR mice revealed either no re-growth or delayed growth, consistent with immune memory being engaged (Fig. 3). In contrast, in the nude mouse model, no CRs were observed in any of the treatment groups (Fig. 4).

Conclusions: This work demonstrates the preclinical feasibility of using FUS/MBs to enhance the efficacy of the clinically relevant combination of aPD-L1+PTX in the treatment of TNBC. Such an approach has the important advantage of not adding to systemic toxicity, as is the case with combining multiple immunotherapies. The results also suggest the effects are mediated by a T-cell mechanism. This potential anti-tumoral immune mechanism elicited by FUS/MBs treatment may have implications in the treatment of metastatic disease and is currently under further investigation.

Acknowledgements: Terry Fox New Frontiers Program Project Grants.

Figure 1. Overview of the set-up used for focused ultrasound treatment.

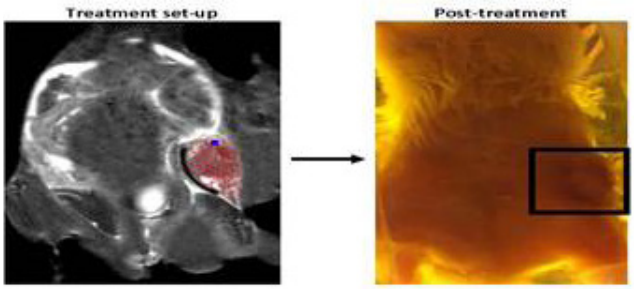

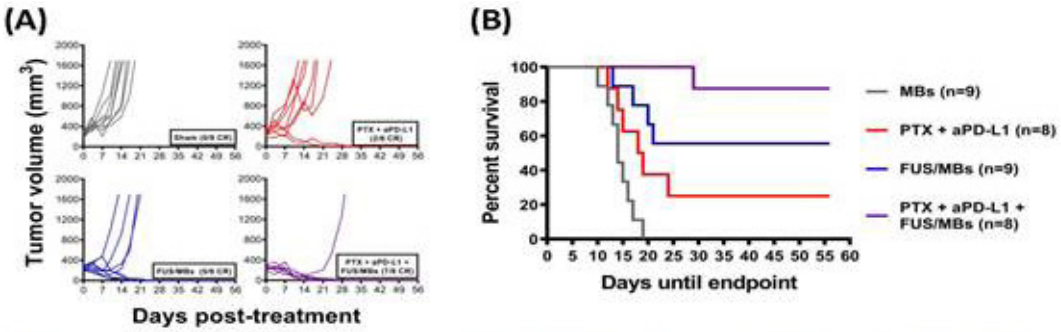

	p-values for Kaplan-Meir	Median survival (d)	Hazard ratio
(MBs) *vs.* (PTX + aPD-L1)	0.0344	14.00 vs. 18.50	0.3795
(MBs) *vs.* (FUS/MB)	0.0005	14.00 vs. Undefined	0.1859
(MBs) *vs.* (PTX + aPD-L1 + FUS/MB)	<0.0001	14.00 vs. Undefined	0.0540
(PTX + aPD-L1) *vs.* (FUS/MB)	0.194	18.50 vs. Undefined	0.4401
(PTX + aPD-L1) *vs.* (PTX + aPD-L1 + FUS/MB)	0.0063	18.50 vs. Undefined	0.0976
(FUS/MB) *vs.* (PTX + aPD-L1 + FUS/MB)	0.1273	Undefined vs. Undefined	0.2146

Figure 2. Combinatorial treatment of PTX + aPD-L1 + FUS/MBs significantly inhibits tumor growth compared to drug only (PTX + aPD-L1) in Balb/c mice.

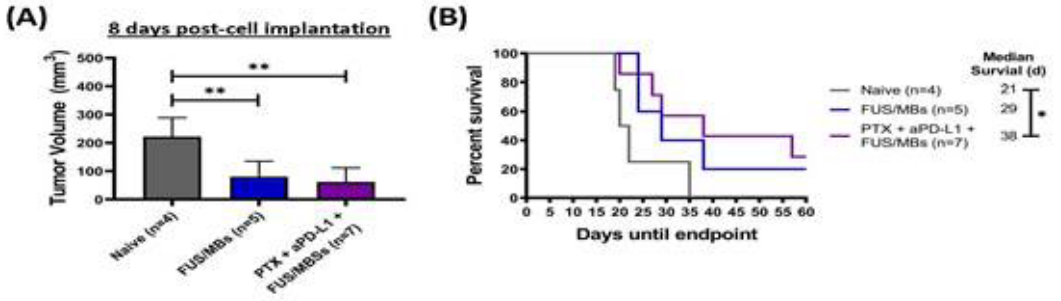

Figure 3. Tumor re-challenge experiments in the contralateral fat pad of immunocompetent mice with CRs revealed either no re-growth or delayed growth, suggesting an immune memory response.

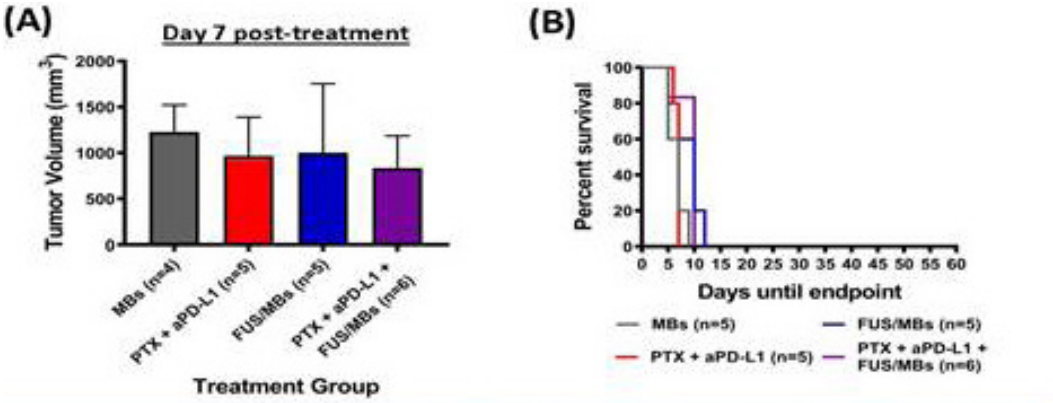

	p-values for One-way ANOVA	p-values for Kaplan-Meir Survival Analysis	Median Survival (days)	Hazard ratio
(MBs) *vs.* (PTX + aPD-L1)	0.8568	0.9555	7.00 vs. 7.00	0.9788
(MBs) *vs.* (FUS/MB)	0.9008	0.0802	7.00 vs. 10.00	0.4359
(MBs) *vs.* (PTX + aPD-L1 + FUS/MB)	0.6113	0.0107	7.00 vs. 10.00	0.3138
(PTX + aPD-L1) *vs.* (FUS/MB)	0.9995	0.1552	7.00 vs. 10.00	0.5517
(PTX + aPD-L1) *vs.* (PTX + aPD-L1 + FUS/MB)	0.9697	0.0318	7.00 vs. 10.00	0.3966
(FUS/MB) *vs.* (PTX + aPD-L1 + FUS/MB)	0.9418	0.9822	10.00 vs. 10.00	0.9922

Figure 4. Combinatorial treatment of PTX + aPD-L1 + FUS/MB in Balb/c nude mice does not recapitulate the same efficacy of tumor growth inhibition as its immunocompetent Balb/c mice counterpart.

IMM-12

Topic: Immuno-oncology
Presentation Type: Oral

Immunomodulation of intracranial melanoma in response to blood-tumor barrier opening with focused ultrasound

Colleen Curley, Aaron Stevens, Alexander Mathew, Katarzyna Stasiak, William Garrison, Grady Wilson Miller, Natasha Sheybani, Victor Engelhard, Timothy Bullock, Richard Price

University of Virginia, Charlottesville, VA, USA

Background: Focused ultrasound (FUS) applied in the presence of circulating microbubbles (MBs) can be used to open the blood-tumor barrier (BTB) and improve the delivery and penetration of agents into brain tumor tissue. It is, therefore, an attractive modality for use in combination with traditional and immune-based therapies targeted to intracranial tumors. Additionally, it is possible that FUS+MBs BTB opening can modulate the immune microenvironment, which could augment the efficacy of immune-targeted therapies. Given the emergence of FUS+MBs BTB opening in combination with immunotherapeutic agents, as well as the progression of FUS into clinical trials of patients with metastatic brain tumors, it is important to understand how FUS+MBs modulates the immune landscape of intracranial tumors.

Materials and Methods: FUS+MBs BTB opening (1.1 MHz, 0.5 MPa peak-negative pressure, 10 ms pulses, 2 s pulsing interval, 2 min duration, 4 spot grid) was performed in and around intracranial B16F1cOVA and B16ZSGreenOVA (i.e. tumor cells stably transfected to express MHC-restricted peptides derived from OVA in frame with ZsGreen fluorescent protein) tumors. Bulk RNA sequencing was performed on tumor (B16F1cOVA) tissue at 6h and 24h post-treatment. Flow cytometry was performed on tumor (B16ZSGreenOVA), meninges, and superficial cervical lymph nodes (SLNs), which drain meningeal lymphatics, at 2d and 4d post-treatment. ZsGreen fluorescence was used as a marker for antigen uptake in dendritic cells (DCs). We also stained for the SIINFEKL peptide MHC class I (H-2Kb) complex on DCs, indicating cross-presentation of the OVA257-364 peptide via MHC I. We also investigated whether FUS+MBs led to differences in expression of cell adhesion molecules (i.e. E-selectin, P-Selectin, ICAM-1, and VCAM-1) on intracranial B16F1cOVA tumor CD31+ endothelial cells at 6h and 24h post-treatment. Finally, we performed adoptive cell transfers of activated OT-1 cells immediately prior to FUS+MBs BTB opening in B16F1cOVA tumors. Eighteen hours post-treatment we harvested the tumors and meninges, and transferred cell numbers in these tissues were assessed by flow cytometry.

Results: Grayscale intensity within the FUS+MBs treated ROI in contrast MR images was significantly increased, indicating successful BTB/BBB disruption (Figure 1). A total of 203 and 37 transcripts were significantly differentially expressed over Sham treated tumors at, respectively, 6h and 24h post-treatment (Figure 2A,B). Several transcripts related to inflammation were significantly upregulated at 6h (Figure 2C-E). Gene set enrichment analysis revealed numerous differentially expressed pathways related to inflammation at 6h and 24h (Figure 3). In studies with B16ZsGreenOVA tumors, the percentage of ZsGreen-positive DCs in FUS+MBs treated tumors was increased at 2d (Figure 4A). We also observed increased CD86 expression (data not shown) and decreased ZsGreen antigen load (Figure 4D) in the meningeal DC population. However, we found no changes in expression of cell adhesion molecules on tumor endothelial cells (data not shown) and no changes in activated T cell homing in FUS+MBs treated tumors

Conclusions: We used RNA sequencing and flow cytometry to assess acute immune responses to FUS+MBs BTB opening in intracranial melanoma tumors. This response was characterized by enhanced gene signatures related to proinflammatory cytokines, chemokines, pattern recognition receptor signaling and antigen processing and presentation. The flow cytometry data support the notion that FUS+MBs can increase antigen presence or distribution within the tumor and contribute to DC maturation. Overall, however, the observed response in intracranial melanoma tumors is mild and transient. Nonetheless, we submit that understanding this response will be important for the rational design of FUS+MBs mediated therapeutic delivery approaches.

Acknowledgements: Supported by National Institutes of Health (NIH) Grants R01EB020147 to R.J.P., R01CA197111 to R.J.P., T.N.J.B. and V.H.E., and Melanoma

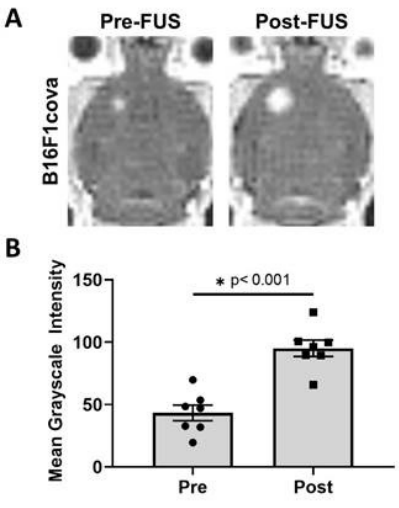

Figure 1. A. Representative images showing enhanced contrast Post-FUS. B. Quantification of pre- and post-FUS grayscale intensity for FUS+MBs treated tumors.

Research Alliance Established Investigator Award 348727 to T.N.J.B. A.D.S. was supported by National Institutes of Health.

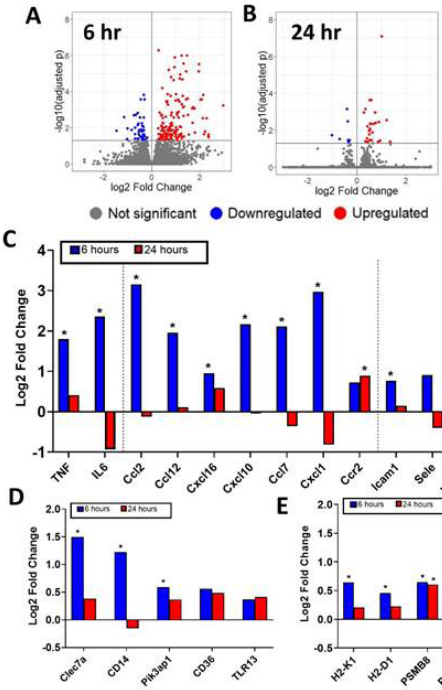

Figure 2. A,B: Volcano plots. C,D,E: Log2 fold change of FUS+MBs treated vs. sham tumors at 6 hours and 24 hours post treatment.

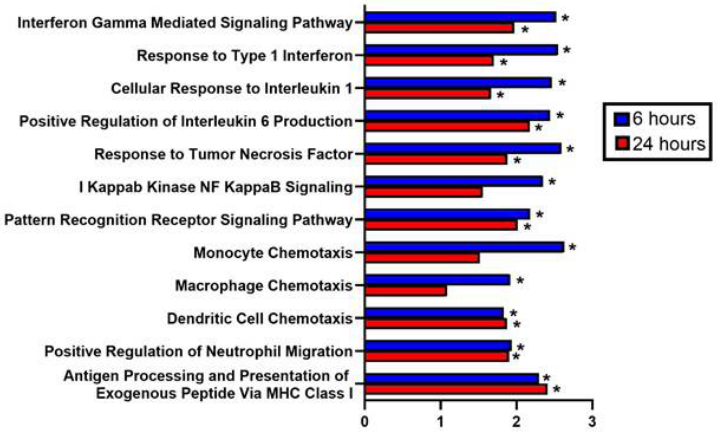

Figure 3. Normalized enrichment scores for selected pathways of FUS+MBs treated relative to sham treated tumors at 6 and 24 hours post FUS+MBs.

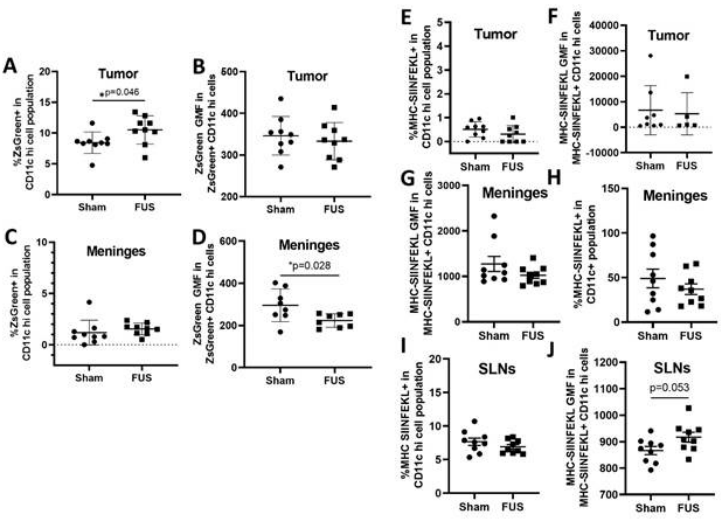

Figure 4. Fig 4: A,C: % ZsGreen positive dendritic cells. B,D: Geometric mean fluorescence of ZsGreen. E,G,I: % MHC-SIINFEKL positive DCs. F,H,J:Geometric mean fluorescence of MHC-SIINFEKL.

IMM-13

Topic: Immuno-oncology
Presentation Type: Oral

Can focused ultrasound enhance the immunogenic properties of doxorubicin and ThermoDox in preclinical and clinical settings?

Ashish Ranjan, Sri Nandhini Sethuraman, Joshua VanOsDol, Harshini Ashar, Mohit Singh Singh, Akansha Singh, Danielle Dugat

Oklahoma State University, Stillwater, OK, USA

Background: Doxorubicin (Dox) is a widely used anticancer agent indicated against sarcoma, breast, and other types of cancer. Recent studies have also found that Dox can aid anti-tumor immunity by inducing immunogenic cell death (ICD) and infiltrations of activated immune cells. Additionally, we and others have shown that FUS-induced local tumor heating (>40ºC) modifies the tumor microenvironment to impart several benefits including enhanced chemotherapy with ThermoDox (TDox), tumor antigen release, expression of heat-shock proteins, upregulation of pro-phagocytic signals such as calreticulin (CRT), and overall tumor immunity. What is not known is whether the application of Dox with FUS can invoke systemic antitumor immunity, and improve the therapeutic effects in malignant cases. The objectives of this study were to combine FUS with Dox or TDox chemotherapy in murine colon cancer and spontaneous canine/feline sarcoma patients and investigate the generation of systemic anti-tumor immunity.

Materials and Methods: To characterize the immune activation mechanisms of Dox with FUS heating (~42-45°C), we began by assessing the therapeutic effects in a bilateral CT26 colorectal tumor model syngeneic with BALB/c mice. CT26 model fits well with human abscopal effects and metastatic disease and is immunogenic, and multiple tumors can be grown on the same mouse with one tumor being treated and another being tracked for systemic effects. We compared the following groups (n=8-10/group, 5mg Dox/kg body weight): 1. Untreated control, 2. Dox, 3. FUS, 4. Dox + FUS, 5. TDox and 6. TDox + FUS. FUS heating of the tumors (~60-100mm3) was performed unilaterally in combination with Dox and TDox infusion for 30 min. The ability of FUS to enhance local and systemic effects of Dox and TDox was determined by immunological characterization of the harvested tumors, and tumor growth delay of local and distant untreated tumors 3-5 wk post-inoculation. To understand the feasibility in a clinical scenario, canine and feline sarcoma patients (n=1) that demonstrate similar microenvironmental features to human sarcoma were treated with TDox + FUS, and immune evaluations of peripheral blood were performed.

Results: TDox (±FUS) demonstrated significant potency compared to other treatments at the treated site. Also, when the monotherapies (Dox, TDox) were combined with FUS, it achieved significant suppression of untreated tumors (> 75%) vs. that seen in controls, and an effect that was ~50-70% greater than that seen with TDox and FUS alone. Notably, TDox + FUS was also relatively more efficacious than Dox + FUS at the untreated site. Immunologically, the enhanced Dox exposures with FUS increased the populations of dendritic cells and M1 macrophages (~2-2.5 fold) in the untreated tumors. Also, the ratio of granzyme B+ CD4+ effector T-cell to regulatory T cell populations was elevated by 3-5-fold in the TDox+ FUS treatment group compared to other treatments. These findings were also observed in the canine and feline patients, wherein FUS+TDox enhanced the populations of IFN-gamma expressing T-cells and concurrently decreased the pro-tumoral T-regulatory cells.

Conclusions: Our preclinical and clinical data is consistent with superior efficacy of TDox in tumors treated simultaneously with a heat source. Activation of immune response and expansion of treatment benefits to distant tumor demonstrate that the local treatment of TDox and Dox produce systemic effects, and that this effect is presumably mediated by activation of systemic immunity. Additional investigations in a combinatorial setting with checkpoint blockade therapy will shed more light on the translational value of this approach.

Acknowledgements: We thank the Celsion Corporation, Focused Ultrasound Foundation, PETCO, National Cancer Institute of the National Institutes of Health under Award numbers 5R37CA239150 (Ranjan), and the Kerr Endowed Chairship at Oklahoma State University for support.

IMM-15

Topic: Immuno-oncology
Presentation Type: Oral

Immuno-PET assessment yields a rational paradigm combining FUS blood brain/tumor barrier disruption with CD47 blockade for glioma therapy

Natasha Sheybani, Victoria Breza, Soumen Paul, Katelyenn McCauley, Stuart Berr, Grady Wilson Miller, Kiel Neumann, Richard Price

University of Virginia, Charlottesville, VA, USA

Background: The natural disease course for glioblastoma (GB) entails invariably grim outcomes for patients, with median survival on the order of 18 months. Phagocytic immunotherapies, such as CD47 blockade (e.g. mCD47), have recently emerged as promising strategies for GB therapy. However, their efficacy is challenged by presence of the blood brain and tumor barriers (BBB/BTB), which hinder drug delivery to the brain. For this reason, transient disruption of the BBB/BTB via focused ultrasound (FUS) and circulating microbubbles (MB) holds promise for improving therapeutic outcomes in the context of mCD47. However, critical questions remain as to the optimal protocol for therapeutic antibody delivery with FUS. This study leverages immuno-PET imaging to spatiotemporally map [89Zr]-mCD47 delivery across the BBB/BTB with FUS in an orthotopic GB model. We then use these insights to design a combinatorial paradigm for mCD47 delivery with repeat FUS BBB/BTB-D.

Materials and Methods: Two weeks following intracranial implantation of GL261 cells, FUS BBB/BTB-D (1.1 MHz, 0.5% duty cycle, 0.4-0.6 MPa) was performed under MRI guidance in the presence of systemically circulating albumin-shelled MBs. Mice received i.v. [89Zr]-mCD47 either without FUS, immediately prior to FUS [FUSPRE] or following FUS [FUSPOST]. Mice underwent serial static PET/CT imaging, followed by harvest of whole brains and peripheral organs for assessment of [89Zr]-mCD47 biodistribution at a terminal time point. A therapeutic paradigm was then executed, wherein i.v. mCD47 (8 mg/kg) was administered to GL261-bearing mice either as monotherapy or in combination with FUS BBB/BTB-D over three sessions spaced three days apart. Overall survival was monitored and tumor outgrowth was tracked via serial contrast-enhanced T1w MR imaging.

Results: Though contrast-enhanced MR imaging confirmed the presence of a tumor in all mice (Fig 1A), PET/CT imaging did not reveal clear preferential [89Zr]-mCD47 uptake in GL261 tumors with or without FUSPRE, suggesting that neither condition improved antibody penetrance over that in naïve brain (Fig 1B-C). Remarkably, however, FUSPOST conferred superlative [89Zr]-mCD47 uptake at the site of BBB/BTB-D, boasting between 4.3- to 6.7-fold greater signal relative to other groups (Fig 1C). This elevation in uptake was sustained over the time points assessed (0-72 hours post-FUS) (Fig 1D). Using these insights, we evaluated a rational paradigm (Fig 2A) combining mCD47 with repeat FUSPOST BBB/BTB-D (Fig 2B-C) for glioma therapy. Delivery of mCD47 across the BBB/BTB with FUS significantly constrained tumor outgrowth (Fig 2D-E) and enhanced survival (Fig 2F) in GL261-bearing mice.

Conclusions: Taken together, our findings suggest that mCD47 delivery with FUS BBB/BTB-D is a promising therapeutic strategy for GB. Moreover, for myriad ongoing pre-clinical and clinical evaluations of FUS-mediated antibody delivery, these findings generate timely and compelling insights regarding the impact of injection timing on antibody penetrance in brain tumors. This study underscores the outstanding potential role of immuno-PET imaging for rational design and monitoring of response to FUS immunotherapy approaches.

Acknowledgements: Supported by National Institutes of Health Grants R01EB020147 and R01CA197111. N.D.S. was supported by NIH F99CA234954, NSF Graduate Research Fellowship, and a UVA School of Medicine Wagner Fellowship.

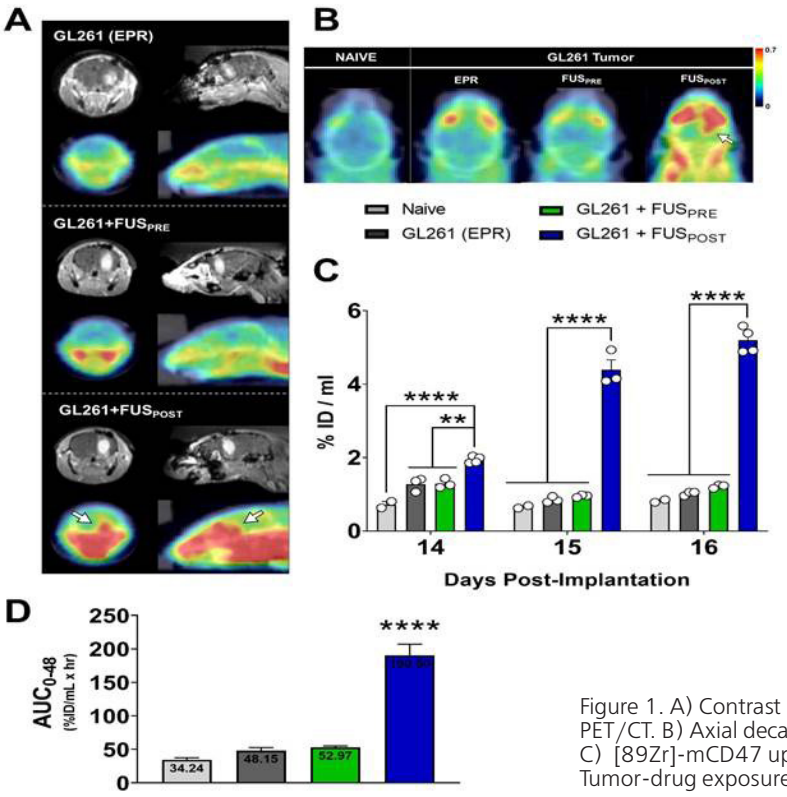

Figure 1. A) Contrast MRI and decay-corrected PET/CT. B) Axial decay-corrected PET/CT. C) [89Zr]-mCD47 uptake values (SUVs). D) Tumor-drug exposure for [89Zr]-mCD47.

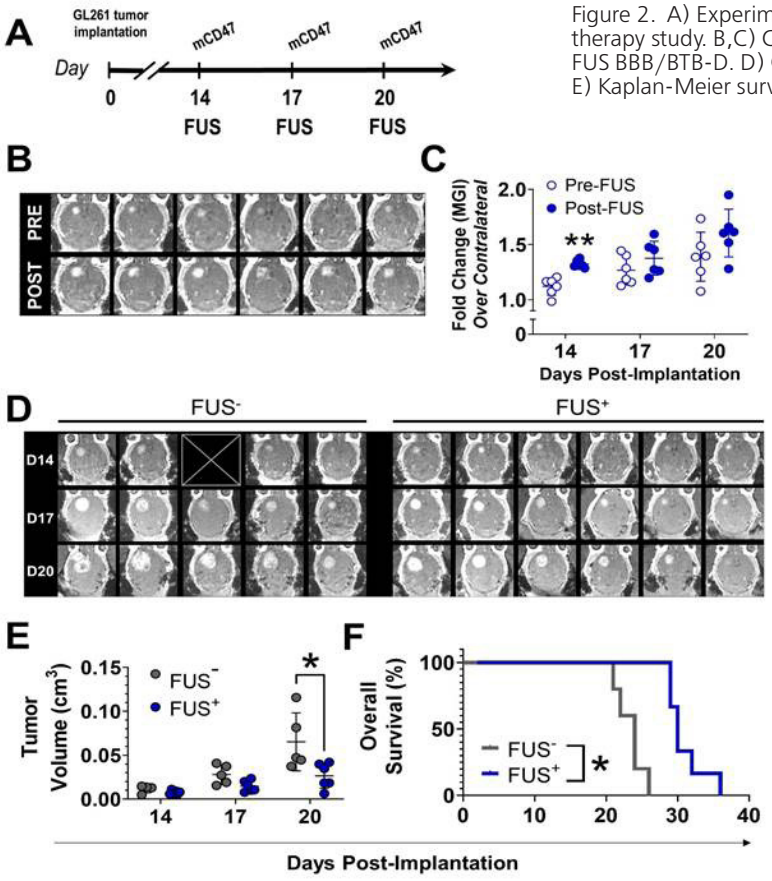

Figure 2. A) Experimental design for mCD47 therapy study. B,C) Contrast enhancement after FUS BBB/BTB-D. D) GL261 tumor outgrowth. E) Kaplan-Meier survival curves.

IMM-16

Topic: Immuno-oncology
Presentation Type: Oral

Combination of thermally ablative focused ultrasound with gemcitabine controls breast cancer via adaptive immunity

Natasha Sheybani, Alexandra Witter, Timothy Bullock, Richard Price

University of Virginia, Charlottesville, VA, USA

Background: Triple negative breast cancer (TNBC) remains recalcitrant to most targeted therapeutic approaches. Among the potential networks in TNBC that could constrain the activity of anti-tumor immunity is the presence of immunosuppressive myeloid cell subsets. These have the capacity to impair adaptive immunity and promote tumor growth and metastasis. Among these cell types, myeloid-derived suppressor cells (MDSCs) limit both T cell activation and effector functions. Recent clinical studies suggest that inducing tumor damage can render TNBC responsive to immunotherapy. We, therefore, tested a strategy for immune sensitization of murine TNBC (4T1 tumors) through a combination of focused ultrasound (FUS) partial thermal ablation and a chemotherapy, gemcitabine (GEM), known to attenuate myeloid derived suppressor cells (MDSCs).

Materials and Methods: To achieve partial thermal ablation of 4T1 tumors, we utilized an ultrasound-guided FUS system equipped with a single element therapeutic transducer driven at 3 MHz. A grid of sonications was overlaid on the ultrasound-visible tumor and ablated in a raster pattern. The exceptionally small focus of this system rendered a low ablation fraction (~10-20% of total tumor volume). In several experiments, we combined sparse scan partial thermal ablation with systemically administered GEM, which was administered i.p. at the time of ablation, as well as 7d and 14d after FUS. Tumor growth and animal survival were recorded. We performed flow cytometry analyses of tumor, lymph nodes, and blood to investigate the roles of mono- and combinatorial therapies in mediating local and systemic immunity. To determine the essentiality of adaptive immunity in tumor growth control and enhanced survival, we also tested the combination of FUS partial thermal ablation and GEM in Rag1-/- (T- and B-cell deficient) mice and WT mice depleted of CD4 and CD8 T cells.

Results: Sparse scan partial thermal ablation monotherapy elicited, in the draining lymph nodes at d7 post-FUS (Fig 1A), a 2.5-fold increase in dendritic cells (DCs) (Fig 1B) and a 3-fold increase in CD86+ DCs (Fig 1C). However, this response neither controlled tumor growth (data not shown) nor promoted a robust T cell response against 4T1 tumors (Fig 1D). As expected, MDSCs were prevalent in 4T1 tumors (Fig 1E). Combining this FUS partial thermal ablation approach with GEM administration (Fig 2A) did, however, significantly constrain primary 4T1 tumor outgrowth (Fig 2B-E) and extend overall survival of mice (Fig 2F). When the combination of FUS and GEM was applied to 4T1 tumors implanted in Rag1-/- mice, tumor growth control (Fig 3A) and survival extension (Fig 3B) were lost. Applying FUS+GEM to CD4 and CD8 T cell-depleted (Fig 3C, D) WT mice yielded similar results. Indeed, both tumor growth control (Fig 3E) and extension of survival (Fig 3F) were abrogated in the absence of T cells.

Conclusions: FUS partial thermal ablation monotherapy of 4T1 tumors elicits DC activation in draining lymph nodes, but is unable to control tumor growth. However, both tumor growth control and animal survival can be markedly improved by combining FUS partial thermal ablation with GEM administration. Experiments performed on the Rag1-/- background and in the setting of T cell depletion definitively established that tumor growth control and improved survival were entirely dependent on adaptive immunity. More specifically, these responses were dependent upon CD8+ and CD4+ T cells. These findings provide strong support for the rapid translation of FUS+GEM combination therapies to clinical trials for women with metastatic TNBC.

Acknowledgements: This study was supported by National Institutes of Health Grants R01CA197111 (R.J.P. and T.N.J.B.) and R21CA230088 (R.J.P.), the Focused Ultrasound Foundation (T.N.J.B. and R.J.P.), and Theraclion (T.N.J.B. and R.J.P.). N.D.S. was supported by a National [text omitted]

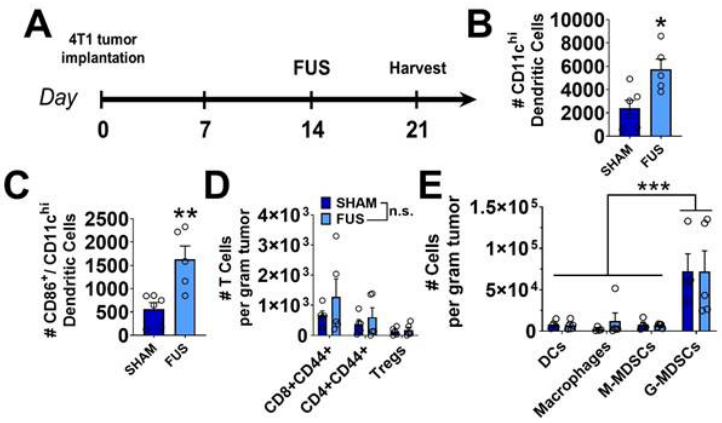

Figure 4. Fig 4: A,C: % ZsGreen positive dendritic cells. B,D: Geometric mean fluorescence of ZsGreen. E,G,I: % MHC-SIINFEKL positive DCs. F,H,J:Geometric mean fluorescence of MHC-SIINFEKL.

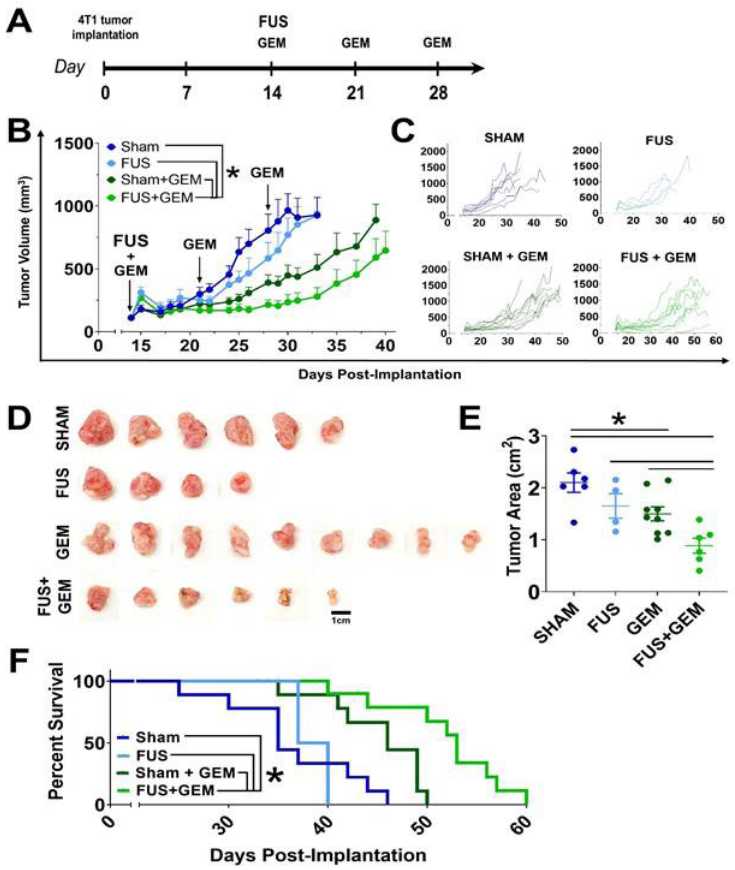

Figure 2. A. Timeline. B,C,D,E: FUS+GEM controls 4T1 tumor growth. F: Improved survival with FUS+GEM

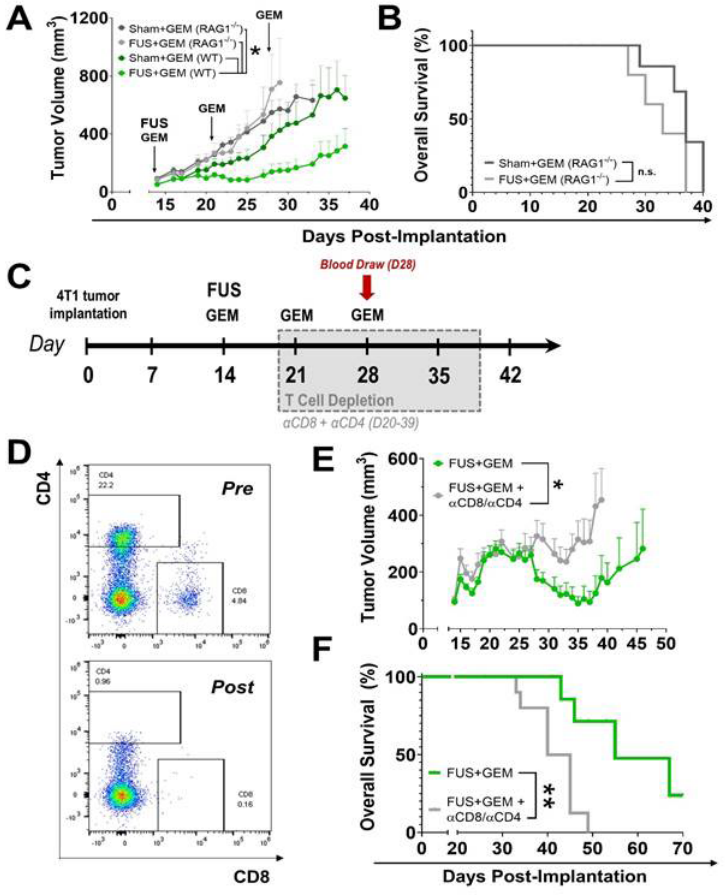

Figure 3. A,B: FUS+GEM tumor growth control and survival are lost in Rag1 mice. C: T cell depletion timeline. D,E: FUS+GEM tumor growth control and survival depend on T cells.

IMM-17

Topic: Immuno-oncology
Presentation Type: Oral

Boiling histotripsy and CD40 activation re-sensitize the immunologically "cold" tumor to checkpoint blockade therapy

Mohit Pratap Singh, Sri Nandhini Sethuraman, Craig Miller, Jerry Malayer, Ashish Ranjan

Oklahoma State University, Stillwater, OK, USA

Background: Immunologically "cold" tumors in advanced stages lack major histocompatibility complex (MHC) and co-stimulatory molecules, exhibit minimal antigen presentation and accumulations of cytotoxic infiltrating lymphocytes, and are refractory to immune checkpoint inhibitors (ICIs). Some recent studies have shown that mechanical tissue fractionation with boiling histotripsy (HT) can improve tumor inflammation. We have also shown that the local anti-CD40 agonistic antibody improves the functional status of T-cells in the early stages of melanoma. However, whether FUS and CD40 are capable of reversing resistance to ICIs in immunologically cold tumors is not known. Herein, we established the late-stage and ICI refractory B16F10 murine melanoma and investigated the role of boiling HT and CD40 antibody (HT+CD40: HT40) in reversing the resistance to ICIs.

Materials and Methods: Large and established ICI refractory tumors (~330-400 mm3) were generated in all the mice by subcutaneous inoculation of B16F10 cells in the flank region. To gain an understanding of immune mechanisms, mice with unilateral flank tumors were assigned to the following groups (n=5/group): 1) Untreated Control, 2) HT, 3) CD40, and 4) HT40. Boiling HT covering 40-50% of tumor volume was performed using a 1.5 MHz transducer operating at 1 Hz PRF, 1% duty cycle, and 450 W acoustic power. Single intratumoral injection of anti-CD40 agonistic antibody (50 μg) was performed within 2h of HT. One-week post-treatment, immunological characterizations of tumors were performed using histology, flow cytometry, and nanostring pancancer-immune gene expression analysis. To assess the sensitization to ICI therapy, we established bilateral tumors by injecting B16F10 cells subcutaneously in right flank on day 0 and in left flank on day 4. We compared the following groups: 1) Untreated Control, 2) HT, 3) CD40, and 4) HT40, each with and without the combination of anti-CTLA-4 and anti-PDL-1 antibody. ICIs (3-doses) were administered every third day intraperitoneally following HT, CD40, or HT40 treatment. Mice were sacrificed when tumors reached ~2 cm in any dimension, or when they reached day 40 post-inoculation. Endpoints were to assess the growth delay of treated and untreated tumors, median survival assessment by the Kaplan-Meier survival curve, and histological analysis of untreated tumors.

Results: HT increased the immune infiltration markers (ICAM2, VCAM1) and chemoattractants (CCL8 and CSF1R) related to antigen-presenting cells in tumors compared to control. Additionally, the inflammatory and immune checkpoint signatures were amplified in a CXCL9 dependent manner upon adding CD40 to the HT regimen. An enhanced population of activated T-cell (~4-fold) and CD8+ T to T regulatory cell ratio (~5-fold) and a significant increase in effector-memory T cell populations for HT40-treated tumors and spleen compared to other groups were noted. Therapeutically, ICI alone was in-effective in inducing tumor growth suppression. However, HT40+ICI significantly suppressed treated and untreated tumors, and enhanced survival compared to the monotherapies. Histopathological evaluations of the untreated tumor showed enhanced lymphocyte infiltrations for HT40 compared to other groups, further establishing the basis of ICI re-sensitization.

Conclusions: HT40 therapy augmented innate and adaptive immunity in the B16F10 model. An inflamed tumor microenvironment with an active interaction of the CXCL9-cytotoxic T cell axis was the likely mechanism responsible for sensitization of HT40 tumors to ICIs and improved survival rates of mice. We propose that combining HT40 with ICIs can enhance outcomes in advanced-stage patients with immunologically cold tumors.

Acknowledgements: National Cancer Institute of the National Institutes of Health under Award Number R37 CA239150-02, Focused Ultrasound Foundation, PETCO and the Kerr (Ranjan) and McCasland Foundation (Malayer) Endowed Chair at Oklahoma State University.

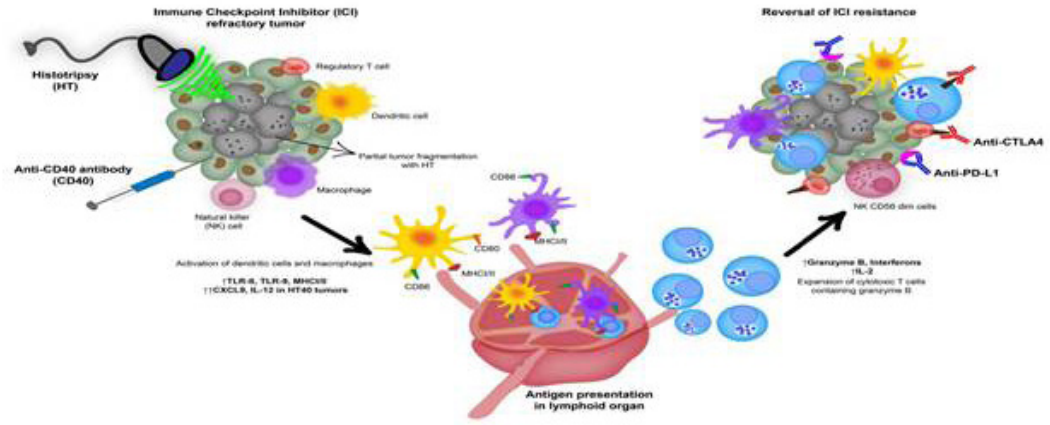

Figure 1. Schematic representation of HT40 induced reprogramming of B16F10 tumor microenvironment and subsequent sensitization of the tumors to ICIs therapy.

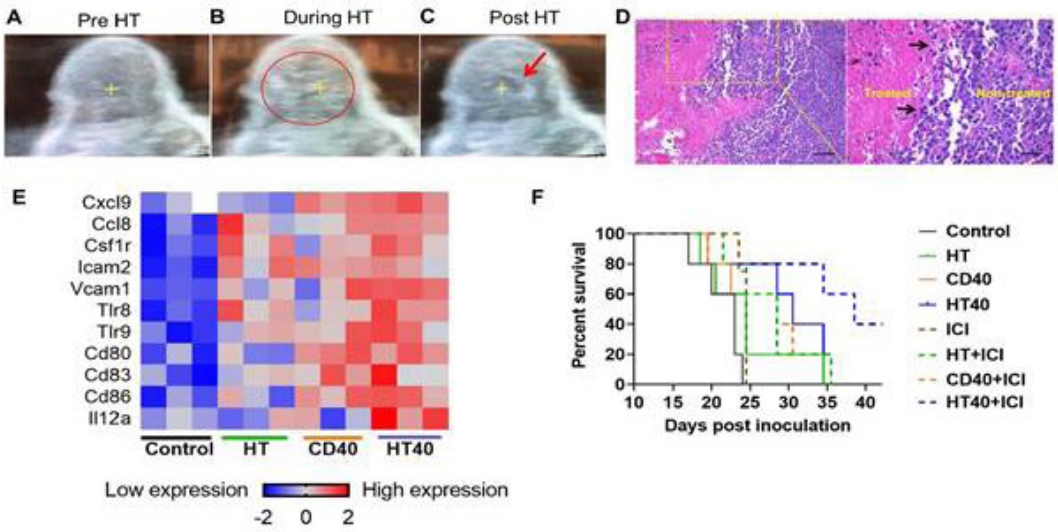

Figure 2. Local HT40 therapy sensitizes large B16F10 melanoma to immune checkpoint inhibitor therapy.

IMM-18

Topic: Immuno-oncology
Presentation Type: Oral

High intensity focused ultrasound thermal ablation in combination with checkpoint inhibitors for the treatment of refractory murine neuroblastoma

Caitlin Tydings[1], Avinash Eranki[2], Karun Sharma[1], AeRang Kim[1]

[1]Children's National Hospital, Washington, DC, USA
[2]India Institute of Technology, Bengaluru, India

Background: Despite an intense, multimodal therapeutic approach, the prognosis for children with high-risk neuroblastoma remains unacceptably poor. Checkpoint inhibitors have revolutionized cancer therapy, but pediatric solid tumors have not shared in that success possibly due to mechanisms impeding effective immune response. High intensity focused ultrasound (HIFU) based thermal ablation is a non-invasive therapy that uses ultrasound wave energy coupled with imaging guidance to precisely destroy targeted tumor via coagulative necrosis. HIFU can cause local inflammatory responses, potentially leading to activation of T-cells toward tumor antigens. Prior work from our group showed a significant survival benefit with increased anti-tumor cytokine and cellular response treating refractory neuroblastoma with HIFU boiling histotripsy and αCTLA-4 + αPD-L1. We sought to establish the reproducibility of these bioeffects using HIFU thermal ablation with αCTLA-4 + αPD-L1 in refractory, murine neuroblastoma.

Materials and Methods: Neuroblastoma tumors were established following a subcutaneous injection of N2A cell line (1x106 cells) in the hind leg of A/J mice. Once tumor sized reached longest diameter 12mm-15mm, mice were treated with 1) HIFU thermal ablation alone (n =36) or 2) HIFU thermal ablation in combination with αCTLA-4 + αPD-L1 (n = 35) or 3) no treatment, control (n = 14). Checkpoint inhibitors, αCTLA-4 + αPD-L1 (100μg per dose) were injected intraperitoneally on days 1, 4 and 7 following HIFU therapy. Mice were anesthetized, positioned on a holder and stage capable of adjusting mouse position in 3 axes and HIFU thermal ablation was performed using a 1.5 MHz transducer, producing about 35 W acoustic power. HIFU ablation therapy was guided by b-mode ultrasound imaging to ensure optimal tumor targeting was performed at three adjacent foci for 5 sec/foci (15 sec total treatment time). This study was approved by the Institutional Animal Care and Use Committee at Children's National Hospital.

Survival was measured for all treatment groups with endpoints being euthanasia due to deteriorating clinical status or tumor size >20mm in longest diameter. At 24, 48 and 72 hour time points following treatment with HIFU thermal ablation alone or in combination with αCTLA-4 + αPD-L1, ELISA was performed on serum obtained by cardiac puncture and flow cytometry was performed on the tumors, draining and contralateral lymph nodes (DLN , CLN), and spleen.

Results: HIFU thermal ablation alone or in combination with αCTLA-4 + αPD-L1 did not provide a significant survival benefit over control animals. Following HIFU thermal ablation alone, there was significant downregulation of CD8α+CD11c+ cells in the tumor and DLN but no other statistically significant changes in immune cell markers compared to control. Following HIFU thermal ablation and αCTLA-4 + αPD-L1, CD8α+ cell proliferation index (CD8α+Ki67+) increased in tumor and DLN, but higher expression of CD3+CD8+ was not observed. CD4+FoxP3- cells remained unchanged but CD4+FoxP3+ population increased in the tumor, DLN, CLN and spleen. Interestingly, PD-1 expression was upregulated on CD3+ and CD8α+ cells in tumor, DLN, CLN and spleen. IFN-γ, CXCL-10 and TNF-α were unchanged after HIFU thermal ablation alone but increased following the combination therapy. IL-10 and VEGF-A were not affected by either treatment and KC/GRO decreased steadily after HIFU thermal ablation with αCTLA-4 + αPD-L1.

Conclusions: HIFU thermal ablation combined with immunotherapy did not improve survival in this neuroblastoma murine model. HIFU thermal ablation and αCTLA-4 + αPD-L1 did not produce a profound immune response and seemed to favor a regulatory T cell response with protumor activity. This is a stark contrast to effects seen with HIFU boiling histotripsy and immunotherapy despite the same murine model system and experimental set up. Understanding the role of PD-1 and other protumoral factors and effect of other HIFU parameters on systemic immune antitumor response will need to be investigated. It will also

be important to assess the effect of HIFU with checkpoint inhibitors in murine models using other tumor cell lines to determine a broader applicability.

Acknowledgements: Curing Kids Cancer

LIV-1

Topic: Liver Tumors
Presentation Type: Oral

Acoustically driven microbubbles enable targeted delivery of microrna-loaded nanoparticles to spontaneous hepatocellular neoplasia in canines

Uday Kumar[1], Huaijun Wang[1], Arsenii Telichko[1], Dongwoon Hyun[1], Eric G. Johnson[2], Michael S. Kent[2], Robert B. Rebhun[2], Jeremy J. Dahl[1], William T. N. Culp[2], Ramasamy Paulmurugan[1]

[1]Stanford University, Stanford, CA, USA
[2]University of California, Davis, Davis, CA, USA

Background: Aberrant expression of miRNAs plays a critical role in cancer initiation, progression, and metastasis. In HCC, miRNA-122 and miRNA-21 have been identified to play pivotal roles in tumor progression, migration, and chemo-resistance. However, the lack of safe and efficient approaches to deliver intact miRNAs to the diseased sites hinders clinical translation of miRNA therapy. Biodegradable PLGA-b-PEG NP are efficient carriers for miRNAs, but their delivery to tumor is limited by tumor heterogeneity and vasculature. The present study addresses this vital gap by using a single curvilinear transducer driven by a research scanner for targeted delivery of nanoparticles loaded with anticancer microRNAs (anti-miR-21 and miR-122) to spontaneous hepatic neoplasia in client owned dogs. The study lays the foundation for the safety and efficient application of US guided spatiotemporal delivery of nanoparticles to dog patients and open-up scope for a smooth transition of this approach to humans.

Materials and Methods: MiRNAs (anti-miR-21 and miR-122) loaded PLGA-b-PEG NPs were formulated by double emulsion solvent evaporation technique with minor modifications. The synthesized NPs size, zeta potential, miRNA entrapment efficiency and endotoxin levels were estimated prior to use for in vivo studies. The curvilinear array transducer (C5-2v; Verasonics) driven by Vantage 256 research scanner (Verasonics Inc., USA) was optimized for targeted US delivery. The client owned dog patients were recruited, screened, and prepared for the study procedure. Prior to the therapy procedure, the liver with tumor was imaged and target tumor mass was identified. A solution of PLGA-b-PEG NPs loaded with microRNAs (5 ml; 8 × 1011 NP/ml) were mixed with 5 ml of SonoVue MB (2.8-5.6 x108 MB/mL), and diluted with sterile 0.9% physiological saline to a final volume of 30 ml. The homogenous MB/NP suspension was infused intravenously at a constant rate using a syringe pump (Medfusion 3500) for the entire duration of the therapy procedure (approximately 35 min) at a constant flow rate. Focused US treatment was performed sequentially across 10 different planes covering the tumor mass in the liver. After 24 hours, each dog underwent an exploratory laparotomy and samples of the tissues with and without US treatment were obtained for ex vivo analysis. Tissue samples collected for RNA extraction were processed by mirVana miRNA Isolation Kit and quantified for delivered microRNAs (anti-miR-21 and miR-122) by TaqMan RT-PCR.

Results: Quantitative estimation of miRNAs delivered using the optimized US-MB mediated delivery conditions revealed that US treated liver tumor showed ~2 - 5 folds ($p<0.001$) higher anti-miR-21 delivery than the untreated tumor or control normal liver tissues. The consistent pattern in delivered miRNAs levels (US treated tumor region > untreated tumor region) ($p<0.001$) in all three dog patients establishes a strong evidence for the versatile noninvasive delivery approach. On the other hand, histological evidences of increased extravasation of nanoparticles from blood vessels into interstitial tumor tissue in US treated region as compared to that of untreated tumor region corroborated well with microRNA quantitation results. A consistent pattern of elevated cytokines IL1b, MYD88 and TNF accompanied by increased prevalence of CD8+ T cells in US treated tumor tissue hints to a hallmark signaling cascade for "cold-to-hot" tumor transition.

Conclusions: Clinical translation of US based therapeutic approaches to large animals and humans have raised doubts considering ultrasound susceptibility to attenuation and reflection due to tissue viscoelasticity and inhomogeneity, especially with increasing depth of target tissues. The present study addresses this vital gap by using a single curvilinear transducer driven by a research scanner at optimized operating parameter for targeted delivery of anticancer microRNAs (anti-miR-21 and miR-122) loaded NPs in canine with spontaneous hepatic neoplasia. To further build on the clinical relevance of this work, we used FDA

approved PLGA-b-PEG polymer based nanocarrier along with commercial clinical grade MB for imaging guided targeted delivery of microRNA.

Acknowledgements: This work was supported by the Focused Ultrasound Foundation and the National Institutes of Health (grants numbers R01CA209888 and R21EB022298).

LIV-2

Topic: Liver Tumors
Presentation Type: Oral

Histotripsy for the treatment of intrahepatic cholangiocarinoma: Feasibility study in excised human tumors

Pete Weber[1], Alissa Hendricks[2], Alex Simon[2], Douglas Grider[1], Irving C Allen[3], Joan Vidal-Jove[4], David Luyimbazi[1], Eli Vlaisavljevich[2]

[1]Virginia Tech Carilion School of Medicine, Roanoke, VA, USA
[2]Virginia Tech, Blacksburg, VA, USA
[3]Virginia Maryland College of Veterinary Medicine, Blacksburg, VA, USA
[4]Institut Khuab for Interventional Oncology, Barcelona, Spain

Background: Cholangiocarcinoma is an aggressive tumor originating within the epithelium of both intrahepatic and extrahepatic bile ducts. It represents 3% of all gastrointestinal tumors. Only a third of these tumors are resectable at diagnosis, contributing to the poor 5-year survival rates associated with this cancer. Intrahepatic cholangiocarcinomas are characterized by a dense desmoplastic fibrotic reaction, making these tumors very stiff and limiting the usefulness of traditional ablative techniques. Histotripsy is a high-intensity focused ultrasound ablation method that uses the precise control of acoustic cavitation to mechanically breakdown tissue. In this study, we investigated the use of histotripsy as a non-invasive ablative modality for the treatment of intrahepatic cholangiocarcinoma. In addition, we compared the treatment of intrahepatic cholangiocarcinoma to two other liver tumors: hepatocellular carcinoma and colorectal liver metastases.

Materials and Methods: Patients with a resectable hepatocellular carcinoma, colorectal liver metastasis, or intrahepatic cholangiocarcinoma were enrolled in an IRB approved (Carilion Clinic, Roanoke, VA) study. Resected tissues were embedded in gelatin tissue phantoms and ablated with a 700 kHz histotripsy transducer with 5 cycle pulses and a pulse repetition rate of 500 Hz. Dosing parameters included: 250, 500, 1000, 1500, 2000, and 4000 pulses/point depending on the tissue type. Treatments were monitored with ultrasound imaging. All treatments were conducted within 48 hours of harvest. Ablated tissue was fixed in 10% formalin for at least 24 hours before being sectioned and stained with hematoxylin and eosin (H&E stain) by Quest Diagnostics (Roanoke, VA). Analysis and scoring of ablations was completed by trained individuals under a coded grading system: 0=no sign of ablation, 1=up to 25% cells ablated, 2=25-75% cells ablated, 3=greater than 75% of cells ablated, 4=no sign of viable cells.

Results: Human hepatocellular carcinoma and liver parenchyma showed nearly complete ablation by a dose of 1000 pulses/point with average ablation scores of 4 +/- 0.00 and 3.5 +/- 0.50, respectively. Colorectal liver metastases were stiffer tissues that required higher doses to achieve a complete ablation. A complete ablation was achievable in these tumors at doses of 1500 and 2000 pulses/point. Cholangiocarcinoma tumors were the stiffest of the three tumors investigated. Partial, but not complete, ablation was achieved in the cholangiocarcinoma treatments up to a dose of 2000 pulses/point (fig. 1). Results from further treatments at a dose of 4000 pulses/point will be presented at the meeting. A comparison of representative histology images for each of the tumor types is shown in figure 2.

Conclusions: Our preliminary results show that histotripsy is capable of successfully ablating both hepatocellular carcinoma tumors and colorectal liver metastases. Results further showed that higher treatment doses are likely required to achieve complete ablations for intrahepatic cholangiocarcinoma tumors. The results of this study will help to inform the treatment and dosing parameters for future clinical trials aimed at developing histotripsy for the treatment of liver cancers.

Acknowledgements: Focused Ultrasound Foundation

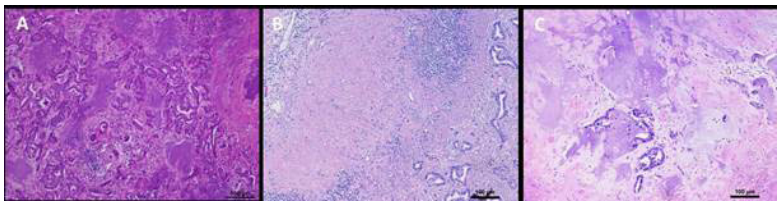

Figure 1. Comparison of human intrahepatic cholangiocarcinoma ablations at A) 1000 pulses, B) 1500 pulses, and C) 2000 pulses. Scale bars = 100 µm.

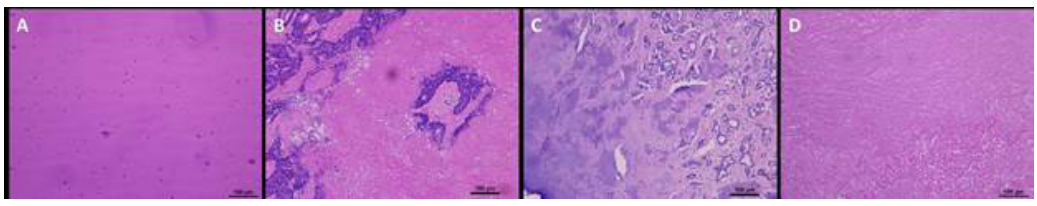

Figure 2. Comparison of human liver tumor ablations at 1000 pulses/point: A) hepatocellular carcinoma, B) colorectal liver metastasis, C) intrahepatic cholangiocarcinoma, and D) liver parenchyma.

LIV-3

Topic: Liver Tumors
Presentation Type: Oral

Phase I-II study of intra-operative high intensity focused ultrasound in 35 patients with colorectal liver metastases

David Melodelima[1], Aurelien Dupre[1], Yao Chen[2], Jeremy Vincenot[3], Michel Rivoire[1]

[1]LabTAU, Lyon, France
[2]Centre Leon Berard, Lyon, France
[3]EDAP-TMS, Vaulx-en-Velin, France

Background: Today, the only potentially curative option in patients with colorectal liver metastases is surgery. However, liver resection is feasible in less than 20% of patients. Surgery has been widely used in association with radiofrequency, cryotherapy, or microwaves to expand the number of treatments performed with a curative intent. Nevertheless, several limitations have been documented when using these techniques (i.e., a traumatic puncture of the parenchyma, a limited size of lesions, and an inability to monitor the treatment in real-time).High-intensity focused ultrasound (HIFU) technology can achieve precise ablations of biological tissues without incisions or radiation. Current HIFU devices are based on an extracorporeal approach with limited access to the liver. We have developed a HIFU device designed for intraoperative use. The use of a toroidal transducer enables an ablation rate (10 cm3/min) higher than any other treatment and without resorting to mechanical scanning.

Materials and Methods: The HIFU transducer has a toroidal shape with a radius of curvature of 70 mm focusing on a circle of 30 mm. The working frequency was 2.5 MHz. The diameter of the transducer was 70 mm. An ultrasound imaging probe working at 7.5 MHz was placed in the center of the HIFU transducer.

The feasibility, safety, and accuracy of intraoperative HIFU ablation were evaluated during an ablate-and-resect prospective study. This clinical phase I and II study was performed in patients undergoing hepatectomy for liver metastases. The protocol was reviewed and validated by a national ethics committee (CPP Sud-Est IV) according to French and European directives. Patients gave written informed consent. In Phase I and IIa, the HIFU treatment was performed on healthy tissue scheduled for resection. Then, 27 liver metastases measuring less than 30 mm in diameter were treated during phase IIb. This set-up allows the real-time evaluation of HIFU ablation while protecting participating patients from any adverse effects related to this new technique.

Results: The phase I study (n=6) showed that use of the HIFU device was feasible and safe and did not damage neighboring tissue. The phase IIa study (n=9) showed that the area of ablation could be precisely targeted on a previously implanted metallic mark. Thirty ablations were carried out in 15 patients. These ablations were all generated within 40 seconds and on average measured 27.5 mm x21.0 mm. Ablations were achieved with a precision of 1-2 mm. The phase IIb study (n=35) demonstrated ablation of metastases with safety margins. Using electronic focusing the volume of ablation was adjusted to the size of the tumor from 7 cm3 (40 seconds of sonication) to 50 cm3 (6 minutes of sonication).

Conclusions: HIFU was feasible, safe, accurate and effective in ablating liver metastases with safety margins. The next step is a multicenter prospective cohort of patients treated with curative-intent with intraoperative HIFU based on this toroidal transducer.

Acknowledgements: This work was performed within the framework of the SIRIC LyriCAN grant INCa_INSERM_DGOS_12563 and was partly funded by the French National Research Agency (ANR-19-CE19-0027-01).

MIS-1

Topic: Miscellaneous Indications

Presentation Type: Oral

High frequency HIFU – A new modality for clinical dermatology

Torsten Bove[1], Joergen Serup[2], Tomasz Zawada[1], Alexander Jessen[1], Mattia Poli[1]

[1]TOOsonix A/S, Hoersholm, Denmark
[2]Bispebjerg University Hospital, Copenhagen, Denmark

Background: HIFU operating at frequencies from 500 kHz to 3 MHz has been demonstrated to be highly efficient for creation of large HIFU focal zones located deep within the body. The method has therefore been very successful in treatment of internal cancers of major organs and cerebral pathologies. By increasing the frequency of the HIFU device, the wavelength is decreased, and the volume of the focal zone is thus reduced accordingly. High frequency HIFU can therefore concentrate and confine treatments to smaller and more specific targets. While use of higher frequencies, and thereby also higher ultrasound attenuation, limits the use for deeper pathologies, it opens for accurate and selective treatments of targets positioned close to the skin surface. The objective of this study is to demonstrate high-frequency HIFU for a wide range of indications in clinical dermatology.

Materials and Methods: The study presents a new commercial 20 MHz HIFU system. At this high operating frequency, the size of the ellipsoidal focal zone is in the range of 500 µm in length and 100 µm in diameter. It can therefore be used to deposit thermal focal points confined to the upper part of the human dermis and epidermis without affecting the deeper fibrotic dermis and subcutaneous layers. Due to the superficially location of these targets, identification of relevant treatment areas and skin response during treatment is directly visible on the surface of the skin. Real-time image guidance during treatment can thereby be achieved from an electronic high-resolution color dermascope integrated into the HIFU handpiece. Treatment is performed manually by creation of "shoulder-by-shoulder" focal points in a pre-specified focal depth covering the target area including a small circumferential margin. A wound crust is thereby formed in a well-defined plane 6 – 10 days after treatment, which subsequently discharges normal and malignant cells as a part of a normal healing phase. Typical treatments consists of administration of 10 to 50 HIFU-doses of 150 ms each with energies of 0.6 – 1.2 J/dose. Focal points are positioned with depths between 0.8 and 2.7 mm depending on treatment type and desired response.

Results: The method is successfully applied to actinic keratosis, basal cell carcinoma, Kaposi's sarcoma and angiomas, where other treatments previously failed. Initial results of more than 200 treated lesions are presented. Treatment efficacy for actinic keratosis, the most frequently treated indication in the study, is 97% without scarring or recurrence after 6-12 months. Successful treatment of malignant indications (basal cell carcinoma and Kaposi's sarcoma) were confirmed by histological verification. Pain level during treatment is reported by patients to be in the range of 40 – 70% of comparable laser or photodynamic treatments. Late wound healing may occur, and attention to aftercare to prevent infection can be necessary.

Conclusions: 20 MHz HIFU is concluded to be a promising new treatment of premalignancies and malignancies of the skin, and offers an alternative to today's treatment with surgery, lasers, photodynamic therapy and X-ray. Treatments do not require any specific pre- or post-treatment, and are applicable to any anatomical site. The method therefore present significant benefits for both patient and clinic in terms of efficacy, cost, time-consumption, and treatment pain-level. With an appropriate treatment strategy and qualified operators, 20 MHz HIFU thereby has the potential to become a leading treatment modality in clinical dermatology and skin oncology.

Acknowledgements: This study has been funded by TOOsonix A/S,

Figure 1. (top) Actinic Keratosis on the neck after failed PDT treatments. Cleared after one HIFU treatment.

Figure 2. (bottom) Basal Cell Carcinoma in scalp. Multiple recurrences after PDT. Cleared after two HIFU treatments.

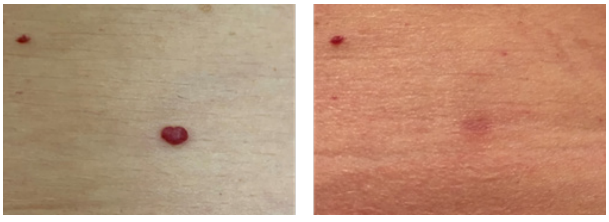

Figure 3. Cherry angioma on the leg. Several recurrences after laser and cryosurgery. Cleared after one HIFU treatment.

MIS-2

Topic: Miscellaneous Indications
Presentation Type: Oral

Focused ultrasound biofilm ablation: investigation of histotripsy and particle-mediated histotripsy for the treatment of catheter-associated urinary tract infections (CAUTIs)

Chris Childers[1], Edsall Connor[2], Jessica Gannon[2], Waleed Mustafa[3], Yasemin Durmaz[3], Alexander Klibanov[4], Abby Whittington[3], Jayasimha Rao[1], Andre Muelenaer[2], Eli Vlaisavljevich[2]

[1]Virginia Tech Carilion School of Medicine, Roanoke, VA, USA
[2]Virginia Tech, Blacksburg, VA, USA
[3]Istanbul Medipol Univeristy, Kavacik Mah., Beykoz, Hungary
[4]University of Virginia, Charlottesville, VA, USA

Background: Urinary catheters often become contaminated with biofilms, resulting in catheter-associated urinary tract infections (CAUTIs) that adversely affect patient outcomes. Histotripsy is a non-invasive focused ultrasound ablation method that is currently being developed for the non-invasive removal of cancerous tumors and other soft tissues. Histotripsy has also previously shown the ability to treat biofilms on glass slides and surgical meshes. Here, we investigate the potential of histotripsy for the treatment of CAUTIs. We also explore the potential of combining histotripsy with acoustically active particles (gas-filled microbubbles, MB, fluid-filled nanocones, NC) in order to develop a particle-mediated histotripsy approach that could non-invasively remove biofilms without the need for the high acoustic pressures and real-time image-guidance required for conventional histotripsy procedures.

Materials and Methods: Clinically relevant catheter materials were tested to determine the feasibility, and acoustic threshold producing conventional luminal cavitation within tygon, silicon, and latex tubes bought from McMaster Carr. A Pseudomonas aeruginosa (strain PA14) biofilm model was developed and tested to produce biofilms on the luminal surface of an in vitro tygon catheter model. This model was then treated with luminal cavitation to determine the ability of conventional histotripsy to remove a luminal biofilm. Further, the bactericidal effect of conventional histotripsy was tested by treating PA14 suspended in LB media. Finally, Particle seeded cavitation was tested to determine the ability of microbubbles (MB) and nanocones (NC) to reduce cavitation threshold, selectively localize cavitation, and remove a biofilm.

Results: Conventional histotripsy produced precise cavitation clouds within the lumen of tygon, silicon, latex, and clinical catheters. Treatment of a PA14 biofilm model with conventional histotripsy significantly reduced luminal biofilm signal. Further, treatment of suspended PA14 in LB showed a substantial reduction in the number of CFU/mL in a dose dependent manner. NC and MB seeded cavitation reduced cavitation threshold within the lumen of a tygon catheter model while allowing for selective cavitation within the lumen of the tygon catheters at lower cavitation pressures. Finally, NC and MB seeded histotripsy reduced the biofilm signal in our PA14 biofilm model as lower pressures than conventional histotripsy.

Conclusions: Overall, the results of this study demonstrate the potential of histotripsy and particle-seeded histotripsy to provide a new modality for removing bacterial biofilms from catheter-based medical devices. These initial feasibility results suggest that additional work is warranted to investigate histotripsy and particle-mediated histotripsy for treatment of CAUTIs and other biomaterial associated infections.

Acknowledgements: The authors would like to thank the Virginia Tech Institute for Critical and Applied Technology (ICTAS), the Center for Engineered Health (CEH), and the VTC School of Medicine for their support of this work.

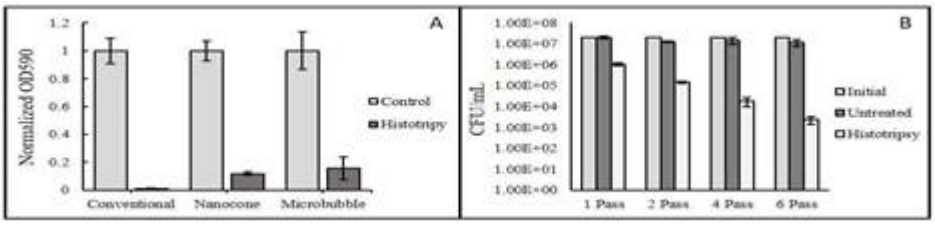

Figure 1: (A) Normalized to 1 OD 590nm biofilm removal. (B) Bactericidal dose response to multiple passes through sample tube.

MIS-3

Topic: Miscellaneous Indications

Presentation Type: Oral

Non-invasive focused ultrasound therapy of calcific aortic stenosis: First-in-man study

Mathieu Pernot[1], Mathieu Rémond[2], Robin Penot[2], Daniel Suarez[2], Guillaume Goudot[2], Wojciech Kwiecinski[3], Ana Fouquier[2], Zahir Larabi[2], Alexander Ijsselmuiden[4], Selina Vlieger[4], Peter Den Heijer[4], Etienne Puymirat[3], Samuel Zarka[3], Bernard Cholley[3], Christian Spaulding[3], Albert Hagege[3], Eloi Marijon[3], Mickael Tanter[1], Benjamin Bertrand[2], René Spaargaren[2], Emmanuel Messas[3]

[1]Institute Physics for Medicine Paris, Paris, France
[2]Cardiawave, Paris, France
[3]Hôpital Européen Georges Pompidou, Paris, France
[4]Heartcenter, Amphia Hospital, Breda, Netherlands

Background: The morbidity associated with surgical and transcatheter aortic valve replacement (SAVR/TAVR) remains high, and valve replacements often lead to complications. Furthermore, not all patients are eligible for open-heart surgery or TAVR. CARDIAWAVE (Paris, France) has developed Valvosoft, a unique non-invasive ultrasound therapy device to treat aortic stenosis. The therapy aims to improve the opening of severely calcified aortic valves by cracking the calcium and reducing the stiffness in the aortic valve tissue by delivering transthoracically local shock waves on the valve leaflets. This study assesses the safety, feasibility and performance of this novel technique.

Materials and Methods: Valvosoft (Cardiawave, Paris, France; Figure 1) is a Non-Invasive Ultrasound Therapy (NIUT) system, designed for transthoracic cardiac focusing. The system is composed of a multi-element transducer driven by high-power electronics. A 2D echocardiographic probe is embedded in the center of the therapeutic transducer to guide and monitor the treatment.

This is a multi-center, prospective, first-in-man study designed to evaluate the safety and feasibility of the Valvosoft device. Ten patients with severe symptomatic calcific aortic stenosis and not eligible for SAVR/TAVR (mainly because of vascular access problems and comorbidities) underwent a Valvosoft ultrasound therapy. Echocardiographic evaluation was performed by an independent core lab at baseline, discharge, and at 1, 3, 6 and 12 months along with clinical follow up.

Results: Enrolled patients were advanced in age (84.1±6.5 yrs) with severe comorbidities (8 with heart failure, 5 with coronary heart disease and 5 with kidney failure). All had extensive aortic valve calcification with mean Aortic Valve Area (AVA) of 0.61±0.17 cm2 and mean pressure gradient of 37.5±10.5 mmHg. At one-month follow-up, six patients had significantly improved their AVA with increase of 27.5% (p=0.03) and mean pressure gradient decrease of 23.2 % (p=0.025). These patients also received the highest dose and longest treatment duration. During one year follow up, 4 patients died due to progression of end stage heart failure not linked to the procedure and one patient had undergone a TAVR procedure. At 12 months, the five remaining patients has no device or procedure related major adverse events nor deterioration of neurological status. Echo, brain-MRI and clinical follow up will be presented.

Conclusions: Non-Invasive Ultrasound Therapy is feasible and safe in patients with severe aortic valve stenosis and can improve AVA and hemodynamic parameters. Larger clinical studies need to be conducted to confirm these preliminary results. NIUT can be an important tool complementary to TAVI in treating patients with aortic valve stenosis.

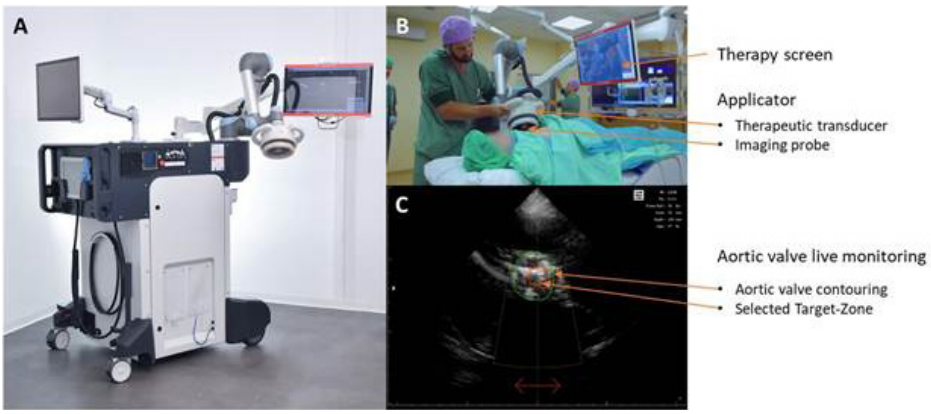

Figure 1. Valvosoft device (Panel A) and treatment overview. During a treatment, the applicator is positioned on the patient's chest (Panel B) and the aortic valve is targeted and live monitored (Panel C).

MIS-4

Topic: Miscellaneous Indications

Presentation Type: Oral

Phase I/II clinical study using low energy focused ultrasound (LoFU) in addition to stem cell for the treatment of peripheral arterial disease

Narendra Sanghvi[1], Mark Carol[2], Roy Carlson[1], Ralf Seip[2], Joseph Frank[3], Wilson Wong[4]

[1]SonaCare Medical, LLC, Indianapolis, IN, USA
[2]SonaCare Medical, LLC, Charlotte, NC, USA
[3]National Institutes of Health, Bethesda, MD, USA
[4]Arkansas Heart Hospital, Little Rock, AR, USA

Background: Annually peripheral arterial disease (PAD) afflicts 8 to 10 million patients in US alone, and 200,000 of them require amputation. Perivascular delivery of autologous adipose derived stem cells (aADSCs) has been shown to improve micro-circulation in ischemic tissues; however, one of the main problems in stem cell therapy is the lack of stem cell (SC) homing in the targeted area. Research at NIH (Tebebi PA, Sci Rep, 2017) has shown an increase of 5-6 fold SC homing in ischemic areas treated by LoFU before SC injection in rodents. The aim of this pilot study was to assess safety and preliminary efficacy of ADSCs in combination to LoFU in patients with severe PAD that exhausted all available clinical non-amputation treatments.

Materials and Methods: This is the first in-human, single center, open label, prospective, randomized study in patients with non-revascularizable moderate or severe lower extremity PAD with Rutherford class 3-5. A total of 13 patients were screened and 10 patients enrolled. Ten patients were randomized 1:1 to one of two groups: ADSCs only and ADSCs + LoFU (SonaCare Medical). ADSCs were isolated from lipo-aspirates of abdominal subcutaneous fat. Both groups received ADSCs, injected intra muscularly along the target vessel path and intra-adventitially proximal to the lesion. In the LoFU group, LoFU was delivered on or near the compromised blood vessels extracorporeally under real time image guidance with a single element transducer (f#=1) operating at 1 MHz, 25 / 225 milli-seconds ON / OFF time, 50 pulses/site with TAP=30-39 Watts to induce mild focal- inflammation to the targeted ischemic area prior to ADSC injection. Main endpoints were for safety and for preliminary efficacy such as change from baseline of Rutherford classification, six minute walk test (6MWT), ankle brachial index (ABI), transcutaneous partial oxygenation (TcPO2) by angiosome and quality of life (EQ- 5D 5L and VascuQol) at 6wks, 3 and 6 months.

Results: For safety endpoints, both groups had 0 procedural complications or investigational product (IP) related adverse events. For efficacy endpoints: ABI and TcPO2 60% (ADSC, n=3) vs 80% (LoFU + ADSC, n=4) of patients were stabilized at 3 months. For ABI, LoFU group shows more patients (4/5) improved at 3 month compared to SC only (3/5). For TcPO2, LoFU group shows more improvement at 3 month in TcPO2 (4/5) and sTcPO2 (3/5), compared to 3/5 and 2/5 in SC only group, respectively. ABI Rutherford, 6MWT and QoL had less decline/deterioration in both groups. Stem cell treatment particularly when used after ultrasound, is safe and shows promise stabilizing vascular hemodynamics of the affected area.

Conclusions: In conclusion, applications of LoFU over the affected areas prior to ADSCs treatment of patients with moderate to severe non-revascularizable PAD is safe and warrants a larger study to quantify significance of LoFU.

Acknowledgements: SonaCare Medical, LLC

MIS-5

Topic: Miscellaneous Indications

Presentation Type: Oral

Transrectal High-intensity focused ultrasound (HIFU) for the management of rectosigmoid deep infiltrating endometriosis: Results of phase I clinical trial

Gil Dubernard

Hospices Civils de Lyon - LabTAU, Lyon, France

Background: Deep invasive endometriosis (DIE) of the rectosigmoid is associated with painful symptoms. When medical treatments are ineffective, surgical resection remains the standard despite significant adverse events. High Intensity Focused Ultrasound (HIFU) is a minimally invasive ablative procedure. FocalOne is a transrectal HIFU (TR-HIFU) device used in prostatic cancer treatment. The primary objective of this study was to confirm the feasibility of TR-HIFU in patients presenting posterior DIE with rectosigmoid involvement. We also assessed its safety and clinical efficacy in this indication.

Materials and Methods: Phase I, non-controlled, prospective monocentric clinical study. The inclusion criteria were patients older than 25, without any project of pregnancy in the next 6 months, who presented a single lesion of posterior DIE with a rectosigmoid invasion and after failure of hormonal therapy. All lesions were assessed using transvaginal sonography and MRI. Patients filled questionnaires on gynecologic and intestinal symptoms, and on quality of life (MOS-SF36 score, EHP-5) before and at one, three and six months after treatment.

Results: Twenty-three patients were included between September 2015 and October 2018. All the lesions were visualized. Twenty lesions were treated ("feasibility rate": 87.0%): thirteen entirely and seven partially. The mean duration of the procedure was 55.6 minutes. We observed a significant improvement in visual analogic scales at six month for dysmenorrhea (-3.6, p=0.004), dyspareunia (-2.4, p=0.006), diarrhea (-3.0, p=0.006), constipation (-3, p=0.002), dyschezia (-3.2, p=0.003), false urges to defecate (-3.3, p=0.007), posterior pelvic pain (-3.8, p=0.002), and asthenia (-4.3, p=0.002).There was also a significant improvement of the MOS-SF36 with an increase of both Physical Composite Score (+9.3%, p=0.002) and Mental Composite Score (+10.9%, p=0.017) at six months. No major complications occurred during and after the procedure.

Conclusions: TR-HIFU therapy for posterior DIE is feasible. It could be an interesting minimally invasive alternative to surgery for the treatment of rectosigmoid endometriosis if its efficacy and safety is confirmed.

Acknowledgements: LabTAU - INSERM U1032 / EDAT-TMS for their Financial Support

Figure 1.

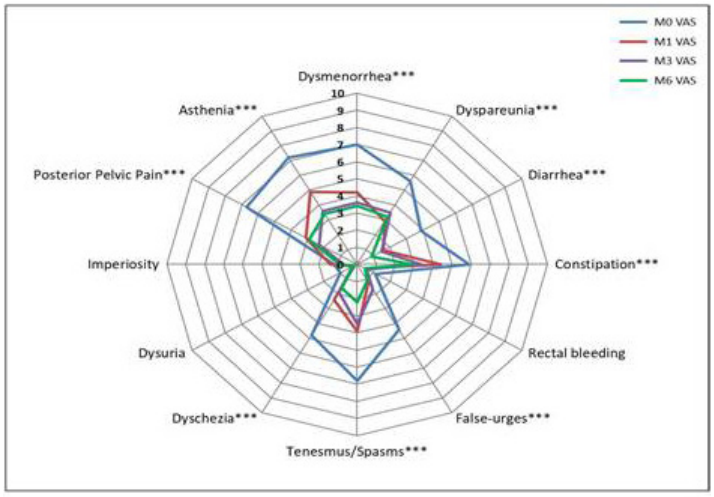

Figure 2.

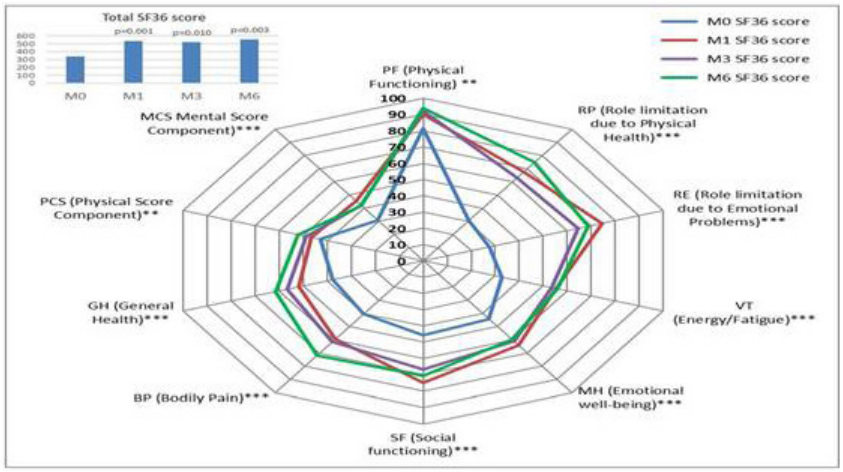

MIT-1

Topic: Miscellaneous Tumors

Presentation Type: Oral

HIFU for the treatment of subcutaneous solid tumors in canines

Jennifer Carroll[1], Sheryl Coutermarsh-Ott[2], Joanne Tuohy[2], Sabrina Barry[2], Shawna Klahn[2], Irving C Allen[2], Jeffery Ruth[3], Nikolaos Dervisis[2]

[1]Virginia Tech, Blacksburg, VA, USA
[2]Virginia Maryland College of Veterinary Medicine, Blacksburg, VA, USA
[3]IDEXX Laboratories (IDEXX telemedicine Consultants), Westbrook, ME, USA

Background: HIFU is a non-invasive ablation technique that has been successfully used to treat a variety of human pathologies and proposed to result in several beneficial bioeffects. Pet dogs have proven useful in translational oncologic research, with veterinary clinical trials focusing on the study of naturally arising tumors in immunocompetent hosts that share the same environment as humans. Current literature detailing the use of HIFU for canine tumors is limited. We designed, executed, and report the results of a pilot trial of HIFU for dogs diagnosed with subcutaneous solid tumors. Our primary objective was to evaluate the safety and feasibility of delivering HIFU to canine cancer patients. Our secondary objectives were to characterize the immediate adverse events, the pathologic changes in the treated tumor tissue, and the changes to the treated tumor microenvironment. Our findings will provide translational insight into the effect of HIFU on malignant tumors and tumor microenvironment.

Materials and Methods: Dogs with subcutaneous solid tumors were recruited and staged with thoracic & abdominal CT. Dogs were considered eligible for inclusion if they had subcutaneous solid tumors measuring >1cm at the largest diameter, adequate liver and kidney function and had an expected survival of > 6 weeks. Exclusion criteria included a modified Karnofsky score of >2, receipt of anti-neoplastic therapy within the previous 3 weeks, patients deemed to be poor anesthetic candidates and those having an expected survival of <6 weeks. Pretreatment biopsies were obtained and a single HIFU treatment for partial tumor ablation was delivered, via a Theraclion Echopulse unit. Tumors were excised 4-6 days post HIFU and submitted for routine histopathology and immunohistochemistry. IHC for CD3 and CD79a was performed on pre and post treatment tumor samples with IHC for CD4, CD8, and iba-1 to follow. Thermal injury post HIFU was classified according to a grading scheme adapted from human medicine. Gene expression analysis was performed on formalin-fixed, parrafin-embeded pre and post-HIFU treatment samples to evaluate the immunologic changes in the intratumoral microenvironment, via custom superarrays containing genes associated with inflammation. Quantitative RT-PCR data was analyzed using the ΔΔCt method. Descriptive statistics were used to describe study population epidemiology. Disease free survival and OS were estimated using the Kaplan-Meier survival analysis method.

Results: 20 dogs were recruited and treated as planned. Tumors targeted included 15 soft tissue sarcomas, 3 mast cells tumors, 1 osteosarcoma, and 1 thyroid carcinoma. 18 dogs were treated according to the treat and resect protocol, while two were treated and monitored overtime. Complications attributed to HIFU treatment were self-limiting and included 5 full thickness skin burns (3rd degree burn), 1 deep partial thickness skin burn (2nd degree), 1 superficial partial thickness skin burn (2nd degree), and 1 degranulation event in a patient with a mast cell tumor. 17/18 dogs treated according to the treat and resect protocol had evidence of complete tumor ablation within the designated treatment field, and 1 deemed geographic miss. Immunohistochemistry revealed an increase in the number of CD3+ cells in the periphery of the ablation zone. Quantitative RT-PCR revealed a > 2 fold increase in genes associated with pro-inflammatory cytokine signaling in post treatment samples.

Conclusions: HIFU appears to be feasible, safe, and results in predictable tumor ablation characterized by discrete regions of coagulative necrosis. HIFU resulted in tentative immunostimulatory alterations to the tumor microenvironment.

Acknowledgements: Focused Ultrasound Foundation and Theraclion

MIT-2

Topic: Miscellaneous Tumors

Presentation Type: Oral

Heat sensitises colon cancer cells to HSP90 inhibition-induced cell death

Petros Mouratidis, Gail ter Haar

The Institute of Cancer Research, London, United Kingdom

Background: High intensity focused ultrasound induces its biological effects, in part, by increasing temperature in the target tissue. Heat activates both programmed cell death and pro-survival processes and their balance decides the fate of heated cells. Pro-survival processes such as the activation of the heat shock response provide opportunities for intervention with pharmacological inhibitors, genetic probes or targeted therapies that could tilt the balance in favour of cell death. This study was designed to assess whether heat can be used in combination with a targeted inhibitor of the heat shock protein HSP90 to augment cell death.

Materials and Methods: The Thermal Isoeffective Dose (TID) was used as a dosimetry parameter to allow comparison of different thermal treatments. 2 human colon cancer cell lines, HCT116 and HT29, were heated at 37, 45 and 46oC for 15 minutes (TID = 0, 60 and 120 CEM43 respectively) using a polymerase chain reaction (PCR) thermal cycler. Temperature was recorded using thermocouples. Cells were also treated with the Hsp90 inhibitor NVP-AUY922 (AUY922) (40nM). Cell viability was estimated using the MTT assay. Flow cytometry was used to study CALRETICULIN, HSP70, HSP90 and CD47 exposure on the plasma membrane. Immunoblotting assessed intracellular HSP70 and HSP90.

Results: Exposure of HCT116 / HT29 cells to TIDs of 60 and 120 CEM43 decreased the cell number immediately, and 1 day after, treatment relative to sham heated cells (TID = 0 CEM43). An increase in live cell number was seen every 24 hours thereafter. Increase in ATP release and downregulation of CD47 1 day after treatment, and increased plasma membrane CALRETICULIN, HSP70 but not HSP90 were seen 2 days after treatment in cells exposed to TID of 120 CEM43 relative to those sham heated. 1 day after treatment of cells with 60 and 120 CEM43 there was increased intracellular HSP70, but not HSP90, relative to cells treated with 0 CEM43. The HSP90 inhibitor AUY922 combined with a TID of 120 CEM43 gave a synergistic increase in thermally-induced cell death associated with reduced expression of CD47. In addition TIDs of 60 and 120 CEM43 enhanced AUY922-induced cell death in the lung cancer A549 cell line and melanoma WM266.4 cells respectively, but not in the breast cancer MCF7 cells.

Conclusions: In this study an increase of biomarkers associated with immunological cell death including ATP release, CALRETICULIN exposure, and CD47 downregulation in the plasma membrane was shown. Also the activation of the heat shock response manifested as an increase in the intracellular and plasma membrane protein levels of HSP70 was shown. Non-ablative heating could sensitise colon cancer cells to the cytotoxic effects of clinically relevant compounds which target HSP90.

Acknowledgements: Cancer Research UK

MIT-3

Topic: Miscellaneous Tumors

Presentation Type: Oral

First experience in the treatment of recurrent, localized and unresectable head and neck tumours using MRIgFUS-based hyperthermia

Samuel Pichardo[1], Huang Yuexi[2], Ruby Endre[2], Merrylee McGuffin[3], Ian Poon[4], Greg Czarnota[3], Kullervo Hynynen[3], Irene Karam[4]

[1]University of Calgary, Calgary, Canada
[2]Sunnybrook Research Institute, Sunnybrook Health Sciences Centre, Toronto, ON, Canada
[3]Sunnybrook Health Sciences Centre and University of Toronto, Toronto, ON, Canada
[4]Odette Cancer Centre and Sunnybrook Health Sciences Centre, Sunnybrook Health Sciences Centre, Toronto, ON, Canada

Background: Cancer of the head and neck is the sixth most common form of cancer diagnosed in the world. Despite combined modality treatments, 20-55% of patients with locally advanced head and cancer will develop locoregional recurrence with an overall survival of approximately 40-60%. There remains a need for therapeutic strategies that can improve locoregional control and provide symptom relief while limiting treatment duration and side effects. Localized hyperthermia (HT) of head and neck tumours has been shown to enhance the cell-killing effect of radiation (thermal radiosensitization) and cytotoxic drugs (thermal chemosensitization). In this report, we present our first experience using hyperthermia delivered with Magnetic Resonance image-guided Focused Ultrasound (MRgFUS) for the treatment of recurrent and unresectable head and neck cancer.

Materials and Methods: A Research Ethics Board (Sunnybrook Health Sciences Centre) approval was obtained for a prospective, pilot, single-center, single-arm, non-randomized trial (NCT03218475). The primary objective is to assess the safety, toxicity and feasibility of MRgFUS-based HT treatments to the head and neck region. The secondary objective is to assess changes caused by MRgFUS within the treated tumour regions based on post-treatment MRI. Figures 1 show the inclusion and exclusion criteria. As indicated in the study flowchart (Fig 2), a total of two HT treatments (separated by one week) were delivered prior to the course of palliative radiotherapy. The [Sonalleve] MRgFUS system [Profound Medical] was modified to accommodate the treatment of head and neck targets (Int J Hyperthermia 30.8, 2014, 579-592). A 3T scanner [Achieva, Philips] was used for planning and real-time imaging of the HT delivery. The patient was positioned on a prone position, with the skin below the tumour mass in direct contact with a custom-made water cushion that acts as neck support as well as acoustic coupling media. The planning of treatment was performed using T1-weighted MRI. A 7-slice 2D echo-planar imaging (EPI) sequence (TE/TR=16/25ms, flip angle=18°, acq. matrix=192×143, ETL=11, voxel size=2mm, slice thickness=7mm, NEX=1) was used for real-time MRI thermometry. The target temperature was set to 42.5°C for 30 min. The patient received radiotherapy delivery in the 1hr following the HT session.

Results: One patient diagnosed with recurrent squamous cell carcinoma of the lip with nodal inolvement (male, 56 years old) was treated to a right supraclavicular nodal mass (dimensions of 3×3×3.5cm) with MRIgFUS-based HT and a course of stereotactic body radioatherapy (SBRT) to a dose of 35 Gy in 5 fractions in April 2020. T1-weighted planning MRI of the tumour is shown in Figure 3. At session 1 of HT treatment, oscillatory artifacts in the thermometry were observed and sudden "jerking" in thermometry at the moment when the ultrasound was activated, which suggested a sudden sensation from the participant. No effective HT delivery was achieved during session 1. In session 2, the following week, the sudden motion was not present, and HT delivery was successfully performed in two sonications (Fig 4), for a total time-in-range of 27 min and a thermal dose of 20 CEM43. No observable tissue modifications were detected at immediate post-procedure MRI.

Conclusions: MRgFUS-based HT was delivered successfully after a proper education of the participant. Breathing-related artifacts in EPI-based thermometry were observed at both sessions. Quality of MRI-thermometry can be improved by a better selection of patient and potential implementation of motion-compensation algorithms for thermometry. Overall, the procedure was well tolerated by the participant and no adverse effects were reported. We anticipate that improvement in patient selection should translate into more effective HT delivery. To the best of our knowledge, this is the first time that MRgFUS-based HT has been delivered to a head and neck tumour in conjunction with SBRT.

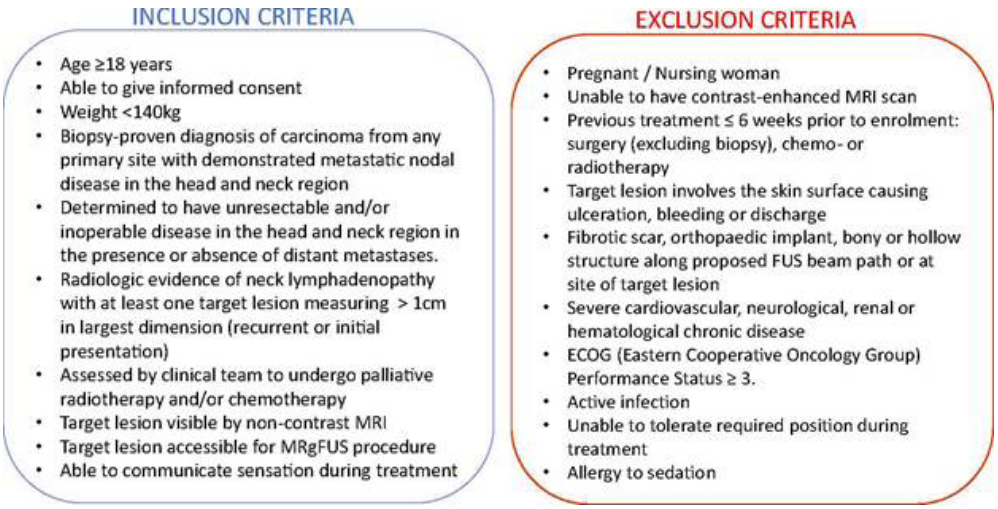

Figure 1. Inclusion and exclusion criteria

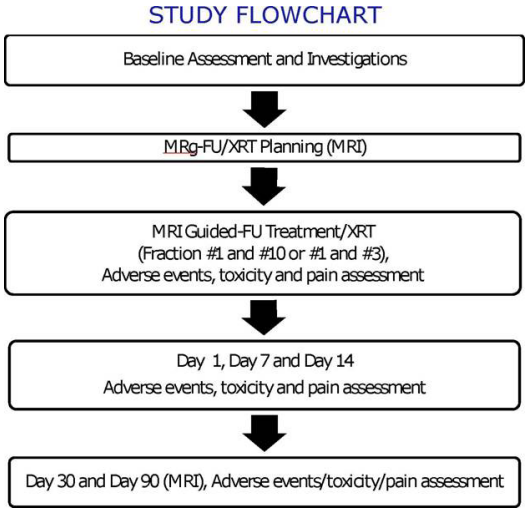

Figure 2. Study flowchart

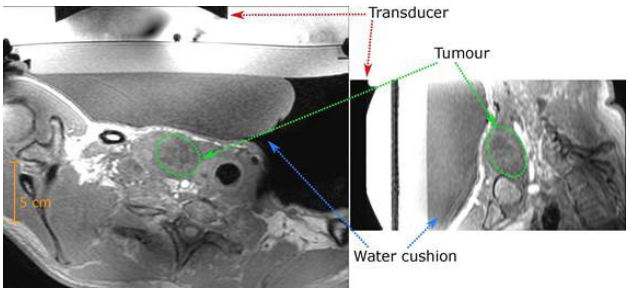

Figure 3. T1-weighted planning imaging showing tumour location, transducer and water cushion. Left) axial view; Right) sagittal view.

Figure 4. Temperature profile of the two sonications delivered on session 2 of HT.

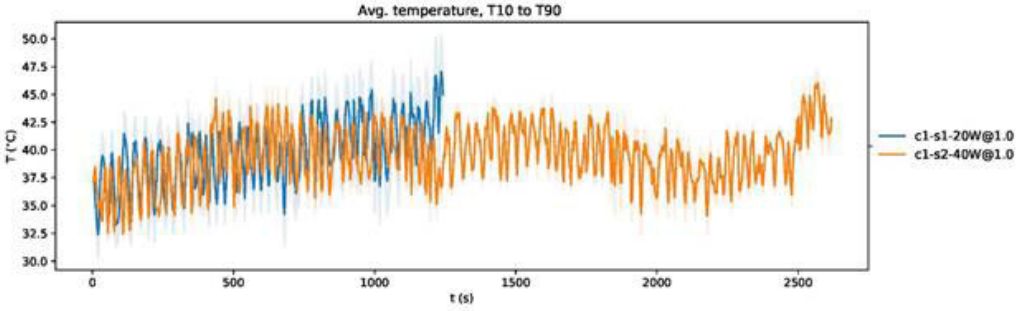

MIT-4

Topic: Miscellaneous Tumors

Presentation Type: Oral

Towards lung FUS: Jet ventilation during one lung flooding optimizes target motion and oxygen-ation independent of positioning

Frank Wolfram[1], Conny Braun[2], Thomas G Lesser[1]

[1]SRH Wald-Klinikum, Gera, Germany
[2]University Hospital Jena, Jena, Germany

Background: HIFU ablation of intrapulmonary targets requires One Lung Flooding (OLF) under ventilation of the contralateral lung. Previous work showed safety and a superior acoustic access to lung tumors during OLF. Prospective application of FUS in lung requires HIFU-System specific patient positioning which might impact the gas exchange as well as the ventilation associated target motion. Superimposed High Frequency Jet Ventilation (sHFJV) is a modern ventilation technique operating with low tidal volumes in contrast to pressure controlled ventilation (PCV). Therefore this study investigated OLF in lateral and supine positions with regard to motion using sHFJV vs. PCV in a large animal model.

Materials and Methods: OLF was performed on ten female pigs (German Landrace, 12.4 weeks, weigh 37 kg (range: 35–40 kg). After onset of anesthesia OLF was performed using a specialized left-sided, double lumen tube (DLT) (Medicoplast, Illingen, Germany) and slow instillation of tempered saline into the left tube leg up to a volume fraction of 12,5ml/kg. Ventilation with FIO2= 0.4 was performed using jet ventilator (TwinStream, CarlReiner, Austria) which was connected to the right DLT lumen. Vital parameters (HR, SO2) were continuously monitored using ECG and Blood Gas Monitor (Rapid Point, Siemens, Germany). In all animals, the position was changed from left lateral (LLP), supine (SP) to right lateral position (RLP). Motion was measured using M-mode sonography (Flex Focus 800, BK Medical, Denmark) with micro-curved 10 - 4 MHz probe of diaphragm and central-pulmonary bronchial markers at the end-expiratory and end-inspiratory level.

Results: Under OLF, no deterioration of oxygenation during sHFJV was found. In lateral left, supine and right position the HR (median 93; bpm) and SaO2 (median 99 %) not differed significantly. All animals survived until the endpoint of complete two lung re-ventilation. Complete lung filling without remaining intrapulmonary air was achieved in the flooded lung.

The diaphragm displacement of the flooded lung side was significant reduced during sHFJV compared to PCV in all animal positions (LLP: 7 mm vs. 17 mm, $p<0.05$; SP: 4 mm vs. 17 mm, $p<0,05$; RLP: 8 mm vs. 20 mm, $p<0.05$). The lowest motion of intrapulmonary bronchial locations was determined in supine position during sHFJV (2 mm).

Conclusions: OLF can be performed without oxygenation deficiency in lateral (left & right) and supine position and therefore applied safely independent on transducer specific patient positioning. Favorable for FUS targeting is sHFJV, enabling continuous ventilation whilst minimizing motion of intrapulmonary targets to a negligible level. Therefore no motion tracking or breath hold techniques for FUS targeting of intrapulmonary nodules are required during sHFJV in contrast to PCV.

Acknowledgements: Approval was provided by the Veterinary Department of the Thuringian State Authority (TLLV Reg. 22-2684-04-WKG-16-002). The study was supported by the SRH Waldklinikum Gera, Germany.

MOV-2

Topic: Movement Disorders

Presentation Type: Oral

Feasibility & efficacy of magnetic resonance guided focused ultrasound surgery (MRgFUS) with autofocusing (AF) echo Imaging

Kyung Won Chang, Jin Woo Chang

Yonsei University College of Medicine, Seoul, South Korea

Background: The skull, which is a major barrier of ultrasound sonication, is round but has an irregular surface and varies its size and shape among individuals. Recently, we developed the concept of skull density ratio (SDR) for the proper selection of the candidate of magnetic resonance guided focused ultrasound surgery (MRgFUS) lesioning for patients with essential tremor (ET). However, SDR alone is not the factor to guarantee the successful treatment of MRgFUS lesioning. Currently, the approach to refine the target by exact measurement of the ultrasonic echo in the transducer has been suggested to improve the efficacy of MRgFUS lesioning, we underwent MRgFUS lesioning with this autofocusing (AF) echo imaging technique.

Materials and Methods: From Dec, 2019 to March, 2020, we recruited 10 patients (ET and PD) with low SDR, 2 patients dropped out of the trial due to screening failure of previous medical history. Total 8 patients were included and underwent MRgFUS thalamotomy in 6 patients with ET and MRgFUS pallidotomy in 2 patients with Parkinson's disease (PD) with AF echo imaging technique.

Results: The mean SDR of the patients with ET was 0.34 (range, 0.29-0.39) and patients with PD was 0.41 (range, 0.38-0.44). The mean skull volume of patients with ET was 280.57 (range, 227–319) cc and patients with PD was 287.13 (range 271-303) cc. During the MRgFUS, average of 15 sonication was performed among average of 5.63 were using AF technique. The mean maximal temperature (Tmax) achieved was 55.88 □ (range, 52-59) and the mean energy delivered was 34.75KJ (range 20~42) in patients with ET and PD. No serious adverse events occurred during and after the treatment. None of the sonication factors (Skull volume, SDR, sonication number, AF score, similarity score, Energy Range & Power) and Max Temperature was correlative with AF echo imaging technique (P>0.05, AF Score showed P=0.071).

Conclusions: With AF echo imaging MRgFUS lesioning technique, safe and efficient treatment is available even for patients with low SDR, which could expand the MRgFUS lesioning indications to SDR < 0.4 for patients with ET and SDR < 0.45 for patients with PD.

Acknowledgements: InSightec®, Ltd, Haifa, Israel

MOV-3

Topic: Movement Disorders
Presentation Type: Oral

The world's first bilateral, staged MRgFUS treatment of medically refractory ET targeting both the ventralis intermedius nucleus and the zona incerta with 12 months follow up results

Ayesha Jameel[1], Wadyslaw Gedroyc [2]

[1]Imperial College, St Marys Hospital, United Kingdom
[2]NHS, St Marys Hospital, United Kingdom

Background: MRgFUS is an effective non-invasive treatment for essential tremor (ET) however only unilateral studies have been performed. Essential tremor is characterised by an action tremor of both limbs, which can spread to involve the head, voice, trunk and legs. The bilateral nature of the disease combined with the success of unilateral studies have led to a burgeoning interest in the potential of bilateral MRgFUS treatments for medication refractory ET.

Previous studies of bilateral treatments of ET using DBS and RFA have demonstrated high complication rates, especially concerning adverse effects on speech; thus there has been a cautionary approach to bilateral MRgFUS treatments for ET. We present the world's first bilateral, staged MRgFUS treatment of medically refractory ET targeting both the Ventralis Intermedius Nucleus (Vim) of the thalamus and the inferior Zona Incerta (ZI) with 12 months follow up results to ascertain its safety and efficacy.

Materials and Methods: In January 2019 we treated one male patient with medically refractory ET for a second unilateral MRgFUS procedure targeting both the VIM and ZI on the right to treat tremor in his left hand. He had previously undergone a unilateral MRgFUS procedure 14 months before, targeting the VIM and ZI on the left with good tremor suppression achieved on his tremor dominant right hand. The patient was screened to ensure there were no persistent adverse effects after the first unilateral treatment to ensure eligibility for a second unilateral treatment.

As with the first unilateral procedure the tremor severity and functional impairment were assessed at baseline and at regular intervals post-treatment (1, 3, 6, 12 months) by a neurologist with a special interest in movement disorders. hese assessments utilised freehand Bain-Findley Spirals (BFS) and the Clinical Rating Scale for Tremor (CRST) a comprehensive essential tremor assessment tool that considers whole body tremor (including an arm tremor score), tremor specific tasks and tremor related disability.

The arm tremor score, derived from the CRST, was analysed in both arms to assess for tremor suppression over the study period.

Full neurological examination was performed at every study visit to monitor for any adverse effects with special consideration given to any change in speech.

Results: At each procedure there was successful thermal ablation of the target tissues at the Vim and ZI with immediate improvement of tremor. This tremor suppression which was sustained over the follow up period.

From baseline to 12 months post the bilateral treatment BFS spirals improved 60.0% in the right arm and 64.3% left arm (Figure 1). The CRST improved 75.4% (Figure 2). The arm tremor score improved by 66.6% in both arms with a small ipsilateral also noted after each treatment (Figure 3).

Adverse events following bilateral treatment were mild and transient, including unsteadiness lasting 2 weeks and dysarthria lasting 3 weeks. However subtle fatigability of speech was noted at the 3 months study visit on clinical assessment by consultant neurologist. This fatigability was not noted by the patient or his wife. At 6 months follow up, speech has returned to pre-procedure status both subjectively and objectively. At 12 months follow up there were no adverse effects.

Conclusions: This pilot study has demonstrated both the safety and efficacy of the world's first staged bilateral MRgFUS procedure for the treatment of ET with stable results at 12 month post bilateral treatment and no long term adverse effects. However, previous bilateral treatments by other methods have demonstrated there is a risk to speech and future bilateral

treatments with MRgFUS should take into consideration potential risks to speech. Further studies are needed with detailed analysis on the effect of bilateral treatments to speech.

Acknowledgements: InsighTec Plc

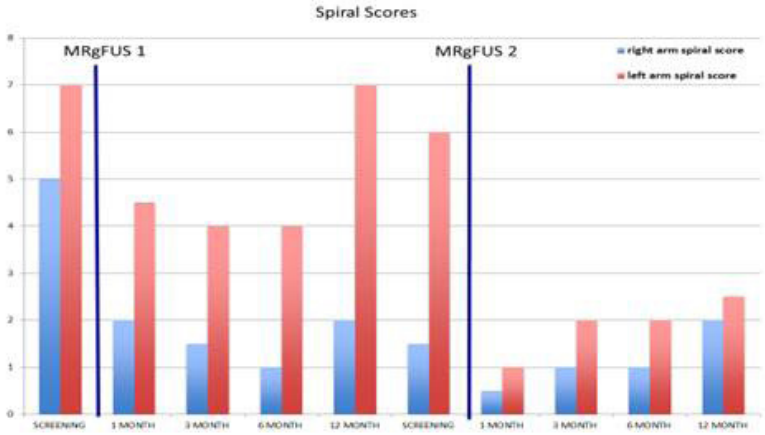

Figure 1. Bain-Findley Spiral Scores for each arm over the study period.

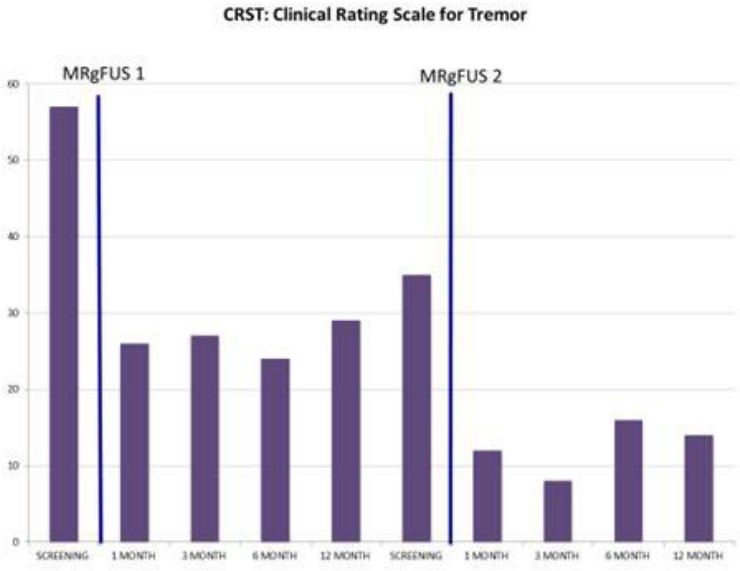

Figure 2. Clinical Rating for Tremor Score over the study period.

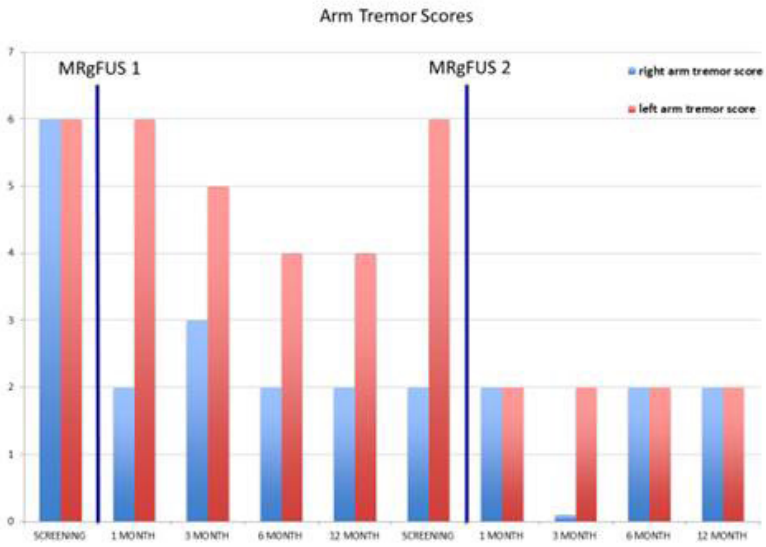

Figure 3. Arm Tremor Score (from CRST) over the study period.

MOV-4

Topic: Movement Disorders
Presentation Type: Oral

Targeting the zona incerta in addition to the ventralis intermedius nucleus with MRgFUS to treat medically refractory essential tremor: Outcomes at two-years

Ayesha Jameel[1], Wadyslaw Gedroyc[2]

[1]Imperial College, St Marys Hospital, United Kingdom
[2]NHS, St Marys Hospital, United Kingdom

Background: Essential Tremor (ET) is defined as an isolated tremor syndrome of bilateral upper limb action tremor, in the absence of other neurological signs. The prevalence of ET is approximately 2% in the US; of which 25%-55% are medication refractory. ET can produce substantial impairment of manual function resulting in significant disability and social handicap.

MR guided focused ultrasound (MRgFUS) has been proven to be a successful non-invasive treatment for ET. Currently, most centres treating ET with MRgFUS place lesions in the Ventralis Intermedius (VIM) nucleus of the thalamus.

Targeting Vim and ZI in the same procedure has been the standard approach of our London (Imperial) and the Oxford functional neurosurgery centres for over 2 decades using RFA and DBS for the treatment of ET. This paper describes our experience of unilateral MRgFUS in patient with medication refractory ET, sequentially treating VIM and ZI in the same procedure.

Materials and Methods: Between July 2016 and November 2017, we treated 14 patients with medically refractory ET. All 14 patients underwent a unilateral MRgFUS procedure where lesions were sequentially placed in the VIM then ZI during the same procedure to treat tremor in the contralateral tremor dominant arm [Fig.1]

Patients were assessed intraoperatively by a neurologist specialising in movement disorders who performed a tremor assessment after each sonication. This tremor assessment included Bain-Findley Spirals from the treated arm (BFS-TA). Post procedure patients were assessed by the neurologist at regular intervals (1, 3, 6, 12 and 24 months). At each follow up visit Bain-Findley Spirals were collated from the treated (BFS-TA) and non-treated (BFS-NTA) arms. These were scored by blinded assessors all of whom were neurologists with a special interest in movement disorders.

Secondary outcome measures were collated at each study visit which included change in the neurologist assessed Clinical Rating Scale for Tremor (CRST) which has three parts – A: whole body tremor, B:tremor specific tasks, C:tremor related disability. Patient self-reported questionnaires (Quality of Life for ET (QUEST) and PHQ-9 depression scores) were also collated.

All outcome measures were compared from baseline to 24 months with the appropriate statistical tests applied.

Results: Across the study, the mean improvement in our primary outcome measure of the treated arm (BFS-TA) from baseline to 24 months was 41.1%($p<0.001$) whilst in the non-treated arm (BFS-NTA) worsened by 8.8%($p<0.001$). [Fig. 2]

The intraoperative BFS-TA scores demonstrated the additional benefit gained from treating ZI after VIM - with 27.9%($p<0.001$) improvement in mean scores post-VIM ablation and an additional 30.1% ($p<0.001$) improvement post-VIM to post-ZI ablation.

Mean improvements at 24 months follow-up in the CRST-parts A, B and C were 60.7%, 30.4% and 65.6% respectively and 37.8% in QUEST-tremor score (all $p<0.001$). From the CRST-A the unilateral tremor severity scores decreased in the treated arm (UETTS-TA) 72.9% ($p=0.001$) and non-treated arm (UETTS-NTA) 30.5% ($p=0.003$) demonstrating some bilateral effects of this treatment. [Fig. 3]

No life threatening adverse effects occurred. At 24 months residual adverse effects were mild unsteadiness (n=1) and hemichorea (n=1).

Conclusions: Our study has demonstrated the utility of targeting the VIM and ZI sequentially in the same MRgFUS treatment to alleviate medically refractory ET in the contralateral arm. Unilateral VIM/ZI MRgFUS diminished contralateral and transiently ipsilateral arm tremor with improvements in arm function, tremor related disability and

quality of life. The adverse effect profile has differed from that described in VIM targeting alone, of note 1 patient had persistent chorea at 24 months which we have attributed to low targeting of the ZI with the sonication spot encroaching on the adjacent subthalamic nucleus. We have since altered our approach to consider potential spot elongation of MRgFUS when targeting deeper tissue.

Acknowledgements: InsighTec Plc

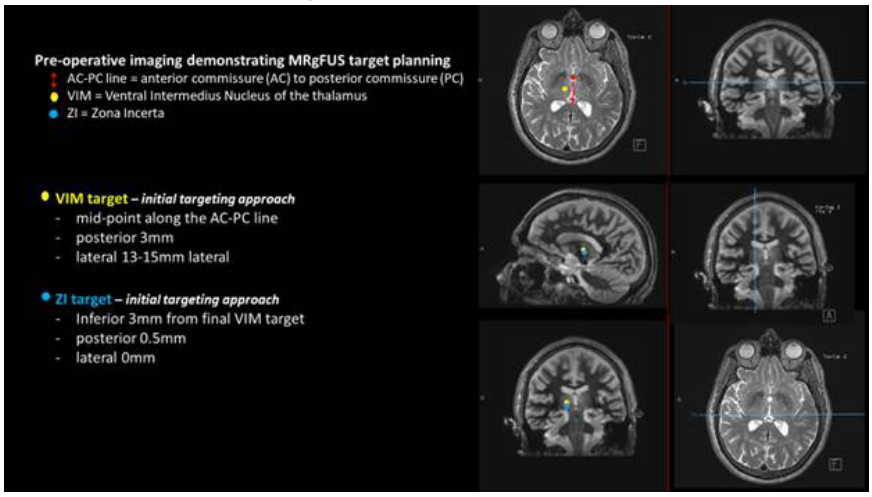

Figure 1. Schematic overlays of preoperative MRI imaging delineating VIM/ZI target planning

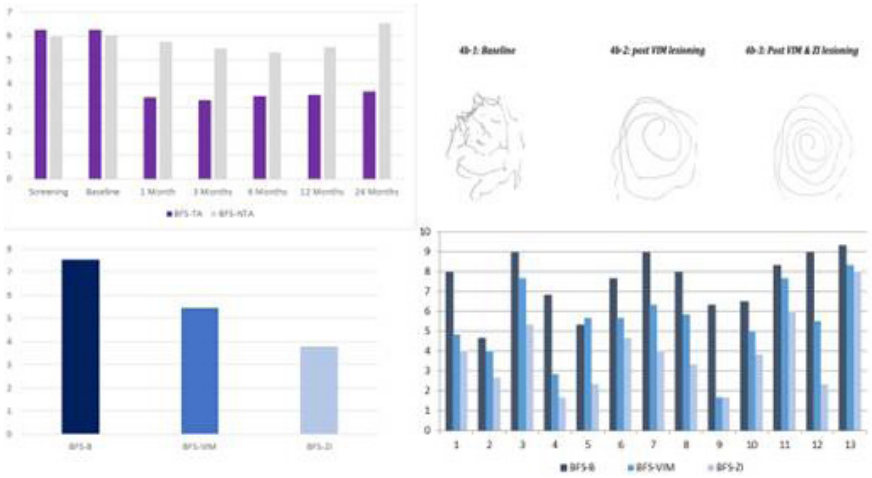

Figure 2. Mean Bain-Findley spiral scores intraoperatively and across the study period.

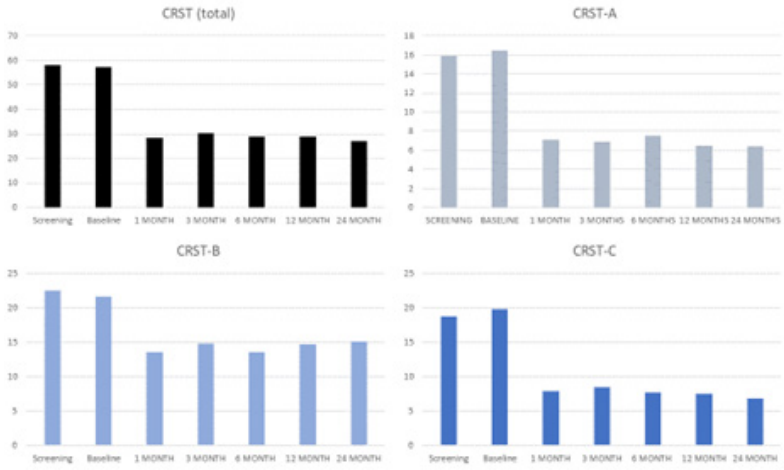

Figure 3. Mean Clinical Rating Scale for tremor across the study period.

MOV-5

Topic: Movement Disorders

Presentation Type: Oral

Connectivity changes in tremor network associated with unilateral focused ultrasound thalamotomy

Francesco Sammartino, Huyen Ngyuen, Michael Knopp, Daniel Boulter, Vibhor Krishna

Ohio State University Wexner Medical Center, Columbus, OH, USA

Background: Abnormal connectivity in the tremor network is thought to underlie the pathophysiology of essential tremor. However, the precise localization of this network is yet to be determined.

Lesion mapping with functional magnetic resonance imaging (fMRI) is a novel technique to identify clinically-relevant brain networks. We sought to define the tremor network by mapping focused ultrasound thalamotomy (FUS-T) lesions.

We tested the hypothesis that functional connectivity is significantly higher in the tremor network in essential tremor (ET) patients than controls (case-control comparison), and that FUS-T reduces functional connectivity in the tremor network (pre-post comparison).

Materials and Methods: Abnormal connectivity in the tremor network is thought to underlie the pathophysiology of essential tremor. However, the precise localization of this network is yet to be determined.

Lesion mapping with functional magnetic resonance imaging (fMRI) is a novel technique to identify clinically-relevant brain networks. We sought to define the tremor network by mapping focused ultrasound thalamotomy (FUS-T) lesions.

We tested the hypothesis that functional connectivity is significantly higher in the tremor network in essential tremor (ET) patients than controls (case-control comparison), and that FUS-T reduces functional connectivity in the tremor network (pre-post comparison).

Results: Tremor network comprised of 18 voxel clusters in the known (contra-lateral cerebellum, ventrolateral thalamus, and bilateral sensorimotor cortex) and distinct (globus pallidus, bilateral occipital cortex and left posterior parietal cortex) brain regions.

Compared to controls, ET patients had significantly higher connectivity in the right cerebellum, left thalamus, bilateral sensorimotor, and left premotor cortex. Connectivity decreased after FUS-T in the contralateral cerebellum and ipsilateral primary motor cortex. The task fMRI analysis confirmed these findings.

Conclusions: Functional connectivity is abnormally high in the tremor network in ET, and it is restored after FUS-T. This connectivity signature should be tested as a diagnostic or treatment response biomarker in future studies.

Acknowledgements: Focused Ultrasound Foundation

MOV-6

Topic: Movement Disorders

Presentation Type: Oral

Safety and efficacy of focused ultrasound staged bilateral thalamotomy for essential tremor

Raul Martinez Fernandez, Jose A Pineda-Pardo, Jorge Máñez-Miró, Marta del Alamo, Frida Hernandez-Fernandez, Rafael Rodríguez-Rojas, David Mata-Marín, Michele Matarazzo, Jose A Obeso

CINAC, Hospital Universitario HM Puerta del Sur, Móstoles, Universidad CEU-San Pablo, Madrid, Mostoles, Spain

Background: Focused ultrasound unilateral thalamotomy is an approved treatment for essential tremor (ET) and has shown to improve both disability and quality of life. One unanswered question is whether magnetic resonance-guided focused ultrasound (MRgFUS) bilateral thalamic ablation can be tolerated, as bilateral radiofrequency thalamotomy was abandoned in the past due to a high rate of worsening of speech and balance. However, the possibility of performing bilateral lesions with a less invasive technique such as focused ultrasound deserves to reconsider this approach. The objective of this study is to report preliminary results on the safety and efficacy of staged bilateral MRgFUS thalamotomy for the treatment of ET.

Materials and Methods: Five patients who had received unilateral MRgFUS thalamotomy at least one year before and who had tremor in the non-treated hand underwent a second thalamotomy on the contralateral hemisphere. The first thalamotomy had not resulted in any permanent side effect and had achieved tremor control in the treated hand. Safety of the second lesion was based on an evaluation of observed and/or reported treatment-related side effects. Additionally, complete neuropsychological testing and voice and gait kinematic analysis were performed. The benefit of the second treatment was assessed through the CRST which includes part A (examination of tremor in each body part), B (task performance) and C (independence for activities of daily living). Three main timepoints were considered: baseline before first thalamotomy (T1); baseline before second thalamotomy (T2); and 6 months after second thalamotomy (T3). Presentation of the data is purely descriptive.

Results: No permanent side effects were registered. All five patients reported mild and transient gait instability after second treatment which resolved within the first few weeks in all cases. One patient reported dysgeusia for a few days following bilateral thalamic ablation. Neither neuropsychological assessment nor voice and kinematic analysis detected any worsening after second thalamotomy as compared to T2. CRST A+B improved by 71% from T1 to T3 (31,8±9,8 to 6,4±9,6) while part C decreased by 87% (13,8±1,0 to 1,8±2,9) [figure 1]. Improvements from T2 to T3 were 55% for parts A+B and 35% for CRST C.

Conclusions: This is the first evidence that MRgFUS bilateral staged thalamotomy is safe and can be applied to treat ET. A larger trial is warranted to confirm this preliminary data.

Acknowledgements: Insightec provided funding to perform patients treatments

MOV-7

Topic: Movement Disorders
Presentation Type: Oral

Optimal parameters for focused ultrasound thermal neuromodulation

Francesco Sammartino[1], John Snell[2], Vibhor Krishna[1]

[1]Ohio State University Wexner Medical Center, Columbus, OH, USA
[2]Focused Ultrasound Foundation, Charlottesville, VA, USA

Background: Focused ultrasound (FUS) induces reversible clinical effects (or thermal neuromodulation, TN) at sub-threshold temperatures (focal temperature <45 0C). This phenomenon is used for physiological exploration and testing during essential tremor treatment. However, the optimal parameters for TN are not well characterized. We sought to define FUS parameters (i.e. temperature threshold and spot size) associated with TN.

Materials and Methods: A retrospective analysis of essential tremor patients (n=24) who underwent FUS ablation of the ventral intermediate nucleus was performed. Intraoperative thermal maps and corresponding writing samples were analyzed. The writing samples (spiral, straight line, and handwriting) were independently rated by two movement disorders specialists (FS and VK) using the clinical rating scale for tremor (individual item scored between 0-4, maximum score=12). Percentage tremor improvement was calculated for each sonication and summarized using mean and standard deviation. A mixed-effects model was used to analyze the association between focal temperature and tremor improvement. We used Pearson's correlation analysis to test the association between spot size and tremor improvement.

Results: One hundred thirty sonications and corresponding writing samples were analyzed, and 29 were identified as subthreshold sonications. Tremor rating was concordant between both raters. Temperature rise was a significant predictor of intraoperative tremor improvement (p=2.2*10-16).

Thermal neuromodulation was observed in 10 out of 29 subthreshold sonications (mean tremor improvement: 22.8±12.2). The mean temperature associated with tremor improvement was 42.6°C (SD:1.9). The bigger spot size was significantly associated with tremor improvement (R2 =0.67, p=5.4*10-5).

Conclusions: TN was observed in a minority of subthreshold sonications. Besides temperature, spot size was significantly associated with tremor improvement. Further investigations are required to prospectively test the optimal focal temperature and spot size required for TN.

MSK-1

Topic: Musculoskeletal
Presentation Type: Oral

Feasibility of treating implant-associated osteomyelitis with focused ultrasound and antibiotic-laden thermally sensitive liposomes

Harshini Ashar, Kalyani Ektate, Ashish Ranjan

Oklahoma State University, Stillwater, OK, USA

Background: Acute and chronic non-healing bone wounds are a serious infection of the musculoskeletal system, typically resulting from diabetes and vascular diseases, open fractures, artificial hip or knee joint replacements, or other bone surgery. In particular, chronic osteomyelitis is a destructive bony lesion typically caused by Staphylococcus aureus biofilms in children and adults and is characterized by a reduced susceptibility to treatment, and poor penetration/non-uniform distribution of antimicrobials within bone tissues. We hypothesized that antibiotic laden Low Temperature-Sensitive Liposomes (LTSLs), applied systemically with Focused Ultrasound (FUS)-induced bone heating (>40°C) can overcome this barrier, by enabling externally-controlled "heat-targeted, on-demand" antibiotic delivery and synergistic bacterial killing within infected bony tissue, reducing or obviating the need for ultimate surgical manipulation and debridement.

Materials and Methods: To investigate our hypothesis, we developed a rat model of metal-implanted osteomyelitis. Briefly, orthopedic K-wires were surgically implanted into both femurs of rats with an inoculum of 10^7 CFU of methicillin-resistant S. aureus (MRSA) strain to induce chronic osteomyelitis. LTSLs were loaded with a model antibiotic agent (Ciprofloxacin or CIP) for controlled and targeted release at >40°C. FUS exposures of infected bone tissues were performed using the ultrasound-guided Alpinion system 10-days post-infection. We compared the following groups (n=3/group): CIP-LTSL (+/- FUS), CIP (+/- FUS) and +/- FUS controls. For ultrasound exposure, the bone was aligned at a fixed focal depth, and the Alipinion software was used to define the target boundary and slice distance in x, y, and z directions for automatic rastering of the transducer during treatment. The following FUS parameters were used: 5 Hz pulse repetition frequency (PRF), 50% duty cycle (DC), and 12 W acoustic power at the focus, for a total of 35-40 min treatment duration. Bone heating was monitored using fiber optic temperature sensors by placing them at the muscle-bone interface. CIP-LTSL and CIP (10 mg CIP/kg body weight) were administered intravenously immediately after the initiation of FUS. 24h later, the rats were sacrificed, and bone delivery of CIP was measured spectrophotometrically. Additionally, the mean colony-forming unit (CFU) analysis of heated and unheated bone and the implanted wires were assessed.

Results: Our surgical method yielded medullary disease by day 10 in bones and adjoining muscle. Histologically, they were characterized by suppurative changes (bacterial and pus pockets) with remodeling and colonization of tissues with S. aureus. Average temperatures for bone calculated from the interface using temperature sensors yielded a mean temperature of ~55°C at the target site. The maximum temperatures were reached within 5-min and could be sustained over the period of treatment. We found the antibiotic delivery in the heated region increased by ~1fold with LTSL(2.16μgCIP/g) vs. CIP(1.47μgCIP/g) and unheated femur(1.33μgCIP/g), demonstrating that this approach can be used to improve drug delivery to infected bones. The increased CIP delivery correlated with the therapeutic effects of the CIP-LTSL combination, achieving significant reductions of biofilm density on the implanted wire(1-1.7log) as well as in the infected bone(0.4-1.8log) compared to CIP and untreated control, respectively.

Conclusions: Our data show that combining FUS bone heating with antibiotic-loaded LTSL can selectively improve bacterial killing rates in osteomyelitic bones vs. those in unheated controls. Although the overall bactericidal effect is significant, improved liposome focusing at infected sites, optimization of FUS treatment durations, and increasing the frequency of treatment can further improve the non-invasively eradication of biofilm-associated chronic bone infections. Studies are currently underway to understand the biofilm disruption and immunopathological mechanisms of FUS in the infected bones. Additionally, the longitudinal treatment success using imaging and ambulatory assessment of rats are in works.

Acknowledgements: We thank the Oklahoma Center for the Advancement of Science and Technology (OCAST) Project # HR17-060, Focused Ultrasound Foundation, and the Kerr Endowed Chair at Oklahoma State University.

MSK-2

Topic: Musculoskeletal
Presentation Type: Oral

Magnetic resonance-guided focused ultrasound for painful bone metastases: A pooled meta-analysis of 33 studies with 1082 patients

Joe Baal[1], William Chen[1], Ulysis Baal[1], Sagar Wagle[2], Jed Baal[1], Thomas Link[1], Matthew Bucknor[1]

[1]University of California, San Francisco, San Francisco, CA, USA
[2]Mayo Clinic, Rochester, MN, USA

Background: The current standard local palliative treatment for painful osseous metastatic disease is external beam radiotherapy. However, local radiotherapy has been associated with delayed side effects and questionable efficacy in the setting of radioresistant cancers. Re-irradiation of recurrent painful bone metastases is restricted by radiation dose limits of the targeted tissue. Magnetic resonance-guided focused ultrasound (MRgFUS) has emerged as an effective ablation technique in the palliative treatment of painful bone metastases as evaluated by several studies in recent years. Available studies are limited in sample size which limits estimation of treatment efficacy and safety. To date, a systematic review and meta-analysis on the treatment efficacy and associated toxicity of MRgFUS for painful bone metastases has not been done. The purpose of this study was to pool selected literature to define the efficacy and safety of MRgFUS for the palliative treatment of painful bone metastases.

Materials and Methods: A systematic search was conducted in March 2020 using the Pubmed and Embase electronic databases with the query: ("mrgfus" or "hifu" or "focused ultrasound") AND ("bone" or "bone metastases" or "bone metastasis"). Studies reporting clinical outcome and/or toxicity data of MRgFUS of painful bone metastases in five or more patients were included in this meta-analysis and systematic review. Studies were excluded if (1) there was no toxicity or outcome data (proportion of patients that respond to treatment and/or pain scores from baseline and follow-up) specific to MRgFUS treatment of painful bone metastases; (2) the follow-up period was less than one month; (3) the study reported redundant patient cohorts already reported in another study; (4) the study was a review, commentary or editorial; or (5) the study had less than 5 patients. Treatment response was a combination of complete response (pain score of 0 after treatment) and partial response, which was defined as ≥2-point reduction in the pain score, per the updated international consensus on palliative radiotherapy endpoints for future clinical trials in bone metastases. A pooled analysis was performed on the study weighted proportion of patients who experienced pain relief following MRgFUS treatment. Both fixed effects and random effects models were applied. Hedges' g statistic was calculated to quantify the change from baseline pain score (NRS or VAS) and follow-up pain scores.

Results: Out of 1335 studies identified on initial search, 33 studies published between 2007 and 2019 met inclusion and exclusion criteria were selected for the meta-analysis (Fig. 1). The selected studies resulted in a total of 1082 patients with painful bone metastases treated with MRgFUS. Random-effects pooled proportion of overall treatment response was 79% (95% CI 73-83%) (Fig. 2). Out of the 20 studies reporting treatment response, 13 studies (N=308) provided the distribution of complete and partial response to the treatment; out of 295 treatment responders, 149 (50.5%) had complete response and 146 (49.5%) achieved partial response. Twenty studies comprising 543 patients demonstrated as pooled mean difference in pain score of -3.8 (95% CI -4.3; -3.3) and -4.4(95% CI -5.0; -3.7) at 1-month and 3-month follow-up, respectively. The overall rate of high grade (CTCAE grade 3 or higher) and low grade (CTCAE grade 2 or lower) MRgFUS-related adverse events were 0.9% and 5.9%, respectively.

Conclusions: Our systematic review and meta-analysis demonstrated that MRgFUS has high efficacy in pain score reduction of symptomatic bone metastases. Our results show safety and efficacy that rival standard radiotherapy treatments for painful bone metastases, based on prior studies. Given the low rates of treatment-related adverse events, MRgFUS may be a viable alternate first option for the palliative treatment of bone metastases in patients with suspected radio-resistant primary cancers. MRgFUS also proves to be an effective salvage therapy option for patients that fail initial radiotherapy.

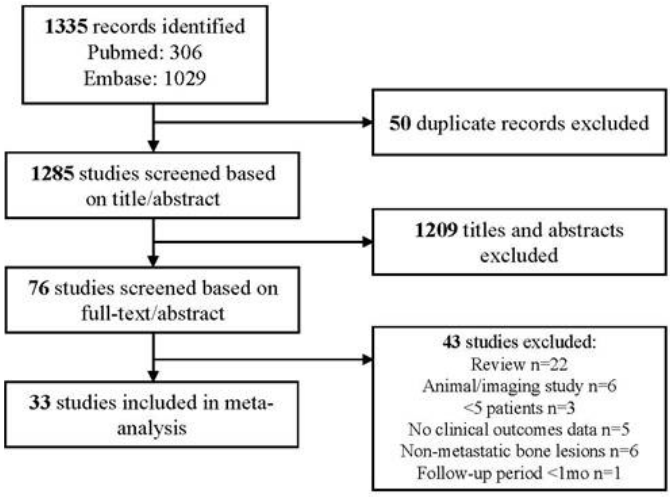

Figure 1. Flowchart of literature search and study selection process.

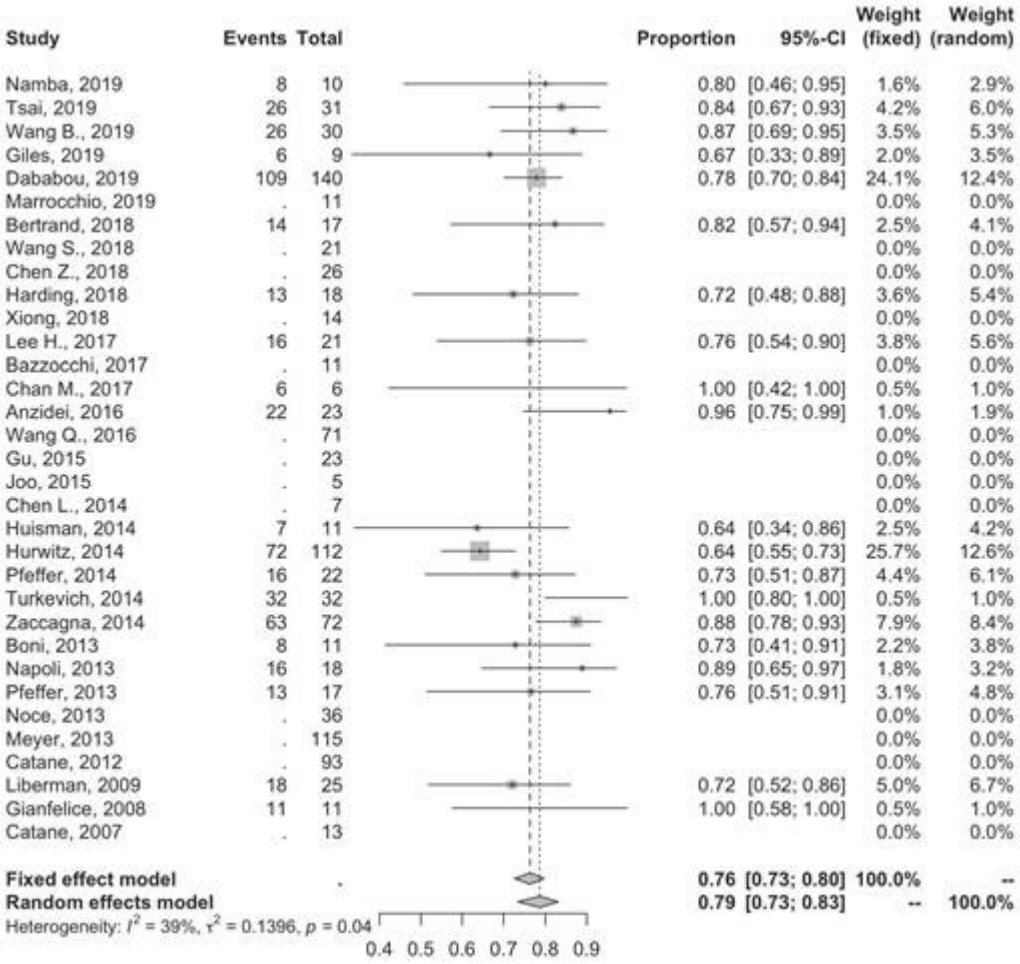

Figure 2. Forest plot for overall treatment response following MRgFUS treatment of painful bone metastases.

MSK-3

Topic: Musculoskeletal
Presentation Type: Oral

MR-guided focused ultrasound versus external radiation therapy for the treatment of pain in bone metastases: A multicenter open-label phase-two clinical trial

Alessandro De Maio[1], Giulia Alfieri[1], Roberto Scipione[1], Francesca De Felice[1], Daniela Musio[1], Alberto Bazzocchi[2], Alessandro Napoli[1]

[1]La Sapienza - University of Rome, Rome, Italy
[2]The Rizzoli Orthopaedic Institute, Bologna, Italy

Background: Recent International consensus and clinical trials study assessed the value of magnetic resonance-guided focused ultrasound surgery (MRgFUS) for the treatment of pain from bone metastases, a common cancer-related morbidity. Options currently available for patients refractory to medical therapy are limited. Today's standard, external radiation therapy (RT), provides pain palliation in 1-4 weeks, over 1-10 typical sessions under exposure of ionizing radiation. On the other hand, MRgFUS, provides pain palliation in 1-3 days after 1 session. The effect of focused ultrasounds to bone is non-invasive, and mainly relies on periosteal nerve ending thermal ablation. The emerging role of MRgFUS is considered as second line option and this study aims at comparing this approach with external radiation therapy.

Materials and Methods: The presented study is a prospective two-center open-label phase-two trial. Patients with painful bone metastases were so allocated in a 1:1 case-matching according to a joint decision between local tumor board and patient. Follow-ups were planned for one year from enrollment with intermediate visits at one, two, three and six months. Assumptions of the study were a two-tailed significance with alpha 5% and 95% statistical power, allowing for 20% dropout. The primary endpoint was improvement in the Visual-Analogue Scale (VAS) at month one after treatment and was analyzed by Chi square test. Provided self-reported quality of life tests were Quality of Life Questionnaire Core 15 Palliative Care (QLQ-C15-PAL), Quality of Life Questionnaire Bone Metastases 22 (QLQ-BM22) and Brief Pain Inventory (BPI). Score differences were analyzed by Mann Whitney U test and repeated measure analysis as Wilcoxon rank-sum test. Area Under the Curve for pain palliation determined overall changes for the entire study timeline. Kaplan Meier curve analysis was adapted both to survival and response to treatment. Cox proportional hazards models were fit to whole dataset, sex, age and pain severity (VAS >7) at baseline. Patient improvement was defined as a decrease in worst reported pain on VAS by 2 or more points from baseline.

Results: A total of 198 patients were enrolled and equally distributed between MRgFUS and external radiation therapy arms.

Improvement proportions were significantly different at month one (primary endpoint), being 0.65 and 0.3 (P=0.0005), and at month twelve 0.79 and 0.35 (P=0.0005), although similarly sustained through month three and not different at month six. Consistently, VAS scores were different with 95% C.I. as -1.89 (-2.60 to -1.19) at month one, then -2.89 (-4.52 to -1.27) at month twelve.

BPI and QLQ-C15-PAL had similar trends, while QLQ-BM22 did not. Subtests for areas of physical function, appetite, nausea and vomiting, dyspnea and quality of life reported significant differences in favor of MRgFUS. Survival was on average 7 and 5.2 months (P<0.0001) respectively for MRgFUS (38% survival at 12 months) and radiotherapy (23%). Hazard ratios were 1.48 (95% C.I. 1.055 - 2.074) for survival, and 1.31 (95% C.I. 1.094-1.312) for pain improvement.

Conclusions: This study demonstrates the potential of MRgFUS technology in the palliation of pain due to bone metastases. External radiation therapy has long been applied to this field and is currently more widely available. The higher rates of improvement documented by MRgFUS use are needed, having shown crucial for patients' quality of life, morbidity and survival. As expected, typical ionizing radiation-related side effects were confirmed to be lower-to-absent in the MRgFUS arm, also reflecting a heightened sensation of quality of life. Larger-scale randomized clinical trials are needed as these, with the spread of technology, may be able to prefer one approach over the other in the line of treatment for such patients.

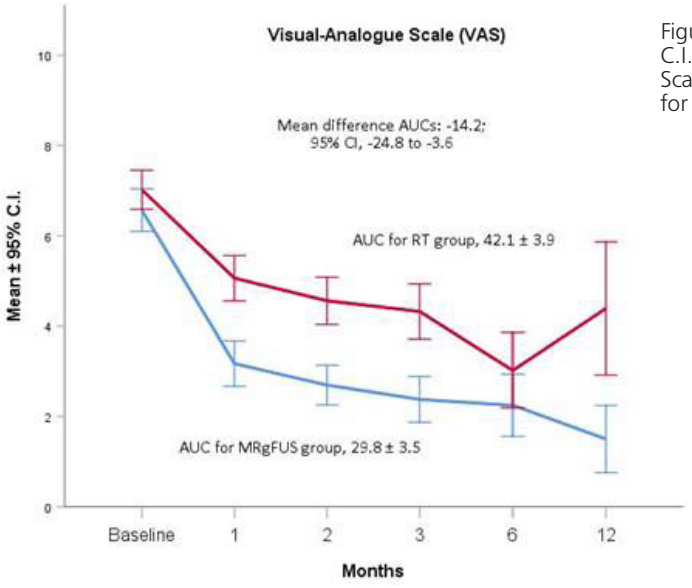

Figure 1. Curves of Mean (± 95% C.I.) Scores on the Visual-Analogue Scale for Bone Pain with overall results for Area Under the Curve analysis.

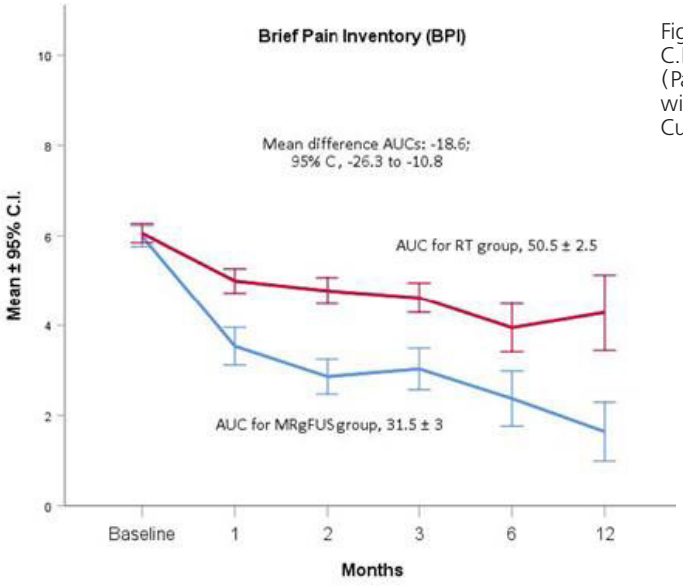

Figure 2. Curves of Mean (± 95% C.I.) Scores on the Brief Pain Inventory (Pain Severity and Interference scores) with overall results for Area Under the Curve analysis.

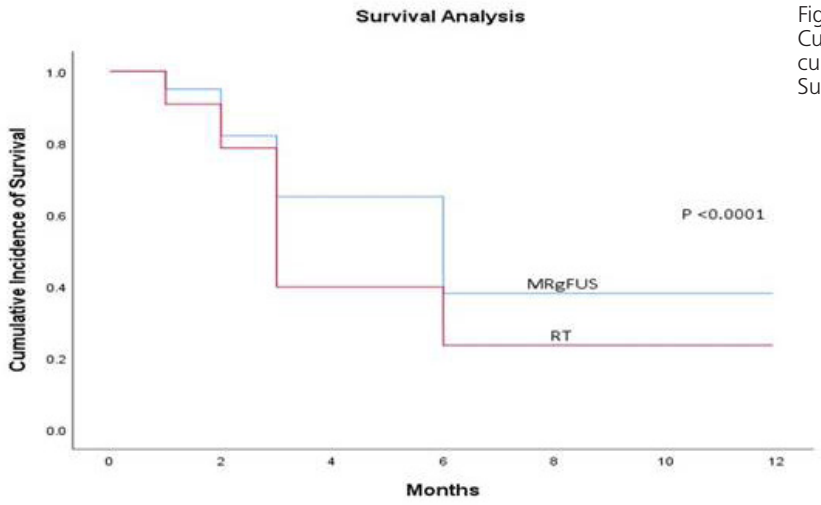

Figure 3. Kaplan–Meier Curves estimating the cumulative incidence of Survival.

MSK-4

Topic: Musculoskeletal
Presentation Type: Oral

Effects of MRgFUS boiling histotripsy combined with ablation in tendons: A pilot study

William Chu Kwan[1], Benjamin Keunen[2], Ari Partanen[3], Grace Lai[4], Karolina Piorkowska[4], Adam Waspe[4], James Drake[4]

[1]University of Toronto, Toronto, ON, Canada
[2]SickKids, Palmerston, ON, Canada
[3]Profound Medical, Mississauga, ON, Canada
[4]Hospital for Sick Children, Toronto, ON, Canada

Background: Tendon resections are used for correcting musculoskeletal conditions such as gait alteration in diabetic foot ulcer or contracture release in cerebral palsy or stroke. During Magnetic Resonance-guided Focused Ultrasound (MRgFUS) ablation, precision of treatment is important for optimal patient outcomes. One potential application of MRgFUS is in the incisionless, non-invasive resection of tendons that replicates the outcomes of surgical tendon release. During MRgFUS thermal ablation of tendons, energies of 2000J (100 W x 20 sec) are sufficient to release tendons. One side effect of these energy doses is heat accumulation that could damage adjacent neurovascular structures. Energy could also accumulate in the near-field or the far-field, potentially leading to skin burns and other thermal damage. The goal of this study is to reduce the energy and limit the thermal spread in ablative treatments by refining MRgFUS ablations with boiling histotripsy and reducing ablation powers.

Materials and Methods: Fresh ex-vivo porcine deep digital flexor tendons were vacuum-degassed in normal saline and embedded in 2% agar phantoms. Physical properties such as temperature, length, and diameter were recorded during preparation. Pre-sonication T1-weighted and T2-weighted MR images were obtained, and sonication monitoring was performed using proton resonance frequency shift thermometry as shown in Figure 1. Treated tendons (n=45) underwent combined boiling histotripsy and ablative FUS treatments using a Sonalleve® V1 (Profound Medical, Canada) at 1.2 MHz. Boiling histotripsy with a burst duration of 4.2ms, pulse repetition frequency of 0.75Hz, and an average peak negative pressure (PNP) of 8.3, 10.6, or 13.4 MPa for 60 seconds was immediately followed by low power continuous exposures of either 20, 30, or 40W for 20 seconds, creating permutations of boiling histotripsy and ablation at different energy dosages. Post-sonication, T1-weighted and T2-weighted MR images were obtained to calculate the volumetric change of signal hyperintensity in the T2-weighted MRI sequences of treated tendons in comparison to adjacent size-matched controls, as shown in Figure 2. Statistical analysis using logistic regression models and predictive probability was performed.

Results: The measured volume corresponding to tendon damage are presented in Figure 3. Following boiling histotripsy, volumetric changes in tendons were observed at ablative powers as low as 20W. An increase in volume was noted as either boiling histotripsy or ablation power was increased. For example, at the given histotripsy dosage with PNP of 8.3MPa, a volume change of 12.8mm3 occured when combined with 20W of ablation, and a volume change of 227.1 mm3 occured when combined with 40W of ablation. Similarly trend occurs when analyzing an ablation dose, the power of 20W caused a volume change of 12.8mm3 when combined with -8.3MPa, and a volume change of 150.8mm3 when combined with -13.4MPa. Logistic regression analysis was performed to quantify the nonlinear volume increase (Fig4). The multiplicative interaction between histotripsy peak negative pressure and ablation power provides the highest correlation to the observed volumetric change when compared to ablation or boiling histotripsy alone.

Conclusions: This pilot study demonstrates the potential of combining boiling histotripsy and ablation with the goal of controlling and producing more precise volume effects in tendons while delivering less ablative power. Deposited energy and thermal spread during an ablation could cause skin burns, adjacent tissue thermal damage, or far-field tissue damage. Therefore, reducing the delivered energy while producing a more controlled desired effect has the potential to increase safety and accuracy of tendon ablation in the setting of tendon resection.

Acknowledgements: CIHR, NSERC, Vanier Scholarship

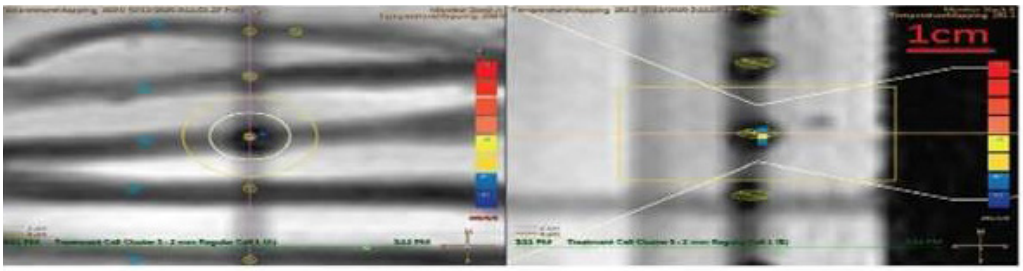

fFigure 1. Temperature map during combined treatment showing minimal increase in temperature during ablation.

Figure 2. Difference in volume of treated tendons with a power of 20W and boiling histotripsy pressures of (A) -8.3MPa, (B) -10.6 MPa, and (C) -13.4MPa.

Ablation Power (W)	Boiling Histotripsy average negative peak pressure (MPa)			Total ablative energy (J)
	-8.3	-10.6	-13.4	
20	12.8(14)	14.6(11.9)	150.8(150.9)	400
30	42.9(94)	415.3(293.5)	478.8(326.5)	600
40	227.1(277.1)	454.6(344.1)	908.3(341.8)	800

Figure 3. Average volume of sonication (mm3) with standard deviation.

	Coefficient Estimate	Standard Error	P-value
Ablation alone	-0.0047550	0.0956417	0.9603
Histotripsy alone	-0.0208169	0.0129382	0.1076
Histotripsy *Ablation	0.0014814	0.0006506	0.0228

Figure 4. Logistic regression model

NDG-2

Topic: Neurodegenerative Disorders
Presentation Type: Oral

The preliminary results of single-center, open, prospective, single-arm, feasibility, assessment of initial efficacy and safety of MRgFUS for blood brain barrier disruption in patients with Alzheimer's disease

Jin Woo Chang

Yonsei University College of Medicine, Seoul, South Korea

Background: Alzheimer's disease (AD) is a progressive neurodegenerative disease and is the most common cause of dementia, with over 5 million people affected in the US. Recently, MR-guided focused ultrasound (MRgFUS) has been attracting attention as a noninvasive means of temporarily disrupting the BBB. Recently, we also demonstrated the excellent recovery of memory and behaviors as well as the reduction of amyloid burden in the pre-clinical FUS studies for AD animal models. As well, we confirmed the safety and feasiblity of MRgFUS BBBD for human glioblastoma (GBM) by finishing phase I trial of MRgFUS BBBD for GBM.

Materials and Methods: This study is a prospective, single-center, single-arm study to evaluate the safety and efficacy of BBB disruption using the ExAblate Model 4000 Type system. Patients with diagnosis of Alzheimer's Disease (NIA/AA criteria), 29 together with their caregivers, will be approached by a team of neurosurgeons and neurologists who specialize in the management of memory disorders and functional neurosurgery. We enrolled 6 patients for this study. The following are inclusion and exclusion criteria.

Inclusion criteria

1. Age: 50-85
2. MMSE ≥ 18
3. 18F-Florbetaben (FBB) PET positive
4. 18F-Fluorodeoxyglucose (FDG) PET suggestive of AD-induced neurodegeneration
5. AD-MCI: Petersen's criteria for amnestic mild cognitive impairment
6. AD-Dementia: NIA-AA criteria for probable AD dementia

Exclusion criteria

1. Severe ischemic changes on MRI: Fazeka's scale of 3 or number of lacunes > 5 or cerebral microbleeds > 3
2. A severity score of 2 more on any of the "delusions", "Hallucinations" or "Agitation/Aggression" of the Caregiver-Administrated Neuropsychiatry Inventory (CGA-NPI)

We underwent two BBBD with 3 months intervals.

Results: We will report our preliminary outcome with the following criteria.

Primary outcome:

- Changes in FBB-PET (global SUVR and regional SUVR, cerebellar gray matter reference)
- Changes in FDG-PET (lobar and global SUVR, Pons reference)

Secondary outcome:

- Safety issue
- Changes in cognitive scores (MMSE, detailed scores in SNSB)
- Structural brain changes: Cortical thickness and Diffusion tensor image markers

Conclusions: MRgFUS BBBD did not make any cognitive or physical side effects for patients with AD patients and seems to be safe even with very wide BBBD.

Acknowledgements: National Research Foundation of Koea under Ministry of Science & ICD, Grant No. 2016M3C&A1914123

NDG-3

Topic: Neurodegenerative Disorders

Presentation Type: Oral

Therapeutic ultrasound as a treatment strategy for improving cognition in physiological and pathological aging

Jürgen Götz, Gerhard Leinenga, Rucha Pandit, Rebecca Nisbet, Daniel Blackmore

The University of Queensland, Brisbane, Australia

Background: Brain functions deteriorate as a consequence of both physiological and pathological aging. My laboratory has a major interest in understanding the pathogenesis of Alzheimer's disease (AD) as a major form of pathological ageing, characterized by the deposition of insoluble protein aggregates (amyloid-beta and tau) and, among others, cognitive impairment. Since several years, we are exploring therapeutic ultrasound together with intravenously injected microbubbles as a treatment modality for brain diseases. In complementing these studies, safety studies have been performed in mice. We have now also assessed very old mice which are cognitively impaired, and determined whether therapeutic ultrasound would also restore their cognition, which is impaired but not because proteins such as amyloid-beta and tau would aggregate.

Materials and Methods: We used the following mouse strains for our analysis: amyloid-beta-depositing APP23 mice (aged: 12-22 months), P301L tau transgenic pR5 mice (aged: 6 months), K369I tau transgenic K3 mice (aged: 5-20 weeks) and C57BL/6 wild-type mice (aged: 4-22 months), which were subjected to several weekly treatment sections with ultrasound in a scanning mode (SUS) together with microbubbles (SUS+MB) compared to sham (microbubbles injected, but no ultrasound delivered). Depending on the genotype, the mice were subjected to various motor and memory tests, different imaging modalities were used, and dissected brains were analysed histologically, biochemically, electrophysiologically, and by quantitative proteomics.

Results: We found that in the different AD mouse models, SUS (with microbubbles) effectively cleared amyloid-beta and tau, using separate mechanisms. Amyloid-beta was mainly cleared by microglial activation, whereas tau was mainly cleared by activating neuronal autophagy. Cognitive functions in SUS+MB-treated APP23 mice were restored to wild-type levels, whereas in the tau transgenic mice there was only a partial amelioration of motor and memory functions observed. A major test used to assess spatial memory functions was the active place avoidance test (APA) which was also used to assess memory functions in very old (22 months old) wild-type mice. Surprisingly we found that SUS achieved major improvements at this age (when wild-type mice are massively impaired in their cognition). The underlying mechanisms will be presented.

Conclusions: Our preclinical data demonstrate the potential of therapeutic ultrasound as a new treatment modality for brain diseases. They illustrate that amyloid-beta is an easier therapeutic target than tau for therapeutic ultrasound. They further present therapeutic ultrasound (SUS+MB) as a modality to improve cognition in physiological ageing.

Acknowledgements: NHMRC, ARC, MRFF, private donors

References:

1. Blackmore et al. *Theranostics* (2018); and under review;
2. Leinenga et al. under review;
3. Pandit R et al., *Adv Drug Del Rev* (2019);
4. Pandit R et al., *Theranostics* (2019);
5. Nisbet R et al., *Brain* (2017);
6. Leinenga & Götz, *Science Translational Medicine* (2015)

NDG-4

Topic: Neurodegenerative Disorders

Presentation Type: Oral

Focused ultrasound-induced blood-brain barrier opening mitigates pathological progression, improves spatial memory and initiates cholesterol changes in the 3xTg-Alzheimer's mouse model

Maria Eleni Karakatsani, Maria Murillo, Robin Ji, Tara Kugelman, Yeh-Hsing Lao, Nancy Kwon, Karen Duff, Elisa Konofagou

Columbia University, New York, NY, USA

Background: Focused ultrasound (FUS) has been proven to reduce amyloid plaques and hyperphosphorylated tau protein from the hippocampal formation and the entorhinal cortex in different mouse models of Alzheimer's disease (AD). Given the beneficial effects of FUS on isolated AD pathologies, we investigate its functional and morphological outcomes on brains bearing both pathologies simultaneously as is the case of human disease.

Materials and Methods: Eleven transgenic mice of the 3xTg-AD line (14 months old) and eleven age-matched wild-type animals received bilateral sonications covering the hippocampus once per week for four consecutive weeks. Following the last treatment, sonicated animals and control littermates underwent behavioral testing in the Morris water maze (MWM). All mice received a 5-day training familiarizing with reaching the escape-platform within 60 seconds. Following the training, the platform was removed and the amount of time spent in each MWM quadrant was quantified. The following week all animals were sacrificed and their brains processed for immunohistochemistry and biochemical analysis.

Results: Animals that received FUS spent significantly more time in the quadrant where the platform was located (Figure 1) while this functional improvement correlated well with a 58.31% decrease in the neuronal length affected by tau confirmed by a 27.2% reduction in tau levels shown by immunoblotting. Amyloid plaque population, volume and overall load were also decreased yet not significantly. Transcriptomic analysis of the sonicated hippocampi revealed upregulation of the low density lipoprotein receptor (LDLr) family, closely associated with cholesterol trafficking in the brain and memory retention.

Conclusions: Overall, we show that both hallmarks of the AD pathology, human amyloid-β42 and tau protein, could be mitigated by repeated ultrasound applications. Significant improvement in the short term memory of non-transgenic animals after repeated sonications leaves room for further investigation of the effect ultrasound has on memory cells including the contribution of the cholesterol levels.

Acknowledgements: National Institutes of Health (R01AG038961 and R01EB009041) and the Focused Ultrasound Foundation.

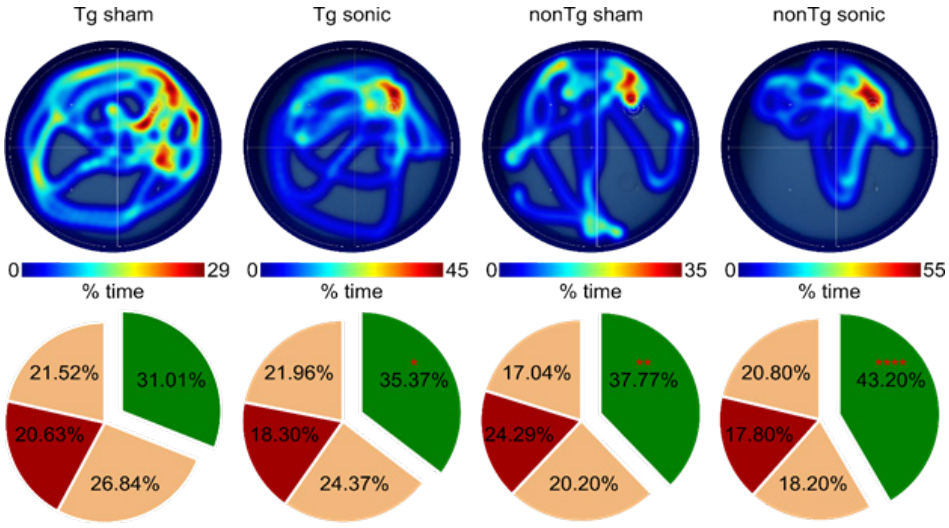

Figure 1. Representative individual heatmaps of the time spent in every quadrant followed by the cumulative results on the probe trial.

NDG-5

Topic: Neurodegenerative Disorders

Presentation Type: Oral

Safety and initial efficacy of hippocampal blood-brain barrier opening for plaque clearance in Alzheimer's disease

Vibhor Krishna, Francesco Sammartino, Michael Knopp, Katherine Binzel, Douglas Scharre

Ohio State University Wexner Medical Center, Columbus, OH, USA

Background: Progressive amyloid deposition and cognitive decline characterize Alzheimer's disease (AD). In preclinical studies, the blood-brain barrier (BBB) opening with focused ultrasound (FUS) reduced plaque. In this Phase-1 trial, we tested the safety of repeated BBB opening with FUS in AD patients.

Materials and Methods: Probable AD patients with mild to moderate dementia symptoms were screened. A high amyloid burden was defined by a standardized uptake value 25% greater than the cerebellum using amyloid positron emission tomography (PET). BBB was opened in five locations in bilateral hippocampi with a high amyloid burden at three time-points two weeks apart. The primary outcome variable was the absence of cognitive decline, hemorrhage, new onset of seizures, or neurological deficits. We also assessed the success of BBB opening (with dynamic contrast imaging) and postoperative PET amyloid levels.

Results: Six patients were screened, four were enrolled, and three treated. No hemorrhage and cerebral edema were observed. BBB opening was focal, immediate, and no contrast enhancement was seen one day postoperative. Seven adverse events were reported, including one serious adverse event (worsening in BEHAVE-AD score from 1 to 3). Two patients reported worsening in cognition at day-1 and five weeks after treatment, respectively. In two patients who completed postoperative PET, the mean amyloid reduced by 21.6% (SE – 1.8) and 40% (SE – 8.6%).

Conclusions: BBB opening with FUS was safe and feasible in AD patients. This strategy needs further testing in a larger cohort as a potential therapeutic for AD.

Acknowledgements: Insightec Inc.

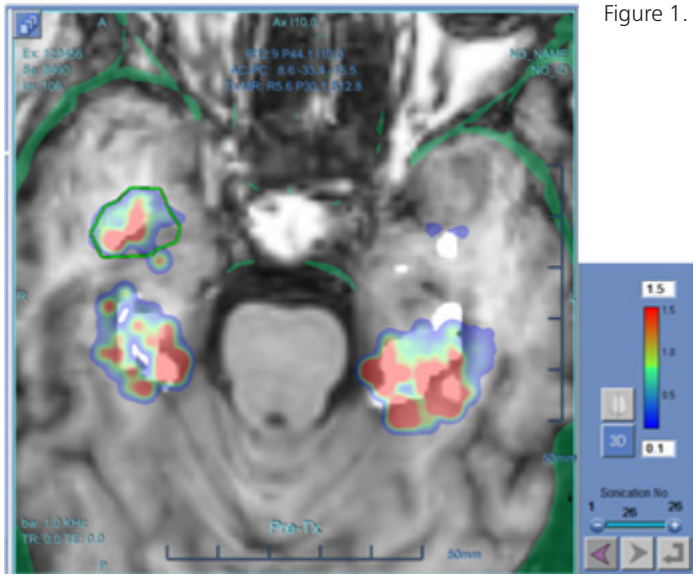

Figure 1.

NDG-6

Topic: Neurodegenerative Disorders
Presentation Type: Oral

Aducanumab delivery by focused ultrasound in APP23 mice

Gerhard Leinenga, Wee Kiat Koh, Juergen Goetz

The University of Queensland, Brisbane, Australia

Background: Immunization strategies targeting amyloid-β (Aβ) in Alzheimer's disease (AD) have generally failed. One exception is Aducanumab for which the slowing of cognitive decline observed in one of two phase III trials was linked to achieving sufficiently high cumulative doses in the brain. A strategy to increase brain levels of vaccines without the need for higher dosing is presented by focused ultrasound in combination with intravenously injected microbubbles that temporarily and safely opens the blood-brain barrier (BBB). We apply focused ultrasound across the brain of a mouse to open the BBB in an approach we named scanning ultrasound (SUS). We have previously shown that repeatedly opening the BBB in mice modelling AD leads to reduction in plaques and improvements in cognitive function. Here, we present a combined approach that increases delivery of aducanumab to the brain which reduced plaques and improved hippocampal-dependent memory function.

Materials and Methods: 13-month old APP23 mice were divided into four groups (sham+vehicle, sham+aducanumab, SUS+vehicle, SUS+aducanumab) in order to achieve matching performance on the active place avoidance test. A dose of 5 mg/kg mouse IgG2a anti-Aβ antibody (aducanumab analog) was injected intravenously concurrent with sham or SUS treatment. SUS was applied with a TIPS System (Philips Research) under anaesthesia after intravenous injection of in-house prepared microbubbles (3x107 microbubbles, average diameter 1.9 μm). 10 ms pulsed sonication at 10 Hz PRF were applied for 6 seconds per spot in a grid pattern of 24 spots at a peak negative pressure of 0.65 MPa. Mice received 4 weekly treatments and were tested again in the APA. Four maintenance treatments were performed over the next 27 weeks and mice were sacrificed at 22 months of age for analysis of amyloid plaque burden.

Results: Combined treatment (SUS+aducanumab) showed improved performance in the APA test as measured by number of shocks and time to enter the shock zone. SUS+vehicle showed a trend towards improved performance. Combined treatment lowered amyloid plaque burden in the cortex as determined by Campbell-Switzer silver staining. Combined treatment, aducanumab alone and SUS alone lowered amyloid plaque burden in the hippocampus. Brain levels of fluorescently-labelled aducanumab, co-administered in the final treatment were increased 5-fold by combining aducanumab with SUS.

Conclusions: Our findings indicate that SUS could have utility in the treatment of AD by increasing the brain uptake of anti-Aβ antibodies. Combining SUS with immunotherapeutic approaches may increase the efficacy of the antibody when compared with the effects of the antibody alone in terms of amyloid clearance and this may lead to beneficial cognitive outcomes.

Acknowledgements: The authors acknowledge funding from the Clem Jones Foundation and the National Health and Medical Council.

NDG-7

Topic: Neurodegenerative Disorders

Presentation Type: Oral

Blood-brain barrier opening of multiple and dispersed brain regions using MR-guided focused ultrasound in Alzheimer's disease

Ying Meng, Maged Goubran, Allison Bethune, Christopher Pople, Jennifer Rabin, Melissa McSweeney, Julie Ottoy, Benjamin Davidson, Clement Hamani, Agessandro Abrahao, Sandra Black, Kullervo Hynynen, Nir Lipsman

Sunnybrook Research Institute, Toronto, ON, Canada

Background: The blood-brain barrier (BBB) restricts the passage of intravascular therapeutics into the brain parenchyma. The BBB also presents a practical challenge in terms of adequate dosing and cost for implementing novel therapeutics effectively in patients with Alzheimer's disease (AD) and other neurological conditions. Microbubble-mediated temporary opening of the BBB using low-intensity MR-guided focused ultrasound (MRgFUS) is a novel approach to targeted drug delivery to the brain. Early phase clinical trials show the MRgFUS procedures in single brain regions, including the eloquent hippocampus, were well-tolerated in patients with AD and not associated with any clinically adverse events. The goal of this study is to establish the safety and feasibility of FUS induced BBB opening in multiple brain regions including the hippocampus, and comprehensive characterization of neuroimaging and biofluid biomarker changes following treatments in patients with AD.

Materials and Methods: We conducted a single-arm, open-labelled study in patients with AD between 50 to 85 years of age and mini-mental status exam (MMSE) 16 or greater (NCT04118764). The study procedures consisted of three MRgFUS procedures every two weeks targeting the bilateral anterior cingulate cortex, bilateral precuneus, and unilateral/bilateral hippocampus. We used the 220 kHz ExAblate Neuro 4000 system type 2.0 (InSightec®, Israel) and ultrasound contrast agent Definity® to conduct BBB opening as described previously. Safety was assessed through clinical examinations and MRI studies. BBB opening was detected with contrast-enhanced T1-weighted MRIs. Cognitive performance was measured using MMSE and Alzheimer's Disease Assessment Scale-Cognitive Subscale (ADAS-Cog). Florbetaben PET imaging, cerebrospinal fluid and blood samples at baseline and one week after the last treatment were also collected for further analysis.

Results: Nine subjects (mean age 70.2+/-7.2 years, five females, four males) were enrolled in the study with mean MMSE of 21.9. The subjects and their primary caregivers provided written informed consent. Overall, 26 MRgFUS procedures were performed with an average sonication volume of 8.4 cm3 covering the bilateral anterior cingulate cortex, bilateral precuneus, as well as unilateral right hippocampus in three subjects and bilateral in six subjects. Spatially-specific and transient BBB opening by focused ultrasound were demonstrated with gadolinium-based contrast leakage in the treatment volumes on MRI. Overall, the procedures were well-tolerated with no grade 3 or worse adverse events by the Common Terminology Criteria for Adverse Events (CTCAE). No worsening of cognitive testing was detected compared to historical data from age and MMSE matched controls.

Conclusions: The current study builds on existing data from two published reports of the clinical safety and technical feasibility of BBB opening of the right frontal lobe and unilateral hippocampus using transcranial MRgFUS in patients with AD. We showed that multiple distributed regions could be accurately targeted and successfully treated in a single sitting with serious adverse events. Further comprehensive characterization of safety and efficacy through advanced neuroimaging and biofluid analysis is ongoing.

Acknowledgements: This study is supported by the Focused Ultrasound Foundation and Weston Brain Institute.

NDG-8

Topic: Neurodegenerative Disorders

Presentation Type: Oral

Young Investigator

Delivery of a selective TrkA agonist to the brain using transcranial focused ultrasound enhances cholinergic function and rescues cognition in a mouse model of Alzheimer's disease

Kristiana Xhima[1], Kelly Markham-Coultes[2], H. Uri Saragovi[3], Kullervo Hynynen[1], Isabelle Aubert[1]

[1]University of Toronto; Sunnybrook Research Institute, Toronto, ON, Canada
[2]Sunnybrook Research Institute, Toronto, ON, Canada
[3]Lady Davis Institute; McGill University, Montreal, QC, Canada

Background: The degeneration of basal forebrain cholinergic neurons (BFCNs) is a cardinal feature of Alzheimer's disease (AD). At present, neuroprotective therapies that delay or halt AD-related neurodegeneration are lacking. Nerve growth factor (NGF) promotes the survival, function and plasticity of BFCNs, yet therapeutic applications of NGF in AD are still limited.

NGF binds to two cell surface receptors, TrkA and p75NTR, that elicit opposing functions–cell survival and cell death, respectively. Pro-degenerative p75NTR is upregulated in AD, thus negating the benefit of TrkA activation by native NGF. We propose that stimulating TrkA (without engaging p75NTR) may address the locus of cholinotrophic deficits in AD, and thereby promote neuronal function and ultimately, cognition. In addition, the poor stability of NGF in the plasma and limited permeability across the blood-brain barrier (BBB) present further challenges for clinical use.

Materials and Methods: We present a therapeutic paradigm to address these translational confines by selectively targeting the TrkA receptor via a small-molecule agonist with favourable pharmacological properties called D3. The in vivo efficacy of D3 and native NGF to engage TrkA-dependent signaling were compared via intracranial injection to the basal forebrain in the TgCRND8 mouse model of amyloidosis, which recapitulates cholinotrophic deficits seen in human AD. To achieve TrkA-related bioeffects using a noninvasive drug delivery platform, systemically administered D3 (16mg/kg) was delivered to the brain using MRI-guided focused ultrasound (MRIgFUS) coupled with intravenously injected Definity microbubbles to transiently and noninvasively induce BBB permeability. MRIgFUS was targeted bilaterally to the basal forebrain using a 1.68 MHz spherically focused transducer with BBB disruption parameters (10 ms bursts, 1 Hz burst repetition frequency, 120 s duration). Control conditions included TgCRND8 and non-transgenic mice treated with MRIgFUS, D3 or vehicle (phosphate-buffered saline; PBS) alone. D3 concentration in the sonicated tissue was quantified by HPLC. Immunohistochemistry and biochemical assays were used to quantify activation of NGF-associated signaling and cholinergic neuronal function. Mice underwent an object recognition task to evaluate recognition memory, Y maze to test for working memory, and Barnes Maze to assess spatial reference memory and cognitive flexibility following treatment.

Results: In the TgCRND8 mouse model of AD, intracranial delivery of D3 induced TrkA-dependent signaling pathways, in contrast to native NGF which was inefficient (Fig. 1). MRIgFUS-induced BBB opening in the basal forebrain was visualized on T1-weighted (T1w) contrast-enhanced MRI (Fig. 2). D3 was detected in sonicated brain regions at 30 min post-MRIgFUS (Fig. 2). Concurrent with D3 delivery by MRIgFUS, FUS-BBB permeabilization alone significantly increased NGF levels in targeted brain areas (Fig. 2). Comparable to levels in non-transgenic controls, intravenous delivery of D3 combined with MRIgFUS in TgCRND8 mice stimulated TrkA-associated signaling cascades (Fig. 3) and enhanced cholinergic function (Fig. 4), in sonicated brain regions where amyloid pathology and neurotrophic imbalances are present. Cognitive function was restored in TgCRND8 mice treated with MRIgFUS-mediated delivery of D3 relative to non-transgenic mice. MRIgFUS alone or D3 alone were not sufficient to rescue cognition.

Conclusions: Our findings demonstrate that the imbalance in TrkA/p75NTR signaling and amyloid pathology can impact NGF bioactivity in vivo, and could, in part, explain the lack of efficacy of NGF therapy in

Figure 1. Intracranial injection of D3, but not native NGF, to the basal forebrain induced TrkA-related signaling, including phosphorylated TrkA (pTrkA), pAkt, pMAPK and pCREB. n=4 per group.

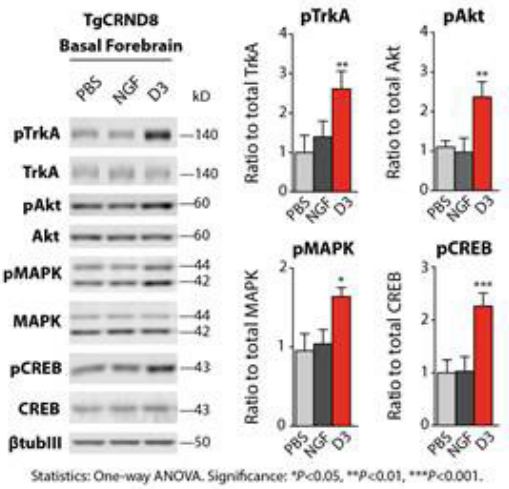

clinical trials for AD. MRIgFUS-mediated delivery of a TrkA agonist enhanced cholinergic function in the presence of amyloid pathology, and improved performance in cholinergic-regulated cognitive tasks. The specific targeting of TrkA, without p75NTR activation, provides a novel therapeutic approach for AD. MRIgFUS BBB permeability itself has been shown to reduce AD-associated pathology and promote neuroplasticity. Therefore, combining TrkA-based therapies with MRIgFUS, represents a promising, multi-target strategy to improve cognitive function in AD.

Acknowledgements: This work was supported by the Canadian Institutes of Health Research (grants to I.A., K.H., and K.X.). Additional funding was received from the FDC Foundation, the WB Family Foundation, Gerald and Carla Connor, the James H. Cummings Foundation, the Westo.

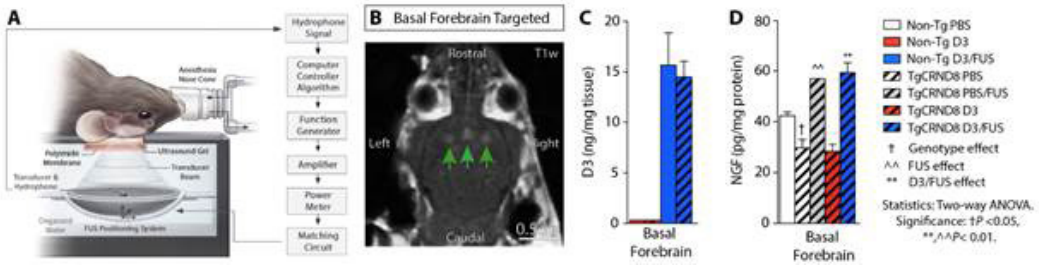

Figure 2. MRIgFUS BBB permeability in the basal forebrain. A) Experimental setup. B) Contrast-enhanced T1w MRI after MRIgFUS. C) D3 and D) endogenous NGF levels were elevated post-MRIgFUS. n=6 per group.

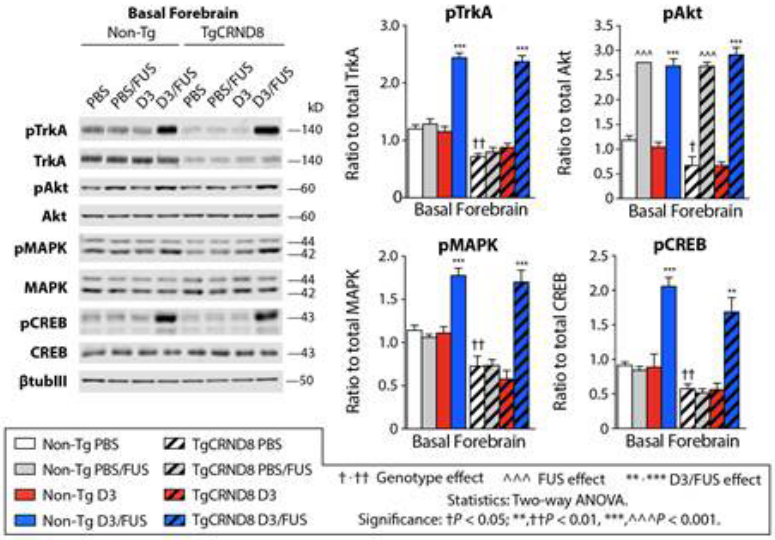

Figure 3. MRIgFUS-mediated delivery of D3 to the basal forebrain in TgCRND8 mice and non-transgenic littermates induced TrkA-associated signaling, including pTrkA, pAkt, pMAPK and pCREB. n=6 per group.

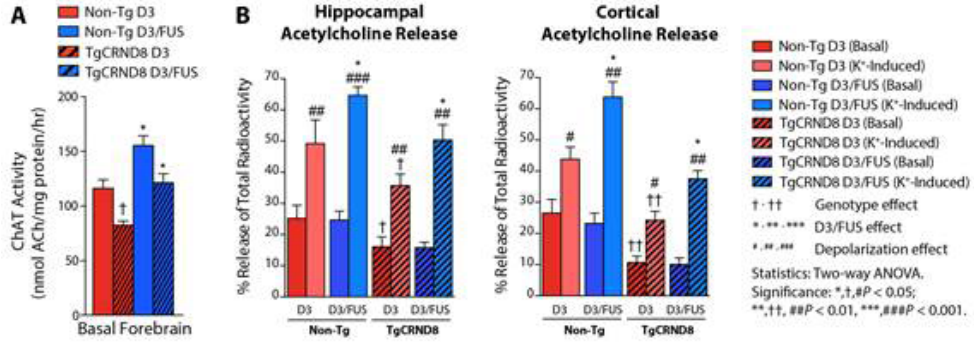

Figure 4. MRIgFUS delivery of D3 enhanced cholinergic function. D3/FUS increased A) ChAT activity, and B) depolarization-evoked release of acetylcholine–key indicators of cholinergic tone. n=5 per group.

NMD-1

Topic: Neuromodulation
Presentation Type: Oral

Sustained, reversible and specific manipulations of oculomotor performance in non-human primates by neuronavigated transcranial ultrasound stimulation with return to baseline

David Attali[1], Pierre Pouget[2], Stephen Frey[3], Harry Ahnine[2], Julien Claron[1], Charlotte Constans[1], Jean-François Aubry[1], Fabrice Arcizet[4]

[1]Physics for Medicine Paris, INSERM, ESPCI Paris, CNRS, PSL Research Univ., Université de Paris, Paris, France
[2]Institute of Brain and Spinal Cord, INSERM, CNRS, UPMC, Paris, France
[3]Rogue Research Inc., Montreal, QC, Canada
[4]Institut de la Vision, CNRS, INSERM, Université de Paris, Paris, France

Background: Transcranial Ultrasound Stimulation (TUS) is an innovative neuromodulation technique allowing non-invasive, targeted and precise stimulation of deep brain areas. TUS brings a lot of promise in the world of neuroscience as well as in neurology and psychiatry, where many disorders suffer from the lack of effective treatments. One of the main advantages of neuromodulation techniques are their reversibility, even if repetitive approaches may be used to obtain long-lasting effects. This is the case with Transcranial Magnetic Stimulation (TMS) and Transcranial Direct-Current Stimulation (tDCS), two non-invasive neuromodulation techniques currently used in psychiatry and neurology. The objective of this study was to assess the sustainability and reversibility of low-intensity focused ultrasound neuromodulation.

Materials and Methods: We applied 20 s trains of neuronavigated TUS in three non-human primates performing an antisaccade task. Two regions-of-interest (ROI) as well as control regions were targeted. The ROIs were the frontal eye fields (FEF) and the supplementary eye fields (SEF), two sophisticated cortical brain areas that play important roles in the control of visual attention and eye movements in primates. We used a single element focused ultrasound transducer operated at a 320kHz frequency with a pulse duration of 30 ms, a pulse repetition frequency of 10 Hz and a total sonication time of 20 s per session. The pressure amplitude was set to 0.76 MPa in water. Animals performed a total of 40 sessions (10 TUS vs 10 sham sessions, in ROIs vs control regions). Each session contained one practice block followed by 7 blocks of 100 antisaccades. Normalized saccade latencies were analyzed for each animal.

Results: We found that TUS trials induced shorter latencies in all 3 animals compared to sham trials ($p<0.001$ for monkey G and monkey S, and $p=0.0064$ for monkey L). This effect was sustained up to 20 min after TUS, and reversible, with behavioral performances returning to baseline after 20 min. In monkey G and monkey L, TUS induced a modulation of behavior when the ultrasound beam was directed to the ROIs only. The third animal (monkey S) performed significantly more anticipated saccades, suggesting the use of an adaptative strategy partially compromising the understanding of its performances.

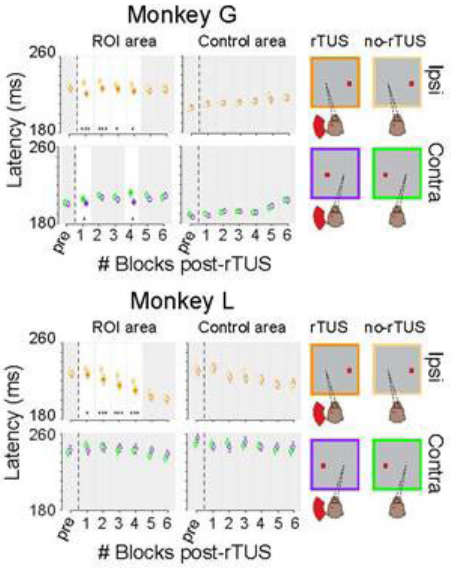

Figure 1. Time course of TUS effect on mean latencies (averaged over all successful trials in each block). Dashed black lines schematize rTUS. Significant differences: * for $p<0.05$ and *** for $p<0.001$.

Conclusions: This study reinforces the feasibility of using neuronavigated TUS as an innovative neuromodulation technique, able to modulate behaviors for a sustained period of several minutes (~20) in the awake non-human primate. For the first time, we have highlighted the return to baseline of these behavioral modifications. Altogether, our results support the use of this approach for exploratory and therapeutic purposes non-invasively and with unprecedented spatial resolution.

Acknowledgements: This work was supported by the Bettencourt Schueller Foundation, Paris, France (UltraBrain project), the 'Agence Nationale de la Recherche' under the program 'Future Investments' with the reference ANR-10-EQPX-15, IHU FOReSIGHT [ANR-18-IAHU-0001].

NMD-2

Topic: Neuromodulation
Presentation Type: Oral

FUS-mediated functional modulation of cortical and thalamic motor areas in awake sheep

Hyun-Chul Kim, Wonhye Lee, Ji Eun Lee, Jennifer Kunes, Kyungho Yoon, Lori Foley, Seung-Schik Yoo

Brigham and Women's Hospital, Boston, MA, USA

Background: Pulsed application of low-intensity transcranial focused ultrasound (FUS) has shown to temporarily modulate regional-specific brain functions in anesthetized sheep. Further investigation is warranted to evaluate the effects of FUS in the absence of anesthesia as the anesthesia confounds the state of brain function. The aim of this study is to establish an experimental setup and a protocol for applying FUS to non-anesthetized sheep and to examine transient modification of the excitability of cortical and thalamic motor areas induced by the sonication.

Materials and Methods: A non-metallic FUS headgear was designed and worn by sheep (n = 6) with respect to tattooed markings on the scalp for magnetic resonance imaging (MRI)-guided navigation. Tattooed skin marking served as reference points for reproducible placement of the headgear. Anatomical and functional head MRI images were obtained from sheep wearing the headgear and were later used for navigation. The targets were the left primary motor (M1) area and its thalamic projection associated with passive actuation of the right hind limb muscles. In a separate session that does not involve any animal, the FUS headgear was placed on a head phantom, and the transducer was aimed at the targets under the image-guidance.

The headgear was applied to sheep right before FUS experiment, and the effects of excitatory/suppressive FUS (250 kHz) on modulating the activity of the target brain areas were evaluated across three conditions: on-target, off-target, and no-FUS. For excitation, 200 ms-long sonication was delivered using tone burst duration of 0.5 ms and 70% duty cycle. For suppression, 1 min-long sonication was delivered at tone burst duration of 0.5 ms at 5% duty cycle. In the off-target condition, sonication was delivered to the non-motor area away from the targets. Electromyography (EMG) was wirelessly collected from both hind limbs while the animal was standing still (in excitatory sonication) or walking on a treadmill (in suppressive sonication).

Results: There were no visible changes in the movement of the hind limbs associated with sonication. In the excitatory stimulation to the M1 and thalamus, the amplitudes of the EMG signals from the right hind limb contralateral to FUS sonication were significantly increased (one-tailed paired t-test, $p < 0.001$) in comparison to those from the left hind limb. There were no statistical differences in the EMG amplitudes between the hind limbs in either the off-target or the no-FUS conditions (Fig. 1). The suppressive stimulation to the M1 (one-way repeated measures analysis of variance; main effect of time, $F(9,45) = 3.51$, $p = 0.002$) and the thalamus (main effect of time, $F(9,45) = 3.40$, $p = 0.003$) yielded significant reduction in the normalized EMG amplitudes. In contrast, none of the off-target and no-FUS conditions showed statistical differences in EMG amplitude between hind limbs (Fig. 2). Behavior monitoring and histological analysis following the sonication did not reveal any abnormalities.

Conclusions: To our knowledge, this is the first study to demonstrate FUS-mediated neuromodulatory effects in an awake large animal model, yielding selective excitation or suppression of the region-specific brain functions. The multiple sonication sessions did not damage the sonicated brain areas based on histological analysis. The results may provide translational information for various clinical applications to humans.

Acknowledgements: This work was supported by National Institutes of Health (NIH Grant R01 MH111763, https://www.nih.gov/). The funders had no role in study design, data collection and analysis, decision to publish or preparation of the manuscript.

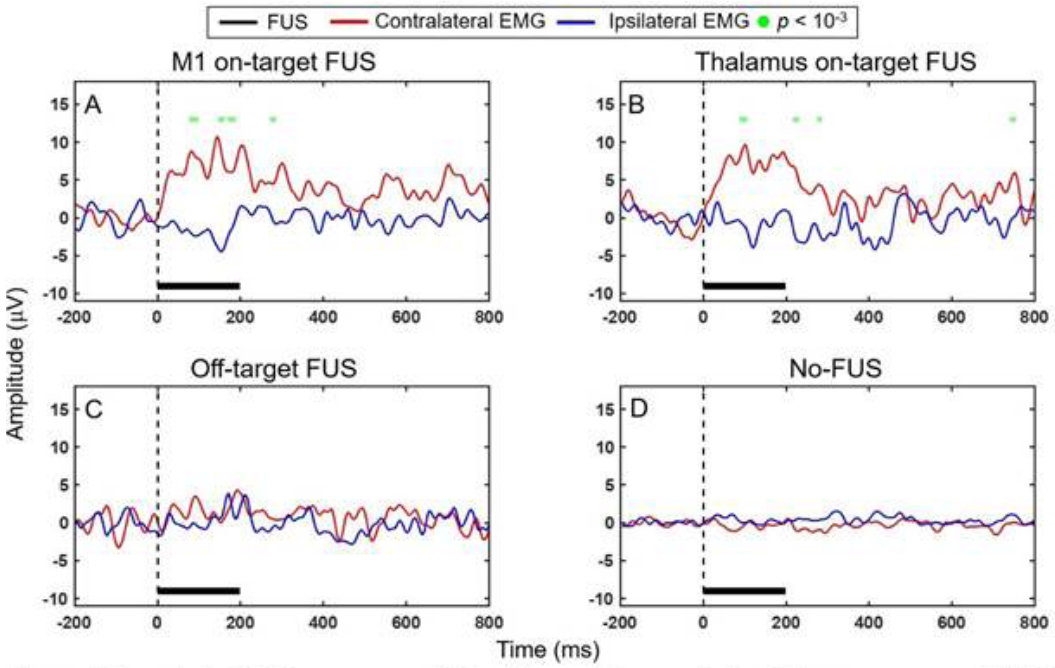

Figure 1. Time-locked EMG measurement from the excitatory sonication.

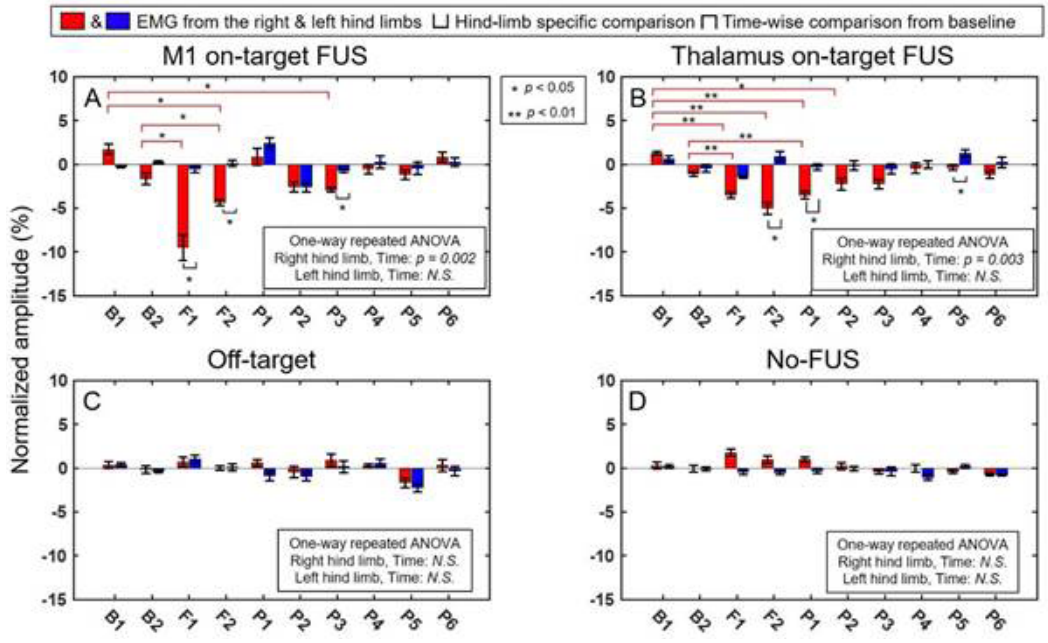

Figure 2. EMG signals acquired during treadmill walking (suppressive sonication).

NMD-3

Topic: Neuromodulation
Presentation Type: Oral

Low intensity focused ultrasound: A possible non-invasive cognitive neural prosthetic

Taylor Kuhn, Norman M Spivak, Bianc Huan Dang, Sergio Becerra, Maya McNealis, Ben Rosenberg, Sonja Hiller, Andrew Swenson, Luka Cvijanovic, Michael Sun, David Kronemyer, Rustin Berlow, Michelle Craske, Nanthia Suthana, Martin Monti, Susan Bookheimer

University of California, Los Angeles, Los Angeles, CA, USA

Background: Both noninvasive and invasive neuromodulation tools have been shown to alter brain function and increase neural activity. There is strong evidence that low intensity transcranial focused ultrasound (tFUS) directly increases neural activity: early histology and animal studies of tFUS have demonstrated its ability to produce reversible physiologic effects on neuron clusters. Further, in studies using fMRI of macaques, tFUS modulated activation in the blood oxygenation level-dependent (BOLD) signal in regional brain targets (e.g. amygdala). Recent fMRI studies in humans demonstrated the ability of tFUS to focally increase BOLD activity in primary somatosensory, primary visual, and thalamus. Importantly, the study involving tFUS stimulation of V1 reported tFUS-evoked increased BOLD fMRI signal in both V1 and functionally associated networks. More work on the safety and clinical utility of tFUS remains before tFUS can be established as a translational clinical tool.

Materials and Methods: We performed a randomized, double blind within-subject crossover study targeting the entorhinal cortex (ErC) with tFUS in six (age(SD) = 61.8(8.25); 50% female) healthy aging adults. tFUS was administered to ErC or amygdala (AG), which served as a control target, exactly 2 weeks apart using BX Pulsar 1002 (BrainSonix Corp, Sherman Oaks, CA) with parameters: 650 kHz, 720 mW/cm2 ISPTA.3, 5% DC, with PRF of 10 Hz for AG and 100 Hz for ErC. The transducer was a circular, single-element, spherically focused transducer, with active aperture 61 mm, 65 mm nominal focal length, hydrophone-measured -6dB focal width of 4 mm in water and -6dB depth range of 50.4-80.5 mm. Prior to and immediately following tFUS, participants underwent neuropsychological assessment of verbal and nonverbal learning and memory as well as MRI assessment of perfusion (Artieral Spin Labelling, ASL) and resting-state functional connectivity. tFUS was conducted in the MR scanner and BOLD data was simultaneously collected during the tFUS administration. Different versions of the tasks, randomized and counterbalanced across participants, were administered at each session. Repeated Measures Analyses of Variance (ANOVA) assessed the impact of ErC and AG tFUS on learning, memory, regional perfusion and functional connectivity. A psychophysiological interaction (PPI) analysis was conducted on the tFUS-simultaneous BOLD data to assess for changes in functional connectivity in line with the on-off sonication paradigm.

Results: ASL MRI revealed tFUS selectively increased blood perfusion in the targeted ERc, cingulate and medial prefrontal regions and not in the control region. Increased regional perfusion was seen at the single-subject and group level. Further, PPI confirmed tFUS focally increased BOLD activity in the targeted ERc and functionally connected regions including bilateral hippocampus, cingulate and anterior thalamic nucleus. Using the amygdala as a control target, we confirmed that these findings were selective to the brain region targeted using tFUS. When targeting the amygdala, increased perfusion was seen in the amygdala and not the ERc. Similarly, when targeting the amygdala, functional connectivity changes were seen in the amygdala, ventral prefrontal and brainstem and not in the ERc or its functional network. Neuropsychological results did not evidence changes (improvement or worsening) in verbal or nonverbal learning or memory following tFUS of either region.

Conclusions: We found a double dissociation between perfusion and connectivity results specific to the region targeted with tFUS which provides early confirmation that affecting local neural activity with ultrasound impacts functionally connected circuits. We have since begun tFUS sonication of ERc in patients with amnestic mild cognitive impairment to determine if tFUS can similarly affect perfusion, connectivity and memory in a neurodegenerative group. Overall, these preliminary results suggest that tFUS: appears safe in humans; targeting is very accurate; can selectively increase regional blood flow in the targeted brain region; can selectively affect functional connectivity of the targeted brain region and its functional network.

Acknowledgements: Center for Cognitive Neuroscience Pilot Fund, University of California, Los Angeles

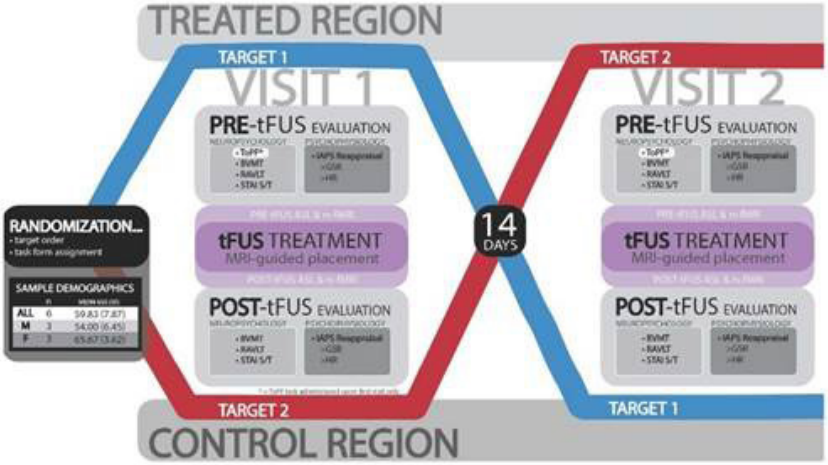

Figure 1.

Figure 2.

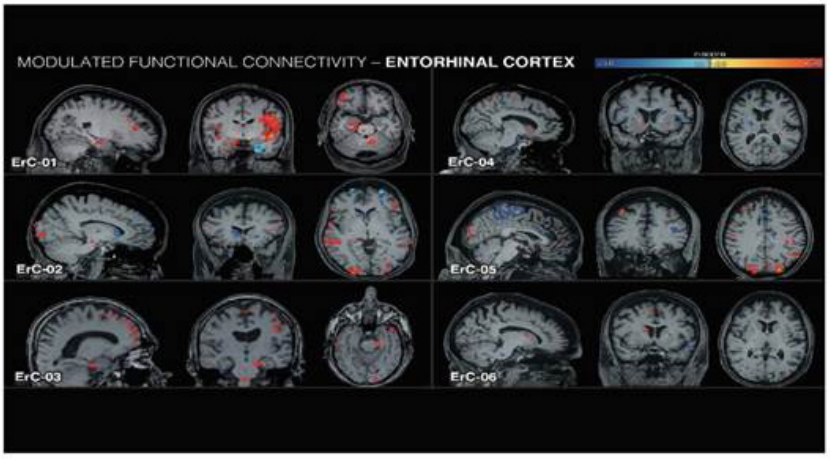

Figure 3.

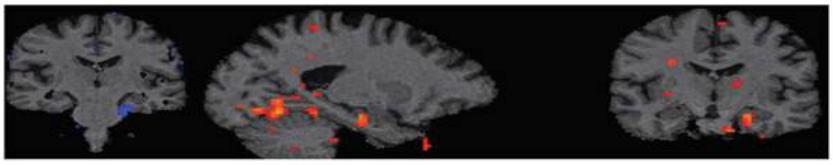

Figure 4.

NMD-4

Topic: Neuromodulation
Presentation Type: Oral

Thalamic low intensity focused ultrasound in acute and chronic disorders of consciousness

Joshua Cain[1], Norman M Spivak[1], Paul Vespa[1], Caroline Schnakers[2], Martin Monti[1]

[1]University of California, Los Angeles, Los Angeles, CA, USA
[2]Casa Colina Hospital and Centers for Healthcare, Pomona, United States Minor Outlying Islands

Background: The processes by which a state of consciousness is regained, after it is lost, remains to be fully understood. In the context of severe brain injury, many patients lose consciousness acutely, entering a state of coma. While many of these patients fully recover consciousness spontaneously in a short period of time, a fraction of patients enter – either temporarily or permanently– a disorder of consciousness (DOC), such as a vegetative state (VS) or a minimally conscious state (MCS). Despite an increasing understanding of the cortico-thalamo-cortical neural circuits that are involved in long-term impairment of consciousness, few therapeutic options effectively leverage this understanding to bring about recovery. Here we present the initial results from a first-in-man clinical trial piloting the use of non-invasive low intensity focused ultrasound pulsation (LIFUP) to target deep nuclei of the brain (i.e., thalamus) in patients with a DOC.

Materials and Methods: Acute patients were recruited shortly after severe brain injury, upon establishing a VS or MCS diagnosis, in the absence of sedatives, approximately 2 weeks post-injury. Chronic patients were recruited, as per international guidelines, starting 3 months post injury, for non-traumatic etiologies, and 12 months post injury, for traumatic etiologies. Each patient was scheduled to undergo two 5-min sessions of MR-guided LIFUP exposures (single element, air-backed, nominal aperture diameter 71.5 mm, fundamental freq = 650 kHz, PRF = 100 Hz, PW = 0.5 ms, Ispta.3 = 720 mW/cm2), one week apart. The 5-min exposure was delivered in 30s blocks, separated by 30s intervals. Safety of the procedure was assessed with contemporaneous vital signs monitoring (i.e., oxygen sat, heart rate, blood pressure) and number of (S)AE—(significant) adverse events—occurring throughout the protocol. Behavioral changes in the patients were assessed with the Coma Recovery Scale-Revised (CRS-R) protocol at 12 time points, before/after exposure.

Results: At present, 13 acute and 9 chronic DOC patients were enrolled in the trial. With respect to safety, no alteration of vital parameters was detected by the clinical staff during LIFUP exposure. No SAEs were reported. Five AEs were reported, 4 in acute patients, 1 in chronic patients. Clinical review of the AEs suggested that none was related to the LIFUP exposure itself. With respect to behavioral change, as a group, acute patients show an increase of 2.4 CRS-R points after the first LIFUP exposure. Chronic patients, who are typically stable, also exhibited increased responsiveness. Importantly, while, on average they demonstrated ~2.5 points increase in CRS-R, a convenience matched comparison cohort of patients who also underwent multiple behavioral testing, without undergoing LIFUP, exhibited no change over a similar week-long assessment.

Conclusions: Overall, this first-in-man study presents preliminary data suggesting that (1) LIFUP exposure at our parameter settings is safe in clinical populations, and (2) this technique may provide an effective treatment for DOC patients, which warrants further investigation with comparative (e.g., sham) cohorts. These results open up a novel, widely applicable, non-invasive, and inexpensive alternative to surgical interventions for direct modulation of deep structures in disorders of consciousness and, potentially, other neurological and mental health conditions.

Acknowledgements: Dana Foundation, Tiny Blue Dot Foundation

NMD-5

Topic: Neuromodulation
Presentation Type: Oral

FUS-induced calcium fluxes in an in-vitro human neural cell model

William Apoutou N'Djin[1], Ivan M. SUAREZ CASTELLANOS[1], Magali Perier[1], Alexandre Carpentier[2]

[1]INSERM, Lyon, France
[2]Pitie Salpetriere Hospital, Paris, France

Background: Focused Ultrasound (FUS) could offer promising alternatives to standard neurostimulation strategies. However, new research models and platforms are still needed to enhance the understanding of FUS neurostimulation phenomena and better control the resulting biological effects on neural structures. The study of Ca2+ dynamics modulated by FUS is essential for describing intercellular signaling and signal transmission across neuronal networks. Here, the feasibility of triggering Ca2+ fluxes by FUS has been studied in vitro at the cell scale on a mixed FUS/fluorescence microscopy platform.

Materials and Methods: The neural cell culture model was obtained after differentiation of Human neural progenitors (ReNcell-VM), labelled with a Ca2+ -sensitive fluorescent dye (Fluo-4). The stimulation platform was built on an inverted microscope that included micromanipulators for positioning FUS sources (Figure 1). FUS sources consisted in a custom-made planar transducer (ø: 10-mm, f = 2.2 MHz) prolonged by an acoustic coupling cone transmitting the ultrasound wave toward the neural cells. Millisecond scale FUS pulses were applied (pressures: 100's of kPa). The neural electrophysiological activities were recorded using fluorescence (Ca2+) imaging (camera: ORCA-Fusion, Hamamatsu; sCMOS 0.7e rms). In this study, fluorescence recordings were captured at 10 fps during ~90s and on an image FOV of ~ 1000 µm x 500 µm (2304 pixels x 1152 pixels). FUS-induced Ca2+ dynamics were compared to those obtained by chemical stimulation (KCl), which could be administrated by perfusion in the petri dish.

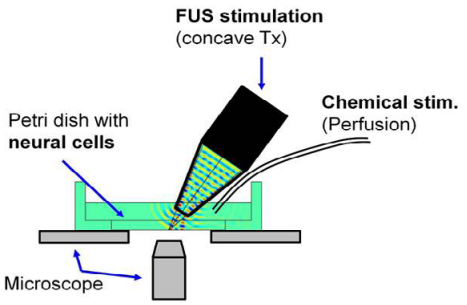

Figure 1: Mixed FUS stimulation / Fluorescence microscopy set-up. FUS stimulation could be directly compared to chemical stimulation (KCl perfusion).

Results: Ca2+ fluxes were successfully induced by FUS in human neural cells. Following FUS, significant Ca2+ signal variations were detectable in several cell clusters simultaneously while observed Ca2+ fluxes propagated in few seconds along axons and across cellular networks (Figure 2). Strong and sustained elevations in florescence intensity were observed immediately after the FUS pulse (~ 1-2s) in several regions spread within the image FOV. In other regions, florescence elevations could start with various delays (t = 2-80s), depending on the locations of the cell clusters in the neural network. After reaching a peak, the fluorescence intensity appeared to begin a progressive return to baseline, also depending on the location of the cells in the petri dish. Overall, the propagation velocity of intercellular Ca2+ fluxes ranged ~10-30 µm/s. Preliminary comparisons showed that Ca2+ fluxes induced by FUS stimulations exhibited similar dynamics to those observed following KCl stimulation.

Conclusions: These results underlined that FUS-stimulated Ca2+ fluxes are transient in nature and are capable of transmitting these responses across several interconnected neurons. Overall, the complex data accessed using this mixed platform should be of critical interest to improve the current knowledge and control on FUS neurostimulation phenomena. Especially, it will allow investigating the effect of various FUS parameters at the neural cell scale and 2D neural network scale, with an eye to consolidate the transfer of FUS techniques for future applications in deep brain neurostimulation.

Acknowledgements: Project support: French Research Agency (ANR-16-TERC-0017), FUS Foundation (Centers of Excellence).

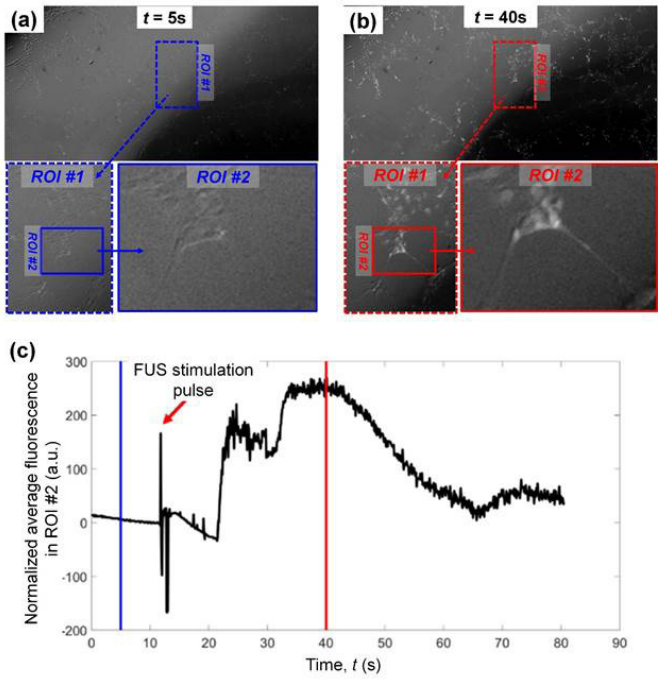

Figure 2: FUS-induced Ca2+ waves in in-vitro Human neural cells. Fluorescence microscopy imaging: (a) before FUS; (b) after FUS. (c) Fluorescence variation (ROI#2) in neural cell bodies.

NMD-6

Topic: Neuromodulation
Presentation Type: Oral

TPS: Shockwave pulses stimulate the brain

Pavel Novak

Storz Medical AG, Tägerwilen, Switzerland

Background: Shockwaves are used in medicine since 1980. First application was for extracorporeal kidney stone disintegration. Meanwhile, low intensity shock waves proofed to be efficient for the treatment of non-unions, tendon and muscular pain, wound healing, heart insufficiency, erectile dysfunction, aesthetics and finally also neurological indications. The working principle is the mechanical stimulation of biological processes called mechanotransduction resulting in increased cell metabolism, release of nitric oxide (eNO) and of numerous growth factors like VEGF, BMP, TGF-β, GABA, BDNF and GDNF. There is also an anti-inflammatory effect, stimulation of stem cells and of the innate immune system.

Materials and Methods: Transcranial Pulse Stimulation (TPS), former under the term TESWT (Transcranial Extracorporeal Shockwave Therapy) uses shockwave pulses for mechanical stimulation of the brain tissue. Compared to focused ultrasound, the applied pulses are shorter (typically 1μs) and have a significantly higher amplitude (up to 150MPa) without any heating effect. Due to the application thru the scull, the intensity is significantly reduced: pressure amplitude down to 35% and energy intensity accordingly to approximately 15%. In order to achieve optimal treatment results, a 3D Infrared navigation system is used. It allow the user to distribute the energy according to the treatment requirements and simultaneously document the treatment process.

35 patients with mild or moderate Alzheimer's disease have been treated in two centers. The treatment was performed with the Neurolith (Storz Medical AG, CE marked) and consisted of 6 approximately 30 minutes sessions within two weeks. Each session à 6000 pulses with 0.2mJ/mm2 at 5Hz. The energy was delivered homogenously over the frontal and parietal lobe as well over precunius for optimal results.

Results: CERAD Plus battery of tests disclosed a statistically significant improvement of the CERAD score of more than 10%. Also long term (2-3 years) evaluation of smaller group of patients shows positive outcome compared to the natural development of the disease using conservative treatment only. The TPS treatment is safe and effective. There are no negative side effect. Placebo controlled, randomized trials are ongoing.

Conclusions: Alzheimer's disease or dementia in general is multi modal disease resulting from different causes like deposition of dedicated proteins (tau, beta-amyloid), inflammation, reduced blood supply and others. The broad scope of shockwave biological effects in soft tissue seems to address very efficiently all known origins of the Alzheimer's disease. Compared to it, pharmaceutical solutions usually treat only one disorder.

Preliminary results show positive treatment outcome also for other neurological indications, like Parkinson.

Acknowledgements: Storz Medical AG employee

NMD-7

Topic: Neuromodulation
Presentation Type: Oral

Young Investigator

Non-invasive receptor-specific millimeter-precision manipulation of brain circuits by ultrasound-mediated aggregation and uncaging of drug carriers: In-vivo results

Mehmet Ozdas[1], Aagam S. Shah[1], Paul M. Johnson[1], Nisheet Patel[1], Markus Marks[1], Tansel Baran Yasar[1], Urs Stalder[2], Laurent Bigler[2], Wolfger von der Behrens[1], Shashank Sirsi[3], Mehmet Fatih Yanik[1]

[1]ETH Zurich, Zurich, Switzerland
[2]University of Zurich, Zurich, Switzerland
[3]UT Dallas, Richardson, TX, USA

Background: Targeted non-invasive, receptor-specific modulation of brain circuits can lead to breakthroughs in the treatment of brain disorders. To address this, we systemically deliver engineered ultrasound-sensitive drug carriers. We then apply a two-component Aggregation and Uncaging focused ultrasound sequence (AU-FUS) to a brain region. The first sequence concentrates the drug carriers with millimeter precision, then second sequence uncages the carrier's cargo focally to achieve high target specificity and low off-target effects without opening BBB. Upon release from the carriers, the drug locally crosses the intact BBB. We show circuit-specific manipulation of sensory signaling in motor cortex in rats by locally concentrating and releasing a GABAA receptor agonist (muscimol) from ultrasound-sensitive carriers. Our focal-concentration approach requires use of orders of magnitude less drug, which significantly reduces off-target effects as we show by recordings from neighboring brain areas.

Materials and Methods: Female Long Evans (200-300 g, n=43 for all experiments) were anesthetized under isoflurane (1.5-2%). A Neuronexus probe (A2x16-10mm) was inserted in the vibrissae motor cortex (vM1) for electrophysiological recordings. A custom 2.5 MHz FUS transducer (Sonic Concepts) was positioned on the skull such that it targets vibrissae sensory cortex (vS1) with the aid of an ultrasound collimator and sterile gel (Fig. 1). vS1 and vM1 are functionally connected however anatomically distant regions from each other. This electrode configuration was used to avoid confounding effects due to possible mechanical FUS effect on the electrodes and the BBB disruption upon electrode insertion itself. Custom liposomes are loaded with muscimol and conjugated with microbubbles then injected through tail-vein (0.2mL/min,6e8/mL concentration for 20-25 mins). 30s following injection start AU-FUS sequence was repeatedly applied until 2-3 mins after injection end. BBB integrity was verified with Evans Blue, gadolinium and PCD. For evoked local field potential (eLFP) analysis, the raw data was low pass filtered (3rd order Butterworth filter) at 300 Hz. The eLFPs were aligned to the whisker stimulus averaged over 2 mins and then normalized to the average response amplitude of the baseline All data shown is mean ± s.e.m. Extracellular spike detection and sorting was done with Klustakwik. All electrophysiological data analysis was done in custom Python scripts.

Results: We show that evoked extra-cellular multi-unit activity and eLFPs in vM1 can reversibly be inhibited (Fig.1b), and our control experiments shows that inhibition in vM1 occurs only when muscimol loaded particles are sonicated with AU-FUS in vS1 (Fig.1c-d). An equivalent inhibition in vM1 with AU-FUS and ultrasound controlled drug carriers can be achieved with orders of magnitude less drug than systemic muscimol injection (Fig. 2). We show that the drug delivery is limited to a small brain region by recording visually evoked activity from a neighboring circuitry (visual cortex) which is not involved in whisker evoked sensory information flow (Fig. 1e-f). Our PCD, Evans Blue and MRI contrast agent experiments show that the drug delivery is done without disruption of the BBB (Fig. 3).

Conclusions: We developed a reliable and safe method for targeted, non-invasive, receptor specific neuromodulation of brain circuits. Our in-vivo results prove that drugs can be delivered to targeted brain regions with high resolution without BBB opening. Our next plan is to deliver FDA approved neuromodulators to specific brain regions to alter the phenotype of animal models of neuro-psychiatric disorders.

Acknowledgements: This project was funded by Swiss Federal Institute of Technology (ETH) Zurich and the European Research Council (ERC) under the European Union's Horizon 2020 research and innovation program (grant agreement No 818179).

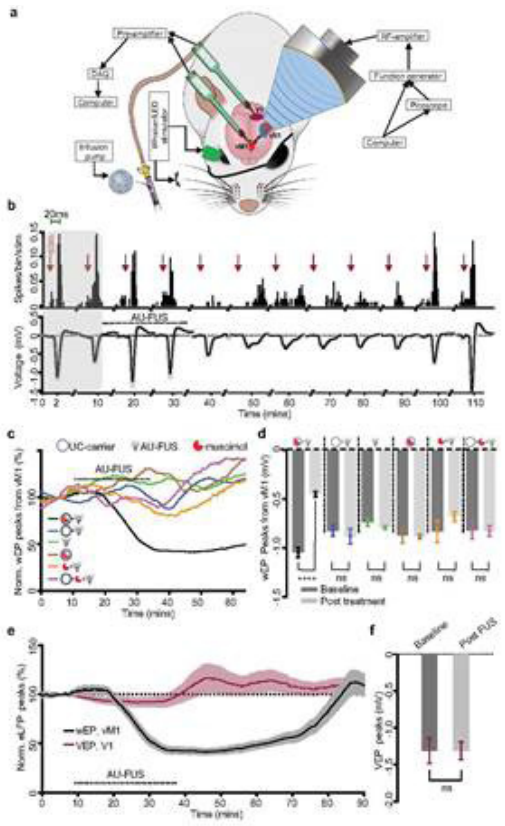

Figure 1.

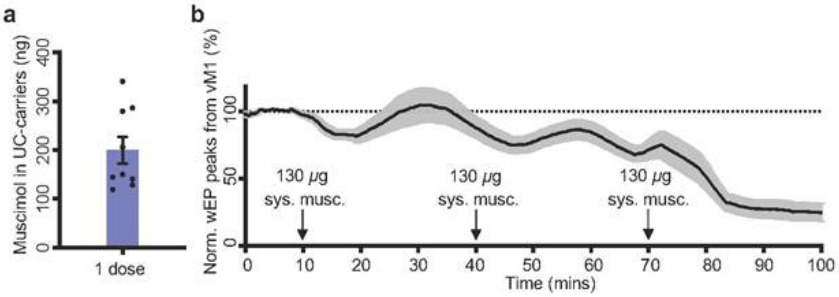

Figure 2.

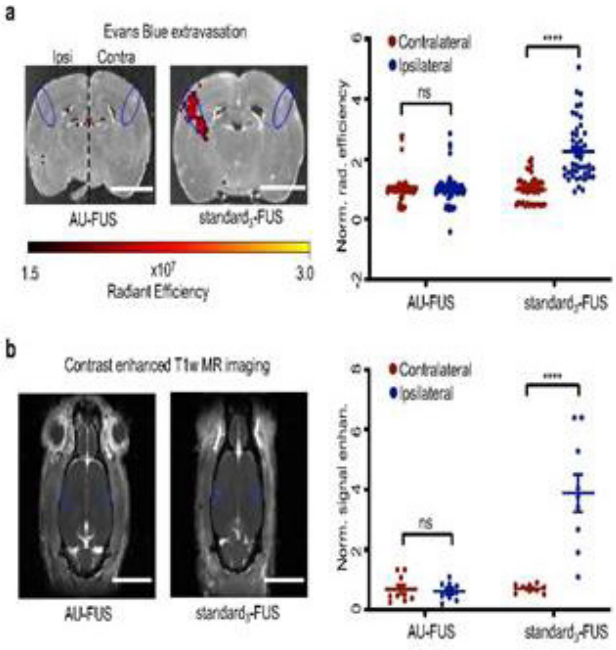

Figure 3.

NMD-8

Topic: Neuromodulation
Presentation Type: Oral

Modulating deep brain circuits with low-intensity focused ultrasound

Lennart Verhagen[1], Davide Folloni[2], Nima Khalighinejad[2], Alessandro Bongioanni[2], Jean-Francois Aubry[3], Jerome Sallet[2], Matthew Rushworth[2]

[1]Radboud University, Nijmegen, Netherlands
[2]University of Oxford, Oxford, United Kingdom
[3]CNRS, Paris, France

Background: To understand brain circuits we need to more than measurement; we need to probe and modulate neural activity. This system-level approach is especially critical in a clinical context. Current interference techniques are either highly invasive, or restricted to the surface of the brain. Focused transcranial ultrasound has the potential to overcome these limitations. I will discuss how we can use low-intensity ultrasound to safely stimulate deep brain structures, such as the amygdala, with high precision. Conventional ultrasound neuromodulation protocols have short-lived effects, limiting its relevance to the clinic.

Materials and Methods: Here we pioneer a novel repetitive ultrasound protocol in non-human primates. We repeat 30ms pulses at 10Hz for up to 40 seconds, intended to induce longer-lasting plastic changes. Whole-brain fMRI allows us to track how ultrasound impacts neural activation across the brain. Behavioural measurements reveal the specific consequences of a focal neural perturbation on cognitive computations.

Results: In a series of experiments we show how the neuromodulatory effects of repetitive ultrasound can last for more than one hour. Analysis of resting-state fMRI reveal modulation of both local and remote circuits. While the focus of ultrasonic intervention might be targeted at a single brain area, the functional impact should be viewed at the circuit level, extending beyond the sonicated region. Likewise, the impact of ultrasound neuromodulation on behaviour reveals a similar juxtaposition of high specificity and functional extension.

Conclusions: At low-intensities focused ultrasound can be used to modulate deep brain circuits in non-human primates with unparalleled precision, with long-lasting effects on neural activity and behaviour.

Acknowledgements: Wellcome Trust

PAC-1

Topic: Pancreatic Cancer
Presentation Type: Oral

Planning and delivery of ultrasound-mediated hyperthermia for clinical targeted drug delivery

Michael Gray[1], Laura Spiers[1], Paul Lyon[2], Constantin Coussios[1]

[1]University of Oxford, Oxford, United Kingdom
[2]Churchill Hospital, Oxford, United Kingdom

Background: Focused ultrasound mediated hyperthermia has been used as a noninvasive method of clinical targeted therapy, particularly for ablative applications and more recently for targeted drug delivery through thermally triggered release from liposomal carriers. In cases where only mild hyperthermia (temperature elevation <6°C) is required, patient-specific treatment planning models are being clinically evaluated as a means to administer therapies without the requirement for real time thermometry. In this talk, we present results from a phase 1 trial for treatment of tumours in the liver and preview an upcoming trial for treatment of pancreatic adenocarcinoma (PDAC) tumours.

Materials and Methods: The TarDox study was a phase 1 clinical trial whose aims were to determine the feasibility, safety, and potential efficacy of targeted drug release from thermosensitive liposomal doxorubicin (ThermoDox) using mild hyperthermia generated by ultrasound guided focused ultrasound (USgFUS). Patient-specific acoustic and thermal models were used to prescribe ultrasonic and volumetric parameters and to predict the resulting tissue temperature elevations. In this ten patient study, six treatments were performed using an implanted sensor to confirm target temperatures, and four treatments were performed without thermometry. Drug delivery was quantified by biopsy before and after FUS.

PanDox is a phase 1 trial applying the principles of TarDox to the treatment of PDAC tumours. Refinements to the treatment planning process include the measurement of pancreatic tissue properties and the inclusion of organ motion in the treatment simulation model.

Results: In the TarDox study, intratumoral biopsy doxorubicin concentrations increased by an average of 3.7x (1.3 – 9.3 range) after FUS-induced mild hyperthermia. The trial goal of 2x enhancement was exceeded in 7 of 10 cases, including 3 of 4 performed without real-time thermometry. No evidence of FUS-related adverse effects was observed during or after treatment.

In support of PanDox, measurements of sound speed and attenuation were made on ex vivo human samples of normal and PDAC tissues. Simulations of the effect of organ motion during FUS-mediated hyperthermia show the value of motion mitigation schemes such as high frequency jet ventilation.

Conclusions: In the TarDox study, it was feasible and safe to use models to plan and deliver mild hyperthermia USgFUS treatments for drug release within oncologically relevant volumes, both with and without real-time thermometry. The methods developed for TarDox may enable hyperthermia across a range of indications including targeted chemotherapy.

Acknowledgements: This research was supported by Supported by the Oxford Biomedical Research Centre, National Institute for Health Research, the Oxford Centre for Drug Delivery Devices (programme grant EP/ L024012/1), and the Engineering and Physical Sciences Research Coun.

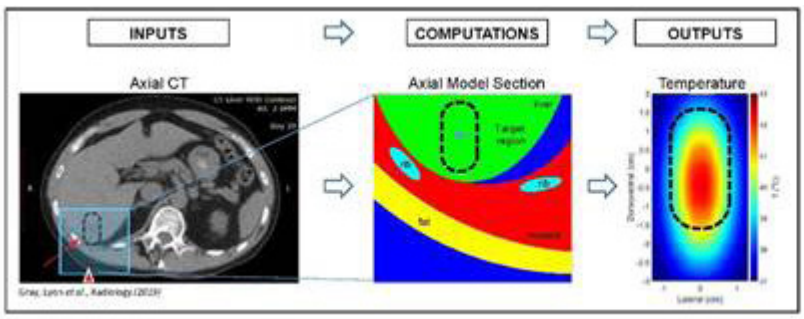

Figure 1. Illustrations of treatment planning model development and output for the targeted region indicated by the black dashed line.

PAC-2

Topic: Pancreatic Cancer
Presentation Type: Oral

Histotripsy is an effective pancreatic tumor ablation strategy that releases immunostimulatory molecules and promotes anti-tumor immunity

Alissa Hendricks[1], Allison Zeher[1], Jacqueline Sereno[1], Jessica Gannon[1], Sheryl Coutermarsh-Ott[2], Eli Vlaisavljevich[1], Irving C Allen[2]

[1]Virginia Tech, Blacksburg, VA, USA
[2]Virginia Maryland College of Veterinary Medicine, Blacksburg, VA, USA

Background: Pancreatic cancer is the fourth leading cause of cancer-related deaths worldwide in part due to a persistent immunosuppressive tumor microenvironment. Histotripsy is a non-thermal, image guided tumor ablation modality that can rapidly kill cells in a targeted region with millimeter precision. Previous work established that there is an immune response to histotripsy ablation, however a mechanism behind this response has not been established. For this study, we utilized an in vitro model of Pan02 (pancreatic adenocarcinoma) transfected with a distinguishable antigen (hemaglutanin/HA), and verified findings in vivo with non-transfected Pan02 tumors. We hypothesized that with no thermal mechanism, histotripsy would not denature potential antigens and with rapid lysis of cells damage associated molecular patterns (DAMPs) could be released in high levels, which would lead to a robust immune response.

Materials and Methods: The effects of this therapy on the innate immune response were quantified through analyzing the relative concentrations of protein and DNA released from treated cells. After identifying protein concentration levels using a BCA assay, the protein samples were loaded for western blot analyses, in order to better visualize and further quantify protein amounts released from partially and fully ablated cell samples. To determine the efficacy of the released molecules to stimulate an immune response, we exposed naïve macrophages to isolated lysate and determined activation at 24 hours through increases in IL-6 expression and release. To show the potential for a systemic immune response, lysate was given to naïve dendritic cells, that were in turn co-cultured with naïve T cells. These in vitro experiments were repeated for thermal ablation, cryoablation, and irreversible electroporation. To verify that immune responses occur comparably in vivo, Pan02 tumors were grown in mice and subsequently treated with histotripsy. RTPCR and flow cytometry were used to determine changes in the tumor microenvironment overtime compared to untreated animals.

Results: Histotripsy is capable of releasing high levels of proteins, even with partial ablations, and, in fully ablated samples, proteins are still able to be clearly identified. Identifiable proteins included antigens (transfected HA) and DAMPs (DNA and HMGB1). The combination of proteins and fragmented DNA released by histotripsy was comparable to levels found in irreversible electroporation, slightly higher than cryoablation, and significantly higher than thermal ablation. Lysates from cells ablated with histotripsy were found to activate macrophages, dendritic cells, and CD4+ and CD8+ T cells. Mice with Pan02 tumors were shown to have significantly increased progression free and overall survival compared to untreated controls. Tumors treated in vivo had increased expression for antigen presentation and damage response pathways. These tumors showed increased macrophages and dendritic cells 24 hours and 7 days, and increased T cell populations at 7 and 14 days after treatment.

Conclusions: A variety of proteins and DNA are released from histotripsy treated cells, which stimulate anti-tumor pathways and lead to an inflammatory immune response. These results show the role of specific DAMPs and immune cell populations in responding to histotripsy ablation. Overall, these results indicate a robust immunomodulatory response to histotripsy ablation and pancreatic cancer.

Acknowledgements: We would like to thank the Focused Ultrasound Foundation for funding this work.

PAC-3

Topic: Pancreatic Cancer
Presentation Type: Oral

Low-intensity focused ultrasound produces immune response in pancreatic tumors

Jordan Joiner, Nancy Kren, Phillip Durham, Yuliya Pylayeva-Gupta, Paul Dayton

University of North Carolina at Chapel Hill, Chapel Hill, NC, USA

Background: Pancreatic cancer has a dismal survival rate due to late diagnosis and therapy resistance. Attempts to invigorate anti-tumor immune responses using checkpoint blockade have been unsuccessful, highlighting the need to understand barriers that impede immunotherapy. Profound immunosuppression, insufficient antigen presentation capacity, and desmoplasia-driven compression of tumor vasculature are thought to account for the failure of cytotoxic T cells to successfully reach and target tumor cells. Low-intensity focused ultrasound has emerged as a potential immunomodulatory treatment modality in several cancer types One of the main consequences of ultrasound application at the tumor site is a transient increase in vascular permeability and availability of antigens that may boost delivery of therapeutics and augment anti-tumor immune responses. However, lack of knowledge regarding optimized FUS parameters that might achieve such effects precludes its current application in patient care.

Materials and Methods: To understand how FUS treatment modulates anti-tumor immunity and vascular parameters, we have used murine syngeneic models of pancreatic cancer. Male and female C57Bl/6J mice were subcutaneously injected with 1x105 KPC cells in 0.1 mL HBSS in the right flank. Mice were treated by intravenously infusing decafluorobutane microbubbles (MBs) with a DSPC-PEG2k lipid shell (7 x 107 MBs total) and scanning the tumor with a Philips Therapy and Imaging Probe System (TIPS). Ultrasound parameters were as follows: 100 Hz PRF, 1 MHz frequency, 0.5 MPa, 10% duty cycle, 0.13 W/cm2, and 2 seconds/spot for a total treatment time of 8-10 minutes. Animals were treated with ultrasound and MBs either once or twice two days apart, and sacrificed at 2 days or 14 days post-treatment to evaluate tumor growth and immune cell filtration in the tumor and lymph node. Tumor tissue was analyzed using immunohistochemistry (HMGB1 and CD8) and flow cytometry (CD11c, I-A/I-E, F4/80, CD45, CD11b, PD-1, CD3, CD8, and CD4) and lymph nodes were analyzed using flow cytometry for the same markers. Histology slides were scanned using a Aperio ScanScope XT at UNC's Translational Pathology Lab and flow cytometry data was acquired on LSRII Fortessa (BD Bioscience) at UNC Flow Cytometry Core Facility. Data was analyzed using FlowJo v. 10.6.2 (Treestar, Inc).

Results: A single LoFU + MB treatment suppressed tumor growth 15 days post-treatment compared to untreated tumors. Significant increases in MHC-II+ dendritic cells and macrophages and expansion of CD8+ T cells were observed in the lymph nodes 2 days after treatment. These increases subsided 15 days post-treatment. Significant increases in intratumoral F4/80+ macrophages were observed 15 days post-treatment. LoFU + MB caused a decrease in PD-1+ expressing CD8+ T cells, signifying a possible decrease in T cell exhaustion. IHC staining of tumors obtained at days 2 and 15 post-treatment did not show an increase in intratumoral CD8+ T cells as a result of LoFU + MB treatment. IHC staining of tumors at 2 days post-treatment demonstrated an increase of HMGB1 due to LoFU + MB. In testing the immune effects of two LoFU + MB treatments in larger tumors, the transient increase in dendritic cells and macrophages was lost, indicating that initial tumor size may be critical for observing immune effects.

Conclusions: Here, we demonstrate that low-intensity focused ultrasound and microbubbles are capable of altering the immune microenvironment, and thus we conclude that this technology may play an important role in future immunotherapy approaches. Further studies are needed to refine ultrasound and microbubble treatment timing in order to optimize approaches, combine with immunotherapy and move this technology towards clinical translation.

Acknowledgements: The authors wish to acknowledge support from the National Science Foundation Graduate Research Fellowship Program (J.B.J.), National Institutes of Health (R21 CA246550 (P.A.D. and Y. P.-G.)), University Cancer Research Fund, UNC Lineberger Comprehensive C.

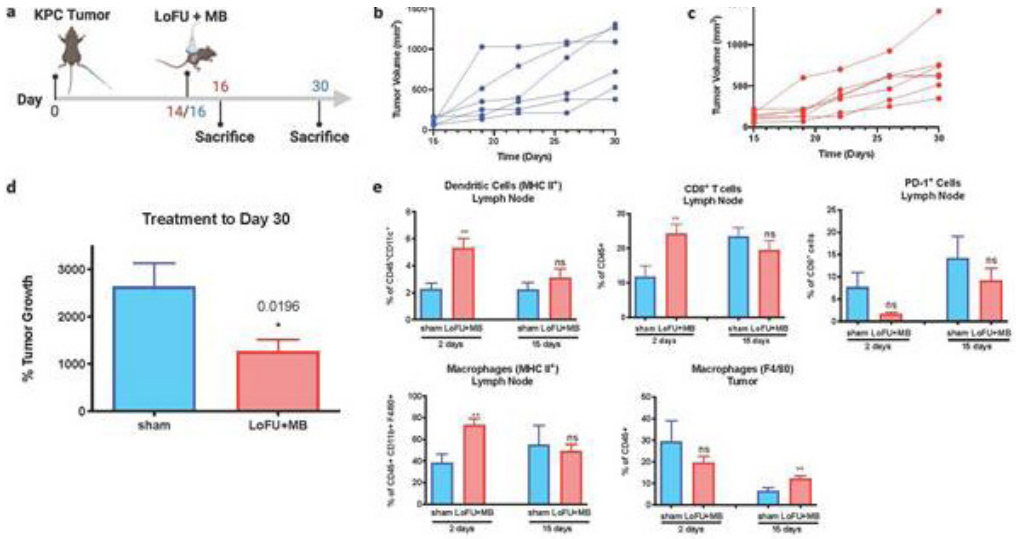

Figure 1. Analysis of KPC tumor growth and time-dependent immune cell infiltration as a result of low-intensity focused ultrasound and microbubbles.

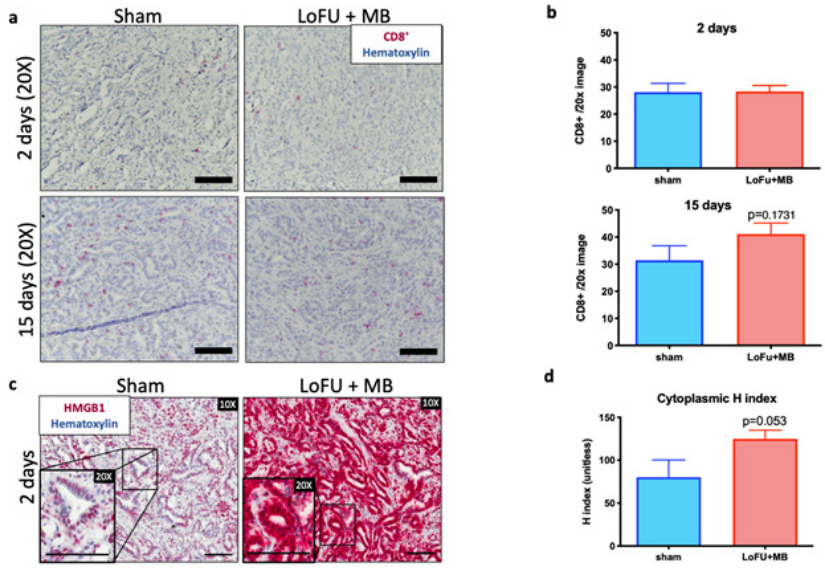

Figure 2. Analysis of CD8 T cell infiltration and HMGB1 expression as a result of low-intensity focused ultrasound and microbubbles. A. Scale bar = 100 um.

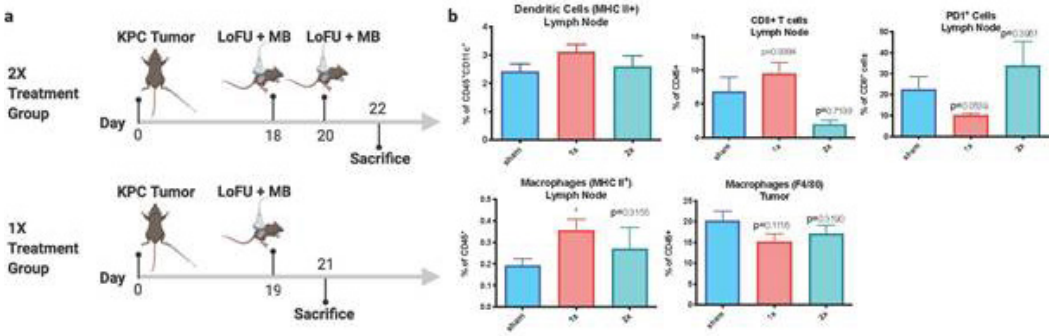

Figure 3. Analysis of immune cell infiltration in KPC tumors as a result of one or two treatments of low-intensity focused ultrasound and microbubbles.

PAC-4

Topic: Pancreatic Cancer
Presentation Type: Oral

Chronic effects of cavitation-aided gemcitabine delivery to pancreas cancer on tumor microenvironment in KPC mouse model

Tatiana Khokhlova[1], Yak-Nam Wang[1], Helena Son[1], Stephanie Totten[1], Stella Whang[1], Kayla Gravelle[1], Joo Ha Hwang[2]

[1]University of Washington, Seattle, WA, USA
[2]Stanford University, Stanford, CA, USA

Background: The ability of inertial cavitation induced by pulsed high intensity focused ultrasound (pHIFU) to permeabilize pancreas tumors and thereby enhance the concentration of systemically administered drug was previously demonstrated in genetically engineered KPC mouse model. The goal of this study was to evaluate the influence of weekly pHIFU-aided administration of chemotherapeutic drug gemcitabine on KPC mouse tumor progression and tumor microenvironment.

Materials and Methods: Tumor-bearing KPC mice were enrolled in the study when the tumor size reached 4-6 mm. Mice were treated once a week with either ultrasound-guided pHIFU and concurrent administration of gemcitabine (n=6) or gemcitabine only (n=5). pHIFU treatment was performed using Alpinion VIFU2000 small animal system along a two dimensional raster trajectory of focal locations spaced 1 mm apart, with the following protocol: frequency 1.5 MHz, pulse duration 1 ms, pulse repetition frequency 1 Hz, peak electric output power 400 W, 60 pulses per focal location. Inertial cavitation activity during each pulse was concurrently monitored with confocal passive cavitation detector (PCD). At the designated end point (doubling of tumor volume, per ultrasound imaging) the animals were euthanized, and excised tumors were processed for histology, immunohistochemistry (CD8 and Granzyme B labeling) and gene expression analysis using Nanostring PanCancer IO360 panel.

Results: In all treatments, consistent inertial cavitation activity was observed. pHIFU-treated region of the tumor turned hypoechoic immediately post treatment in all mice, suggesting localized edema and/or loss of tissue structure; this effect persisted throughout the survival period. Survival was improved in the group treated with pHIFU and gemcitabine compared to gemcitabine only (Fig.1). Histological examination revealed disrupted tumor cells and stromal structure within the treated area of the tumor. Enhanced labeling by Granzyme B was observed within and immediately adjacent to the treated area, but not in non-treated tumor tissue (Fig.2). No difference in CD8+ staining was observed between treated and non-treated tumors, suggesting the involvement of NK cells rather than T cells in response to treatment. Gene expression analysis showed that pHIFU treatment lead to downregulation of genes related to negative lymphocyte regulation (havcr2, siglec-f, cxcr2), migration and invasiveness.

Conclusions: Weekly combination treatment of pancreas tumors in KPC mice with pHIFU and gemcitabine resulted in only minor improvement in survival, most probably due to excessively conservative choice of the end point. However, partial mechanical disruption of tumor and stroma cells by pHIFU-induced cavitation appeared to not only facilitate gemcitabine penetration, but also to sensitize the tumor to gemcitabine therapy and alter immunosuppressive tumor microenvironment.

Acknowledgements: NCI R01CA154451

Figure 1. (top) Kaplan-Meier curve for mice with tumors treated with pHIFU and gemcitabine (pHIFU with Gem) compared to tumors treated with gemcitabine only (Gem only).

Figure 2. (bottom) Hematoxylin and Eosin stained section (middle pannel) showing the treated region of the tumor outlined by a green dashed line. Magnified images from treated (right) and untreated (left) regions labeled for Granzyme B. The treated region showed positive staining for Gramzyme B. Scale bar represents 100 mm.

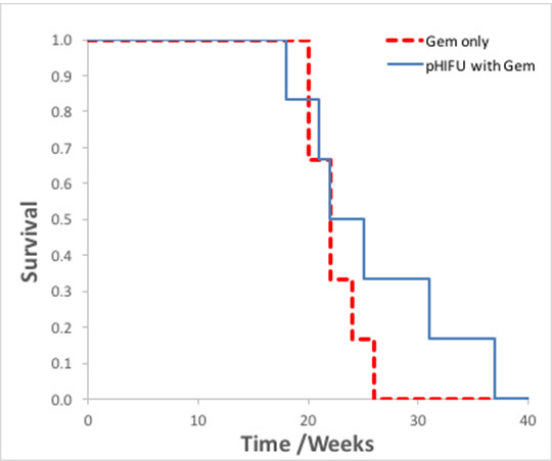

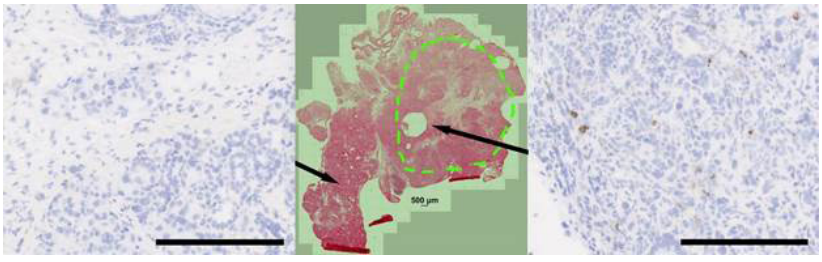

Figure 3. Statistically significant ($p<0.03$) reduction in gene expression (shown as log2 fold change) in gem+pHIFU vs gem only treated tumor.

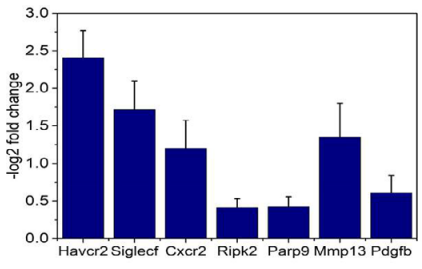

PAC-5

Topic: Pancreatic Cancer
Presentation Type: Oral

Demonstration of the use of microbubbles combined with low pressure pHIFU to induce cavitation and anti-cancer effects in pancreatic tumours

Petros Mouratidis, Gail ter Haar

The Institute of Cancer Research, London, United Kingdom

Background: High intensity focused ultrasound (HIFU) can be used for the treatment of solid tumours by creating cavitation which results in mechanical disruption of their microenvironment. Pancreatic tumours, which are characterised by a dense stroma should be particularly prone to these acoustic cavitation effects. Our pilot preclinical studies have shown that treatment of pancreatic tumours with pulsed HIFU (pHIFU) using high acoustic pressures (peak negative pressure (P-) > 10 MPa) in combination with immune checkpoint inhibitors (ICIs) can result in anticancer effects. The application of these pHIFU exposure parameters in a clinical setting is, in part, hindered by the high acoustic pressures required, which are considered to be neither practical nor safe for the patient. The aim of this study was to investigate the feasibility of combining pHIFU with microbubbles to induce similar anticancer effects in pancreatic tumours at clinically-relevant low rarefactional pressures

Materials and Methods: Syngeneic orthotopic pancreatic KPC tumours (KrasLSL.G12D/+; p53R172H/+; PdxCre tg/+) were grown in immune-competent murine C57BL/6 subjects. Tumours were exposed to pHIFU (P- = 17.6 to 3.8 MPa, duty cycle = 1 %, 15 repeats, f = 1.5 MHz) in the presence or absence of intravenously (IV) injected microbubbles. The small animal Alpinion VIFU 2000 Therapeutic ultrasound platform was used to treat the murine subjects with pHIFU. Acoustic cavitation was monitored during pHIFU bursts using a weakly focused polyvinylidine fluoride, broadband (0.1 to 20 MHz) passive cavitation detector. Data recording was controlled and processed using custom-written MatLab software. Tumours were imaged using 2D high frequency (14 MHz) B-mode ultrasound before exposure and measured with callipers at the time of culling. A combination of anti-CTLA4 / anti-PD-1 antibodies (200ug/ antibody/ dose/ subject) were administered intra-peritoneally 3 days before treatment, and every 3 days thereafter.

Results: Treatment of subjects with pHIFU (P- of 17.6 MPa) without microbubbles resulted in broadband and half harmonic emissions in orthotopic pancreatic KPC tumours. Exposure of tumours to pHIFU (P- of 6.1 MPa) without microbubbles resulted in no detectable broadband emissions. In contrast, increases in broadband and half harmonic emissions were detected when subjects were injected with a bolus dose of 100 ul of microbubble contrast agent and exposed to pHIFU (P- of 5.5 and 3.8 MPa) immediately after. Treatments lasted approximately 20 minutes in total with cavitation mainly detected in the first few minutes after microbubble injection. No side effects, including skin damage, were observed. A single pHIFU exposure at P- = 5.5 MPa combined with administration of microbubbles and ICIs extended the survival of subjects relative to non-treated animals. However no significant destruction of tumours or increases in tumour infiltrating lymphocytes (TIL) at these low P- was observed.

Conclusions: The use of microbubbles in combination with pHIFU reduces the pressure threshold needed for the induction of acoustic cavitation in pHIFU treated tumours. Some reduction in the rate of tumour growth was observed but without significant levels of necrosis or infiltration of the tumours but TIL. The results of this ongoing study suggest that increased levels of cavitation dose may be needed to produce significant anti-cancer effects.

Acknowledgements: Insightec ltd

PAC-6

Topic: Pancreatic Cancer
Presentation Type: Oral

Sonodynamic therapy for pancreatic cancer

Eleanor Stride[1], John Callan[2], Anthony McHale[2]

[1]University of Oxford, Oxford, United Kingdom
[2]Ulster University, Biomedical Sciences Research Institute, Coleraine, Northern Ireland

Background: Despite significant improvements in the survival rates for multiple forms of cancer over the past three decades, the prognosis for pancreatic cancer patients has remained extremely poor. This is due to a combination of late diagnosis, reducing treatment options for patients; and the nature of the tumours themselves, typically consisting of dense, poorly vascularised masses that are consequently strongly hypoxic and resistant to most conventional forms of therapy. Sonodynamic therapy (SDT) utilises drugs that can be locally activated using focused ultrasound thereby minimising systemic toxicity. Its effectiveness is however limited in the absence of molecular oxygen. The aim of this study was to conjugate SDT drugs to oxygen carrying microbubbles to address this limitation and to simultaneously exploit the delivery enhancement enabled by exposing microbubbles to focused ultrasound.

Materials and Methods: In the initial study, 1,2-Distearoyl-sn-glycero-3-phosphocholine (DSPC) coated microbubbles containing either oxygen (O2) or sulphur hexafluoride (SF6) were produced by sonication and conjugated to a sonosensitiser (Rose Bengal RB) via an Avidin-Biotin linker. Tumours were induced in BALB/c SCID mice using the BxPc-3 human pancreatic cell line and exposed to ultrasound for 3.5 mins (3.5 Wcm-2 at 1MHz centre frequency, 100 Hz pulse repetition frequency and 30% duty cycle) following intratumoural injection of either O2 or SF6 microbubbles. Following promising results from the intial pilot, 1,2-dibehenoyl-sn-glycero-3-phosphocholine coated microbubbles containing oxygen and 50nm spherical magnetite particles were produced by sonication and conjugated to the SDT drug Rose Bengal via an Avidin-Biotin linker. The substitution of the phospholipid was found to substantially enhance the stability of the microbubbles to changes in size and concentration. Orthotopic tumours were induced in BALB/c SCID mice using the BxPc-3 human pancreatic cell line and exposed to ultrasound for 3.5 mins (3.5Wcm-2 at 1MHz centre frequency, 100Hz pulse repetition frequency, 30% duty cycle) following intravenous injection of the microbubbles with or without application of a 0.1T magnetic field.

Results: In the pilot animals, 5 days after treatment a 45% reduction in tumour volume was seen in the mice receiving the O2 bubbles, compared with a 35% increase in volume for those receiving the SF6 microbubbles. The control group showed an increase of 180% in tumour volume over the same period. Fibre optic oxygen probe measurements and subsequent analysis of the levels of hypoxia inducible factor (HIF1-α) confirmed an increase in the partial pressure of oxygen in the tumour. In the larger study, 38 days post implantation the tumours treated with both ultrasound and the magnet were 50% smaller than the control tumours and exhibited a 3-fold increase in active caspase as a marker of apoptosis. There was no statistically significant effect of ultrasound alone.

Conclusions: The results indicate that intravenously administered oxygen filled microbubbles can temporarily reduce tumour hypoxia and facilitate sonodynamic therapy and efficacy can be enhanced by magnetic targeting. This potentially represents a new treatment option for recalcitrant tumours for which existing therapeutic options are extremely limited.

Acknowledgements: We thank the Engineering and Physical Sciences Research Council for supporting this work through EP/I021795/1. John Callan thanks Norbrook Laboratories Ltd. for an endowed chair.

PRO-1

Topic: Prostate
Presentation Type: Oral

MRI-guided transurethral ultrasound ablation (TULSA) in men with localized prostate cancer: Two-year follow-up

Sandeep Arora[1], Steven Raman[2], Christian Pavlovich[3], Jurgen Fütterer[4], Gencay Hatiboglu[5], Temel Tirkes[6], Aytekin Oto[7], Masoom Haider[8], Derek Cool[9], James Relle[10], Marc Serrallach[11], Daniel Costa[12], Thorsten Persigehl[13], Katarzyna Macura[3], Michiel Sedelaar[4], Joyce Bomers[4], Michael Koch[6], David Bonekamp[5], David Penson[1], Allan Pantuck[2], Carlos Nicolau[11], Gregory Zagaja[7], Yair Lotan[12], Axel Heidenreich[13], Andrei Purysko[14], Robert Staruch[15], Mathieu Burtnyk[15], Joseph Chin[9], Laurence Klotz[8], Scott Eggener[7]

[1]Vanderbilt University Medical Center, Nashville, TN, USA
[2]University of California, Los Angeles Health Sciences, Santa Monica, CA, USA
[3]Johns Hopkins University, Baltimore, MD, USA
[4]Radboud University Medical Center, Nijmegen, Netherlands
[5]University Hospital Heidelberg, German Cancer Research Center (DKFZ), Heidelberg, Germany
[6]Indiana University, Indianapolis, IN, USA
[7]University of Chicago, Chicago, IL, USA
[8]University of Toronto, Toronto, ON, Canada
[9]Western University, London Health Sciences Centre, London, ON, Canada
[10]Beaumont Health System, Royal Oak, MI, USA
[11]Clinic Hospital of Barcelona, Barcelona, Spain
[12]UT Southwestern Medical Center, Dallas, TX, USA
[13]University Hospital Cologne, Köln, Germany
[14]Cleveland Clinic, Cleveland, OH, USA
[15]Profound Medical, Mississauga, ON, Canada

Background: MRI-guided transurethral ultrasound ablation (TULSA) is an incision-free in-bore procedure for customized prostate ablation using directional ultrasound under real-time MRI thermometry guidance and control. We report two-year (2y) outcomes from the TULSA-PRO Ablation Clinical Trial (TACT) pivotal study.

Materials and Methods: TACT enrolled 115 men with organ-confined prostate cancer (≤T2b, PSA ≤15 ng/ml, Gleason Grade Group 1-2) across 13 centers in USA, Europe, and Canada. Median (IQR) age was 65 (59-69) years and PSA was 6.3 (4.6-7.9) ng/ml. Clinically significant Gleason Grade Group 2 (GG2) prostate cancer (PCa) was present in 72/115 (63%) men, and highly suspicious MRI lesions (PI-RADS score >=4) in 77/115 (67%). High volume disease (>= 3 biopsy cores positive) was present in 71% and bilateral disease in 44%. The TULSA procedure was performed by a urologist and radiologist, with customized treatment plans designed to achieve whole-gland ablation sparing the urethra and urinary sphincter. Primary regulatory endpoints were safety and PSA reduction at 1y. Clinical outcomes at 1y included 10-core biopsy and multiparametric MRI assessed by a central radiologist for prostate volume reduction and residual disease. 2y outcomes included PSA stability, rate of salvage treatment, adverse events, and quality of life.

Results: Target volumes of 40 (32-50) cc were ablated in 51 (39-66) min. MRI thermometry measured 98% ablation coverage, confirmed by CE-MRI. PSA decreased 95% to nadir of 0.3 (0.1-0.6) ng/ml, 0.6 (0.3-1.2) ng/ml at 2y. Prostate volume decreased 91% to 3 cc. At 1y biopsy, GG2 PCa was eliminated in 54/68 (79%) men, 72/111 (65%) had no evidence of any PCa. Multivariate predictors of residual GG2 included intraprostatic calcifications, thermal dose coverage, and MRI lesions at 1y. MRI at 1y had negative predictive value of 93% for residual GG2. Eight men (7%) underwent post-TULSA salvage. There were no rectal injuries, severe urinary incontinence (UI), or severe erectile dysfunction (ED). Grade 3 adverse events in 9 (8%) men resolved by 1y. Urinary symptoms (IPSS) recovered to baseline by 3 months. Moderate UI (pads) present in 2.6% at 1y, no new onset at 2y. Moderate ED (oral medication) present in 23% at 1y, one new at 2y. Erections sufficient for penetration maintained by 75% at 1y, 83% at 2y.

Conclusions: Two-year follow-up in men with localized prostate cancer indicates that whole-gland TULSA conferred effective disease control with low toxicity and stable quality of life. Further studies are ongoing of TULSA for benign prostatic hyperplasia, partial gland ablation, and radio-recurrent salvage.

Acknowledgements: This study was sponsored by Profound Medical. RS and MB receive a salary and stock options from Profound Medical.

PRO-2

Topic: Prostate
Presentation Type: Oral

HIFU prostate ablation results in a single-center community practice

Robert Lemme[1], Rahul Mehan[2], Harpreet Wadhwa[2]

[1]A.T. Still University - Kirksville College of Osteopathic Medicine, Kirksville, MO, USA
[2]East Valley Urology Center, Mesa, AZ, USA

Background: High-intensity focused ultrasound (HIFU) received US authorization in 2015 for the ablation of prostate tissue and is used most commonly for the treatment of prostate cancer. Reported here is a summary of near-term results for safety, functional outcomes and disease control on patients undergoing HIFU ablation for prostate cancer at a single-center community practice.

Materials and Methods: Between January 2018 and June 2020, forty (40) consecutive patients underwent prostate HIFU ablation using the Sonablate device. One patient with metastatic prostate cancer was referred by an Oncologists for compassionate HIFU treatment and excluded from this analysis. For the remaining thirty-nine men the average age was 72 (51-86), prostate volume averaged 36cc (20-60cc), pretreatment PSA averaged 7.3 ng/mL (3.8-16) and clinical stage T1c-T2c. MpMRI was performed on 85% of men with a mode PIRADs score of 4.0 (3-5). Pretreatment biopsies included sixty-five percent (62%) targeted and thirty-five (38%) template with an average of 14 cores (3-24) yielding 4.75 positive (3-24).

Seventy-nine percent (79%) of men had intermediate or greater disease (Gleason 3+4 = 53%, 4+3 = 21%, 4+4 = 3%, 4+5 = 3%). Ninety percent (92%) of patients completed the pretreatment baseline questionnaires including IPSS and IIEF5. Postop HIFU follow-up protocol includes repeat of all preop tests, PSA evaluations every three-six months during the first year and annual thereafter and MRI / fusion guided biopsy scheduled at 12 months or at any time for cause. Complications were assessed by the Clavien-Dindo classification. Average treatment time and catheterization was 119 minutes and 6 days respectively. A urethral sparing technique was utilized for all procedures. Eighteen percent of patients received pre-HIFU hormones and 20% underwent a pre-HIFU photoselective vaporization of the prostate (PVP).

Results: Following HIFU, all men evidenced a drop in PSA to an average nadir of 1.3 with 88% of men maintaining a lower PSA at their 12 month follow-up. No de-novo urinary incontinence or bladder outlet obstruction was reported, and the majority of men preserved continence and erectile function at their pretreatment levels. Using Clavien-Dindo classification the primary complications were acute urinary retention (10%) and urinary tract infections (5%) with only one late Grade III complication, stemming from a prior PVP procedure.

Four patients were diagnosed positive for prostate cancer following HIFU treatment. Three patients had an infield recurrence and one patient had a new out-of-field occurrence. Two patients are currently scheduled for a repeat HIFU procedure, one patient is on Active Surveillance and one patient was referred for radiation treatment.

Conclusions: For thirty-nine (39) men undergoing prostate HIFU ablation for prostate cancer, the procedure was safe and provided excellent potency and continence preservation along with good short-term disease control, albeit with limited duration follow-up. No serious complications were noted. Urethral sparing techniques appear promising in minimizing urinary side effects Further data collection and evaluation is ongoing to confirm that good cancer control is maintained over time.

PRO-3

Topic: Prostate
Presentation Type: Oral

Monitoring clinical HIFU lesion in prostate cancer using passive elastography based on conventional B-mode images

Thomas Payen[1], Sébastien Crouzet[1], Nicolas Guillen[2], Jean-Yves Chapelon[3], Cyril Lafon[1], Stefan Catheline[1]

[1]LabTau, Lyon, France
[2]EDAP TMS, Vaulx-en-Velin, France
[3]INSERM, Lyon, France

Background: High intensity focused ultrasound (HIFU) is clinically used in the context of non-metastatic prostate cancer, where it provides an efficient, local, non-ionizing and minimally invasive treatment option. In order to preserve the surrounding tissues and limit the side effects for the patient, it is however crucial to monitor the sudden rise in temperature in the treated area which results in definitive necrosis. A significant increase in tissue stiffness is a well-known marker of HIFU lesions and elastography has been thoroughly investigated as a monitoring technique. However, the deep-seeded prostate remains a challenge for techniques relying on external perturbations. In contrast, passive elastography uses the wave field naturally present in the human body to estimate elasticity in the whole organ. The objective of this work is to evaluate how passive elastography can be implemented in a clinical system for monitoring the progress of HIFU treatment using Bmode images.

Materials and Methods: Passive elasticity maps were first obtained in a vibrated calibrated phantom with stiff inclusions. Raw IQ data was acquired and B-mode images were reconstructed from the same data set. Frame-to-frame displacement was estimated by phase tracking and the GLobal Ultrasound Elastography (GLUE) technique, respectively. Elasticity was then estimated using an autocorrelation-based algorithm. Five prostate cancer HIFU patients with various Gleason scores were imaged for 10 seconds before and after HIFU treatment using the Focal One® system. The GLUE method was again used to estimate the displacement in this slow-rate acquisition (22 Hz). The resulting pre and post passive elastography maps were compared to estimate the treatment effect on the prostatic tissue. Per-operative contrast-enhanced ultrasound and post-operative multiparametric MRI were used as comparators to assess the treatment success.

Results: In the phantom, the shear wave velocity was estimated in the background and in the inclusion at 2.93 ± 0.71 and 5.53 ± 0.89 m/s, respectively, using IQ data, and 3.13 ± 0.81 and 5.17 ± 0.95 m/s using the reconstructed B-mode images, in good agreement to the manufacturer's values of 2.89 and 5.16 m/s. In addition, the maps demonstrated sharp boundaries for inclusion delineation. In patients, the shear wavelength was in average 37% higher in the tumor than in adjacent prostate tissue prior to treatment indicating stiffer tissue. In addition, the elasticity values increased by 26% after treatment in the ablated region while they remained similar in untreated areas.

Conclusions: Passive elastography can be performed using B-mode images acquired with low frame rate conventional US scanners with results comparable to the ones obtained based on ultrafast IQ data. The direct comparison between IQ data-based and B-mode-based results showed good agreement between the two methods. In addition, B-mode passive elastography was able to detect tumor in the prostate as well as show the stiffness increase resulting from HIFU treatment. This technique compatible with clinical systems has the potential to see a quick transfer to the clinic for prostate cancer diagnostic and HIFU monitoring.

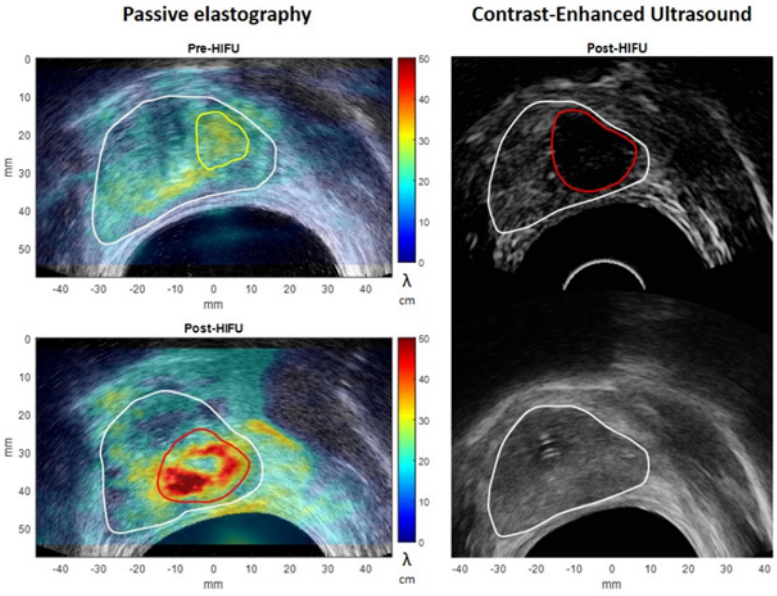

Figure 1. Passive elastography (left) before and after HIFU treatment in a cancerous prostate (tumor in yellow). Vascular depletion was confirmed with contrast agents (top right) in the treated region (red).

Acknowledgements: This work was supported by the RHU PERFUSE (ANR-17-RHUS-0006) of Université Claude Bernard Lyon 1 (UCBL), within the program "Investissements d'Avenir" operated by the French National Research Agency (ANR).

PRO-4

Topic: Prostate
Presentation Type: Oral

Oncological outcomes of 356 patients undergoing focal ablative salvage therapy (HIFU or cryotherapy) following radiation failure for prostate cancer

Deepika Reddy[1], Taimur Shah[1], Marieke van Son[2], Max Peters[2], Feargus Hosking-Jervis[1], Tim Dudderidge[3], Stuart McCracken[4], Raj Nigam[5], Richard Hindley[6], Amr Emara[6], Neil McCartan[7], Naveed Afzal[8], Henry Lewi[9], Raj Persad[10], Jaspal Virdi[11], Clement Orczyk[7], Caroline Moore[7], Manit Arya[1], Mark Emberton[7], Mathias Winkler[1], Hashim Ahmed[1]

[1]Imperial Prostate, Imperial College London, London, United Kingdom
[2]Utrecht Medical Centre, Utrecht, Netherlands
[3]University Hospital Southampton, Southampton, United Kingdom
[4]Sunderland Royal Hospital, Sunderland, United Kingdom
[5]Royal County Surrey Hospital NHS Trust, Guildford, United Kingdom
[6]Basingstoke and North Hampshire Hospital, Basingstoke, United Kingdom
[7]University College London, London, United Kingdom
[8]Dorset County Hospital Foundation Trust, Dorchester, United Kingdom
[9]Springfield Hospital, Chelmsford, United Kingdom
[10]North Bristol NHS Trust, Bristol, United Kingdom
[11]The Princess Alexandra Hospital, Harlow, United Kingdom

Background: Patients that have previously failed radiotherapy for prostate cancer is usually limited to systemic therapy due to morbidity from salvage prostatectomy. Such management is non-curative and impacts significantly upon quality of life. Focal salvage therapy may provide oncological control in select patient groups. We reviewed the outcomes following focal salvage ablative therapy with HIFU or cryotherapy within the UK's HEAT and ICE registries.

Materials and Methods: 356 consecutive patients underwent focal ablative treatment after initial radiation treatment failure (28/1/2004-1/10/2019, 194 (54.5%) underwent HIFU for posterior recurrence and 162 (45.5%) underwent cryotherapy for mostly anterior or T3b disease. Primary outcome was failure-free survival (FFS) defined as no systemic therapy, whole-gland treatment, metastases or prostate cancer-specific death. Secondary outcomes were overall survival, ADT free survival, metastases free survival and adverse events. Analysis of predictors of failure was also performed.

Results: Median (IQR) age was 69years (65-73) and PSA (IQR) was 4.0ng/ml (1-7-7.2). Overall median (IQR) follow-up was 41.3 months (21.4-58.5). Quadrant ablation was performed in 128 (36.0%), hemi-ablation performed in 64 (18.0%), hockey-stick in 5 (1.4%) and 159 (43.8%) had unknown ablative patterns. Due to histological or MRI proven recurrence/residual disease, 31 (8.7%) underwent further focal salvage re-treatment.

FFS (95%CI) at 3 and 6 years were 81% (76-87%) and 75% (68-83%) respectively (figure 1). Median (IQR) time to failure was 15.5 months (19.7). Overall survival (95%CI) at 3 and 6 years were 97% (95-100%) and 88% (81-96%) respectively (figure 2). Prostate-specific mortality was 2.8%. Overall 1 (0.3%) patient was managed for fistula formation, 16 (4.5%) were treated for UTIs.

Conclusions: Salvage focal ablative therapy for radio-recurrent prostate cancer is safe and provides good short to medium-term oncological control. The FORECAST study is awaited to further determine oncological outcomes in this cohort.

Acknowledgements: Sonacare and support the HIFU UK national registry (called HEAT) through an unrestricted grant. Galil/BTG Ltd previously supported the cryotherapy UK registry (called ICE, previously known as EuCAP) through unrestricted grants. None of the funding sources.

Figure 1. Kaplan-Meyer Curve demonstrating failure free survival after focal ablative salvage therapy.

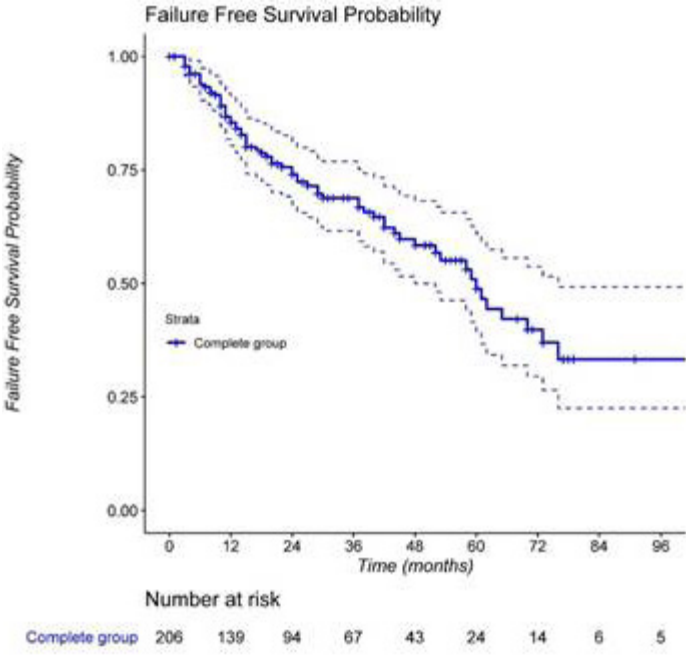

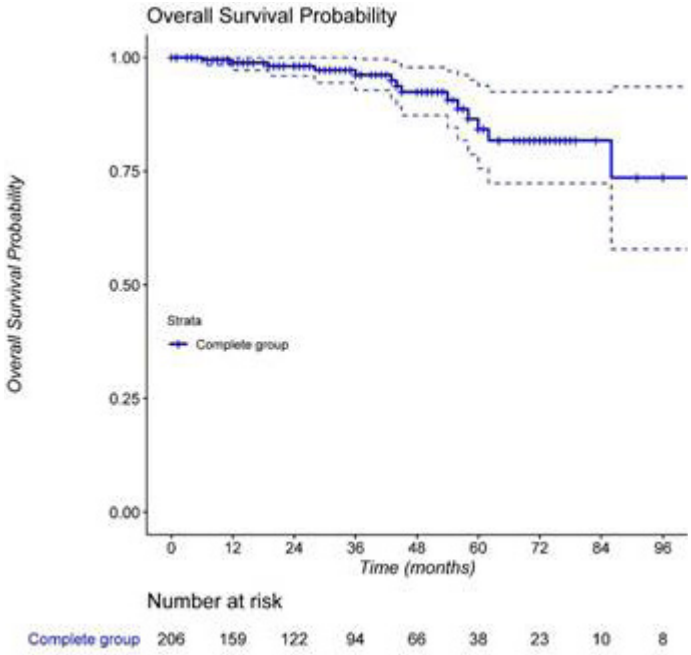

Figure 2. Kaplan-Meyer Curve demonstrating overall survival after focal ablative salvage therapy.

PRO-5

Topic: Prostate
Presentation Type: Oral

Cancer control outcomes following focal therapy using HIFU in 1,793 men with non-metastatic prostate cancer treated over 15 years

Deepika Reddy[1], Taimur Shah[1], Marieke van Son[2], Max Peters[2], Saiful Miah[3], David Eldred- Evans[1], Stephanie Guillaumier[4], Feargus Hosking- Jervis[1], Ryan Engle[1], Tim Dudderidge[5], Richard Hindley[6], Amr Emara[6], Raj Nigam[7], Neil McCartan[4], Valerio Massimo[8], Suks Minhas[9], Naveed Afzal[10], Henry Lewi[11], Clement Orczyk[4], Chris Ogden[12], Raj Persad[13], Jaspal Virdi[14], Caroline Moore[4], Manit Arya[1], Mark Emberton[4], Mathias Winkler[1], Hashim Ahmed[1]

[1]Imperial Prostate, Imperial College London, London, United Kingdom
[2]Utrecht Medical Centre, Utrecht, Netherlands
[3]Addenbrookes Hospital, Cambridge University Hospitals, Cambridge, United Kingdom
[4]University College London, London, United Kingdom
[5]University Hospital Southampton, Southampton, United Kingdom
[6]Basingstoke and North Hampshire Hospital, Basingstoke, United Kingdom
[7]Royal County Surrey Hospital NHS Trust, Guildford, United Kingdom
[8]Lausanne University Hospital, Lausanne, Switzerland
[9]Charing Cross Hospital, Imperial College Healthcare NHS Trust, London, United Kingdom
[10]Dorset County Hospital Foundation Trust, Dorchester, United Kingdom
[11]Springfield Hospital, Chelmsford, United Kingdom
[12]The Royal Marsden Hospital NHS Foundation Trust, Royal Marsden Hospital, London, United Kingdom
[13]North Bristol NHS Trust, Bristol, United Kingdom
[14]The Princess Alexandra Hospital NHS Trust, Harlow, United Kingdom

Background: Focal therapy is a treatment modality aiming to treat areas of cancer in order to confer acceptable oncological control, whilst reducing treatment-related functional detriment.

We report on oncological outcomes of patients undergoing focal HIFU recorded in the UK HEAT registry.

Materials and Methods: Of 1793 consecutive patients undergoing primary focal HIFU (17/11/2005-13/12/2019), across 6 UK sites, 1307 (72.9%) had a minimum of 6 months follow up. Focal intervention involved up to 2 sessions. Failure-free survival (FFS) was primarily defined as avoidance of salvage whole-gland or systemic treatment, metastases or prostate cancer-specific mortality. Differences in FFS between D'Amico risk groups were determined using log rank analysis.

Results: Of all patients treated median (IQR) age was 66 (60-71) years and PSA 6.90 (4.9-9.4) ng/ml. D'Amico low, intermediate and high-risk cancer occurred in 5.7% (102/1793), 62.6% (1124/1793), 25.8% (462/1793), respectively. Median follow-up for all 1793 patients was 27.5 (13.3-55.4) months and 32.6 (17.3-58.2) months for those with at least 6 months follow-up.

Complications were reported in 96/1793 (5.4%); 3.8% (68/1793) had urine infections or epididymitis with 0.6% (11/1793) having Clavien-Dindo >2 complications.

Of the 1307 evaluated for cancer control, 242(18.5%) had a second focal ablation due to residual or recurrent cancer and 32(2.4%) had salvage radiotherapy and 47(3.6%) salvage radical prostatectomy. Overall, Kaplan-Meier 2, 4 and 6 year FFS was 96% (95%CI 95-97%), 87% (95%CI 85-90%), and 77%(95%CI 73-81%), respectively. There was no statistically significant difference in 6 year FFS between intermediate and high- risk disease(78% [95%CI 73-84%] and 72% [95%CI 65-80%], p=0.30).

Conclusions: Of men undergoing focal HIFU, 89% had intermediate and high-risk prostate cancer. Focal HIFU is a safe procedure demonstrating good medium oncological outcomes.

Acknowledgements: Sonacare and support the HIFU UK national registry (called HEAT) through an unrestricted grant. No funding sources had any role or input into the design and conduct of the study; collection, management, analysis, and interpretation of the data; and preparation, review, or approval of the manuscript.

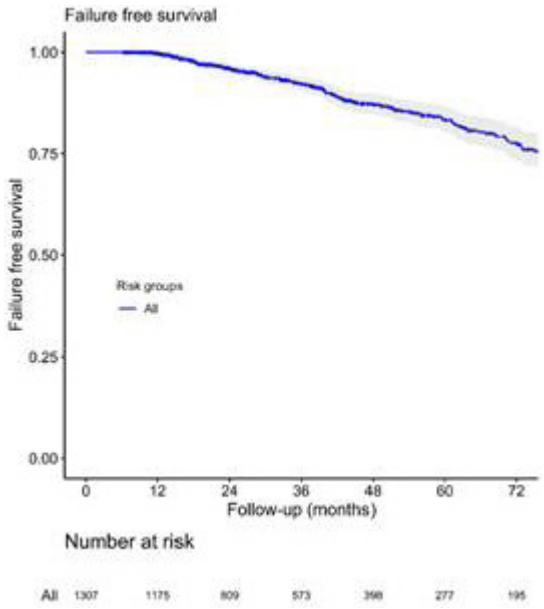

Figure 1. Failure free survival in 1307 patient undergoing focal HIFU for non-metastatic prostate cancer with at least 6 months follow-up.

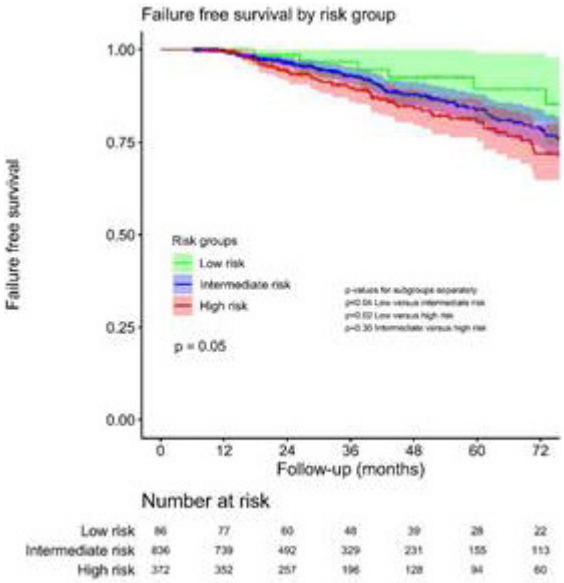

Figure 2. Failure free survival comparing D'amico risk groups in 1307 patient undergoing focal HIFU for non-metastatic prostate cancer with at least 6 months follow-up.

PRO-6

Topic: Prostate
Presentation Type: Oral

Focal therapy compared to radical prostatectomy for non-metastatic prostate cancer: A propensity score matched study

Deepika Reddy[1], Taimur Shah[1], Max Peters[2], Daniel Ball[3], Na Hyun Kim[4], Enrique Gomez-Gomez[5], Saiful Miah[6], David Eldred- Evans[1], Stephanie Guillaumier[7], Peter S. N. van Rossum[2], Marieke van Son[2], Feargus Hosking- Jervis[1], Tim Dudderidge[8], Richard Hindley[9], Stuart McCracken[10], Damian Greene[11], Amr Emara[9], Raj Nigam[12], Neil McCartan[7], Valerio Massimo[13], Suks Minhas[14], Naveed Afzal[15], Henry Lewi[16], Chris Ogden[17], Raj Persad[18], Jaspal Virdi[17], Clement Orczyk[7], Manit Arya[1], Mark Emberton[7], Hashim Ahmed[1], Mathias Winkler[1]

[1]Imperial Prostate, Imperial College London, London, United Kingdom
[2]Utrecht Medical Centre, Utrecht, Netherlands
[3]London North West University Healthcare NHS Trust, Northwick Park Hospital, London, United Kingdom
[4]Northwick Park Hospital, London, United Kingdom
[5]Reina Sofia University Hospital, University of Cordoba, Cordoba, Spain
[6]Addenbrookes Hospital, Cambridge University Hospitals, Cambridge, United Kingdom
[7]University College London, London, United Kingdom
[8]University Hospital Southampton NHS Trust, Southampton, United Kingdom
[9]Basingstoke and North Hampshire Hospital, Basingstoke, United Kingdom
[10]Sunderland Royal Hospital, City Hospital Fundation Trust, Sunderland, United Kingdom
[11]Spire Hospital, Newcastle, United Kingdom
[12]Royal County Surrey Hospital NHS Trust, Guildford, United Kingdom
[13]Lausanne University Hospital, Lausanne, Switzerland
[14]Charing Cross Hospital, Imperial College Healthcare NHS Trust, London, United Kingdom
[15]Dorset County Hospital Foundation Trust, Dorchester, United Kingdom
[16]Springfield Hospital, Chelmsford, United Kingdom
[17]The Royal Marsden Hospital, London, United Kingdom
[18]North Bristol NHS Trust, Bristol, United Kingdom
[17]The Princess Alexandra Hospital, Harlow, United Kingdom

Background: Focal therapy (FT) ablates areas of prostate cancer rather than treating the whole gland. We compared oncological outcomes of FT to radical prostatectomy (RP).

Materials and Methods: Using prospective multicentre databases of 761 FT and 572 RP cases (November/2005-September/2018), patients with PSA <20ng/ml, Gleason </=4+3 and stage </=T2c were 1-1 propensity score-matched for treatment year, age, PSA, Gleason, T-stage, cancer core length and use of neoadjuvant hormones. FT included 1-2 sessions. Primary outcome was failure-free survival (FFS) defined by need for salvage local or systemic therapy or metastases.

Results: 335 undergoing RP and 501 undergoing FT were eligible for matching. For FT, 420 had high intensity focused ultrasound and 81 cryotherapy. After matching, 246 RP and 246 FT cases were identified [Figure 1]. For RP, mean (SD) age was 63.4 (5.6) years, median (IQR) PSA 7.9g/ml (6-10) and median (IQR) follow-up 64 (30-89) months. For FT, these were 63.3 (6.9) years, 7.9ng/ml (5.5-10.6) and 49 [34-67] months, respectively. At 3, 5 and 8 years, FFS (95%CI) was 86% (81-91%), 82% (77-88%) and 79% (73-86%) for RP compared to 91% (87-95%), 86% (81-92%) and 83% (76-90%) following FT (p=0.12) [figure 2].

Conclusions: Focal therapy provides an alternative treatment method for patients with clinically significant localised prostate cancer that confers equivalent cancer control to radical prostatectomy in the medium term.

Acknowledgements: Sonacare and support the HIFU UK national registry (called HEAT) through an unrestricted grant. Galil/BTG Ltd previously supported the cryotherapy UK registry (called ICE, previously known as EuCAP) through unrestricted grants. None of the funding sources.

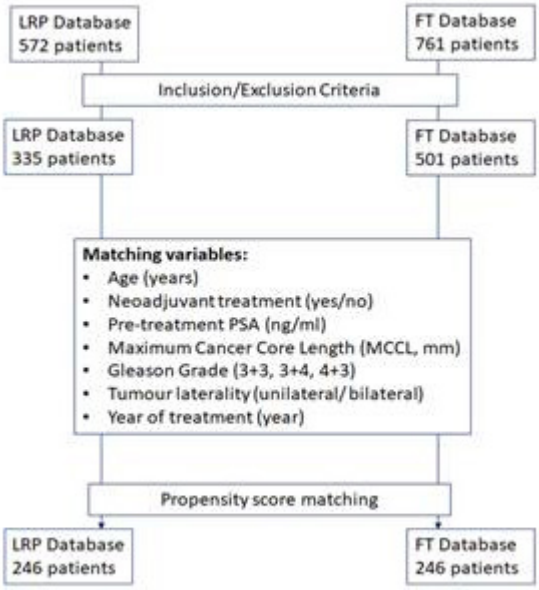

Figure 1. Flow diagram demonstrating matching variables and cohort development for the primary outcomes.

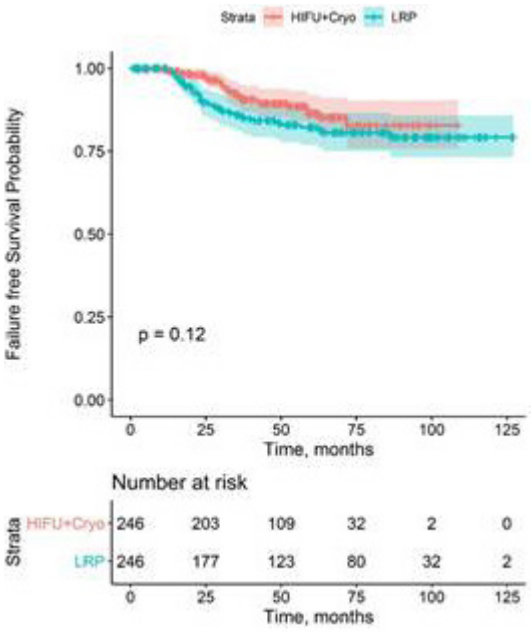

Figure 2. Primary outcome: Kaplan- Meier curver reporting failure free survival against time for radical prostatectomy and focal therapy, after 1-1 matching and single imputation.

PRO-7

Topic: Prostate
Presentation Type: Oral

Transrectal boiling histotripsy of the prostate: initial pre-clinical results with a prototype device

George Schade, Rishi Sekar, Tatiana Khokhlova, Alex Peek, Yak-Nam Wang, Stephanie Totten, Wayne Kreider, Yashwanth Kumar, Oleg Sapozhnikov, Adam Maxwell, Vera Khokhlova

University of Washington, Seattle, WA, USA

Background: Histotripsy ablation of the prostate may offer benefits over thermal High Intensity Focused Ultrasound (HIFU) due to its precise non-thermal mechanism and real-time visualization using B-mode ultrasound (US). Prior studies have evaluated transabdominal and transperineal shock scattering cavitation histotripsy, based on using microsecond-long pulses, for treating benign prostatic hyperplasia and prostate cancer. Our group has been developing a transrectal boiling histotripsy (BH) method, which uses sequences of millisecond-long pulses with shock fronts to produce vapor bubbles at the focus. Interaction between the vapor bubbles and ensuing shocks produces non-thermal mechanical tissue ablation. In this study, we assessed the feasibility of BH ablation of the prostate using a prototype transrectal device.

Materials and Methods: A custom-built transrectal BH system comprising a 2 MHz HIFU transducer (5.0 x 3.5 cm, focal length 4.0 cm) with in-line B-mode imaging (BK 3000, probe E14C4) (Fig. 1) mounted onto an automated translation/rotation stage. To confirm prostate BH pulse parameters, fresh ex vivo prostate tissue specimens were collected (N = 3 canines and N = 3 humans (IRB approved procurement protocol)), embedded in degassed 1.5% agarose gel and then treated with BH. Following tissue experiments, in vivo transrectal BH was assessed in N = 6 anesthetized canine subjects. Immediately following BH treatment, the subjects were euthanized and the prostate was harvested. During the treatment, input power was titrated up to establish the threshold for vapor bubble formation as seen with B-mode ultrasound imaging. BH pulses were 10 ms duration with pulse repetition frequency of 1 Hz. Single-foci and volumetric lesions were created by mechanically translating the focus through the tissue with 1 mm increments. A total of 10-60 BH pulses per focus were administered. Specimens were formalin-fixed and evaluated histologically.

Results: BH tissue liquefaction was feasible in all ex vivo tissues and in vivo experiments. The bubble threshold was similar in ex vivo canine and human tissue corresponding to a shock amplitude of 58-68 MPa at the focus. BH produced discrete lesions of mechanically disintegrated tissue in both canine and human tissue, however, human tissue was more resistant to BH, requiring more pulses to achieve similar degrees of disintegration. (Fig. 2) In vivo, the threshold for BH vapor bubble initiation was greater corresponding to at least 88 MPa shock amplitude. On B-mode, BH produced well defined hypoechoic lesions that corresponded well with gross and histologic findings (Fig. 3). On histology, well-defined lesions were observed containing homogenized tissue debris with areas of erythrocytes. At necropsy, no evidence of collateral injury was observed.

Conclusions: Transrectal BH ablation of the prostate is feasible using a preclinical prototype BH system. Further ex vivo and in vivo studies are needed to characterize the impact of tissue properties and surrounding anatomic structures on histotripsy parameters and optimize future clinical implementations.

Acknowledgements: Funding: NIH R01EB007643, R21CA219793, R01DK119310, and RFBR 175433034.

Figure 1. Transrectal BH device consisting of a 2 MHz transrectal HIFU transducer and in-line B-mode imaging array.

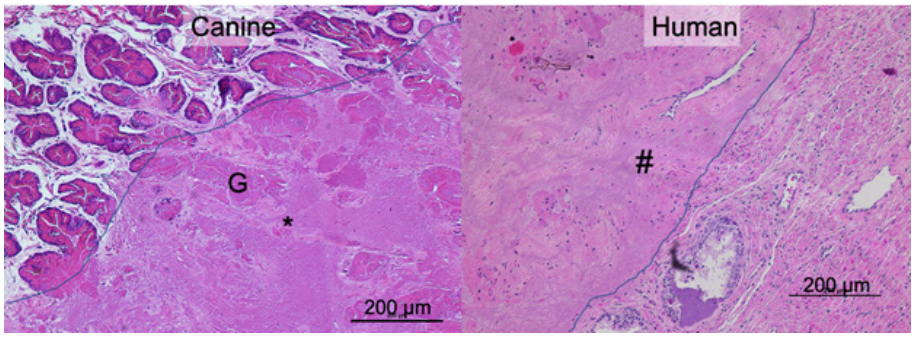

Figure 2. Fresh ex vivo canine and human prostate treated with transrectal BH (10 ms pulses, 1 Hz prf, 10 pulses/focus). Canine tissue was more sensitive to BH, with nearly complete homogenization (*).

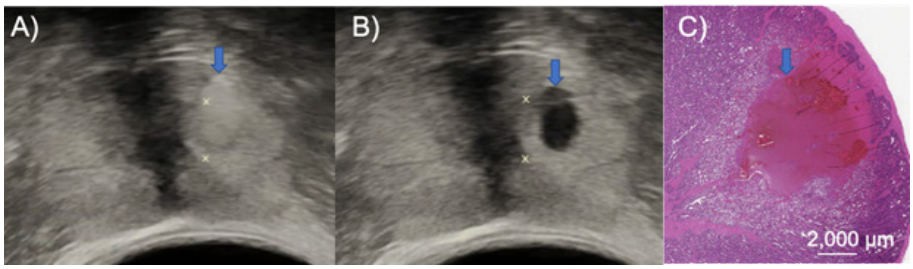

Figure 3. Results of transrectal BH prostate ablation in the canine model in vivo. On B-mode, during treatment BH appears as a hyperechoic bubble cloud (arrow) (A) that evolves into a hypoechoic cavit.

PRO-8

Topic: Prostate
Presentation Type: Oral

Focal therapy with high-intensity focused ultrasound for the localized prostate cancer for Asian patients: Prospective analysis of oncological and functional outcomes

Sunao Shoji[1], Kohei Uemura[2], Masanori Hasegawa[1], Takuma Tajiri[3], Akira Miyajima[1]

[1]Tokai University School of Medicine, Isehara, Japan
[2]The University of Tokyo, Bunkyo-ku, Japan
[3]Tokai University Hachioji Hospital, Hachioji, Japan

Background: Multiparametric (mp) magnetic resonance imaging (MRI) is increasingly used to diagnose clinically significant prostate cancer (csPCa), because of its growing availability, and advances that combine anatomic and functional data. Based on diagnoses of csPCa, focal therapy for localized PCa treatment has been designed to treat significant cancer with minimal injury to the urethra, sphincter, neurovascular bundle (NVB), and bladder neck. Because high-intensity focused ultrasound (HIFU) is an extracorporeal ablative technology that delivers ultrasonic energy to pinpoint foci only millimeters wide, and only minor temperature changes are observed outside of the focal zone, making it an attractive modality for focal therapy. The objectives of the present study to evaluate the oncological and functional outcomes of the region target focal therapy with HIFU for localized PCa for Asian in prospective study.

Materials and Methods: Patients who had (a) serum PSA levels ≤ 20 ng/ml, (b) significant PCa that had been located using MRI-TRUS elastic fusion image-guided transperineal prostate biopsy and 12-cores transperineal systematic biopsy, (c) life expectancies longer than 10 years, (d) no metastasis, (e) no bilateral cancers with Gleason scores ≥ 7, (f) no severe anal strictures, and (g) no previous history of treatment for PCa, were included in the present study. All patients were followed up for at least 1 year in the present report. We performed MRI-TRUS elastic fusion image-guided transperineal prostate biopsy with BioJet system (D&K Technologies GmbH, Barum, Germany). Locations of mpMRI-visible csPCa were recorded by the partitioned regions of the prostate. The recorded localization of each mpMRI-visible csPCa was converted to the treatment planning screen of TRUS image on the HIFU work station of Sonablate® 500 (SonaCare Medical, Indianapolis, IN, USA), and treatment range was determined. Oncological outcomes were evaluated with PSA kinetics and follow-up biopsy results. Functional outcomes were evaluated with International Prostate Symptom Score (IPSS), IPSS Quality of Life (QOL), Overactive Bladder Symptom Score (OABSS), uroflowmetry, Expanded Prostate Cancer Index Composite (EPIC) health-related domain summary and International Index of Erectile Function (IIEF)-5 scores.

Results: We treated 90 men (median age: 70 years; median PSA level: 7.26 ng/ml). The treated areas were completely devascularized a on dynamic contrast-enhanced MRI at 2 weeks after tre treatment. Catheterization was performed within 24 hours after the treatment in all patients. Biochemical disease-free rate was 92.2% during 21 months follow-up when use of Phoenix ASTRO definition. In follow-up biopsy, significant cancer was detected in 8.9% of the patients in un-treated areas. Urinary functions, including International Prostate Symptom Score (IPSS) ($P<0.0001$), IPSS quality of life (QOL) ($P=0.001$), Overactive Bladder Symptom Score (OABSS) ($P<0.0001$), EPIC urinary domain ($P<0.0001$), maximum urinary flow rate ($P<0.0001$), and IIEF-5 ($P=0.001$), had significantly deteriorated at 1 month after treatment, but improved to preoperative levels at 3 or 6 months. Rates of erectile dysfunction and ejaculation who had the functions were 86% and 70%, respectively, at 12 months after treatment.

Conclusions: In conclusion, focal therapy with HIFU for localized PCa based on the mpMRI localization of csPCa for Asian patients would have similar oncological and functional outcomes to those in previous reports in Europe. The present results demonstrated the promise of localized PCa as a novel treatment option for Asian patients. Further large studies are required to verify oncological and functional outcomes from this treatment for patients with localized PCa.

PRO-9

Topic: Prostate
Presentation Type: Oral

Real-time US imaging of HIFU field and applications to focal therapy of the prostate

Shmuel Ben-Ezra[1], Yoni Hertzberg[1], Tal Sommer[2], Amit Bar Masada[1], Alex Volovick[1], Doron Kopelman[3], David Margel[4], Ori Katz[2]

[1]NINA Medical, Nazareth, Israel
[2]The Hebrew University of Jerusalem, Jerusalem, Israel
[3]Rappaport Faculty of Medicine, Technion Israel, Institute of Technology, Haifa, Israel
[4]Tel Aviv University, Tel-Aviv, Israel

Background: The adoption of HIFU technology for various clinical applications is expected to get boost-up upon the introduction of an accurate, affordable, and intuitive guidance method. We present here a method for live imaging of the HIFU field by diagnostic ultrasound. The method can be helpful for various focal therapy applications, specifically for prostate focal therapy in which focal point localization and hot spot monitoring are highly desired to prevent adverse events.

Materials and Methods: An integrated transducer combines a HIFU transducer with an imaging probe. By intermittently replacing the imaging pulse with a short pulse from the HIFU transducer, an image of the HIFU beam profile is generated. The result is a high framerate, live video of the beam profile inside the body, including focal point tracking and hot spots monitoring.

The system consists of a HIFU transducer (H-184, Sonic-Concepts, WA) and an imaging probe (ATL/Philips P4-2) connected to an open ultrasound research platform (VANTAGE 64 VeraSonics, WA). The imaging probe is installed into the central opening in the HIFU transducer, such that diagnostic and therapeutic fields are aligned to each other [Figure 1]. The HIFU imaging is performed by driving the HIFU transducer at low power (less than 10W of peak power) with a single cycle sine wave pulse of 1MHz, far below the threshold for tissue damage. This pulse is synchronized in time through a trigger with the ultrasound imaging system which receives the echo of this pulse and performs the image reconstruction. The received echo signal is reconstructed to an image of the HIFU field by delay and sum (DAS) algorithm. The time delay per pixel is calculated with respect to the curved shape of the HIFU transducer, its orientation, and the time synchronization between the imaging and HIFU systems. The HIFU image may be fused into the B-mode image as a color image on top of a gray level image.

Results: An US image of a HIFU beam profile has been acquired [Figure 2]. The HIFU image has been plotted on top of a gray scale B-mode image of the phantom.

The image intensity at each pixel represents the amplitude of the HIFU field multiplied by the localized reflection coefficient of the medium. To extract the HIFU field from the intensity image, it can be divided by the reflection coefficient of the medium at each pixel, which can be derived from the B-mode image intensity. This eliminates the dependency of the HIFU image intensity by the medium reflection coefficient.

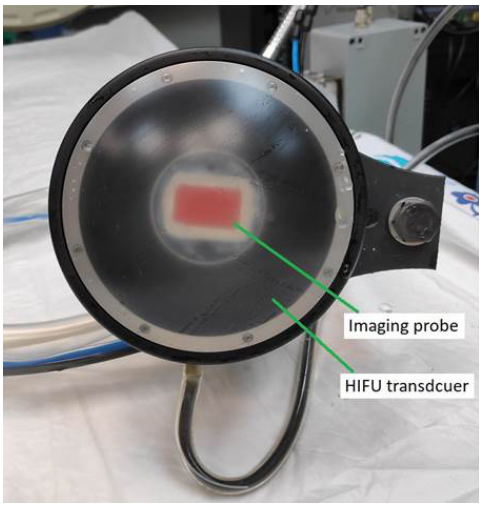

Figure 1. The integrated transducer, combines a therapeutic HIFU with a transducer, and a diagnostic probe.

Conclusions: A new imaging method of a HIFU field intensity has been introduced. This imaging method can be used safely in real-time during USgHIFU procedures to provide a live image of the treatment beam and focal point tracking to the practitioner and to improve treatment efficacy and safety.

The inhomogeneity of the human tissue causes deformations of the HIFU field. The field deformations might cause efficacy and safety issues such as reduction in the focal intensity, geometrical shift of the focal point, and formation of unsafe hot spots. Determining the intensity of the HIFU field inside the body can be useful for HIFU focal point localization, for detecting of hot spots and for ensuring the HIFU field power at the focal point is optimal.

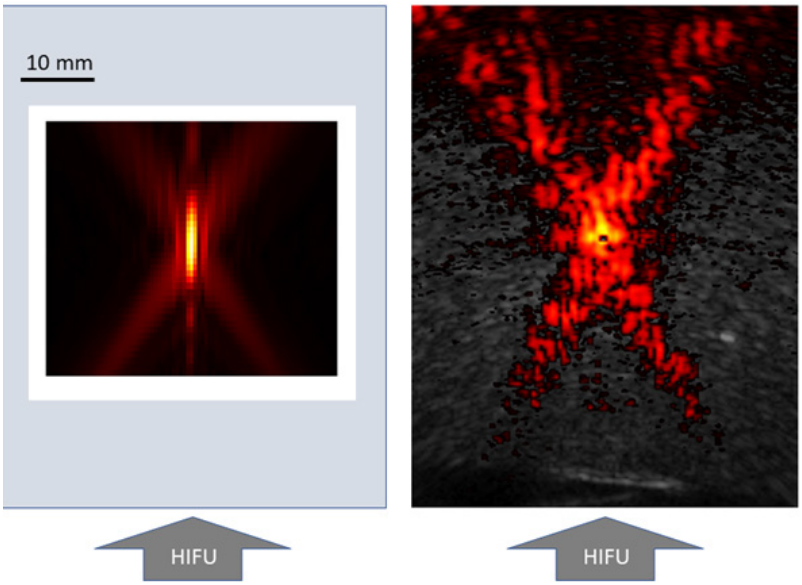

Figure 2. The acoustic field of a therapeutic transducer at 1 MHz. Left - hydrophone scan in degassed water, Right - live imaging of the HIFU field in a phantom (~ 10 fps) on top of a standard B-mode image.

PSY-1

Topic: Psychiatric Disorders
Presentation Type: Oral

Young Investigator

Magnetic resonance guided focuses ultrasound capsulotomy for psychiatric disorders: Clinical results and neuroimaging analysis

Benjamin Davidson, Ying Meng, Peter Giacobbe, Clement Hamani, Kullervo Hynynen, Nir Lipsman

Sunnybrook Research Institute, Toronto, ON, Canada

Background: One in four people worldwide are affected by a psychiatric illness – most commonly major depressive disorder (MDD) or obsessive compulsive disorder (OCD). Although approximately two-thirds of these patients recover through conventional treatments like psychotherapy and pharmacotherapy, up to one third are treatment resistant, suffering from a 20-fold increased risk of suicide. Recently, it has become possible to perform magnetic resonance guided focused ultrasound (MRgFUS) capsulotomy, an ablative neuromodulatory treatment. Here we report the clinical, safety, and neuropsychological results of two phase-1 clinical trials treating OCD and MDD using MRgFUS capsulotomy. We then demonstrate metabolic and structural changes occurring within the cortico-striatal circuitry underlying OCD and MDD.

Materials and Methods: Twelve patients under MRgFUS capsulotomy (6 OCD, 6 MDD). Adverse clinical and radiographic events were recorded at regular intervals postoperatively. Clinical outcomes were assessed using the Yale Brown Obsessive Compulsive Scale (YBOCS) for OCD patients and the Hamilton Depression Rating Scale (HAMD) for MDD patients (n=6). Neurocognitive performance was assessed at baseline and 6 months. Metabolic changes were quantified using 5-fluorodeoxy glucose positron emission tomography (PET). Changes in cortical thickness and subcortical volume from baseline to 3 months were quantified using the longitudinal processing stream of Freesurfer, a surface-based approach. In order to assess changes in white-matter tracts, a constrained spherical deconvolution processing pipeline was used, constructing 20 million streamlines in each brain at each timepoint. Tracts connecting the mediodorsal thalamus with the medial/lateral orbitofrontal cortex, anterior cingulate cortex, inferior, and middle frontal gyrus were extracted from the whole-brain tractogram. Tract counts were compared between preoperative and 3 month timepoints, adjusting for age and total intracranial volume.

Results: There were no serious adverse clinical or radiographic events. 4/6 OCD patients and 2/6 MDD patients met pre-established clinical response criteria (Figure 1). Neurocognitive performance improved significantly on several measures of executive function ($p<0.05$) (Table 1). By 6 months, there were significant reductions in cerebral glucose metabolism (Figure 2). Among 12 cortical regions, at 3 months postoperatively, there was a significant reduction in cortical thickness of the left pars orbitalis, bilateral orbitofrontal cortex, and right cingulate cortex ($p<0.05$).

There were significant reductions in the bilateral tracts connecting the thalamus with the orbitofrontal cortices, anterior cingulate cortex, inferior frontal cortex, and middle frontal cortex ($p<0.05$) (Figure 3). Tract reductions were significantly correlated with the postoperative day 1 lesion volume on the left, however there was no correlation with the right-sided lesion volume.

Conclusions: 12 patients underwent MRgFUS capsulotomy without serious adverse events. The clinical response rate was favourable, and comparable with more invasive methods of performing capsulotomy. MRgFUS capsulotomy also resulted in widespread reductions in cerebral and subcortical metabolism. The mechanism of MRgFUS is likely mediated through Wallerian degeneration of the white matter tracts passing through the anterior limbi of the internal capsule, therefore resulting in reduced tract counts, but also subtle reductions in cortical thickness at the tract enpoints in the ventral prefrontal cortex. Future directions will involve using structural imaging to personalize targeting for symptom subtypes.

Acknowledgements: Focused Ultrasound Foundation, Harquail Center for Neuromodulation.

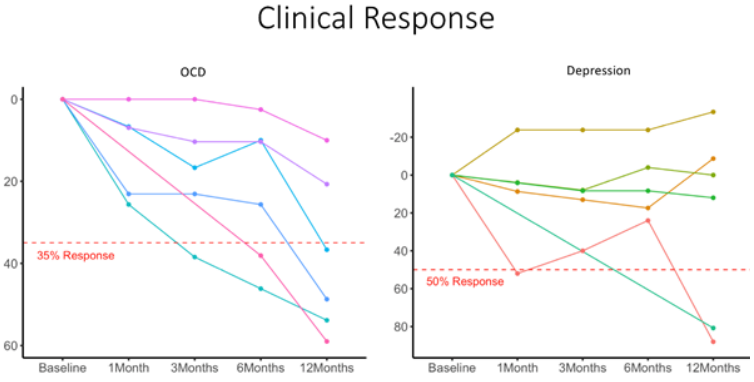

Figure 1. Clinical response among OCD patients (left) and MDD patients (right). The red dotted line indicates literature-accepted cutoff thresholds for a clinically significant improvement.

Table 1. Neuropsychological Testing on 9 patients

Measure	Preoperative	Last followup	P-value
CVLT-II: Total acquisition[a]	53.78 +/- 8.57	55.89 +/- 10.46	0.37
CVLT-II: Delayed free recall[c]	0.22 +/- 0.97	0.61 +/- 0.82	0.17
BVMT-R: Immediate recall[a]	41.67 +/- 16.86	50.44 +/- 12.21	0.09
BVMT-R: Delayed recall[a]	45.33 +/- 17.39	54.22 +/- 9.58	0.03
Oral SDMT[c]	-0.99 +/- 1.01	-0.58 +/- 1.02	0.10
D-KEFS Sorting Task: Correct number of sorts[b]	10.11 +/- 2.93	13.89 +/- 2.89	0.02
D-KEFS Sorting Task: Description score[b]	10.00 +/- 2.45	13.33 +/- 2.50	0.02
FrSBe (Self version): Dysexecutive scale[a]	70.00 +/- 14.53	60.67 +/- 13.56	0.03
FrSBe (Self version): Disinhibition scale[a]	58.89 +/- 21.15	50.78 +/- 20.35	0.11
FrSBE(Self version): Apathy scale[a]	86.11 +/- 16.40	72.89 +/- 23.71	0.02
FrSBe (Self version): Total[a]	73.78 +/- 14.69	62.22 +/- 17.25	0.02
WTAR IQ	108.78 +/- 7.69	*	-

Scores were standardized with published normative data, and reported in the following format: a T-Score (mean of 50, SD of 10); b Scaled Score (mean of 10, SD of 3); c Z-Score (mean of 0; SD of 1) BVMT-R: Brief Visuospatial Memory Test - Revised; D-KEFS: Delis–Kaplan Executive Function System; FrSBe-self version: Frontal Systems Behavior Scale (note that on this scale, lower scores represent fewer behavioural symptoms); CVLT-II: California Verbal Learning Test, Second Edition; SDMT: Symbol Digit Modalities Test; WTAR: Wechsler Test of Adult Reading; *WTAR was only performed at baseline to estimate premorbid intellectual functioning. p-values reflect the results of a Wilcoxon signed rank test.

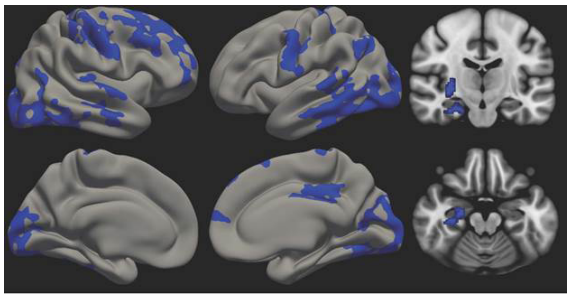

Figure 2. Results of the 5-Fluorodeoxyglucose positron emission tomography analysis. Reductions in cerebral (first and middle columns)and subcortical(third column) metabolism are indicated in blue.

Tract	Baseline	3 Month	p-value
Thalamus – Right Medial OFC	1.1	0.8	<0.001
Thalamus – Left Medial OFC	1.1	0.7	<0.001
Thalamus – Right Lateral OFC	1.9	1.4	<0.001
Thalamus – Left Lateral OFC	1.9	1.4	<0.001

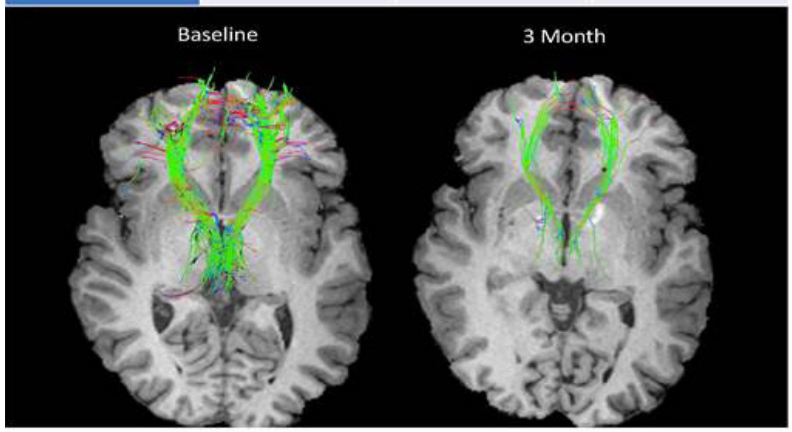

Figure 3. Top: Table indicating changes in structural connectivity between baseline and 3 months. Botton: Representative images from a patient at baseline (left) and 3 months (right).

PSY-2

Topic: Psychiatric Disorders
Presentation Type: Oral

Effect of low-intensity focused ultrasound stimulation in patients with major depressive disorder

Jeong-Ho Seok[1], Seung-Schik Yoo[2], Jooyoung Oh[1]

[1]Gangnam Severance Hospital, Yonsei University College of Medicine, Seoul, South Korea
[2]Brigham and Women's Hospital, Boston, MA, USA

Background: For the treatment of major depressive disorder (MDD), brain stimulation may provide alternative or supplementary options to conventional pharmacotherapy. Recently, low-intensity transcranial focused ultrasound (tFUS) stimulation has emerged as a promising neuromodulation technique due to its non-invasiveness, high spatial selectivity, and deep brain penetration. In this study, we investigated the effect of tFUS stimulation of the left dorsolateral prefrontal cortex (DLPFC) in patients with MDD.

Materials and Methods: Participants were recruited in the psychiatric outpatient clinics of the Gangnam Severance Hospital, and provided written informed consent. All participants were randomly assigned to either active tFUS or sham group. Under the image-guidance, six tFUS stimulation sessions were given to the individual, approximately a day apart, across 2-week period. In each session, FUS (250 kHz), each 300 ms long, was delivered to the left DLPFC every 6 s for the duration of 20 min. Each sonication was pulsed at 50 % duty cycle with tone burst duration of 1 ms. With an estimated derating factor of ~40% intensity transmission by the skull, estimated in situ peak negative pressure (Pr) at the focus was ~135 kPa with an in situ spatial-peak temporal-average acoustic intensity (Ispta) of ~600 mW/cm2. The sham group underwent the same study procedure without the sonication. Clinical assessments were conducted before the first FUS session (as baseline assessment), immediately after, and 2 weeks after the completion of the tFUS sessions. Repeated measures of analyses of variance were performed to analyze the clinical scores. Resting-state functional magnetic resonance imaging (rsfMRI) data were acquired prior to the treatment, and 2 weeks after the completion of the treatment to find differences in functional connectivity between the groups.

Results: Participants in both tFUS and sham stimulation groups did not report any auditory sensations during the sonication. Clinical assessment data from 18 subjects and rsfMRI data from 14 subjects were analyzed. There was a significant main effect of time and a significant interaction between the time and the group in terms of the Montgomery-Asberg Depression Rating Scale scores. The functional connectivity analysis of rsfMRI revealed that tFUS stimulation yielded differential connectivity patterns between the groups. The repeated tFUS sessions were tolerated well by all participants, without generating any particular neurological symptoms.

Conclusions: This randomized, sham-controlled clinical trial, the first study of its kind, demonstrated safety and probable efficacy of tFUS stimulation in the treatment of depression. The participants were not able to distinguish which group they were assigned to in the absence of auditory cues generated by FUS. The network-level modulation of the DLPFC and the subgenual anterior cingulate cortex is hypothesized as the main mechanism behind the observed efficacy.

Acknowledgements: This work was partially supported by the Neurosona Co. Ltd., Republic of Korea.

PSY-3

Topic: Psychiatric Disorders
Presentation Type: Oral

Transcranial focused ultrasound may disrupt amygdalar function

Norman M Spivak, Bianca Dang, Sergio Becerra, Maya McNealis, Ben M Rosenberg, Sonja Hiller, Andrew Swenson, Luka Cvijanovic, Michael Sun, David Kronemyer, Rustin Berlow, Michelle Craske, Nanthia Suthana, Martin Monti, Susan Y Bookheimer, Taylor Kuhn

University of California, Los Angeles, Los Angeles, CA, USA

Background: Non-Invasive Brain Stimulation is an emerging therapy in treating psychiatric and neurological disorders via methods such as TMS and tDCS. Many disorders involve dysfunction in regions that are not easily reached using TMS. Anxiety disorders arise from dysregulated amygdalar circuits, which are known to play a critical role in the brain and the body's response to external stimuli. In this study conducted over two visits, tFUS was administered to the right amygdala (AG) to disrupt emotional activity and behavior. On the second visit, tFUS was applied to the entorhinal cortex (ErC), which served as a control region. Regardless of the region of sonication, subjects performed a series of tasks assessing the level of emotional reactivity and cognitive reappraisal ability, both immediately prior to, and after tFUS administration.

Materials and Methods: This study sought to determine whether MR-guided low-intensity tFUS can selectively modulate amygdalar activity. The tFUS was administered using the BX Pulsar 1002 (BrainSonix Corp, Sherman Oaks, CA). The parameters were as follows: 650 kHz, 720 mW/cm2 ISPTA.3, 5% DC, with a PRF of 10 Hz for AG and 100 Hz for the ErC. The transducer was a circular, single-element, spherically focused transducer, with an active aperture of 61 mm, 65 mm nominal focal length, with a hydrophone-measured -6 dB focal width of 4 mm in water and - 6 dB depth range of 50.4 - 80.5 mm.

Our study had a total of six healthy subjects (N = 6; age (SD) = 61.8 (8.25); 50% female), who were recruited to come in exactly two weeks apart for the tFUS sessions; one session targeting the entorhinal cortex (ERc) and one targeting the amygdala (AG). The tFUS was administered under MR guidance using a Siemens 3T Prisma.

Subjects were asked to look at a series of images taken from the International Affective Picture System, and to WATCH (look at negative images), VIEW (look at neutral images), and REAPPRAISE (cognitively reappraise negative images). After each image, subjects were asked to rate levels of valence (higher more positive) and arousal. For each, we calculated the mean skin conductance level (SCL). We then generated indices of negative reactivity (WATCH-VIEW) and reappraisal (WATCH-REAPPRAISE) for valence, arousal, and SCL, and compared how these values changed after tFUS to AG and ErC.

Results: NEGATIVE REACTIVITY

AG tFUS had a moderate effect size for SCL (Cohen's d=0.49), and large effect size for arousal (d= 0.73), meaning that there was an increase in the SCL and arousal after sonication when viewing negative images. There was no effect for valence (d=0.12).

There was no effect for arousal (d=.16) or valence (d=0.09) for ErC tFUS. However, there was a moderate decrease in SCL when viewing negative images following sonication (d=-0.45)

REAPPRAISAL

AG tFUS had no effect on SCL (d= 0.13). Arousal had a large effect size (d=0.82) and a moderate effect size for self-reported valence (d=-0.46), suggesting that there was decreased arousal and increased valence when reappraising negative images after sonication.

There was no effect of tFUS of ErC for either SCL (d=0.03) or self-reported arousal (d=0.004). However, there was a large effect of self-reported valence (d=0.7), suggesting that there was decreased valence when reappraising the negative images after sonication.

Conclusions: These very preliminary data suggest that tFUS may be able to downregulate or disrupt amygdalar activity. While not yet definitive, this approach has the potential to be a future treatment for neuropsychiatric conditions with hyperactive amygdalae. Such conditions include anxiety disorders, phobias, and obsessive-compulsive disorders. Replication in larger samples is needed and work on this study is ongoing to study the potential tFUS has to directly enhance emotional regulation via modulation of the amygdala. These early findings

offer novel and exciting insight into the potential future application of tFUS as an accessible, safe, and non-invasive therapeutic device for a wide variety of patient populations.

Acknowledgements: Cognitive Center for Neuroscience Pilot Funding, University of California, Los Angeles.

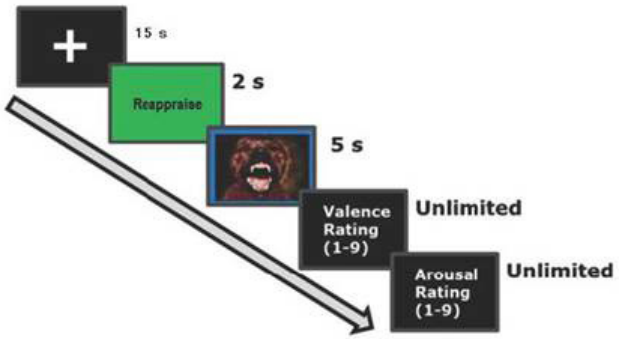

Figure 1. Each trial began with a white fixation cross in the center of a black screen for 15 s, followed by an instruction cue (VIEW, WATCH, or REAPPRAISE) for another 2 seconds, and then by an image occupying approximately 85% of the entire screen for 5 seconds. After the offset of each image, participants rated their level of valence, followed by their level of arousal. The ratings for both affective dimensions were obtained on a 1-9 scale using the Self-Assessment Manikin.

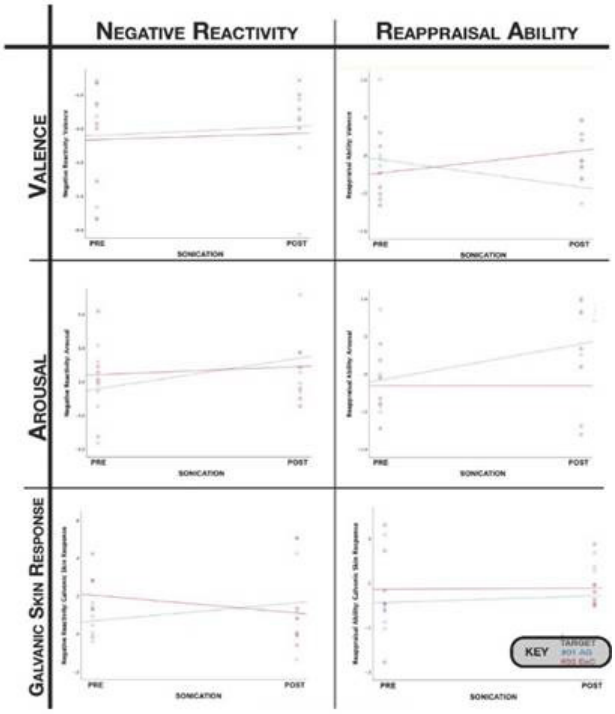

Figure 2. Participants completed an IAPS emotional reactivity and cognitive reappraisal task where they saw neutral or negatively rated (e.g. disgusting, frightening) images and were asked to either simply react (simple reaction) to the images or attempt to consciously minimize their emotional response using cognitive strategies (e.g. reminding themselves that the images are not real). After each image, participants reported their subjective arousal level, the degree of affect of the image (valence) and Galvanic skin conductance response (SCR) was simultaneously collected. Simple reaction to negative images was normalized by the reaction to neutral images in order to create a "Negative Reactivity" component. Reaction following cognitive remediation was normalized to simple reaction to negative images to create the "Cognitive Reappraisal" component. Graphs above compare longitudinal changes in arousal, valence and SCR between tFUS targeting the amygdala (AG) and tFUS targeting the entorhinal cortex (ErC). Given the small sample size, results are reported using effect sizes (Cohen's d). For the negative reactivity contrast, AG tFUS resulted in moderate increase in SCR and self-reported arousal. Similarly, ErC tFUS resulted in moderate increased SCR but not arousal or valence. For the cognitive reappraisal contrast, AG tFUS resulted in a large decrease in arousal and a moderate improvement in valence such that disgusting and frightening images were rated as less negative. Conversely, following ErC tFUS, there was a moderate-to-large decline in valence such that disgusting and frightening images were rated as more negative.

TEC-1

Topic: Technical
Presentation Type: Oral

Thermal dose performance temperature: A measure to evaluate MR-HIFU hyperthermia treatments

Edwin Heijman, Holger Grüll

University of Cologne, Cologne, Germany

Background: We enter an era where hyperthermia control is not always based on discrete sensors and patients' feedback but can be controlled by near-real-time temperature maps and algorithms (e.g. model predictive control). Since focused ultrasound can heat tissue within seconds deep inside the body, algorithmic control of the acoustic output is a necessity.

These new developments require new ways to evaluate the performance and its ability to reach a predefined goal of the hyperthermia controller. We present a novel performance indicator, called the Thermal Dose Performance Temperature (TDPT), to compare the performance of different MR-HIFU hyperthermia treatments.

Materials and Methods: The success of an RF hyperthermia treatment is quantified by, the so-called, T10, T50 and T90 temperatures at equilibrium, where the numbers stand for 90th, 50th, and 10th percentile of the temperature distribution, respectively. The MR-HIFU hyperthermia control is not based on reaching a hyperthermic equilibrium, but on maintaining a constant temperature over the whole treatment time. This asks for a different approach where spatial temperature distribution and time play a role. The thermal dose has been seen as the parameter which unifies time and temperature into a biologically effective dose. Although, there is not a certain amount of thermal dose required for hyperthermia, like an ablation. The contrary, a hyperthermia treatment should have a very low thermal dose preventing additional tissue damage. Secondly, we would like to benchmark the therapy to a set therapy goal: target temperature and time. Therefore, we normalize the thermal dose of the treatment to the thermal dose of the optimal treatment (fixed target temperature over the whole treatment time). We call the ratio between the real thermal dose and the optimal thermal dose the Thermal Dose Performance (TDP). Due to the non-linear nature of the thermal dose, the values of the TDP are challenging to interpret as a performance indicator. Therefore, we transfer the TDP to a Thermal Dose Performance Temperature by pretending that the controller was able to stabilize this TDPT for the whole treatment at this TDP.

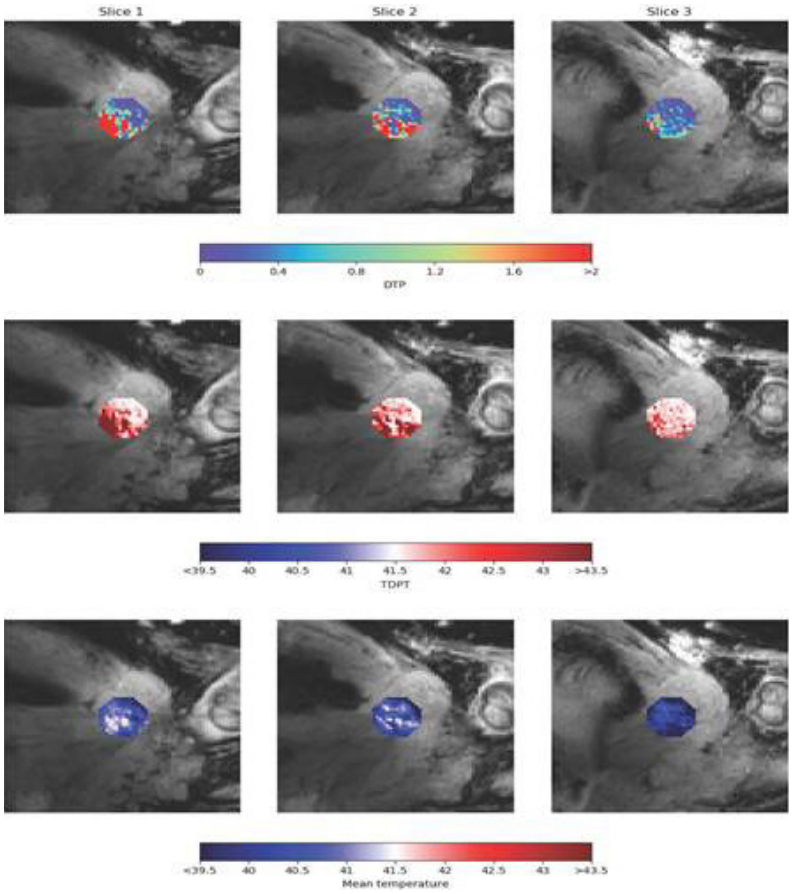

Figure 1. The calculated Thermal Dose Performance (TDP), Thermal Dose Performance Temperature (TDPT) and the mean temperature of the first treatment session in all sagittal slices within the cell.

Results: The TDP and TDPT were pixel-wise calculated by using, previous reported, data of an MR-HIFU hyperthermia therapy of a 52-year-old patient with a dedifferentiated liposarcoma. Figure 1 shows the different parameters (TDP, TDPT and mean temperature) at the three sagittal slices, orthogonal to the transducer beam axes, within the 3.2cm multi-position hyperthermia cell. Since the TDP has logarithmic behaviour, the TPDT looks more natural and more quickly to interpret as a performance indicator. In all slices, the pixel-values of the TDPT are higher compared to the mean temperature due to the exponential weighting of the higher temperature values. The used hyperthermia control algorithm only uses slice 2. According to the TDPT the algorithm underperformed on the lower part of the sonication cell, which is not visible in the mean temperature.

Conclusions: From our first analysis, we conclude that the TPDT gives us more insights on the performance of the hyperthermia control algorithm, regardless of the set target temperature and treatment time. Further data are needed to evaluate in more detail the value of the TDPT.

TEC-2

Topic: Technical
Presentation Type: Oral

A prototype system for boiling histotripsy in abdominal targets comprising a 256-element spiral array combined with a power-enhanced Verasonics engine

Vera Khokhlova, Bryan Cunitz, Mohamed Ghanem, Wayne Kreider, Christopher Hunter, Christopher Bawiec, Adam Maxwell, George Schade, Oleg Sapozhnikov, Minho Song, Tatiana Khokhlova

University of Washington, Seattle, WA, USA

Background: Boiling histotripsy (BH) uses sequences of millisecond-long ultrasound pulses with high amplitude shocks to mechanically liquefy target tissue with real-time monitoring of the treatment by ultrasound imaging. For pre-clinical BH treatment of abdominal organs, a high-power multi-element phased array system is needed to enable electronic focus steering for creating volumetric lesions and to introduce aberration corrections when focusing through inhomogeneous body wall. In addition, most BH studies have been performed under B-mode imaging of bubbles generated at the treatment site, which does not allow quantitative assessment of the degree of tissue liquefaction. Development of more comprehensive imaging modalities is therefore needed to enhance BH treatments.

Materials and Methods: A prototype BH system was built comprising a custom 256-element 1.5 MHz phased array (Imasonic, Voray sur l'Ognon, France) for pre-clinical studies in porcine kidney and liver (Fig.1). The array has a focal distance of 120 mm, an outer diameter of 144 mm, and a 40 mm central opening for holding a coaxially aligned ultrasound imaging probe (ATL P6-3) to monitor the treatment. The BH array was electronically matched to the Verasonics V1 engine with a 1.2 kW external power source. Driving electronics were supplemented by an extra capacitor bank and software was custom-modified to deliver BH exposures, providing a pulse average acoustic power of up to 2.2 kW sustained for 10 ms with 1-2 Hz repetition rate. System performance was characterized by hydrophone measurements in water. Electronic steering capabilities of the array were evaluated for shock-producing conditions at the focus and power compensation was introduced to equalize BH exposures at multiple focal locations across the treatment regions. Volumetric mechanical lesions were generated in ex vivo liver tissue with 1 mm spacing between individual foci, 10 ms pulse length, 5 - 10 pulses/focus, and 1% duty cycle. Plane wave Doppler followed by B-mode imaging were implemented immediately after each BH pulse to visualize residual bubble motion during the treatments. The changes in the Doppler power and speed were used as metrics to assess the degree of tissue liquefaction.

Results: Fully developed shocks of 100 MPa amplitude formed at the array focus in water at 275 W (12.5% of the maximum acoustic power of the system). Steering ranges of either 12 mm laterally or 24 mm axially corresponded to peak pressures of at least 90% of the maximum. Volumetric BH exposures in bovine liver with 10 pulses/per focus resulted in uniform tissue liquefaction with completely merged individual lesions while sparing connective tissue structures within the lesion (Fig. 2). Gross analysis showed a clear demarcation between the lesion and intact tissue with no apparent thermal damage. Additional exposures in porcine liver showed that maximum residual bubble velocities measured by Doppler were reached right after each BH pulse and increased from 18 to 30 cm/s as the treatment progressed with increased number of pulses per focus thus providing a quantitative metric for real-time control of tissue liquefaction (Fig. 3).

Conclusions: A pre-clinical BH prototype system was developed and successfully implemented to produce volumetric mechanical lesions in ex vivo tissue using electronic focus steering. Lesion formation was confirmed in real time by evaluating the degree of tissue liquefaction using color Doppler US imaging. This newly developed system should be capable, in terms of the power achievable, of delivering BH treatments transcutaneously in porcine liver and kidney in vivo. On-going work is aimed at using the array capabilities to introduce aberration correction for in vivo BH sonications through inhomogeneous body wall.

Acknowledgements: Work supported by NIH R01EB7643, R01GM122859, R01EB25187, and RSF 20-12-00145.

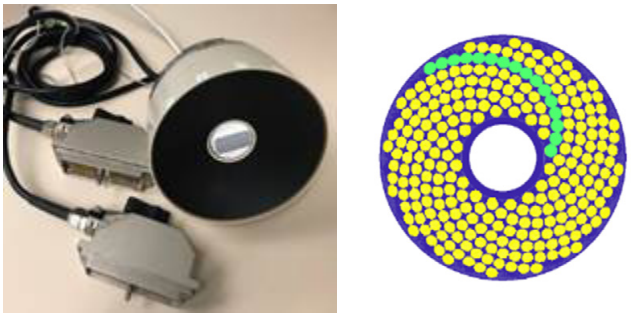

Figure 1. Photograph and sketch of a 256-element 16-arm spiral array.

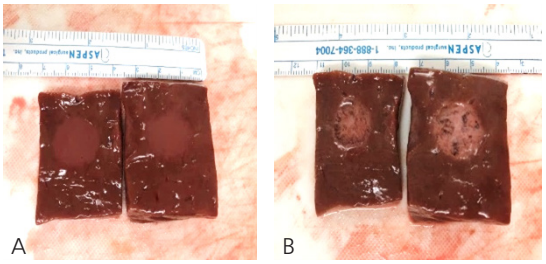

Figure 2. Bisected volumetric BH lesions generated in ex vivo bovine liver (A) with and (B) without liquefied content.

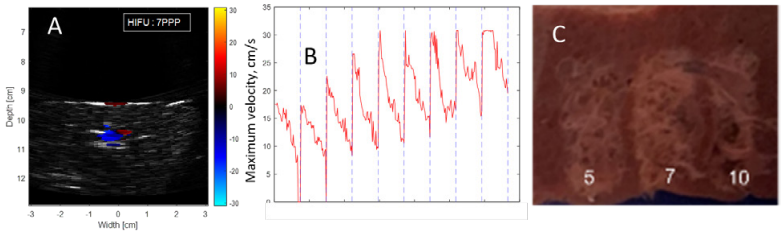

Figure 3. (A) Color Doppler image in ex vivo liver after the 7th BH pulse. (B) Residual bubble velocity after each BH pulse. (C) Rinsed volumetric BH lesions produced with 5, 7, and 10 pulses/focus.

TEC-3

Topic: Technical
Presentation Type: Oral

Motion-robust, multi-slice, real-time MR PRFS thermometry for MR-guided ultrasound thermal therapy in abdominal organs

Kisoo Kim, Chris J Diederich, Eugene Ozhinsky

University of California, San Francisco, San Francisco, CA, USA

Background: Proton resonance frequency shift (PRFS) based MR thermometry provides fast and accurate temperature monitoring for clinical MR-guided ultrasound thermal therapy. Real-time 3D MR PRFS thermometry is desirable for volumetric monitoring of thermal therapy. However, acquiring 3D PRFS data is time-consuming and is sensitive to motion artefacts induced by respiration and organ movement because it relies on voxel-wise analysis of phase difference between measured gradient echo (GRE) images. In particular, for the use of ultrasound thermal therapy on abdominal or pelvic organs, motion-robust, multi-slice, real-time MR thermometry is essential to meet the spatial and temporal requirements. The goal of this project is to develop and evaluate a real-time volumetric MR thermometry acquisition and reconstruction pipeline for monitoring thermal therapy in abdominal organs.

Materials and Methods: The accelerated multi-slice MR PRFS thermometry application was developed on the RTHawk Research Platform (HeartVista, Menlo Park, CA). It featured an accelerated GRE sequence with a spiral readout trajectory (spiral readout length = 10.7 ms, interleave=5) to achieve real-time volumetric imaging and a multi-baseline reconstruction pipeline for the correction of motion artefacts in PRFS measurements (Fig.1). Respiratory motion was tracked with an integrated pencil-beam navigator sequence and quantified with a temporal window of 150 ms. Real-time displacement measurements were used to route data in the multi-baseline reconstruction pipeline.

First, this approach was demonstrated in a simulation using a virtual phantom with respiratory motion integrated in the RTHawk Platform. Single- and multi-baseline approaches were compared to evaluate the performance of all-in-one MR thermometry applications. Second, the technique was validated in an experiment with a 3T MRI scanner (GE Healthcare, Waukesha, WI). A low-cost MR compatible respiratory motion simulator was developed (Fig.2) and implemented for non-heating experiments with a tissue-mimicking phantom (InSightec, Israel). The motion simulator performed cyclical motion of the phantom (~ 7.5 mm along z-axis) to simulate breathing. Multi-baseline images were collected as 10 phases of breathing cycle. The MRI parameters included TR/TE = 26/14.78 ms, FOV = 500 (simulation)/240 (experiment) mm2 (resolution of 3.3/1.52 mm2).

Results: Multi-baseline PRFS method provided more stable temperature measurements compared to single baseline PRFS method in both simulation and phantom experiments (Fig.3-4). Figure 3a shows simulated PRFS temperature maps with single- and multi-baseline approached at two positions of the respiratory cycle. The error from motion of the phantom was clearly observed in the single baseline PRFS map (middle, right, Fig.3a), while the multi-baseline PRFS map showed the artifacts to be mitigated (bottom, right, Fig.3a). The accuracy and stability of measurements was evaluated by the standard deviation of the mean values in the ROI across the time course. The multi-baseline PRFS measurement was found to be -0.19±0.35(simulation)/-1.48 ±0.17(experiment), and those of single baseline was 0.67±0.47(simulation)/-0.03 ±0.3(experiment). Although the field drift correction was not applied in the phantom experiment, the standard deviation of multi-baseline PRFS was lower than single baseline PRFS (Fig.4b).

Conclusions: Motion-robust, multi-slice, and real-time MR thermometry method developed here enables stable temperature measurement during the phantom movement simulating free breathing. Compared to real-time 3D MR echo planar imaging with a GRE sequence, the spiral MR sequence does not show any geometric distortion or shifting due to low bandwidth of the spiral readout. This preliminary study indicates the all-in-one PRFS MR thermometry method has potential to provide for real-time multi-

Figure 1. (a) a schematic diagram of spiral-based MR GRE sequence. (b) real-time reconstruction pipeline on the RTHawk platform.

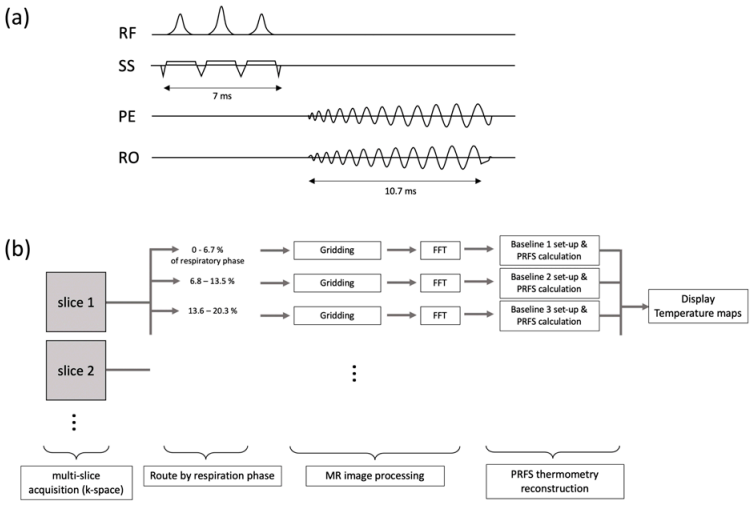

slice temperature monitoring during free breathing with applications for hyperthermia or thermal ablation.

Acknowledgements: **Acknowledgements:** NIH R21EB026018, R01EB025990, R21CA230120

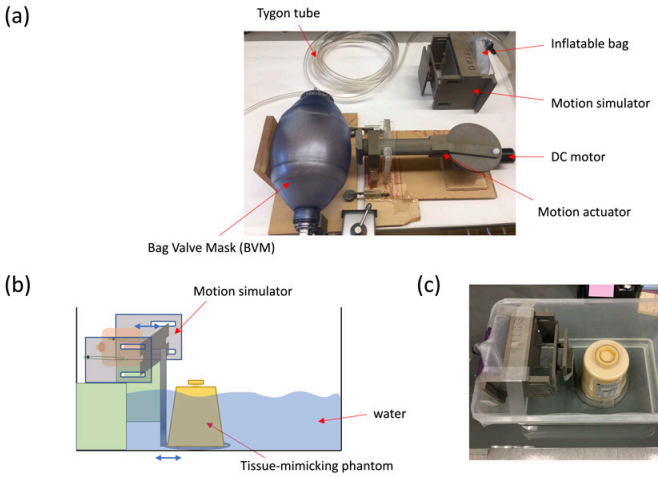

Figure 2. (a) a photo of the respiratory motion simulator. (b) an illustration and (c) a photo of the simulator setup within the MRI scanner.

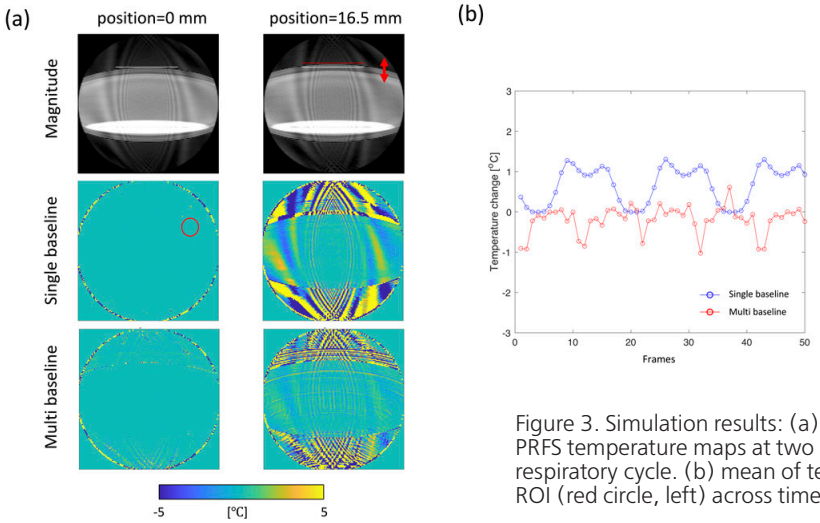

Figure 3. Simulation results: (a) single-/multi-baseline PRFS temperature maps at two positions of the respiratory cycle. (b) mean of temperature within the ROI (red circle, left) across time for each approach.

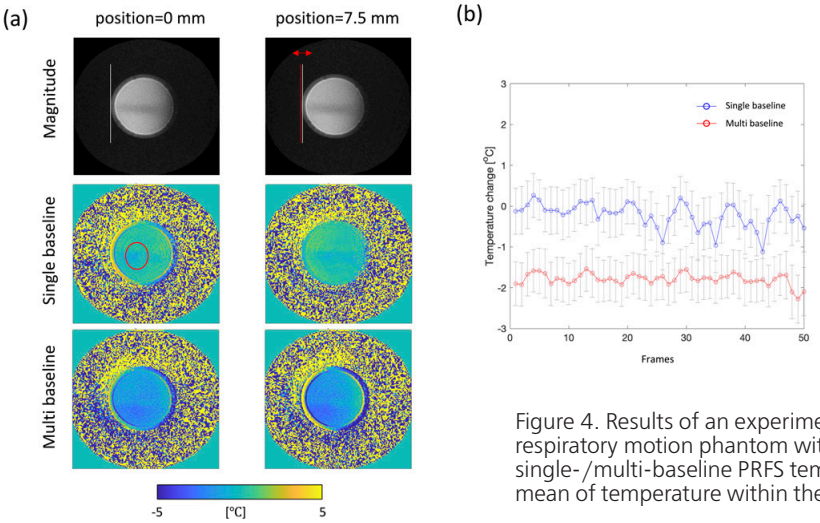

Figure 4. Results of an experiment with simulated respiratory motion phantom without heating. (a) single-/multi-baseline PRFS temperature maps, (b) mean of temperature within the ROI (red circle, left).

TEC-4

Topic: Technical
Presentation Type: Oral

Gas-filled protein nanostructures as cavitation nuclei for molecule-specific sonodynamic therapy

Lin Song, Lei Sun

The Hong Kong Polytechnic University, Hong Kong, China

Background: Sonodynamic therapy (SDT) is a promising alternative for cancer therapy, understood to exert cytotoxicity through cavitation and subsequent production of large amounts of reactive oxygen species (ROS). Targeted microbubbles (MBs) have a demonstrated ability to induce acoustic cavitation under ultrasound exposure, leading to excessive ROS production and enhanced SDT efficacy at specific sites. However, the inherent instability and relatively large size of MBs prevent them from crossing vasculature and limit their potential for deep tumor therapy. Gas-filled protein nanostructures (gas vesicles or GVs) produced by cyanobacteria have a hollow structure similar to MBs and have demonstrated comparable enhancement of ultrasound imaging contrast.

Materials and Methods: We thus hypothesized that GVs may act as stable nuclei for inertial cavitation to enhance SDT with improved EPR effects due to their nanometer scale.

Results: In solution, we found that GVs successfully increased cavitation and enhanced ROS production in a dose- and time-dependent manner. The presence of GVs increased ROS production and enhanced cellular toxicity during SDT in vitro. In vivo, surface-modified GVs targeting CD44+ cells were found to accumulate specifically at the tumor site, inhibit tumor growth and to produce greater tumor damage after SDT treatment.

Conclusions: Our results thus show that GVs can function as stable, nanosized, nuclei for spatially-accurate and cell-targeted SDT.

TEC-6

Topic: Technical
Presentation Type: Oral

Magnetic resonance-guided high-intensity focused ultrasound (MRgHIFU)-induced large-volume hyperthermia is feasible in deep and superficial targets in a porcine model

Lifei Zhu[1], Dao Lam[1], Christopher Pacia[1], Michael Gach[1], Ari Partanen[2], Michael Talcott[1], Suellen Greco[1], Imran Zoberi[1], Hallahan Dennis[1], Hong Chen[1], Michael Altman[1]

[1]Washington University in St. Louis, St. Louis, MO, USA
[2]Profound Medical, Mississauga, ON, Canada

Background: Hyperthermia (HT) refers to increasing tissue temperature to 40–45°C for an extended duration. It is one of the most potent treatment modalities for enhancing the efficacy of radiation therapy (RT) and/or chemotherapy. Magnetic resonance-guided high-intensity focused ultrasound (MRgHIFU) has been recently employed to induce HT under real-time MR thermometry and temperature feedback control. A commercial MRgHIFU system (Sonalleve® V2, Profound Medical) has shown an acceptable safety profile in the muscles and uterus of porcine models in vivo when employing heating fields (target-regions-of interest (tROI)) of ≤44 mm in cross-sectional diameter. Herein, we aim to characterize heating fields and potential tissue damage of large-volume (tROI diameter of 58 mm) HT induced by MRgHIFU in both deep and superficial targets in vivo in a porcine model.

Materials and Methods: Nineteen HT sessions were performed in vivo with the Sonalleve® V2 in hind leg muscles of eight pigs with tROI diameters of 58 mm. Target plane depths were approximately 20 mm (superficial, N=11) and 60 mm (deep, N=8) from the skin. A "threshold-plane" was used for temperature regulation at one or more user-defined positions, either proximal (the "near-field") or distal (the "far-field") to the transducer relative to the target plane. The near-field-only, the far-field-only, and/or both the near- and far- fields were selected as the threshold-plane for both target depths. Temperature statistics evaluated in the tROI included accuracy, precision, temporal variation, and uniformity. Accuracy was calculated by subtracting the desired temperature of 42°C from the achieved average temperature (Tavg) within the tROI. Precision was quantified by averaging the standard deviation of the temperature of each pixel within the tROI. Temporal variation was gauged by the standard deviation of the Tavg of tROI across all dynamics. Heating uniformity was assessed by the temporal average of the largest difference between the Tavg and either the 10th or 90th percentile of the temperature of pixels within the tROI. Temperature fields were characterized by time-in-range (TIR-X, the duration each voxel stays within 40–45°C for X minutes) maps. Tissue damage was analyzed by histopathology.

Results: Fig 1 presents the HT and off-line processing, including tROI denoted by the red dashed circle overlaid on a representative axial MRI target slice (Fig 1A), the corresponding Tavg map of the target slice (Fig 1B), and the TIR-10/TIR-20/TIR-25 map (Fig 1C). For this tROI, Fig 1D presents the temporal Tavg/Tmax/Tmin of all voxels within the tROI. Fig 2 shows the metrics in the tROI for different locations of threshold-plane in both deep and superficial HT. Overall, the accuracy was -0.4±0.5°C (Fig 2A); precision was 1.2±0.2°C (Fig 2C); temporal variation of Tavg for 30-min HT was 0.6±0.2°C (Fig 2B), and the temperature uniformity was 1.5±0.2°C (Fig 2D). A 34.6% difference in the TIR-20 along the sagittal dimension was observed when applying threshold-plane to near-field compared to applying it to far-field. Histopathology showed 75.0% of the examined HT sessions presenting myofiber degeneration or necrosis within the tROI, while 18.8% of the sessions presented only edema within the tROI.

Conclusions: MRgHIFU-induced large-volume HT is feasible in both deep and superficial targets. Target tissue histology showed some localized tissue damage within the HT volume, implying care must be taken for employing these fields to treat deep tumors in a clinical setting. No skin or subcutaneous tissue damage was observed with near-field being included in the threshold-plane. The results of this study also demonstrated the potential of using threshold-planes to spatially tailor the thermal dose to the target, and/or away from critical structures. This study thus lays the foundation for the future development of spatial-feedback controlled HT.

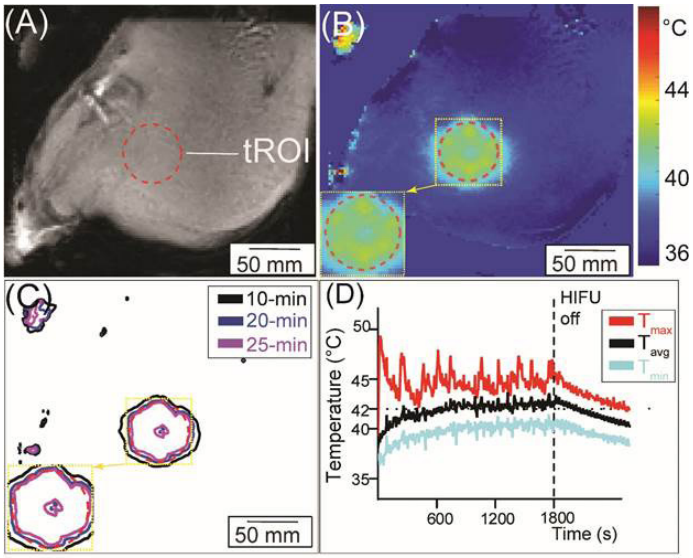

Figure 1. Workflow of the HT to thigh muscle and off-line temperature processing.

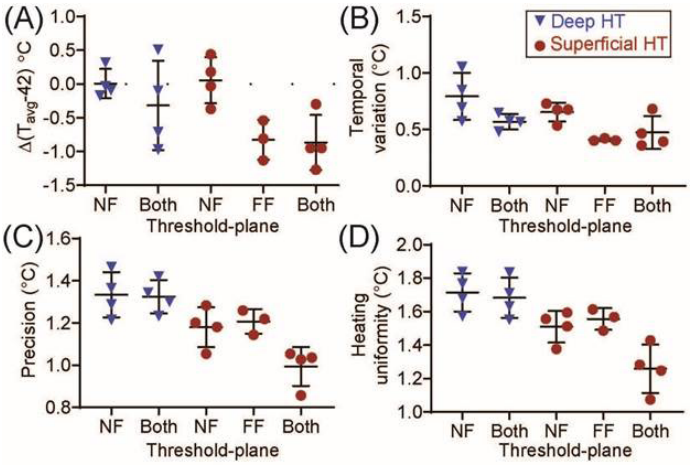

Figure 2. Temperature metrics for both deep HT (blue triangles) and superficial HT (red dots) in thigh muscle.

TEC-7

Topic: Technical
Presentation Type: Oral

Harmonic motion imaging guided focused ultrasound (HMIgFUS) in an in vivo breast cancer mouse model for monitoring and assessment of lesion formation

Xiaoyue Li[1], Niloufar Saharkhiz[1], Saurabh Singh[2], Indranil Basu[2], Chandan Guha[2], Elisa Konofagou[1]

[1]Columbia University, New York, NY, USA
[2]Albert Einstein Cancer Center, The Bronx, NY, USA

Background: Focused ultrasound surgery (FUS) is a noninvasive treatment procedure in which ultrasound energy deposition causes localized temperature rise and cell necrosis. In recent years, there has been increased interest in using FUS for breast tumor ablation, due to its shorter recovery times compared to invasive methods, lack of ionizing radiation, and targeting specificity. There is thus a need for further study on the effects of FUS and techniques for FUS monitoring and guidance. In this study, harmonic motion imaging (HMI) is performed simultaneously with FUS treatment in order to measure tissue elasticity changes with treatment in real time. HMIgFUS is here demonstrated, for the first time, in an orthotopic mouse model of breast cancer (4T1) in vivo.

Materials and Methods: 4T1 mammary carcinoma cells were injected into the 5th inguinal mammary fat pad of 8 week old female BalbC mice (1x10^5 cells/mouse, n=4). Scanning and ablation was performed 16 days post-injection (tumor average diameter: 7.3 +/- 0.9 mm). All mice were sacrificed immediately following ablation.

The HMI transducer assembly consisted of a 15.6 MHz linear array imaging probe confocally aligned with a 4 MHz FUS transducer. 2D HMI was performed prior to and following FUS ablation. A 3D positioning system was used to move the HMI transducer assembly to acquire point-by-point 2D raster scans (5 points laterally, 3 points axially; lateral and axial step size: 3 mm). FUS exposure (15.8 MPa peak positive) during the displacement mapping stage lasted 0.2 seconds at each point. During the ablation stage, FUS was performed for 50 seconds (21.4 MPa peak positive) at a single spot at the center of the tumor, and single point HMI was acquired during FUS with a duration of 0.1 seconds every 3 seconds. Induced axial displacements were estimated using a 1-D cross correlation technique. Peak-to-peak displacements were used to construct HMI displacement maps. The lesion location was automatically segmented based on HMI single spot displacement maps and was defined as the +/-1 dB displacement region around the geometric focus. Histological examination (H&E) was performed on excised tumor samples following ablation by an expert pathologist.

Results: An initial increase in HMI displacement was observed within the defined region during the first few seconds of FUS ablation (from 0 to 15-20 seconds) followed by a decrease in displacement in subsequent time-points, indicating lesion stiffening. Histological examination confirmed the presence of cell necrosis inside of a well-defined lesion that was circumscribed within the tumor. Histology results showed that tumor margins were not ablated, and skin burning was not found in all four mice. The mean estimated lesion diameter was found to be 5.9 +/- 0.25 mm among the four mice, as defined by histology. We used a 6 mm diameter circular ROI area around the geometric focus to estimate displacement before and after FUS ablation in 2D HMI displacement maps. A mean decrease in HMI displacement of 4.5 µm before and after FUS tumor ablation identified the lesion due to the associated stiffening in 4 mice.

Conclusions: In this study, we have shown that HMI can be used to monitor FUS ablation in mammary breast tumors in mice

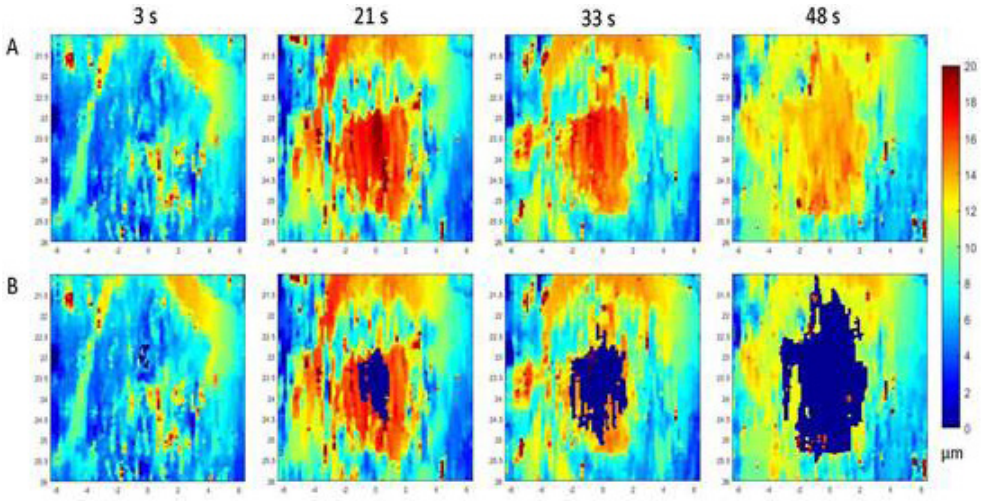

Figure 1. FUS lesion estimation from single spot HMI maps acquired over time during FUS ablation in a mammary tumor mouse model.

using simultaneous 2D imaging for the first time. Histology verified the presence of ablation, and showed that the HMIgFUS lesion was well-localized at the center of the tumor. Ongoing investigations include assessment of degree of stiffening with tumor debulking and effect on metastasis.

Acknowledgements: NIH

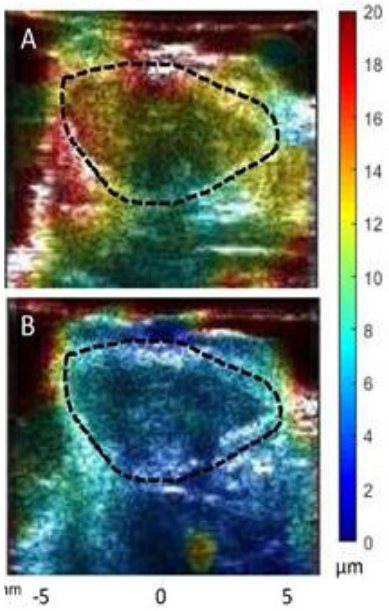

Figure 2. 2D raster-scanned HMI displacement maps overlaid on B-mode of the tumor of one 4T1 orthotopic mouse model before and after FUS ablation.

SAVE THE DATE

8th International Symposium on Focused Ultrasound

October 23-28, 2022

Bethesda North Marriott Hotel & Conference Center
Bethesda, MD, USA

Hybrid Format
In-Person & Virtual

Focused Ultrasound Foundation

FOCUSED
ULTRASOUND
FOUNDATION

Focused Ultrasound Foundation
1230 Cedars Court | Suite 206 | Charlottesville, VA, USA
+1 434.220.4993
www.fusfoundation.org